UNIVERSIDAD AUTÓNOMA DE BAJA CALIFORNIA

FACULTAD DE INGENIERÍA

DOCTORADO EN CIENCIAS E INGENIERÍA

"SISTEMA DE BARRIDO ÓPTICO PASIVO PARA MONITOREO DE DEFORMACIONES EN OBJETOS DE GRANDES DIMENSIONES"

TESIS

QUE PARA OBTENER EL GRADO DE DOCTOR EN CIENCIAS

PRESENTA

MOISÉS RIVAS LÓPEZ

DIRECTOR

OLEG SERGIYENKO

Mexicali, B. C. ***Febrero de 2010***

AGRADECIMIENTOS

A mi esposa Guillermina y a mis hijos Moisés, Aarón, Abraham y Consuelo, por su paciencia y sus muestras de amor en los momentos difíciles que se presentaron durante el desarrollo del presente trabajo.

A Valentín Tyrsa, como un homenaje a su memoria, por haberme motivado para incorporarme al programa de doctorado.

A mi madre y hermanos Consuelo, Tarsicio y Enriqueta, por su cariño y la confianza que siempre han depositado en mi.

A mi director de tesis, Oleg Sergiyenko por brindarme su amistad y estar siempre dispuesto a dirigirme, aconsejarme y apoyarme para concluir exitosamente mis estudios de doctorado.

A Benjamín Valdez Salas, quien como amigo y Director del Instituto de Ingeniería, me brindó su apoyo y me dio todas las facilidades para el desarrollo de este trabajo.

A los integrantes del comité revisor, Larysa Burtseva, Miguel Enrique Bravo Zanoguera, Yuriy S. Shmaliy y Juan Iván Nieto Hipólito, por sus valiosas recomendaciones y por el tiempo que dedicaron para la revisión de esta tesis.

A mis amigos Javier Rivera Castillo, Félix Fernando González Navarro, Noé Carrillo Gallardo y Georgina Carrillo Cabrera, por su solidaridad, su afecto y el apoyo que me brindaron cuando necesité de Ellos.

RESUMEN de la tesis Moisés Rivas López , presentada como requisito parcial para la obtención del grado de DOCTOR EN CIENCIAS, EN EL ÁREA DE ELÉCTRICA. Mexicali, Baja California, México. Febrero de 2010.

SISTEMA DE BARRIDO ÓPTICO PASIVO PARA MONITOREO DE DEFORMACIONES EN OBJETOS DE GRANDES DIMENSIONES.

Resumen aprobado por:

________________ ________________

Dr. Oleg Sergiyenko

Las deformaciones que sufren las grandes estructuras de ingeniería como puentes, túneles, edificios históricos, presas, e incluso los desplazamientos de fallas geológicas, pueden ser medidas con un práctico pero eficiente método de barrido óptico.

El monitoreo con dispositivos geodésicos o con tecnología GPS no es siempre apropiado, a veces puede ser irrealizable, por ejemplo: la tecnología GPS no puede ser utilizada fuera de la zona de recepción de señales de radio tales como túneles, minas, bosques etc.

Por lo tanto nuevos y apropiados métodos y dispositivos para monitoreo automático deben ser creados.

En esta tesis se presenta un método original y un prototipo de un sistema de barrido óptico pasivo el cual puede ser utilizado en el campo del monitoreo de deformaciones.

El método de barrido óptico pasivo puede ser usado con éxito, donde los métodos geodésicos y la tecnología GPS, no funcionan adecuadamente.

Este prototipo tiene una unidad de barrido con una apertura para captar la luz emitida por una fuente localizada en puntos estratégicos sobre la estructura monitoreada.

Un espejo cilíndrico con un corte a 45° montado en un motor de c.c dentro de la apertura, es rotado para captar la luz emitida por la fuente. Esta luz es reflejada hacia un sensor óptico el cual convierte la señal de luz en una señal eléctrica. El procesamiento de esta señal aunado a la señal de posición "cero" permite calcular el ángulo medido con alta resolución. La variación de velocidad de barrido y frecuencia estándar junto con métodos de control de estabilidad de barrido, permiten para este método, aumentar significativamente la resolución angular del sistema, y adecuarla de manera óptima para los requerimientos de la aplicación práctica. Se utiliza también un método novedoso para buscar el centro energético de la señal que contribuye a reducir la incertidumbre.

Los parámetros más importantes del prototipo, cuales fueron definidas en esta tesis, son: exactitud, velocidad de operación, rango de acción y requerimientos de potencia.

Las principales características están basadas en simplicidad, versatilidad y accesibilidad económica.

ABSTRACT of the thesis of Moisés Rivas López as partial requirement for obtaining the degree of DOCTOR IN SCIENCES, ELECTRICAL AREA. Mexicali, Baja California, México. February 2010.
PASSIVE OPTICAL SCANNING SYSTEM FOR DEFORMATION MONITORING IN LARGE DIMENSION OBJECTS
Summary approved by:

____

Dr. Oleg Sergiyenko
Thesis director

Deformations that occurred in any large engineering structures, like bridges, tunnels, historical building, dams, including landmarks displacement during natural land movements can be measured with a very simple but efficient optical scanning method.
The monitoring with geodetic devices or GPS technology is not always appropriate, sometimes it is unrealizable, for example; GPS technology can not be used outside the zone of radio signals reception such as tunnel, mines, forest etc., therefore, new and appropriate methods and devices for automatic monitoring should be created.
This thesis introduces an original method and an optical passive scanning system as a prototype, which may be applicable to the field of deformation monitoring.
The passive optical scanning method can be successful where the geodetic methods do not work appropriately. The prototype has a scanning unit with an aperture to collect the light emitted by a source fixed in strategic points on the monitored structure.
A cylindrical mirror with 45° cut mounted in a DC motor inside the aperture is revolving for collect the emitted light by the source.
This light is reflected towards an optical sensor which converts the light to electrical signal. The processing of this signal jointly with position "zero"signal allows to calculate the angle measured in high resolution. The variation of scanning speed, standard frequency jointly with methods of scanning stability control allows for this method to increase significantly the angular resolution of the system, and to adjust it in an ideal way for the requirements of the practical application. Use of a novel method of the energy center search of the signal helps to reduce significantly the uncertainty.
The most important parameters of the prototype, which were defined in this thesis, are: accuracy, operation speed, operation range and power requirements.
The main characteristics is based in simplicity, versatility, and economical accessibility.

ÍNDICE

Página

CAPÍTULO I

1. INTRODUCCIÓN 1

1.1. Planteamiento del problema. 1

1.1.1. Antecedentes. 2

1.1.2. Medios utilizados en la medición de deformaciones en objetos de grandes dimensiones. 3

1.1.2.1. Redes a base de sensores inalámbricos. 3

1.1.2.2. Sistemas de monitoreo con sensores de fibra óptica (SOFO). 4

1.1.2.3. Métodos Topográficos y Geodésicos. 6

1.1.3. Los sistemas de barrido óptico. 7

1.1.3.1. Sistemas basados en cámaras de video. 8

1.1.3.2. Sistemas de visión basados en el principio del láser. 9

1.2 Hipótesis. 10

1.3 Objetivos. 11

1.3.1 . Objetivo General. 11

1.3.2. Objetivos particulares. 11

1.4 Alcance. 12

CAPÍTULO II

2. FUNDAMENSTOS TEÓRICOS 13

2.1 Medición de ángulos con el sistema de barrido óptico pasivo. 13

2.2 Conversión de señal física a señal eléctrica. 17

2.3 Búsqueda del centro de la señal generada por el emisor de luz. 17

2.4 Método de triangulación. 19

2.5. Conversión de coordenadas angulares a coordenadas cartesianas. 22

ÍNDICE

Página

CAPÍTULO III

3. CONSTRUCCIÓN DE PROTOTIPO Y EXPERIMENTACIÓN 24

3.1. Construcción del prototipo. 24

3.2. Experimentación. 27

3.2.1 Búsqueda del centro de señal. 30

CAPÍTULO IV

4. ANÁLISIS DE RESULTADOS E INCERTIDUMBRE 35

4.1. Análisis de resultados y fuentes de error. 35

CAPÍTULO IV

5. CONCLUSIONES Y RECOMENDACIONES 39

5.1. Conclusiones. 39

5.2. Rcomendaciones y trabajo futuro 41

CAPITULO VI

6. PRODUCTOS DE LA INVESTIGACIÓN 42

REFERNCIAS BIBLIOGRÁFICAS. 44

ANEXO I (Publicaciones en extenso) 51

LISTA DE FIGURAS Página

Figura 1.1. Sistema de monitoreo en base a sensores inalámbricos 4

Figura 1.2 Configuración básica del método con sensor óptico distribuido 5

Figura 1.3. Principio de funcionamiento del sistema GPS 7

Figura 1.4 Sistema de estereovión 8

Figura. 1.5. Dos principios de triangulación láser (a. con ángulo de emission fija; b. con distancia de triangulación fija. (Petrov et al., 1998) 10

Figura 2.1 Elementos principales del sistema de barrido óptico 13

Figura 2.2 Señales de inicio y fin de la medición 14

Figura 2.3 Proceso de medición del ángulo en forma independiente de t. 15

Figura 2.4 Señal generada por el fotodetector 18

Figura 2.5 Aproximación a una señal rectangular 18

Figura 2.6 Estimación de coordenadas por triangulacón 19

Figura 2.7 Triangulación en la medición de distancia 20

Figura 3.1. Prototipo del Sistema de barrido óptico pasivo 24

Figura 3.2 Especificaciones de los dispositivos ópticos utilizados en la construcción prototipo 25

Figura 3.3 Dispositivos electrónicos y electromecánicos del SBOP 26

Figura 3.4 Circuito de acondicionamiento de señal 26

Figura 3.5 Medición de coordenadas para un ángulo mayor de 90° 28

Figura 3.6 Medición de coordenadas para un ángulo mayor de 70° 29

Figura 3.7 Medición de coordenadas para un ángulo de 45° 29

Figura 3.8 Rectificación de una señal senoidal como aproximación a una señal gaussiana 30

Figura 3.9 Derivada de la señal gaussiana simulada 31

Figura 3.10 Pulso de disparo en el valor extremo de la señal 32

Figura 3.11 Señal real generada por el fotodetector 32

Figura 3.12 Transformación de la señal gaussiana a una señal rectangular 33

Figura 3.13 Integración de la señal rectangular 34

Figura 3.14 Pulso generado en el centro geométrico de la señal 34

LISTA DE FIGURAS Página

Figura 4.1 Medición de coordenadas con fuente emisor láser 35

Figura 4.2 Variación de exactitud de coordenadas dentro del ángulo θ del sistema 36

Figura 4.3 Simulación de la medición del ángulo del cono formado por la trayectoria de la luz 37

Figura 4.4 Cálculo de ángulos de 6 puntos equidistantes a 10m entre sí a diferentes distancias del SB y su tiempo de medición con un barrido de 20rps 38

Figura 4.5 Cálculo de ángulos de 6 puntos equidistantes a 10m entre sí a diferentes distancias del SB y su tiempo de medición con un barrido de 60rps 38

CAPÍTULO I

1. INTRODUCCIÓN

En las últimas décadas el monitoreo de deformaciones en grandes objetos se ha vuelto una necesidad apremiante, para la prevensión de desastres, pues si no se detectan a tiempo los daños que sufren las estructuras de edificios, puentes, minas y otras obras civiles, debidos a esfuerzos críticos, por la operación diaria de éstas o provocadas por fenómenos naturales como terremotos, entre otros, las consecuencias se traducen en la pérdida de vidas humanas.

Durante los últimos 20 años se ha desarrollado una rama de la ingeniería conocida como Monitoreo de la Integridad de Estructuras (Structural Health Monitoring), que permite identificar o prevenir daños en estructuras mediante el monitoreo de éstas, métodos e instrumentos de medición, que permiten la comparación entre dos estados del sistema (Worden, Farrar., Manson, Park ,2005).

Este monitoreo normalmente se lleva a cabo manualmente mediante inspecciones que realiza personal especializado, lo que dificulta la obtención continua de datos. Sin embargo, es posible realizarse de manera automatizada utilizando sistemas de monitoreo asistidos por computadora, que permiten llevar un registro permanente de datos asociados a la integridad de las estructuras, facilitando la implementación de medidas para alargar su tiempo de vida, reducir costos de operación y mejorar la seguridad pública (Chintalapudi, Fu, Kothary, 2006).

En el presente trabajo se propone un método de monitoreo basado en un sistema de barrido óptico pasivo, que a diferencia de otros sistemas de monitoreo, este tiene un alcance superior a los 100 metros y puede trabajar en condiciones climatolológicas adversas, lo que le da la ventaja de poder ser utilizado también en el monitoreo de desplazamiento o discontinuidad de capas tectónicas como son las fallas geológicas, entre otras (Tyrza, Rivas, 2004).

1.1. Planteamiento del problema

Como ya se mencionó en la sección anterior, las fallas estructurales en grandes obras civiles como puentes y edificios ocasionan la pérdida de vidas humanas, siendo una parte del problema la falta de información oportuna sobre la integridad de las estructuras en este tipo de obras.

En este contexto, se presenta una alternativa para el monitoreo de deformaciones en objetos de grandes dimensiones, basado en un sistema de barrido óptico pasivo que utiliza fuentes emisoras de luz puntuales o fuentes puntuales tipo spot, que a diferencia de un emisor direccional la luz es emitida en todas direcciones, permitiendo ser captada por un receptor en condiciones adversas. El receptor detecta la intensidad de la luz del emisor desde el inicio del ángulo de visión. Sin embargo, se presenta el problema de identificar en que momento se debe generar el impulso que permitirá detectar la posición del emisor, una forma es considerar el flanco de subida al iniciar la detección, pero esta opción presenta inconvenientes si la amplitud de la señal disminuye, por lo que se propone considerar el centro de la señal generada por el receptor que la cual coincide con el centro de señal y es aquí donde se presenta uno de los principales problemas del sistema que es el de contar con un método para detectar el centro de la señal minimizando el error.

En síntesis, existen dos problemas principales asociados al proyecto:

1. La necesidad de contar con un métodos de monitoreo que permita obtener un registro permanente de las deformaciones en puntos estratégicos de estructuras bajo riesgo o en fallas ocasionadas por fenómenos naturales, con exactitud definida de medición de las coordenadas respectivas en intervalos de tiempo lo más corto posible.

2. En condiciones reales la existencia ruido óptico de naturaleza múltiple por un lado, y por otro, la necesidad de tener un ciclo de barrido giratorio lento, para ofrecer la resolución suficiente del sistema, hace que tome especial relevancia el método para detectar el centro de señal, asociado al centro de energía de las fuentes emisoras.

1.1.1. Antecedentes

El monitoreo de objetos de grandes dimensiones se llevó a cabo durante muchos años utilizando técnicas topográficas y geodésicas apoyadas en instrumentos como el teodolito.

Actualmente, existen registros de monitoreos que se han llevado a cabo en fallas geológicas, utilizando estaciones topográficas totales y GPS, para realizar estudios microtectónicos (Olivera, Fleta , Susagna,2003), (Zippelt,2003) (Cosser, Gethin, 2003)

También existen registros de monitoreo de estructuras mineras, que se han llevado a cabo utilizando sistemas de posicionamiento global y teodolito (Herrera, Contreras,1998). En estos y otros casos, el monitoreo se lleva a cabo a intervalos por lo general mayores a un año, lo que resulta insuficiente para poder predecir el momento en que la deformación llegue al umbral y producir una fractura. Otros medios han sido utilizados recientemente, como son aquellos a base de fibras ópticas (Kihara, Ohno, 2002), las redes inalámbricas a base de sensores bluetooth (Metha, El Zarky, 2004), y radiofrecuencia (Chintalapudi, Fu, Paek, 2006), Sin embargo, debido a sus limitaciones en alcance o interferencia, estos medios se están utilizando principalmente en el monitoreo de la integridad estructural de obras civiles como puentes y edificios.

En el caso de estructuras mineras, desplazamientos en capas tectónicas o descontinuidades, como fallas geológicas, entre otras, sería impráctico el monitoreo con estos medios, debido a sus limitaciones. En estos casos resulta más conveniente utilizar sistemas de barrido óptico.

A continuación se describen los medios utilizados actualmente en el monitoreo de deformaciones en objetos de grandes dimensiones.

1.1.2. Medios utilizados en la medición de deformaciones en objetos de grandes dimensiones.

1.1.2.1 Redes a base de sensores inalámbricos.

Este sistema de monitoreo se basa en instalar una malla de sensores inalámbricos (figura 1.1) como es el caso de tecnologías bluetooth y radiofrecuencia, que permiten medir diferentes parámetros en una estructura, es un modelo muy reconocido debido a su gran aplicación en monitoreo de obras civiles principalmente en edificios, disminuyendo

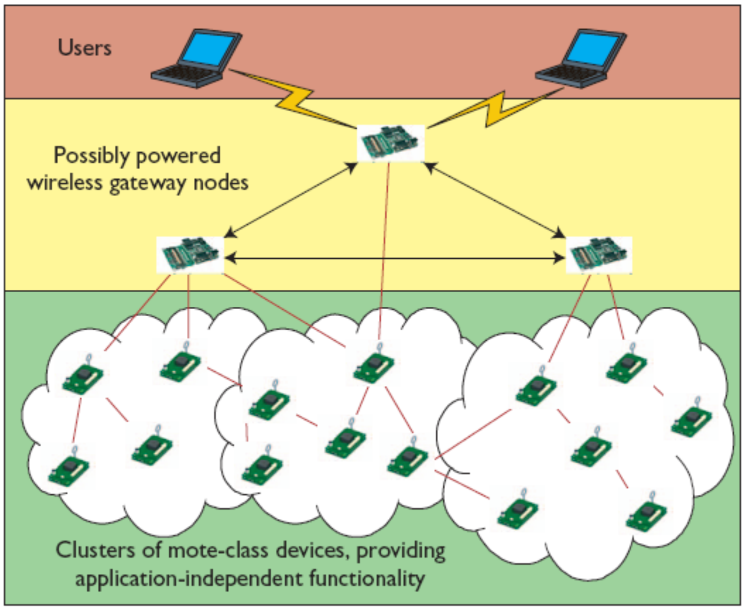

Figura 1.1. Sistema de monitoreo en base a sensores inalámbricos

costos por el uso de cableados, en ocasiones cuentan con un procesador interno y sistemas microelectromecánicos (Chintalapudi, et. al, 2006), pero la mayoría de los sitemas disponibles o en desarrollo, tienen el inconveniente de manejar demasiado volumen de información ocasionando un déficit en el procesamiento debido a la complejidad del software, disminuyendo la velocidad de respuesta (Allen, Park, Farrar, 2005), utiliza demasiados canales de comunicación, tiene la ventaja de trabajar con modelos de bajo consumo de energía (Metha et**.** al,2004), lo cual a su vez se convierte en una desventaja, porque su alcance se reduce a una distancia de diez metros lo cual resulta impráctico en monitoreo de grandes objetos como puentes, minas y fallas geológicas entre otros.

1.1.2.2. Sistemas de monitoreo con sensores de fibra óptica (SOFO).

Otros sistemas de monitoreo son aquellos a base de tecnologías de fibras ópticas (Werner, Fritz, 2003) estos sistemas operan con un mecanismo en el que un espectro de luz es transmitido a través de una fibra óptica, el cual cambia en proporción al estiramiento que sufre una fibra óptica cuando esta es sometida a una tensión, como se muestra en la figura 1. 2 ((Kihara, et al 2002).

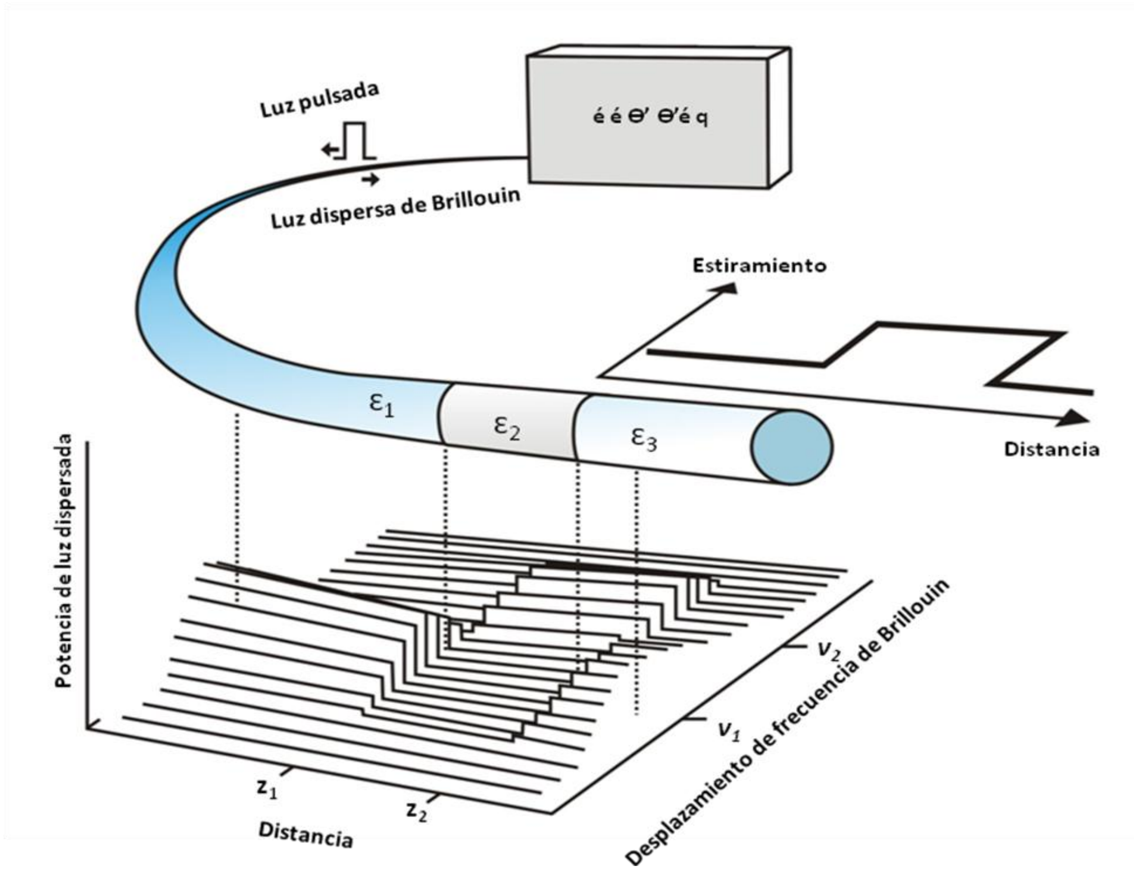

Figura 1.2 Configuración básica del método con sensor óptico distribuido

Los sensores de fibra óptica para monitoreo de estructuras son diseñados para ser sensibles a la tensión y a la flexión y si bien es cierto que los requerimientos y los métodos de medición son diferentes en cada obra que se desea monitorear, en la actualidad muchas de las aplicaciones se basan en el interferómetro de Michelson (Lee,Zhang,2004) (Leng,Winter,Barnes,2005), (Griffin, Connelly,2004)(Player,Slade, 2005) y el principio de luz dispersa de Brillouin. Los sitemas de barrido con sensores de fibra óptica han sido probados obteniendo resultados exitosos en la medición de deformaciones en obras civiles. Sin embargo, estos sistemas tienen como desventaja la alta fragilidad de las fibras, la necesidad de utilizar transmisores y receptores caros, los empalmes entre fibras son difíciles de realizar, lo que dificulta las reparaciones en caso de una ruptura, entre otras, por lo que resulta muy costoso utilizarlos en el monitoreo de largas longitudes, como el caso de una falla geológica o el monitoreo de una línea de transmisión.

1.1.2.3. Métodos Topográficos y Geodésicos.

Durante muchos años los métodos más utilizados para el monitoreo de objetos de grandes dimensiones fueron los métodos geodésicos apoyados en instrumentos como el teodolito mecánico, teodolito electrónico, distanciómetro y nivel. Con estos instrumentos el monitoreo se lleva a cabo midiendo ángulos planos en un espacio esférico dentro de un ángulo sólido $\Omega = 4\pi$ Sr, debido que se trabaja sobre la superficie de la tierra (Tyrsa, Burtseva, Rivas, 2004), (Rivas,Sergiyenko, Tyrsa, 2009) considerando al ángulo sólido como la unidad de medida en un espacio tridimensional cuya magnitud estándar es el estereoradián (sr), (Hemerson,Differing, 2005). En este contexto el monitoreo con teodolito tiene una baja productividad debido al tiempo que se requiere para medir diferentes puntos y la periodicidad de las mediciones, resultando más ventajoso el uso de sistemas de barrido automatizados (Tyrsa et al, 2004).

Otro instrumento muy utilizado como apoyo a los métodos geodésicos es el GPS o sistema de posicionamiento Global, (Global Positioning System), que es un sistema de orientación y navegación cuyo funcionamiento está basado en la recepción y procesamiento de información emitidas por una constelación de 24 satélites, permitiendo determinar por triangulación las coordenadas de cualquier objeto en la superficie terrestre (Herring, 1996). (Fotiou , Kagiadakis , Pikridas,2003)

Es un sistema que por lo general recibe de cuatro a ocho señales de satélites con posición orbital conocida con respecto a la tierra, también se conoce el tiempo que las señales tardan en recorrer el camino entre el satélite y el receptor y la velocidad de propagación de las señales lo cual permite establecer por triangulación posición del receptor en términos absolutos (Pozo,2005) Como se muestra en la figura 1.3.

Existen registros de varias aplicaciones de monitoreo utilizando GPS (Rutledge , Gnipp Kramer,2003)(Dai, Wang, Rizos,2001). Sin embargo, las mediciones con estos sistemas se ven afectadas por diferentes fuentes de error, ocasionadas por perturbaciones atmósfericas, fenómenos meterorológicos, imprecisión de los de las estaciones receptoras con respecto a los relojes atómicos de los satélites, interferencia de disponibilidad selectiva, introducida por el estamento militar, traduciéndose en un mayor grado de incertidumbre (Pozo, Ribeiro, , 2001).

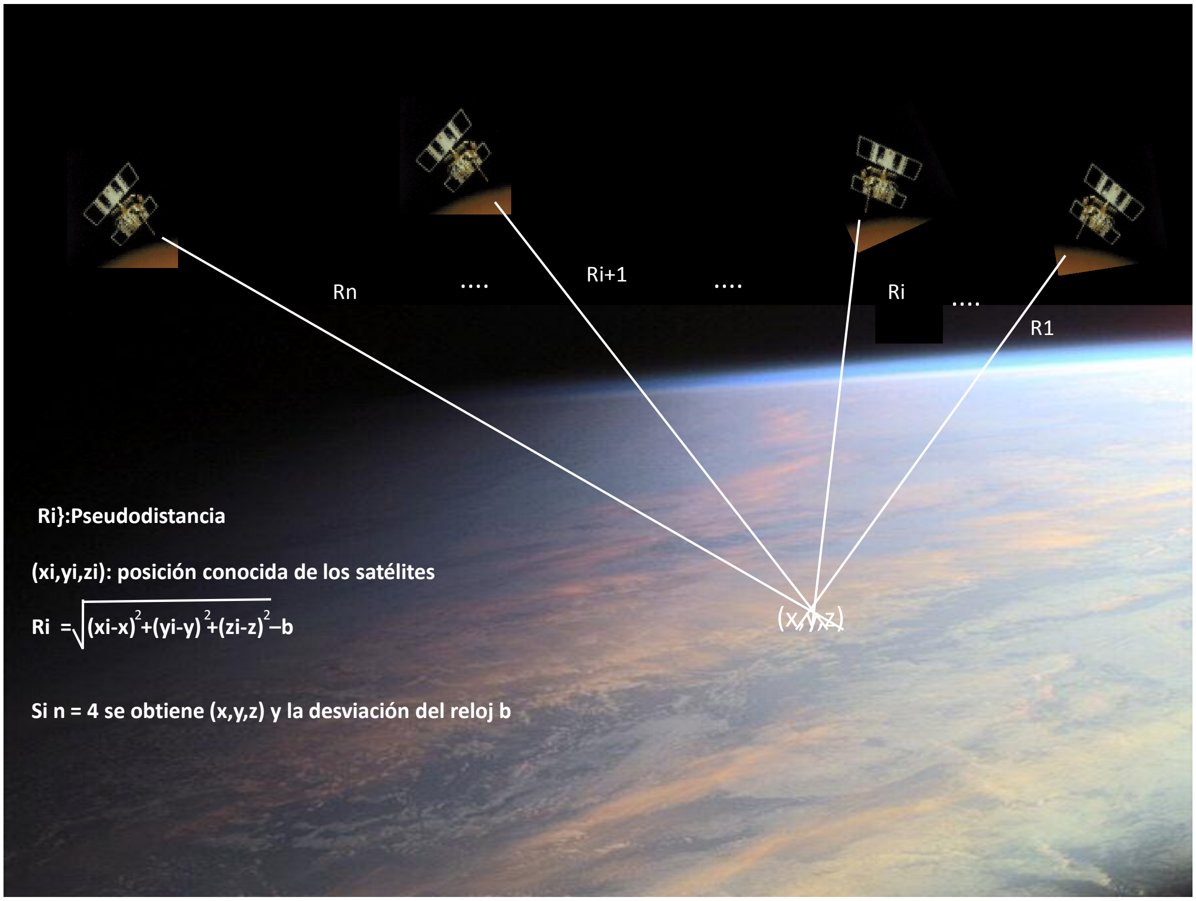

Figura 1.3. Principio de funcionamiento del sistema GPS

Debido a las desventajas anteriores, estos sistemas no son recomendables para aplicaciones en lugares donde el número de satélites visibles es insuficiente para lograr una buena incertidumbre, como es el caso de minas y zonas boscosas entre otras.

En algunos casos la incertidumbre puede reducirse mediante el uso de pseusatélites, pero esto eleva demasiado el costo del monitoreo (Dai, Wang, Rizoz,Han, 2001).

1.1.3. **Los sistemas de barrido óptico.**

Dadas las desventajas de los métodos presentados con anterioridad y con el propósito de llevar un registro de datos de manera continua, se han desarrollado los sistemas de barrido óptico apoyados en tecnología láser (Gordon,Lichti,Stewart, 2004)(Bosch, Donati,2001) o apoyados en cámaras de video (Audbert, Miller, Paindavoine, 2002). Ambos sistemas trabajan a base de técnicas para la reconstrucción de imágenes 3D.

1.1.3.1. Sistemas basados en cámaras de video

La base de cualquier método de cámaras, es el principio de la visión volumétrica de los seres humanos, capaces de reconstruir una imagen tridimensional (3-D) y calcular aproximadamente las distancias hasta los objetos en la escena. Esto, es en otras palabras, la estereovisión.

Un sistema técnico de estereovisión es un enfoque de sistema multicámara en donde se considera como caso elemental un sistema de dos cámaras (García,Orteu,2001). Si un sistema de estereovisión (Chaumette y Hutchinson, 2006) se utiliza, y, un punto 3-D es visible tanto en la imagen izquierda como en la derecha (ver Figura 1.4), es posible utilizar como características visuales el vector S que contiene los valores deseados de la escena /características:

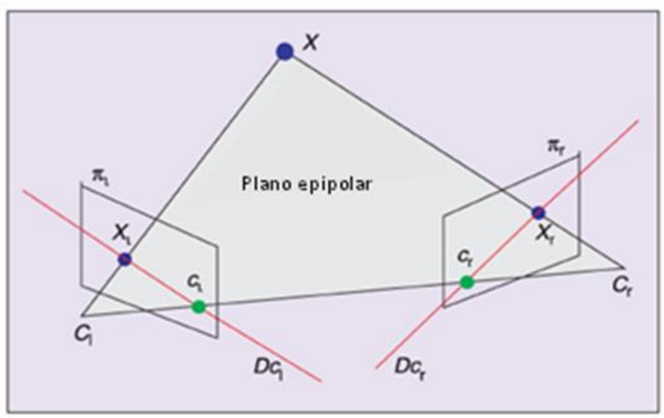

Figura 1.4. Sistema de estereovión

$$s = xs = (xl, xr) = (xl, y\ l, xr, yr), \qquad (1.1)$$

i.e., para representar el punto sólo apilando en s las coordenadas X e Y del punto observado en las imágenes de la izquierda y derecha.

Para un punto 3-D con coordenadas X = *(X,Y,Z)* en el cuadro de la cámara, que proyecta en dos imágenes 2-D con coordenadas **x** = *(x, y)*, tenemos (Chaumette & Hutchinson, 2006):

$$\begin{cases} x = X/Z = (u - c_u)/ f\alpha \\ y = Y/Z = (v - c_v)/ f, \end{cases} \qquad (1.2)$$

En donde la matriz medición de la imagen m = (u, v) da las coordenadas del punto de la imagen expresada en unidades de píxel, y a= (Cu, Cv, f, α) es el conjunto de parámetros intrínsecos de la cámara: Cu y Cv son las coordenadas del punto principal, f es la longitud focal, y α es la relación de las dimensiones en píxeles. En este caso, tenemos s = x = (x, y), la imagen de plano las coordenadas del punto.

Aunque estos métodos están siendo utilizados para el monitoreo de deformaciones geométricas (Audbert et al, 2002), tienen la principal desventaja en la correspondencia de las imágenes monoculares haciendo más complejos los algoritmos para realizar estas tareas, elevando el costo de computación (Cristina, Dapoto, Vegas, 2007), teniendo además limitaciones en condiciones de brillo, sombras, y sombreados. Estos sistemas son más adecuados para monitoreo de imágenes u objetos con mucho movimiento.

1.1.3.2. Sistemas de visión basados en el principio del láser.

Las tecnologías modernas de sensores láser han hecho posible la adquisición de datos 3-D de una manera rápida y exacta, (Tyrsa et al., 2004), (Peng-Hsiang y Weng Fu-Jen Kao, 2004), (Diosi Y Kleeman, 2005), (França et al., 2005), (Surmann et al., 2003), (Lavelle et al., 2004), (Handbook of Optical and Laser Scanning, 2004), (Forman & Parry, 2001), (Pierce et al., 1992), (LICHTI et al., 2000), (Petrov et al., 1998). A diferencia de otras tecnologías 3-D existentes basadas en la reconstrucción de imágenes 2-D provenientes de CCD's, estos sensores 3-D permiten determinar la ubicación de objetos mediante el barrido por láser y metodologías geométricas tales como la triangulación (Petrov et al., 1998), (Tyrsa et al., 2006, a), (Tyrsa et al., 2006, b), (Rivas et al., 2008).

El principio de triangulación láser (Handbook of Optical and Laser Scanning, 2004) en general puede ser basado en dos esquemas como se representa en la figura 1.5 (a y b).

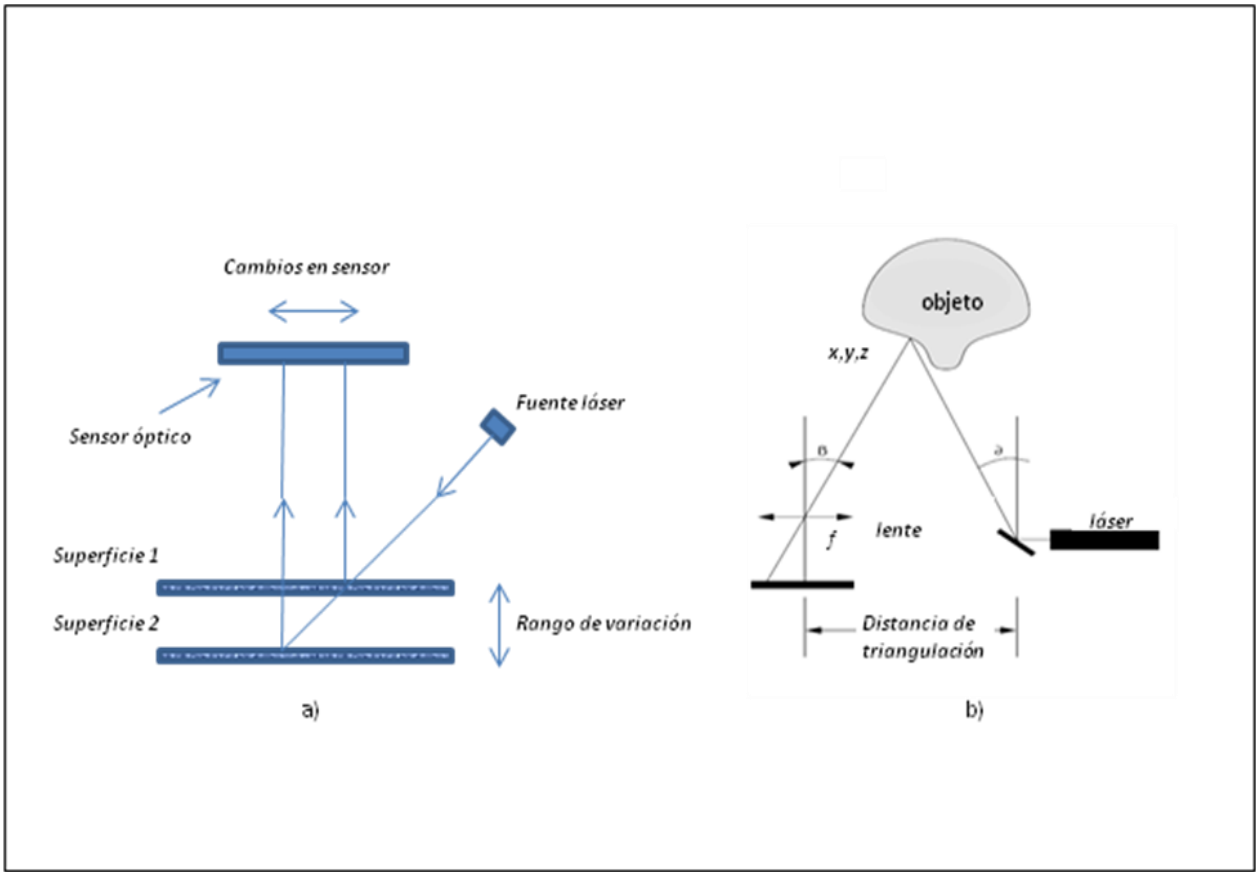

Figura. 1.5. Dos principios de triangulación láser (a. con ángulo de emission fija; b.con distancia de triangulación fija. (Petrov et al., 1998)

El primero de ellos utiliza un ángulo de emisión fijo y distancia variable; el segundo, por el contrario, emplea una base de triangulación fija y ángulo de barrido variable. Sin embargo, en el monitoreo de grandes objetos, presentan algunas restricciones, pues en materiales opacos a distancias muy alejadas el rendimiento es muy bajo al regresar la señal (Gordon, et al, 2004).

Otra desventaja de estos sistemas es el rendimiento en condiciones climatológicas adversas como el caso de lluvia y brisa que afectan la recepción de la señal.

1.2. Hipótesis.

Con la presente investigación se pretende comprobar la hipótesis de que, es posible medir de manera remota las deformaciones en objetos de grandes dimensiones, a intervalos de tiempo menores de un minuto, con una incertidumbre menor a 10^{-3}m, en distancias de 10m a 100m, utilizando un sistema automático de barrido óptico pasivo.

1.3. Objetivos.

1.3.1. Objetivo General.

Desarrollar un nuevo método teórico y formalismo matemático correspondiente, para demostrar que es posible monitorear deformaciones en objetos de grandes dimensiones, a intervalos de tiempo menores de un minuto, con una incertidumbre menor a 10^{-3}, utilizando un sistema automático de barrido óptico pasivo.

1.3.2. Objetivos particulares.

Analizar diferentes sistemas utilizados para monitoreo de deformaciones en objetos de grandes dimensiones, para aprovechar en nuestra investigación las ventajas de los mejores sistemas que actualmente existen en el mercado.

Diseñar un sistema de barrido óptico pasivo optimizando distancia y ángulo de barrido.

Complementar las condiciones del canal óptico en el par "emisor-receptor" teniendo en cuenta la tarea de monitoreo de grandes estructuras.

Desarrollar el principio eléctrico y formalismo matemático para conversión del ángulo sólido a la señal eléctrica que permitirá obtener su valor numérico.

Diseñar el circuito de acondicionamiento de la señal optoelectrónica

Desarrollar los métodos inéditos para procesamiento de la señal eléctrica que permitan aumentar la resolución angular (búsqueda del centro geométrico del emisor; método de Sergiyenko- Hernández aplicado en las mediciones angulares repetitivas)

Construir el prototipo del sistema de barrido óptico pasivo para monitoreo y realizar experimentación en el laboratorio, para comprobar la funcionalidad del método propuesto.

Proponer una metodología para monitorear deformación de un objeto utilizando el sistema de barrido óptico pasivo.

Estimar la incertidumbre/exactitud de las mediciones

Analizar y evaluar los resultados obtenidos.

1.4. Alcance.

El presente trabajo consiste en la propuesta de un método de monitoreo basado en un sistema de barrido óptico pasivo, que a diferencia de los sistemas basados en redes inalámbricas se tiene la ventaja de un alcance mayor a los 100 metros y menor interferencia. Este sistema también tiene ventajas sobre los sistemas geodésicos pues mientras un sistema GPS requiere de un tiempo largo (en una observación se requieren por lo menos 27 satélites diferentes para llegar a nivel de incertidumbre de mm (Kee,Park, 2008) para hacer una nueva medición de coordenadas de un mismo punto. Con el sistema propuesto se pueden tener 10 mediciones por segundo permitiendo detectar variaciones en las coordenadas de un punto estratégico del objeto bajo prueba, en cortos periodos de tiempo. Cabe mencionar que el método de medición, se probó mediante la construcción del prototipo en condiciones de laboratorio, las mediciónes se presentan en el capítulo IV.

CAPITULO II

2.FUNDAMENTOS TEÓRICOS.

2.1. Medición de ángulos con el sistema de barrido óptico pasivo.

En la figura 2.1 se muestra un diagrama esquemático general que contiene los principales elementos propuestos para construir un sistema de barrido óptico pasivo.

Como se puede observar, el sistema de barrido se compone de emisores de luz, colocados a una distancia l, del receptor, el cual se conforma de un espejo e, que gira con una velocidad ω.

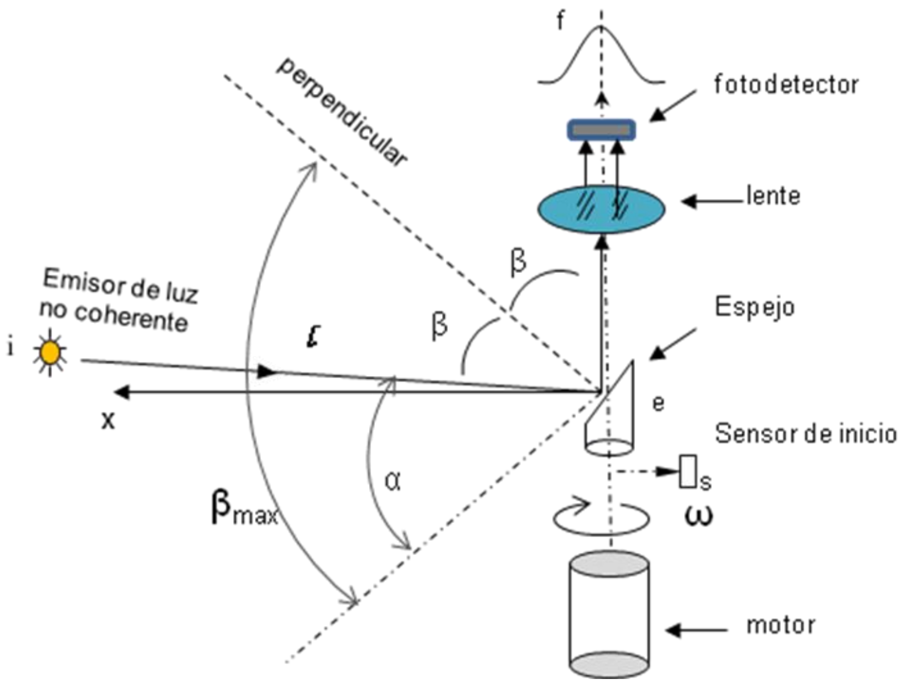

Figura 2.1 Elementos principales del sistema de barrido óptico

El rayo emitido llega con un ángulo de incidencia β, con respecto a la perpendicular del espejo, por lo que es reflejado con un mismo ángulo β, de acuerdo a la ley de reflexión (C.L. Wyatt ,1991)., para pasar a través de un lente que concentra el haz para ser captado por un fotodetector, el cual genera una señal f en forma de una función gaussiana que posteriormente será procesada.

Cuando el espejo empieza a girar, un sensor s es sincronizado con el origen generando un pulso que indica el inicio de la medición, la cual termina cuando el fotodetector emite la señal de alto para finalizar la medición como se muestra en la figura 2.2.

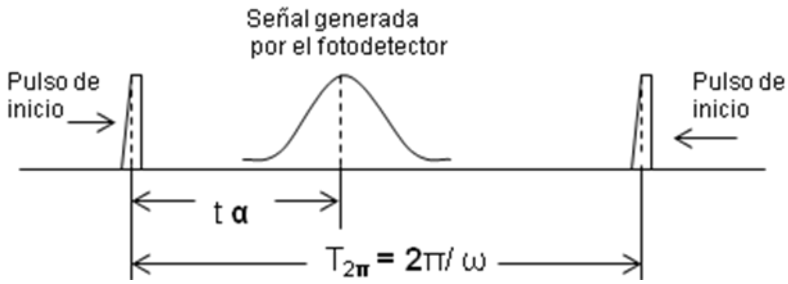

Figura 2.2 Señales de inicio y fin de la medición

En esta figura 2.2 se puede apreciar que la intensidad de la luz se incrementa en el centro de la fuente emisora, por lo que el sensor s deberá generar la señal de inicio en el flanco de subida del pulso generado por el mismo, mientras que el fotodetector deberá emitir las señal de fin de medición cuando detecte el centro geométrico del emisor, para disminuir posibles errores en la medición.

Conforme a lo anterior el tiempo entre la señal de inicio y la señal de alto, está dado como sigue:

$$t_{\alpha} = \alpha / \omega \qquad (2.1)$$

donde α es el ángulo entre la dirección instantánea al punto de emisión y cero de la escala angular , ω es la velocidad angular de barrido (velocidad programada del motor de c.d. de la apertura de barrido) y t_{α} representa el tiempo desde que el sensor respectivo emite la señal de inicio, hasta que un circuito de acondicionamiento de señal encuentra el centro de la señal generada por fotodetector.

Por otra parte, se conoce que en una revolución completa $\alpha = 2\pi$, por lo que el periodo de tiempo en una revolución $T_{2\pi}$, está dado conforme a la siguiente expresión matemática:

$$T_{2\pi} = 2\pi / \omega \tag{2.2}$$

finalmente despejando α de la fórmula (2.1) se obtiene lo siguiente:

$$\alpha = \omega \, t_{\alpha} \tag{2.3}$$

De acuerdo con la ecuación (2.3) la medición del mensurando α, prácticamente se convierte en la tarea de medir el intervalo de tiempo $t_{\alpha,}$ lo cual se puede realizar por métodos conocidos (Hernández, Sergiyenko, Rivas, 2009), (Lombardi, 2006). Sin embargo, la medición de intervalos cortos de tiempo (ω =10r/s, $T_{2\pi}$ = 100 μs), se convierte en una tarea complicada. Por esta razón es conveniente excluir de la ecuación (2.3) la variable tiempo. La manera de hacerlo se presenta en la figura 2.3.

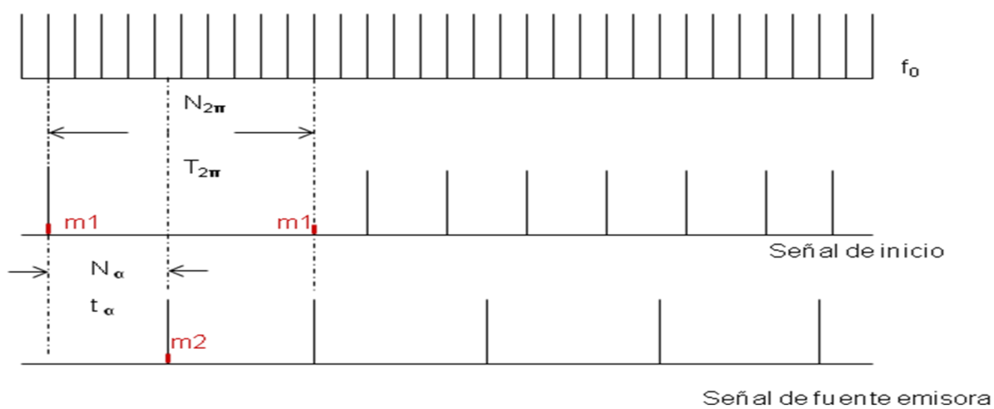

Figura 2.3 Proceso de medición del ángulo en forma independiente de t

Como se puede observar de la figura 2.3, el intervalo $T_{2\pi}$ es igual a la distancia entre las marcas m1 y m1, el cual está expresado por el código $N_{2\pi}$ definido en la ecuación (2.4).

$$N_{2\pi} = T2\pi \cdot f_0 \tag{2.4}$$

Por otro lado, el intervalo de tiempo t_{α} que es igual a la distancia entre las marcas m1 y m2, puede ser expresado por el código $N\alpha$ que se define como sigue:

$$N\alpha = t_{\alpha} \cdot f_0 \tag{2.5}$$

donde f_0 es una frecuencia de referencia estandar. De esta manera se puede excluir la variable tiempo de la ecuación (2.3) para expresarla en la forma siguiente (Rivas, Sergiyenko, Tyrsa,2009):

$$\alpha = 2\pi \cdot N_{\alpha} / N_{2\pi} \tag{2.6}$$

donde α es valor de coordenada angular del emisor de luz, colocado en un punto de interés. Esta ecuación se puede generalizar como se expresa en (2.7), debido a que el punto de interés puede ser colocado en diferentes posiciones o bién, pueden existir diferentes puntos de interés ubicados sobre el eje vertical (subíndice j) u horizontal (subíndice *i*) .

$$\alpha_{ij} = 2\pi \cdot N_{\alpha_{ij}} / N_{2\pi_{ij}} \tag{2.7}$$

Al excluir la variable tiempo en la estimación de α, se obtuvo un resultado teórico muy significativo. Todas las fuentes de incertidumbre asociadas con medición de tiempo mencionados en (Hernández, et al, 2009), (Lombardi, 2006) son iguales para ambos intervalos N_{α} y $N_{2\pi}$, por lo que todos los errores instrumentales se eliminan en la operación de división en las fórmulas (2.6) y (2.7).

Para la tarea técnica bajo consideración, eso establece una incertidumbre a nivel prácticamente despreciable por ejemplo: para una f_0 igual a 1MHz tenemos una graduación distinguible angular igual a 360°/ 1000000= 0.00036°, este resultado para cualquier aplicación técnica moderna es más que suficiente. Aunado a lo anterior, el método teórico propuesto todavía tiene recursos para aumentar la resolución, eso puede ser viable para las tareas de monitoreo que no están limitadas por criterio de tiempo de medición. En este caso, se puede aplicar el método realizando ciclos de barrido consecutivos y repetitivos, “continued time stamping” (Staffan Johansson, 2004,2005), que permite aplicar una búsqueda de las mejores coincidencias entre la escala desconocida y la estandar, utilizando el método de Sergiyenko-Hernández (Hernández et al, 2009).

2.2. Conversión de señal física a señal eléctrica.

Para llevar a cabo electrónicamente la medición del ángulo, mediante el método representado en forma gráfica en la figura 2.3, se requieren los siguientes procedimientos y dispositivos técnicos: 1) detectar marcas m1y m2 , mediante un fotodetector ; 2) contar los códigos $N_{2\pi}$ y $N\alpha$ mediante contadores de pulsos ; 3) realizar sincronización de contadores con señales fotovoltaicas, las cuales en este caso serían las señales de control para los contadores. 4) desarrollar interface que permita pasar toda la información en tiempo real y en paralelo al procesador (en este caso computadora) que va a realizar los cálculos para cada paso ij según (2.4) y (2.5).

Para realizar dichos procedimientos 1-4 se requiere resolver las siguientes tareas Prácticas: 1) Seleccionar el fotodetector cuyos parámetros técnicos serían más adecuados para las tareas de monitoreo 2) definir la velocidad óptima de barrido y adecuar los parámetros técnicos de los contadores a las necesidades requeridas 3) desarrollar un algoritmo de control de los dispositivos electrónicos mediante un procesador central (computadora), 4) definir la cantidad óptima de pasos ij suficientes para la tarea de monitoreo y en base a ello seleccionar el procesador central que permita en tiempo real realizar los cálculos necesarios según el formalismo matemático y almacenamiento de los datos recibidos en archivo matriz de tamaño $i \times j$.

2.3. Búsqueda del centro de la señal generada por el emisor de luz.

Para realizar el cálculo del ángulo mensurando conforme a lo descrito en 2.2 se tiene solamente una simplificación teórica. Se supone que la coordenada del emisor está descrita solamente en un punto en el espacio, mientras en la realidad la fuente de luz no coherente tiene cierta distribución espacial. Teóricamente sería conveniente asociar esta fuente distribuida con la coordenada geométrica de su centro, para minimizar posibles errores, pues un problema que se presenta en la medición de α cuando se utilizan emisores de luz no coherente, es que la luz se propaga en todas direcciones y el espejo capta la luz desde que inicia su ángulo de visión, por lo que el fotodetector genera una curva gaussiana (o más compleja como se presentará en la sección de experimentación), aumentando la probabilidad de error en el disparo de la señal de alto.

Para disminuir este error se propone que el disparo se genere cuando se detecte el centro de la señal, el cual se puede determinar derivando la señal generada para encontrar el punto máximo como se muestra a continuación.

Si V(t) representa la señal generada siendo una función como la que se muestra en la figura 2.8, donde v es el voltaje y t es el tiempo, entonces de acuerdo con el teorema de Rolle y al teorema del valor extremo (Leithold, 1994) :

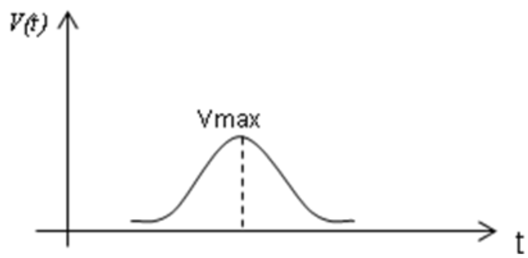

Figura 2.4 Señal generada por el fotodetector

$$v(t) = V\max \quad \text{si} \quad dv(t)/dt = 0 \qquad (2.8)$$

En condiciones ideales este método resulta apropiado (Rivas, et al ,2009). Sin embargo, si la señal presenta varios puntos de inflexión, este método no será muy eficiente, por lo que se propone aproximar la señal generada a una señal rectangular como se muestra en la figura 2.5.

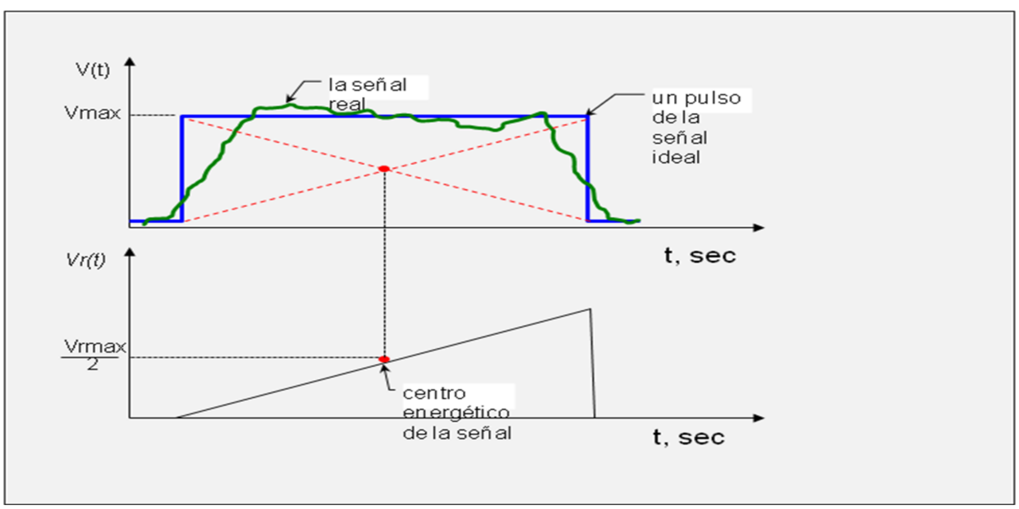

Figura 2.5 Aproximación a una señal rectangular

De acuerdo con la figura 2.5 si *Vr*(t) es una señal rectangular con Valor máximo igual a *Vr* max, entonces se tiene lo siguiente:

$$Vr(t) = \int v(t)dt \tag{2.9}$$

El centro de la señal se encuentra entonces en:

$$Vr(t) = Vr\max/2 \tag{2.10}$$

2.4. Método de triangulación.

Este método permite encontrar las coordenadas de un punto como se muestra en la figura 2.6. si se conocen al menos tres de los elementos del tríangulo (Barchett, Raymond, 1984). (Bannister ., Raymond ., Baker,2002) ., Técnicas modernas en topografía,7ma

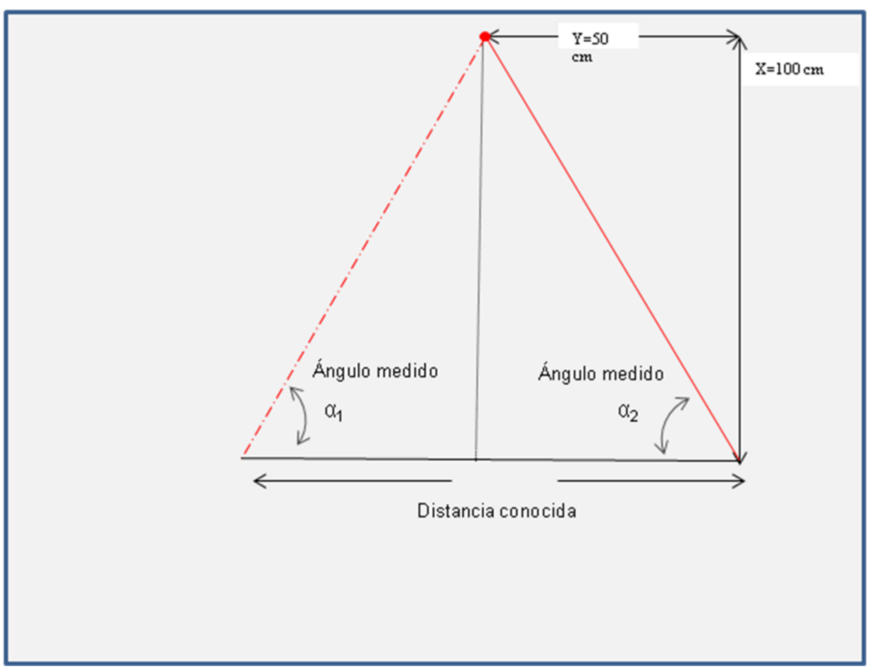

Figura 2.6. Estimación de coordenadas por triangulacón

Para la tarea práctica presentada en esta tesis, la medición de la coordenada angular es suficiente. Sin embargo, si en cada ciclo de medición podemos medir la coordenada angular de un punto de referencia fijado sobre la estructura bajo control, entonces podemos detectar la deformación si la coordenada del próximo ciclo de medición es distinta. El valor de la deformación es proporcional al cambio del valor de la coordenada en su forma angular.

No obstante a lo anterior, para los ingenieros responsables de la obra bajo control, así como para almacenamiento y comparación de la información sobre deformaciones, la forma más cómoda y útil son las coordenadas cartesianas. Por eso se requiere configurar el sistema y el formalismo matemático del mismo, para la obtención de coordenadas en esta forma.

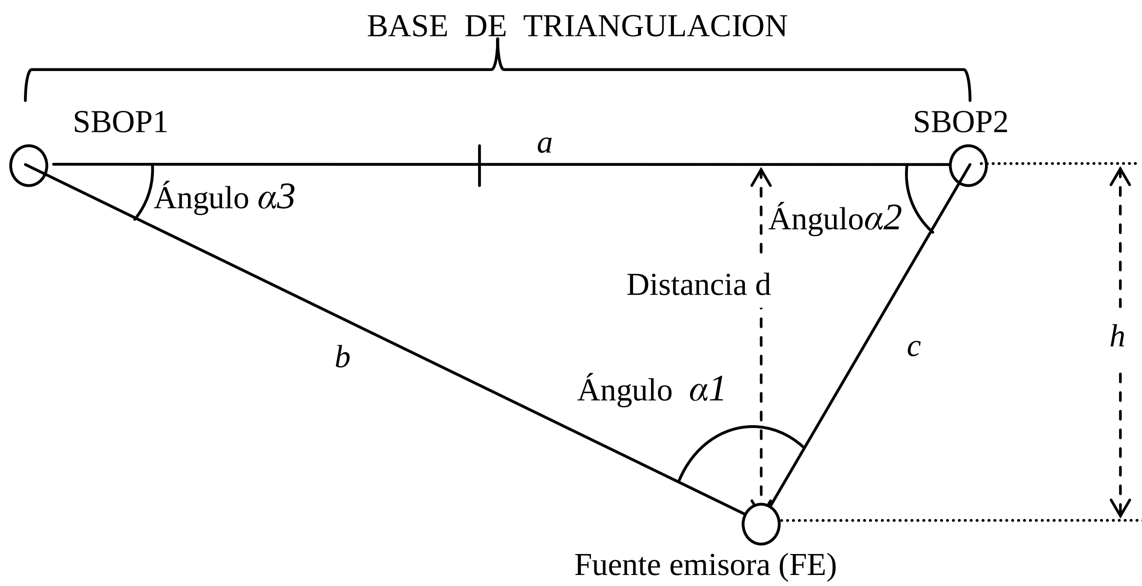

Figura2.7. Triangulación en la medición de distancia

Como se observa en la figura 2.7 para realizar una triangulación correcta según las bases teóricas de la trigonometría (Barchett, Raymond,1984), hay que aplicar dos de nuestros sistemas de medición de coordenada angular en la medición de los ángulos α_2 y α_3 según procedimiento descrito en 2.1. En este caso se conocen dos elementos (dos ángulos) del triángulo y para conocer el tercero se requiere solamente definir con alta exactitud la distancia a entre los dos sistemas de barrido óptico pasivo (SBOP1 y SBOP2) en la etapa de diseño de barrido físico (en otras palabras, medir la base con instrumentos de medición de distancias lineales).

En este caso el formalismo matemático para determinar las coordenadas cartesianas de la fuente emisora (FE) está basado en las siguientes consideraciones.

Existe una función matemática D(a,α_3,α_2) para el valor de distancia que depende de las variables a, α_2 *y* α_3 . Dicha función se deduce a partir de algunas propiedades de los triángulos. La primera que se utiliza es la Ley de senos :

$$\frac{a}{sen(\alpha_1)} = \frac{b}{sen(\alpha_2)} = \frac{c}{sen(\alpha_3)} \quad . \qquad (2.11)$$

En la Figura 2.7 se puede ver que la distancia desconocida *d* coincide con la altura del triángulo formado por el SBOP1-Proyección-SBOP2. Y matemáticamente se establece que:

$$sen(\alpha_3) = \frac{d}{b}, \text{ despejando b, se tiene: } b = \frac{d}{sen(\alpha_3)} . \qquad (2.12)$$

$$sen(\alpha_2) = \frac{d}{c}, \text{ despejando c, se tiene: } c = \frac{d}{sen(\alpha_2)} . \qquad (2.13)$$

Reemplazando ecuaciones (3.2) y (3.3) en (3.1) se eliminan las distancias (desconocidas) ***b*** y ***c***, y se obtiene la siguiente relación:

$$\frac{d}{sen(\alpha_3) sen(\alpha_2)} = \frac{a}{sen(\alpha_1)} \qquad (2.14)$$

Por propiedad general de los triángulos se sabe que la suma de los ángulos internos α_1, α_2 y α_3 es 180°, así se obtiene que:

$$\alpha_1 = 180° - (\alpha_2 + \alpha_3) \qquad (2.15)$$

Sustituyendo la ecuación (2.15) en (2.14) se tiene:

$$\frac{d}{sen(\alpha_3)sen(\alpha_2)} = \frac{a}{sen(180° - (\alpha_2 + \alpha_3))}$$

Despejando *d*, se obtiene la función **d(*a*,α2,α3)**:

$$\mathrm{d}(\mathrm{a}, \alpha_2, \alpha_3) = \frac{a.sen(\alpha_2).sen(\alpha_3)}{sen(180 - (\alpha_2 + \alpha_3))} \qquad (2.16)$$

De esta forma, a partir del teorema de senos y de tres parámetros iniciales (ángulos de recepción α_2 y α_3, y distancia entre los dos SBOP , se determina la distancia *d* desde la base hasta la proyección de un haz de luz en la fuente emisora.

2.5. Conversión de coordenadas angulares a coordenadas cartesianas.

La distancia ***d*(*a*, *α2*, *α3*)**, es el valor de distancia entre el SBOP1 y SBOP 2 y la fuente emisora que está en el ángulo sólido del campo de visión θ de nuestro sistema.

Para poder cubrir la superficie completa de la estructura bajo observación se necesita en el caso general $i \times j$ puntos, donde i corresponde a desplazamiento horizontal y j al desplazamiento vertical.

Para obtener las coordenadas cartesianas de los resultados de mediciones angulares del sistema en cada paso de barrido ij, (Rivas, Sergiyenko, Burtseva, 2008), se utilizarán las siguientes expresiones matemáticas que pueden ser deducidas del parámetro básico d_{ij} y del triángulo básico de la figura 2.7, utilizando la relación entre lados y ángulos de un triángulo (Barchett, Raymond A,1984). donde d_{ij} se puede expresar como sigue:

$$d_{ij} = a\frac{Sen\alpha_{2ij} \cdot Sen\alpha_{3ij}}{Sen\left[180^\circ - \left(\alpha_{2ij} + \alpha_{3ij}\right)\right]} \qquad (2.17)$$

De igual manera las coordenadas en el punto ij (x_{ij},y_{ij},z_{ij}) se pueden determinar con las fórmulas (2.18),(2.19),(2.20) como se muestra a continuación:

$$\mathrm{x}_{\mathrm{ij}} = a \cdot \frac{Sen\alpha_{2ij} \cdot Sen\alpha_{3ij} Cos\sum_{j=1}^{j}\beta_j}{Sen\left[180^\circ - \left(\alpha_{2ij} + \alpha_{3ij}\right)\right]} \tag{2.18}$$

$$\mathrm{y}_{\mathrm{ij}} = -a \cdot \left(\frac{1}{2} + \frac{Sen\alpha_{2ij} \cdot Cos\alpha_{3ij}}{Sen\left[180^\circ - \left(\alpha_{2ij} + \alpha 3_{ij}\right)\right]}\right) \tag{2.19}$$

$$\mathrm{z}_{\mathrm{ij}} = a \cdot \frac{Sen\alpha_{2ij} \cdot Sen\alpha_{3ij} Sen\sum_{j=1}^{j}\beta_j}{Sen\left[180^\circ - \left(\alpha_{2ij} + \alpha_{3ij}\right)\right]} \tag{2.20}$$

Una vez definidos los fundamentos teóricos, se procedió a la construcción del sistema de barrido y a la experimentación como se presenta en el capítulo III.

CAPITULO III

3. CONSTRUCCIÓN DE PROTOTIPO Y EXPERIMENTACIÓN

Con el propósito de probar el método de medición propuesto, se construyó un prototipo de apertura de barrido pasivo y se llevó a cabo la experimentación correspondiente. Una parte de la experimentación se realizó con el prototipo y otra se llevó a cabo mediante la simulación, como se presenta a continuación.

3.1. Construcción del prototipo.

El prototipo fue diseñado y construido para operar conforme a los fundamentos teóricos, presentados en la sección 2 y utilizando componentes comerciales con los parámetros técnicos adecuados para su funcionamiento y con costos acordes a los recursos disponibles para el proyecto (Rivas,Sergiyenko,Aguirre,2009).

El prototipo quedó construido como se muestra en la figura 3.1.

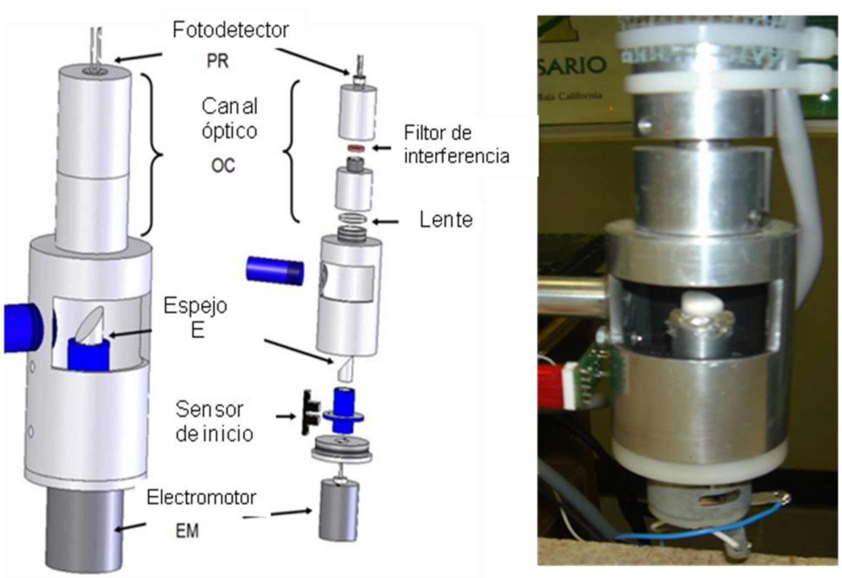

Figura 3.1. Prototipo del Sistema de barrido óptico pasivo

Los dispositivos ópticos y electrónicos utilizados en la construcción del prototipo se muestran en las figuras 3.2 y 3.3 respectivamente.

Edmund optics | america

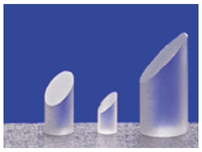

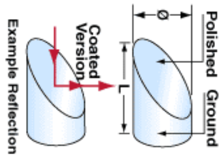

Description	Dia. (mm)	Height (mm)
• LENS 45 ROD 5MM DIA AL CTD	5.0	10.0
• LENS 45 ROD 10MM DIA AL CTD	10.0	15.0
• LENS 45 ROD 15MM DIA AL CTD	12.0	20.0

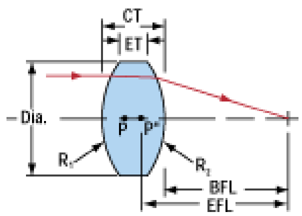

Description	Dia. (mm)	E.F.L. (mm)	Back F.L. (mm)	C.T. (mm)	E.T. (mm)	Radius R1 (mm)	Radius R2 (mm)	Glass Type
• LENS DCX 20 x 30 MgF2 TS	20.0	30.0	28.20	5.30	1.88	30.08	-30.08	BK7
• LENS DCX 20 x 30 UNCTD TS	20.0	30.0	28.20	5.30	1.88	30.08	-30.08	BK7
• LENS DCX 20 x 30 VIS-NIR CTD	20.0	30.0	28.20	5.30	1.88	30.08	-30.08	BK7

Figura 3.2. Especificaciones de los dispositivos ópticos utilizados en la construcción prototipo

Como se puede apreciar los principales dispositivos ópticos utilizados fueron un espejo cilíndrico con 10mm de diámetro y un corte a 45°, el cual refleja la luz del emisor hacia un lente biconvex, que es el otro dispositivo óptico utilizado, con un díametro de 20mm y una distancia focal de 30mm. La ventaja de este lente es que toda la luz captada es concentrada en el centro de un fotodetector ubicado a una distancia igual a la distancia focal.

Ambos dispositivos tienen tolerancias muy pequeñas (del orden de .03 mm) lo que permite minimizar el error en el proceso de barrido.

Por otra parte, los principales dispositivos electrónicos y electromecánicos utilizados se presentan en la figura 3.3.

El fotodetector utilizado fue un fotodiodo de silicio con una superficie de captación rectangular de 15mm^2 y una alta velocidad de respuesta (mayor de 10MHz) suficientes para su aplicación en el SBOP propuesto.

Description	Type	Area (mm2)	Responsivity (A/W)	Detectivity (cm*Hz1/2/W)	Capacitance (pF) at 0V	Rise Time	Noise Equivalent Power (W/H1/2)	Operating Temp. (°C)	Lead Length (inches)	Max. Dia. (inches)	Mount
• SILICON DETECTOR 100MM2	Biased: Normal Response	100.0mm²	0.65	2.56 x 10^{13}	1550pF	43 nsec	3.9 x 10^{-14}	-10°C to 60°C	BNC	0.975"	BNC
• SILICON DETECTOR 100MM2 BLUE	Unbiased: Blue Enhanced Response	100.0mm²	0.20	5.00 x 10^{12}	8800pF	2.0 µsec	2.0 x 10^{-13}	-10°C to 60°C	BNC	0.98"	BNC
• SILICON DETECTOR 100MM2 UV	Unbiased: UV Enhanced Response	100.0mm²	0.14	2.22 x 10^{12}	4500pF	5.9 µsec	4.5 x 10^{-13}	-10°C to 60°C	BNC	0.98"	BNC
• SILICON DETECTOR 15.0MM2 HIGH SPEED	Biased: High Speed Response	15.0mm²	0.55	1.94 x 10^{12}	82pF	2 ns	2.0 x 10^{-13}	-40°C to 110°C	0.5"	0.33"	TO-5

MODEL	VOLTAGE		NO LOAD		AT MAXIMUM EFFICIENCY					STALL	
	OPERATING RANGE	NOMNAL	SPEED	CURRENT	SPEED	CURRENT	TORQUE	OUTPUT	EFF	CURRENT	TORQUE
			rpm	A	rpm	A	g-cm	W	%	A	g-cm
MD5-2554AS-AA	6.0 – 12.0	12.0V CONSTANT	20800	0.55	17000	1.70	72.92	12.72	62.38	7.70	400
MD5-2450AS-AA	6.0 – 12.0	12.0V CONSTANT	22000	0.60	17200	2.00	77.50	13.73	55.91	7.40	360
MD5-1980AS-AA	12.0 – 24.0	24.0V CONSTANT	27000	0.40	22600	1.43	88.50	20.55	60.92	5.87	470
MD5-15120AS-AA	12.0 – 24.0	24.0V CONSTANT	18800	0.24	15100	0.70	66.68	10.34	61.54	2.86	340

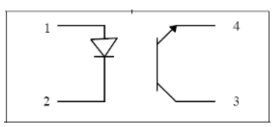

Transistor Slotted Interrupter
Single Channel (4-Pin Slot)

- With mounting tabs
- VF=1.7V max @ 60mA
- BVceo (Ic=1mA): 30V min.
- BVeco (IE=100uA): 6V min.
- Iceo max. (Vce=25V Ih=0): 100nA

Figura 3.3. Dispositivos electrónicos y electromecánicos del SBOP

Para acondicionar la señal del fotodetector se utilizó un circuito como el que se muestra en la figura 3.4, en donde se puede apreciar que la señal del fotodetector es amplificada

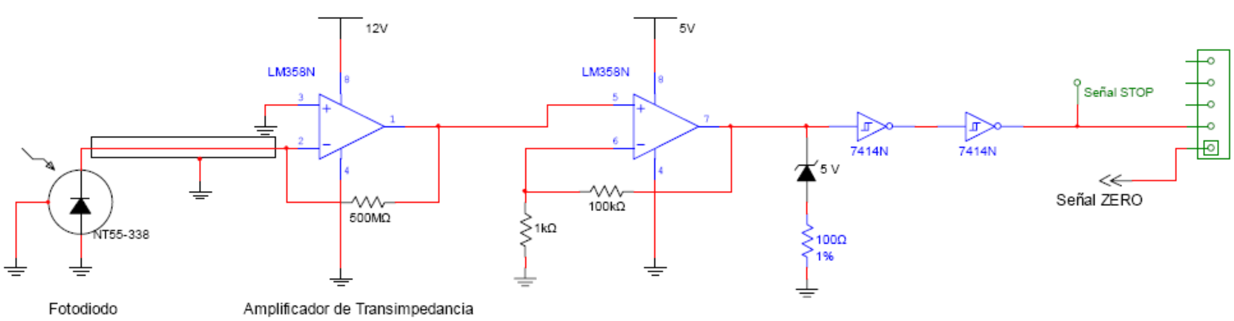

figura 3.4 Circuito de acondicionamiento de señal

Otro dispositivo utilizado fue el motor que permite la rotación del espejo para llevar a cabo el barrido respectivo.

El motor utilizado fue un motor de corriente directa con un rango de voltaje de operación de 6.0 a 12.0 volts y una velocidad de 17000 rpm a máxima eficiencia, lo cual es más que suficiente para nuestra aplicación debido a que el barrido se lleva a cabo a baja velocidad (600 rpm).

El otro dispositivo utilizado fue un optointerruptor diodo emisor de luz-optotransistor, para generar el pulso de inicio.

Una vez construido el prototipo con los dispositivos descritos se procedió a llevar a cabo la experimentación como se presenta en la siguiente sección.

3.2. Experimentación.

La experimentación se llevó a cabo posicionando geométricamente en diferentes coordenadas una lámpara incandecente de 24w sobre una mesa de planitud y haciendo girar el espejo del prototipo a diferentes velocidades.

En la figura 3.2 se muestran los resultados de la medición, posicionando la fuente emisora de luz a un ángulo mayor de 90° y una frecuencia de rotación de 8.49 rev/min.

Figura 3.5 Medición de coordenadas para un ángulo mayor de 90°

Las coordenadas obtenidas bajo estas condiciones fueron (x,y)= (0,0.499999) y el ángulo medido fue de 99.2137°.

El resultado de una segunda medición para un ángulo mayor de 70° y una frecuencia de rotación de 14.8 rev/min se muestra en la figura3.3

En esta medición se obtuvieron las coordenadas (x,y) = (0,0.500002) y un ángulo de 73.6603°.

Figura 3.6 Medición de coordenadas para un ángulo mayor de 70°

Una tercera medición se presenta en la figura 3.4, en donde el posicionamiento de la fuente emisora de luz ubicada a 45° y utilizando una frecuencia de rotación de 6.4

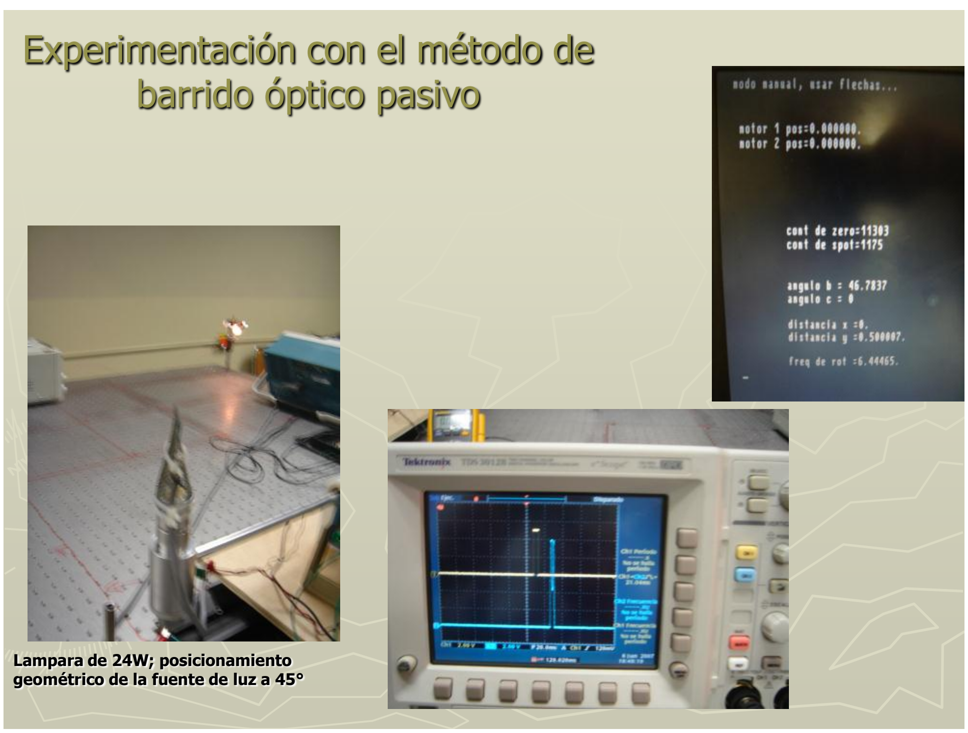

Figura 3.7 Medición de coordenadas para un ángulo de 45°

Las coordenadas encontradas en esta medición fueron (x,y) = (0,0.500007) y el ángulo medido ángulo de 46.7037°.

En una sección posterior se presentará un análisis de los resultados y la incertidumbre del sistema.

3.2.1. Búsqueda del centro de señal.

Las mediciones presentadas en la sección anterior se realizaron utlizando como señal de control el flanco de subida generado por el sensor de inicio y el fotodetector.

Paralelamente se realizaron simulaciones para probar los métodos de búsqueda del centro de señal.

Por principio, se simuló la señal gaussiana con un generador de funciones y un diodo rectificador como se presenta en la figura 3.5

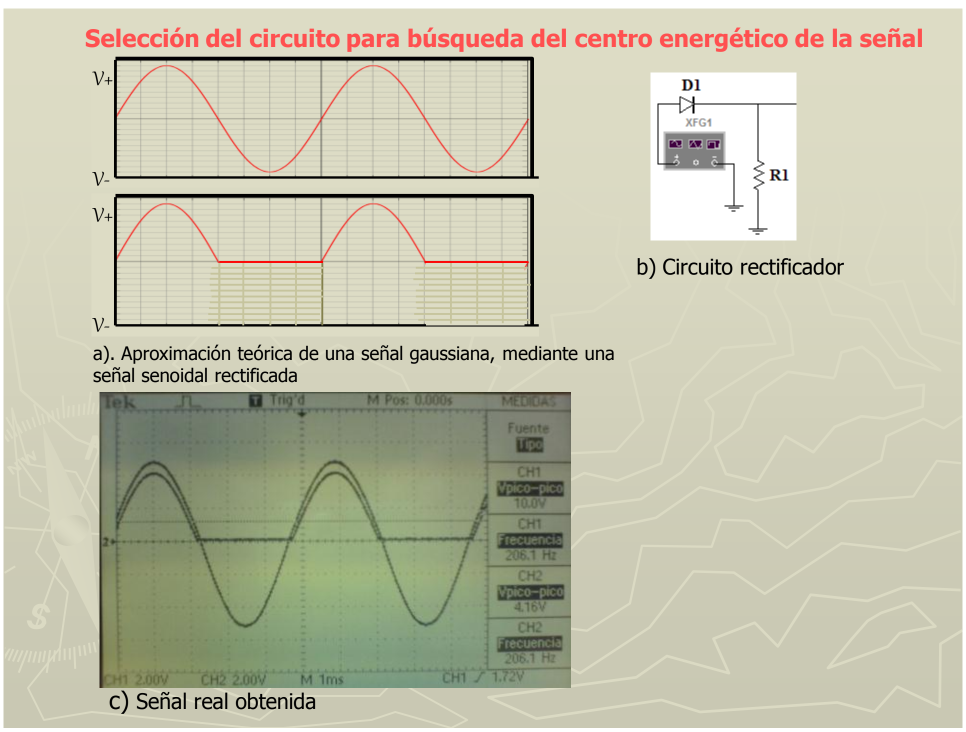

Figura 3.8 Rectificación de una señal senoidal como aproximación a una señal gaussiana

La respuesta esperada al rectificar la una señal senoidal se presenta en la figura 3.5 a), una vez construido el circuito mostrado en la figura 3.5b), se obtuvo como resultado la señal que aparece en la figura 3.5 c). Como se puede apreciar la respuesta obtenida es una señal que se asemeja a una curva gaussiana.

Esta señal se consideró como aproximación a la respuesta ideal del fotodetector, por lo que fue introducida a un circuito diferenciador como se aprecia en la figura 3.6 b).

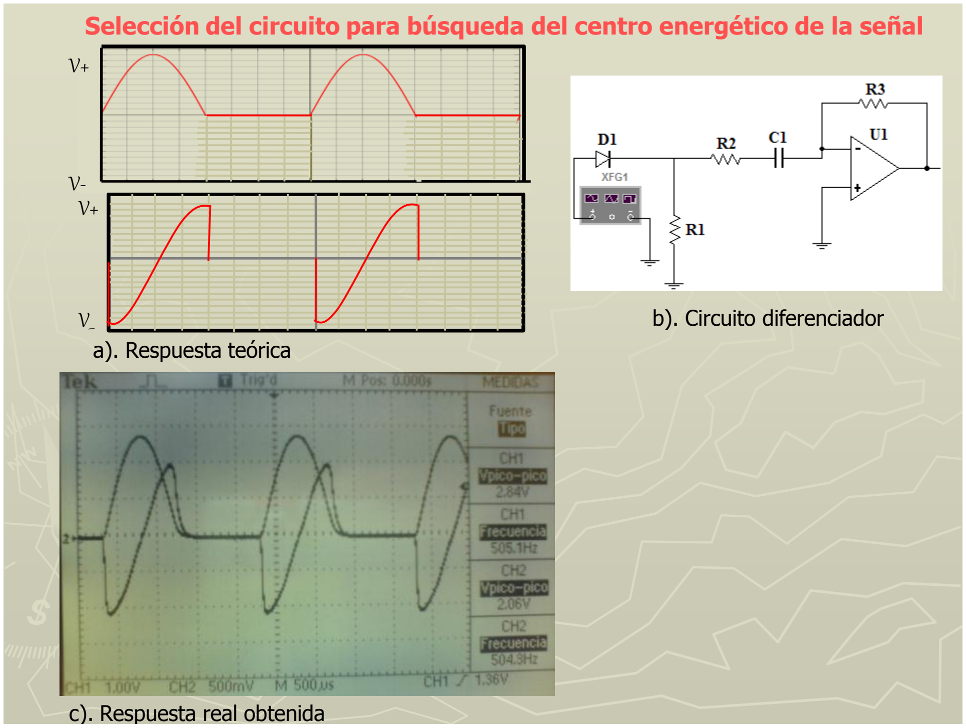

Figura 3.9 Derivada de la señal gaussiana simulada

Para obtener su derivada conforme a los fundamentos teóricos presentados en la sección 2.2, para posteriormente encontrar el máximo de la función que teóricamente representa el centro de energía de la fuente emisora.

Para encontrar el punto máximo se consideró la ecuación (4) de la sección 2.2, de la que se deduce que el punto máximo se encuentra cuando la derivada de la función es igual a cero. Esto considerando que la derivada de una función representa el valor de la pendiente de la recta tangente en un punto de la misma, como se aprecia en la figura 3.7

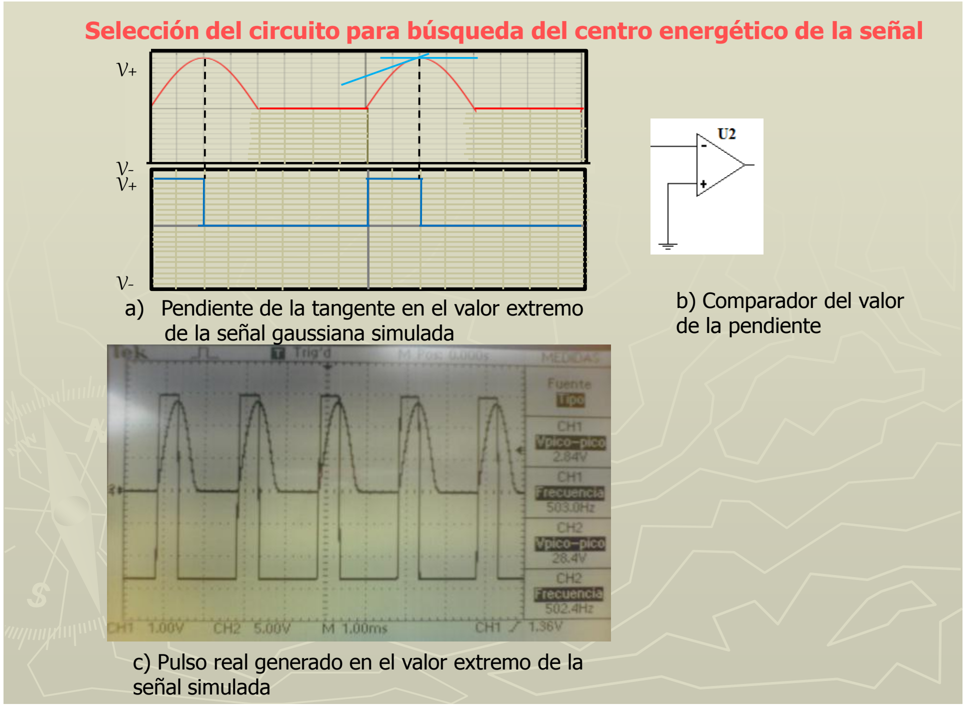

Figura 3.10 Pulso de disparo en el valor extremo de la señal

En condiciones ideales este circuito podría detectar el centro de la señal sin problema. Sin embargo, en condiciones reales el fotodetector generó respuestas como la que se muestra en la figura 3.8

Figura 3.11 Señal real generada por el fotodetector

Cuando se presenta una señal como la que se muestra en la figura 3.8 utilizar un circuito diferenciador para encontrar el centro de la señal se vuelve ineficiente.

En este sentido se propuso evaluar un nuevo método utilizando un circuito integrador, para lo cual se debe aproximar la señal gaussiana a un pulso rectangular como se expuso en la sección 2.2.

Esta aproximación se puede lograr introduciendo la señal gaussiana a un circuito comparador de lazo abierto como se muestra en la figura 3.9

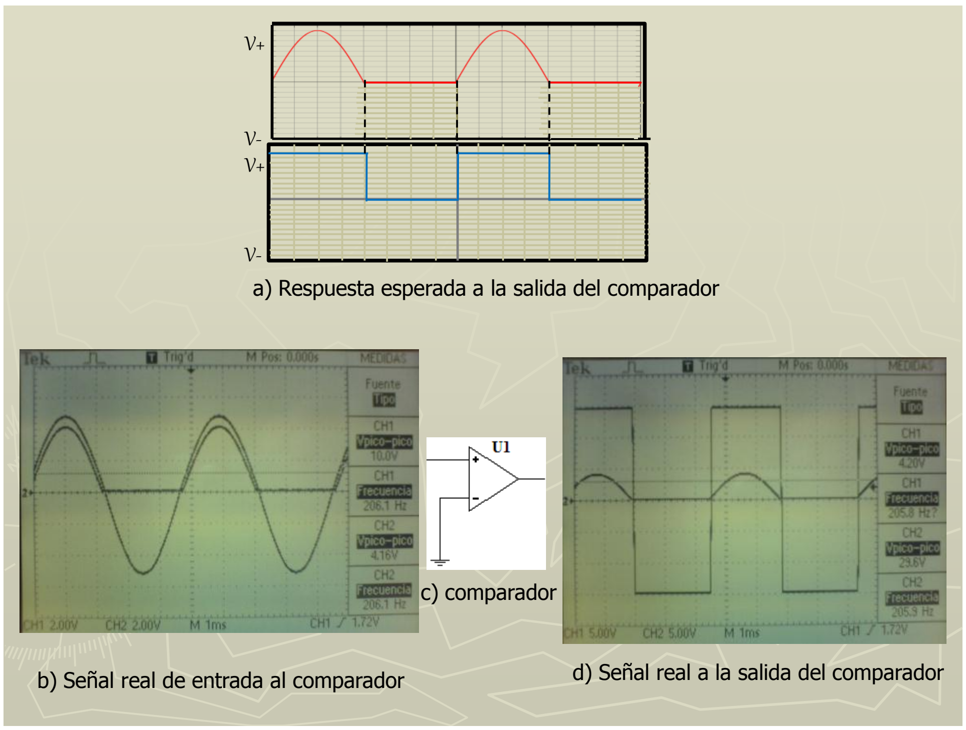

Figura 3.12 Transformación de la señal gaussiana a una señal rectangular

De acuerdo con los fundamentos teóricos presentados en la sección 2.2 al integrar una señal rectangular se obtiene como resultado una señal triangular, lo cual se logra con un circuito integrador como el que se muestra en la figura 3.10 .

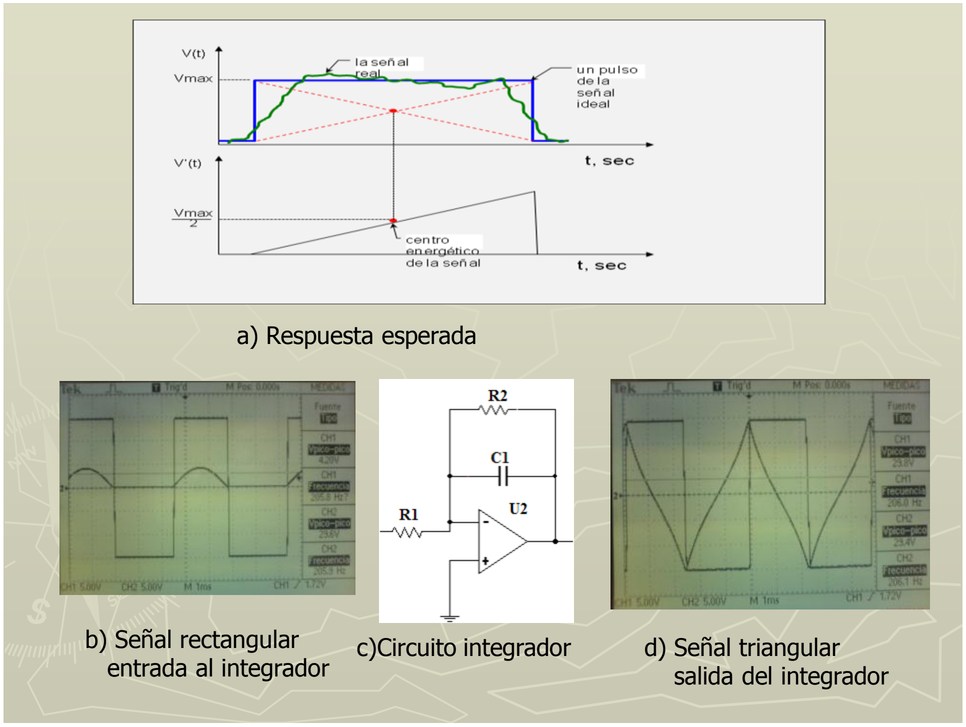

Figura 3.13 Integración de la señal rectangular

finalmente para encontrar el centro de la señal se utilizó un circuito comparador como el que se muestra en la figura 3.11.

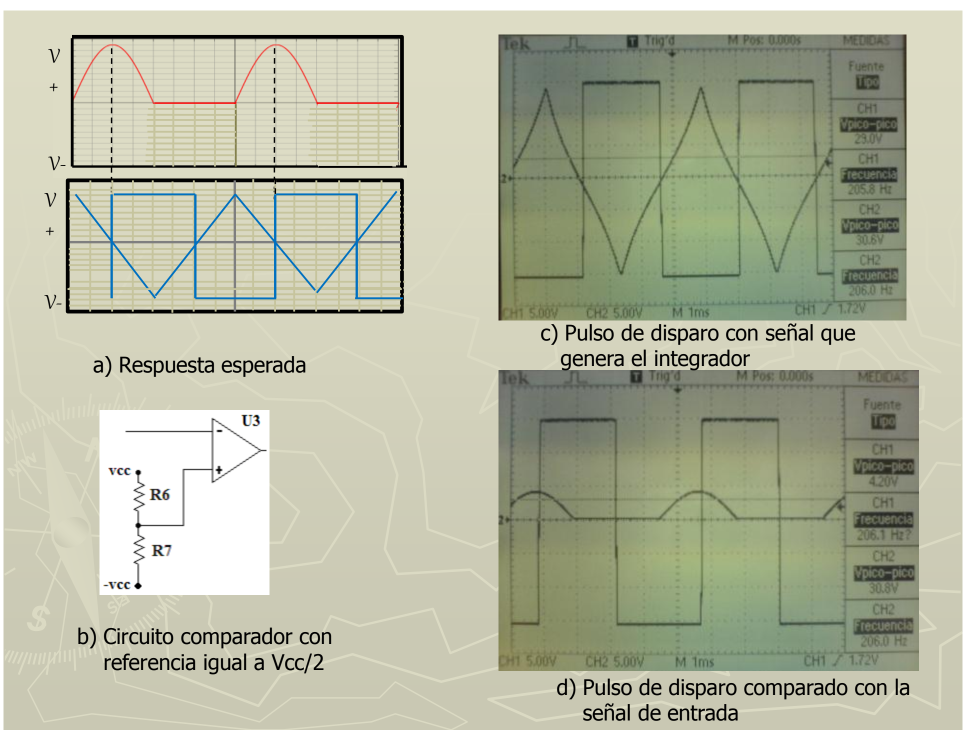

Figura 3.14 Pulso generado en el centro geométrico de la señal

CAPITULO IV

4. ANÁLISIS DE RESULTADOS E INCERTIDUMBRE

4.1. Análisis de resultados y fuentes de error.

Además de las mediciones tomando como fuente emisora una lámpara incandecente, también se realizaron mediciones utilizando un láser obteniéndose los resultados que se muestran en la figura 4.1.

MEDICION DE COORDENADAS

PUNTO DE PRUEBA	VALORES TEÓRICOS				VALORES MEDIDOS			
	X (m)	Y (m)	B (°)	C (°)	x(m)	y(m)	B (°)	C (°)
A	0.75	0.75	108.43	30.96	0.79	0.77	109.29	31.81
B	1	0.75	104.04	38.66	1.06	0.77	104.38	39.9
C	1	0.5	90.00	45.00	1.12	0.56	93.55	46.4
D	0.75	0.5	90.00	36.87	0.76	0.48	89.16	37.61
E	0.5	0.5	90.00	26.57	0.503	0.506	90.07	26.71
F	0.5	0.25	63.43	33.69	0.49	0.22	60.51	34.27
G	0.75	0.25	71.57	45.00	0.77	0.23	71.22	46.5
H	1	0.25	75.96	53.13	1.06	0.249	76.75	54.84
I	1	0	63.43	63.43	1.1	0.01	66.28	65.21
J	0.75	0	56.31	56.31	0.74	-0.01	55.34	56.77
K	0.5	0	45.00	45.00	0.49	-0.01	43.73	45
L	0.5	-0.25	33.69	63.43	0.52	-0.25	34.73	65.21
M	0.75	-0.25	45.00	71.57	0.81	-0.24	47.68	72.77
N	1	-0.25	53.13	75.96	1.11	-0.24	56.47	76.81
O	1	-0.5	45.00	90.00	1.26	-0.5	51.49	90.17
P	0.75	-0.5	36.87	90.00	0.8	-0.51	38.62	90.87

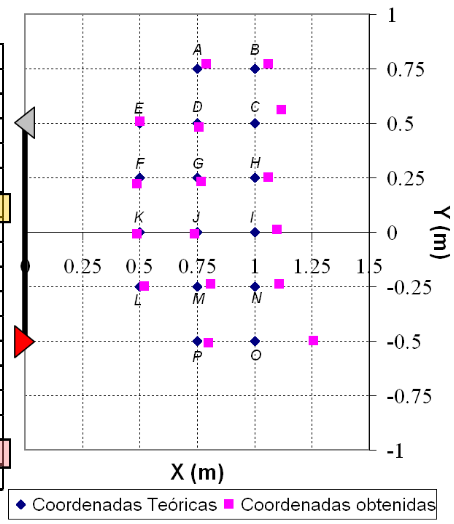

Error Máximo…..(1.26 - 1.00) / 1.00 * 100 = 26%

Error Mínimo……(90.07-90.00)*90.00*100= 0.07%

Figura 4.1 Medición de coordenadas con fuente emisor láser.

Como se puede observar el máximo error obtenido en la medición fue del 26% y el error mínimo fue del 0.07%, este error se obtuvo como resultado de una sola medición en cada uno de los puntos ubicados en una superficie de $2\,\mathrm{m} \times 1.5m$

Este error se puede disminuir realizando un mayor número de mediciones consecutivas y obteniendo el promedio de las mismas (Blaza,2006) como se muestra en la figura 4.2.

Con esta promediación la exactitud del mensurando crece $\sqrt{n}$ veces (Downie,1967), (Grave 2006), donde n representa la cantidad de mediciones consecutivas.

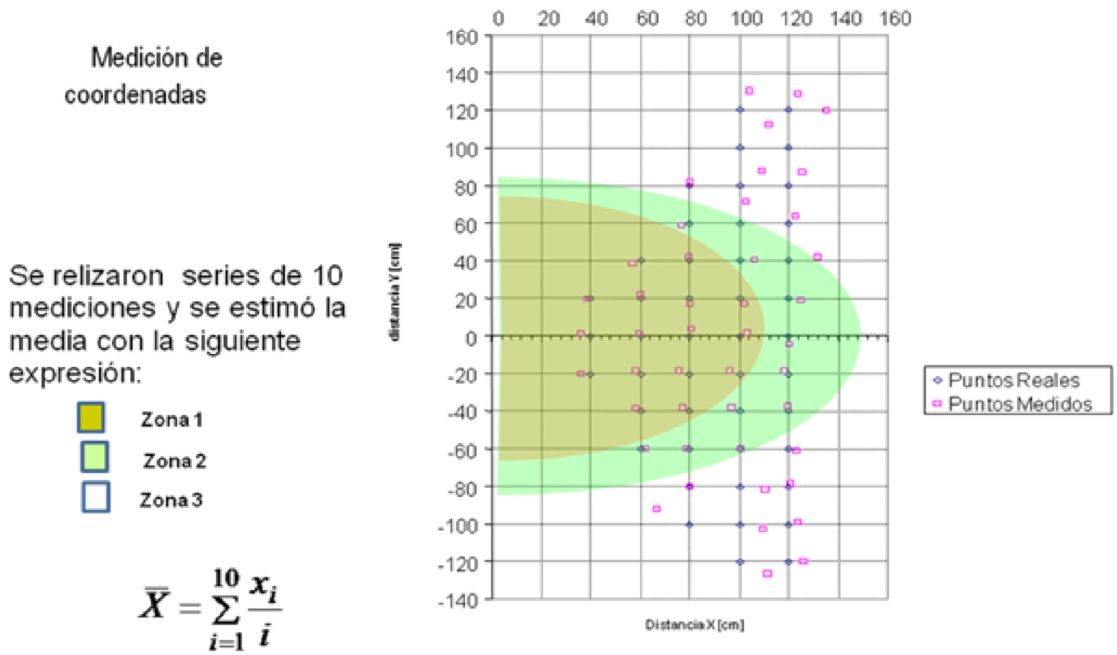

Figura 4.2. Variación de exactitud de coordenadas dentro del ángulo θ del Sistema.

En la figura 4.2 se identifican las zonas de mayor exactitud. Como se puede apreciar en distancia menor de 2 m la zona de menor error es la zona comprendida entre -80 y 80 cm (zona1) 1m .

Otra posible fuente de error que se consideró, es debido al ángulo del cono que se forma por el tiempo que tarda la luz en llegar desde el punto de origen hasta el sistema de barrido, este ángulo se estimó mediante una simulación para una distancia de 20m a 800m, como se muestra en la figura 4.3., en esta simulación también se consideraron diferentes frecuencias de rotación.

Para estimar el tiempo de recorrido de la luz, se consideró que ésta viaja a una velocidad de 299796±2Km/s (Bergstrand, 1949).

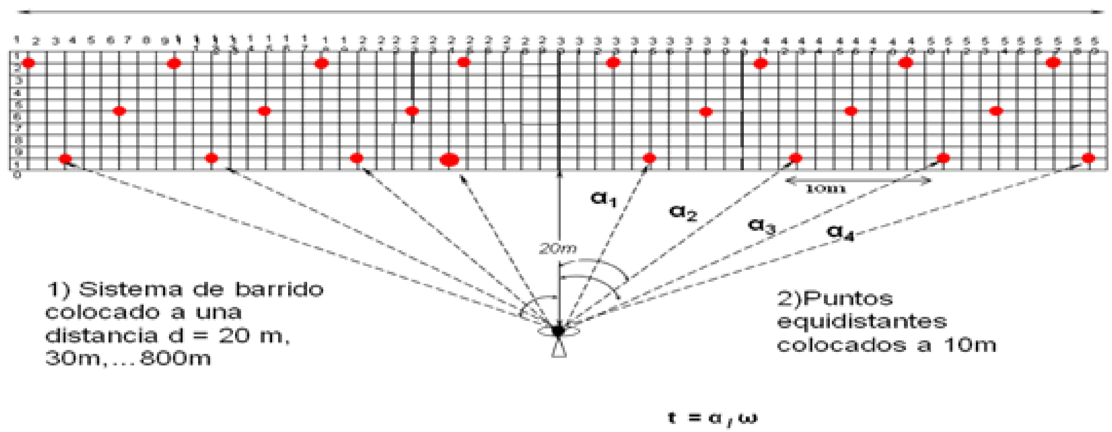

Figura 4.3. Simulación de la medición del ángulo del cono formado por la trayectoria de la luz.

Con esta consideración el tiempo de recorrido de la luz se obtiene de la siguiente manera:

$$t_d = l_c / c \qquad (4.1)$$

Donde C representa la velocidad de la luz, t_d es es el tiempo de recorrido de la luz y l_c es la distancia del punto de medición al sistema de barrido .

De esta manera , si se considera que el tiempo de recorrido es el mismo tiempo en que se da el desplazamiento angular α , entonces t_α se puede obtener con la ecuación 4.2.

$$t_d = t_\alpha \qquad (4.2)$$

Por otra parte se tiene que t_α también es igual al desplazamiento angular entre la velocidad angular como se expresa en la ecuación 4.3

$$t_\alpha = \alpha / \omega \qquad (4.3)$$

Despejando α se obtiene la siguiente expresión:

$$\alpha = \omega \cdot t_\alpha \qquad (4.4)$$

Aplicando estas ecuaciones, se obtuvieron los resultados que se muestran en las figuras 4.4 y 4.5.

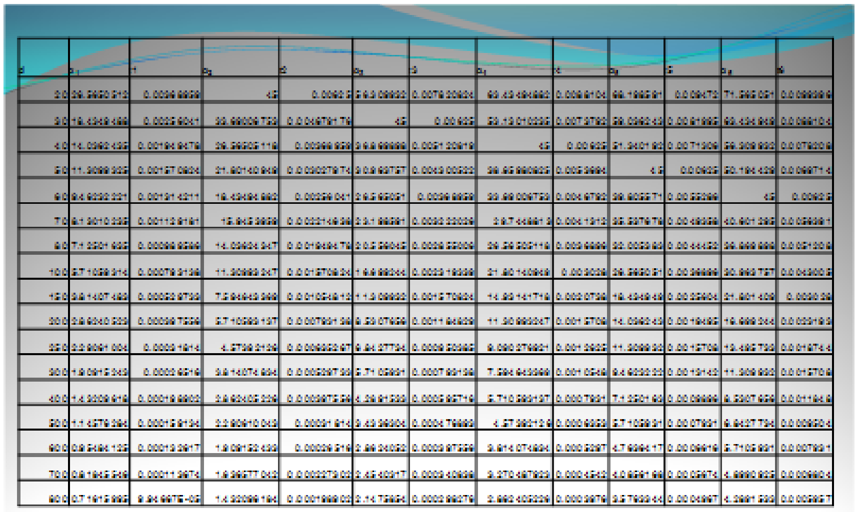

Figura 4.4. Cálculo de ángulos de 6 puntos equidistantes a 10 m entre sí a diferentes distancias del SB y su tiempo de medición con un barrido de 20 rps

d	t_d	α
20	6.66667E-08	4.18879E-07
30	0.0000001	6.28319E-07
40	1.33333E-07	8.37758E-07
50	1.66667E-07	1.0472E-06
60	0.0000002	1.25664E-06
70	2.33333E-07	1.46608E-06
80	2.66667E-07	1.67552E-06
90	0.0000003	1.88496E-06
100	3.33333E-07	2.0944E-06
150	0.0000005	3.14159E-06
200	6.66667E-07	4.18879E-06
250	8.33333E-07	5.23599E-06
300	0.000001	6.28319E-06
400	1.33333E-06	8.37758E-06
500	1.66667E-06	1.0472E-05
600	0.000002	1.25664E-05
700	2.33333E-06	1.46608E-05
800	2.66667E-06	1.67552E-05

Figura 4.5. Desplazamiento angular en el tiempo de recorrido de la luz a diferentes distancias

en ellas se puede apreciar que el tiempo de recorrido de la luz, en el trayecto de la fuente emisora al receptor es muy pequeño (del orden de 10^{-5} a 10^{-5}) y el ángulo que se forma es del orden de 10^{-7} de por lo que se puede considerar prácticamente despreciable, para los fines que se buscan.

En Síntesis, la distancia en la que se debe colocar el sistema si para minimizar el error debido a este ángulo es entre 20 y 40 metros.

CAPITULO IV

5. CONCLUSIONES Y RECOMENDACIONES

5.1. Conclusiones.

Una vez concluido el análisis de resultados se pudo comprobar que es posible medir las deformaciones en objetos de grandes dimensiones utilizando un sistema de barrido óptico pasivo propuesto, permitiendo obtener más de 10 mediciones en un minuto y una incertidumbre menor a menor a 10^{-3}.

- El sistema de monitoreo desarrollado posee las mejores propiedades de los métodos que existen actualmente: puede detectar deformaciones peligrosas de estructuras en tiempo real; pueden detectar daños internos de la estructura con resolución que depende del paso ij de las FE (fuentes emisoras); El error relativo de la medición remota en Zona 1(figura 4.2) del ángulo sólido θ del sistema no excede el 1% ; como se ve de la lista de elementos utilizados para el sistema el costo total es muy bajo, lo que significa que para monitoreo de alta resolución pueden ser usados n sistemas colocados alrededor de la estructura en un espacio 3D.
- El sistema propuesto tiene buena inmunidad contra interferencia de las señales y ondas electromagnéticas ; permite aplicar los métodos muy básicos contra ruido óptico; no requiere penetrar dentro de estructura bajo control; permite aplicar métodos muy sencillos de instalación sobre estructura.
- El método de barrido permite realizar monitoreo de deformaciones de manera remota en modo automático en las distancias entre 1m -100m con la resolución 10^{-3}m

- El principio eléctrico y formalismo matemático permiten realizar medición de ángulos con alta resolución. Por su carácter la variación de la velocidad de barrido y el valor de la frecuencia estándar, se puede de manera sencilla variar la resolución del sistema debido a la tarea concreta (disminuyendo la velocidad de barrido por ejemplo usando motor tipo reloj, también usando patrón de frecuencia de 10 MHz, se puede incrementar la resolución angular en 10-3600 veces)
- Aplicación de métodos novedosos de búsqueda del centro energético de la señal del emisor y método de coincidencias perfectas de pulsos, esto nos permite disminuir errores causados por formas geométricas imperfectas de las fuentes y rayos de luz reales, y considerarlos como objetos puros teóricos (puntos y líneas rectas)
- En la experimentación con el primer prototipo del sistema se comprobó exitosamente la funcionalidad del método propuesto lo que permitió analizar sus incertidumbres las cuales fueron presentadas antes.
- La experimentación permitió prácticamente verificar y ordenar por importancia las fuentes eléctricas y mecánicas de incertidumbre (incertidumbre por: movimiento vertical hacia adelante del eje del motor, movimiento vertical lateral y movimiento y giro sobre el propio eje, la incertidumbre por fuentes eléctricas son mínimas y facilmente compensables mediante programación), cuales serían tomadas en cuenta en la construcción del segundo prototipo que ya está en proceso de terminar su construcción,

5.2. Recomendaciones y trabajo futuro

En este trabajo se presentó un método original de barrido óptico y un prototipo preliminar que puede ser utilizado en el monitoreo de desplazamiento y defromaciones en objetos de grandes dimensiones y en sistemas de navegación de robots móviles. Este primer prototipo fue construido utilizando dispositivos electrónicos de calidad comercial, disponibles en el mercado. La parte electromecánica fue construida con herramientas manuales, dando origen a diferentes fuentes de error.

El método de barrido y el prototipo respectivo, fueron probados en condiciones de laboratorio y en algunos casos se realizaron simulaciones, principalmente en el caso del método de búsqueda del centro energético de señal de luz, de la fuente emisora.

Actualmente, se encuentra en construcción un segundo prototipo, el cual se está fabricando con equipo automático industrial de alta precisión.

En este contexto, se recomienda para trabajos futuros, investigar la posibilidad de reducir las pérdidas en el canal óptico, trabajando en modo pulsado, determinar experimentalmente el periodo de barrido para diferentes aplicaciones prácticas, diseñar y construir un circuito más eficiente para encontrar el centro energético de la señal de luz y probarlo experimentalmente.

Se recomienda como una primera aplicación práctica, probar el sistema de barrido óptico midiendo el desplazamiento en una torre de enfriamiento ubicada en la Planta Geotérmica de Cerro Prieto y estudiar el comportamiento del sistema de barrido en condiciones reales.

CAPITULO VI

6. PRODUCTOS DE LA INVESTIGACIÓN

Como resultado de la investigación se produjeron diferentes pulicaciones en revistas arbitradas, memorias de congresos y un capítulo de libro.
A continuación se presenta una relación de dichas publicaciones, cuyos documentos en extenso se pueden encotrar en el ANEXO I.

RELACION DE PUBLICACIONES

M. Rivas Lopez, Oleg Sergiyenko, Vera Tyrsa, "Computer vision" book. Edited by Xiong Zhihui / Chapter 22 "Machine vision: approaches and limitations" pp. 395-428. Editorial: IN-TECH, Vienna, Austria, 2008. - 538 p. ISBN 978-953-7619-21-3

Moisés Rivas López, Oleg Sergiyenko, Vera Tyrsa, Wilmar Hernandez Perdomo, Daniel Hernández Balbuena, Luis Devia Cruz, Larisa Burtseva, Juan Iván Nieto Hipólito. Optoelectronic method for structural health monitoring. SAGE Publications, "International Journal of Structural Health Monitoring", Vol. 9. No.2, pp.105-120,March , 2010, ISSN 1475-9217 / doi: 10.1177/1475921709340975

Moisés Rivas, Oleg Sergiyenko, Mario Aguirre, Luis Devia, Vera Tyrsa, and Ismael Rendón Spatial data acquisition by laser scanning for robot or SHM task. IEEE-IES Proceedings "International Symposium on Industrial Electronics"(ISIE-2008), Cambridge, United Kingdom, 30 de junio -2 de julio de 2008, 2008, p.1458-1463, ISBN 978-1-4244-1666-0, ISSN/Library of Congress Number 2007936380.

O. Sergiyenko, V. Tyrsa, D. Hernandez-Balbuena, **M. Rivas López**, I. Rendón López, L. Devia Cruz. Precise Optical Scanning for practical multiapplications. Proceedings of IEEE-34th Annual Conference of IEEE Industrial Electronics (IECON'08), Florida, USA, 10-13 November, 2008. pp.1656-1661, ISBN 978-1-4244-1766-7.

Tyrsa Valentin,Burtseva Larisa, Rivas López Moisés, Tyrsa Vera, Monitoring of Civil Engineering Structures, Healt Monitoring and Smart Nondestructive Evaluation of Structural and Biological Systems III, Editor: TribikranKundu,March, 2004 , San Diego CA., USA, pp485-492.

Daniel Hernández Balbuena, Oleg Sergiyenko, Vera Tyrsa, Larysa Burtseva, **Moisés Rivas López.** Signal frequency measurement by rational approximations. Elsevier, "Measurement", Volume 42, Issue 1, January 2009, Pages 136-144. ISSN: 0263-2241 - doi:10.1016/j.measurement.2008.04.009

Oleg Y. Sergiyenko, Vera V. Tyrsa, Luis F. Devia, Wilmar Hernandez, Oleg Starostenko, **Moisés Rivas Lopez.** Dynamic Laser Scanning method for Mobile Robot Navigation. Proceedings of ICCAS-SICE 2009, ICROS-SICE International Joint Conference, Fukuoka, JAPAN, August 18-21, 2009, pp. 4884-4889, PR0002/09/0000-4884 2009SICE

Daniel Hernández B., **Moisés Rivas L**., Larisa Burtseva, Oleg Sergiyenko, Vera Tyrsa. Method for Phase Shift Measurement using Farey Fractions. IEEE-LEOS Proceedings "Multiconference on Electronics and Photonics"(MEP-2006), Guanajuato, Mexico, Guanajuato, 7-10 de noviembre 2006, 2006, p. 181 -185, ISBN 1-4244-0627-7, ISSN/Library of Congress Number 2006932321

REFERNCIAS BIBLIOGRÁFICAS.

1. Allen D.W., Park G., Farrar C.R. Overview of Wireless Active Sensing Systems for Structural Healt Monitoring, publicado en Structural Health Monitoring, Advancements and Challenges for Implementation, Fu Kuo Chang(ed.), DEStech publications inc., Lancaster, Pennsylvania, U.S.A., 2005, pp. 1578-1585.

2. Aubert Damien, Miller Philippe, Paindavoine, Geometric deformation measurement and correction applied to dynamic streak camera images, Measurement Science and Techology, 13(2002), pp1910-1923, impreso en UK.
3. Bannister A., Raymond S., Baker R., Técnicas modernas en topografía,7ma edición, Alfaomega, México, D.F., 2002.

4. Barchett, Raymond A., College Algebra with Trigonometry. ISBN: 0-07-003864-3. Mc graw hill . USA 1984

5. Bergstrand. Erik, Velocity of light. “Nature”, February 26, 1949, p.338, or Vol.165, No.4193, p.405-406 in “Nature Catalogue"

6. Blaza toman, Linear statistical models in presence of systematic effects requiring a type B evaluation of uncertainty, Metrología, international Journal of pure and applied metrology, vol. 43, Num. 1, august, 2006, Institute of Physics publishing, pp. 27-32, Philadelphia, PA, USA.

7. Bosch T., Donati S. (Guest Editors): ‘Distance and Displacement Measurements by LaserTechniques’, Special Issue of Optical Engineering, vol.40, (2001), pp.1-99.

8. C.L. Wyatt (1991). Electro-Optical System Design: For Information Processing (NY: McGraw-Hill). – 343 p.

9. Cosser Emily , Gethin W Roberts, Xiaolin Meng, Alan H Dodson. Measuring the Dynamic Deformation of BridgesUsing A Total Station. Proceedings, 11th FIG Symposium on Deformation Measurements, Santorini, Greece, 2003.

10. Chaumette, F. & Hutchinson, S. (2006). Visual servo control PART I: basic approaches. IEEE Robotics & Automation Magazine, December 2006, pp.82-90.

11. Cristina Federico, Dapoto H. Sebastián, Vegas Javier, Artola Verónica, Russo Claudia, Abásolo María José, Desarrollo de un escáner 3D mediante cámaras estereoscópicas e iluminación laser, V Workshop de Computación Gráfica, Imágenes y Visualización, XIII Congreso Argentino de Ciencias de la Computación CACIC 200 7, Instituto de Investigación en Informática LIDIFacultad de Informática. Universidad Nacional de La Plata.La Plata, Buenos Aires, Argentina.

12. Chintalapudi Krishna, Fu tat, Paek Jeongeup, Kothary Nupur, Monitoring Civil Structures With a Wireless Sensor Network, IEE Internet Computer, IEE computer society, marzo de 2006, pp. 27-34

13. Dai Liwen, Wang Jinling, Rizos Chris and Shaowei Han. Applications of Pseudolites in Deformation Monitoring Systems. The 10th FIG International Symposium on Deformation Measurements. 19 – 22 March 2001 Orange, California, USA. pp 11-20.

14. Diosi, A. & Kleeman, L. (2005). Laser scan matching in polar coordinates with application to SLAM. Proceedings of IEEE/RSJ International Conference on Intelligent Robots and Systems (IROS 2005), pp. 3317- 3322, ISBN: 0-7803-8912-3, august 2005.

15. Downie N.M., Fundamentals of Measurement: Techniques and Practices, New York: Oxford University Press., 1967 – 482 p.

16. França, J.; Gazziro, M.; Ide, A. & Saito, J. (2005). A 3D scanning system based on laser triangulation an variable field of view, Proceedings of the 2005 International Conference on Image Processing (ICIP 2005), pp. 425-428, IEEE Volume 1, Italy, 2005, Genoa.

17. Fotiou Aristidis , Kagiadakis Vardis , Pikridas Christos and Rossikopoulos Dimitrios, Geodetically Derived Displacements and Crustal Deformation Analysis: Applicationin the Volvi Area. Proceedings, 11th FIG Symposium on Deformation Measurements, Santorini, Greece, 2003.

18. Forman, P. & Parry, I. (2001). Rapid Data Collection at Major Incident Scenes using Three Dimensional Laser Scanning Techniques. 2001 IEEE 35th International Carnahan Conference on Security Technology, pp. 60-67, october 2001

19. França, J.; Gazziro, M.; Ide, A. & Saito, J. (2005). A 3D scanning system based on laser triangulation an variable field of view, *Proceedings of the 2005 International Conference on Image Processing (ICIP 2005),* pp. 425-428, IEEE Volume 1, Italy, 2005, Genoa.

20. Garcia Dorian , Orteu Jean-José . 3D Deformation Measurement Using Stereocorrelation Applied to Experimental Mechanics. Session II: New Techniques in Monitoring Surveys II. The 10th FIG International Symposium on Deformation Measurements. 19 – 22 March 2001 Orange, California, USA. Pages 50-59.

21. Grabe Michael. Measurement Uncertainties in Science and Technologies, Springer Verlag GmbH; 1 edition, 2006 - 270 p.

22. Griffin Barry, Connelly Michael J., Digital Signal Processing of Interferometric Fiber Optic Sensors, IEEE LTIMC 2004 – Lightwave Technologies in Instrumentation & Measurement Conference, Palisades, New York, USA, 19 – 20 October 2004.

23. Gordon, S., Lichti, D., Franke, J. and Stewart, M., 2004. Measurement of structural deformation using terrestrial laser scanners. In: 1st FIG International Symposium on Engineering Surveys for ConstructionWorks and Structural Engineering, Nottingham, United Kingdom.

24. Handbook of Optical and Laser Scanning. (2004).Edited by Gerald F. Marshall, 769 p., ISBN: 0-8247-5569-3, Marcel Dekker, Inc., New York – Basel, 2004

25. Hans-Gerd Maas, Photogrammetric techniques for deformation measurements on reservoir walls, Delft University of Technology, Faculty of Civil Engineering and Geo Sciences, Thijsseweg 11, 2629JA Delft, The Netherlands.

26. Hmerson W. H., Differing angles on angle, Short communication, Metrología, international Journal of pure and applied metrology, vol. 42, Num. 4, august, 2005, Institute of Physics publishing, pp. 123-126, Philadelphia,PA, USA.

27. Hernández Balbuena Daniel, Sergiyenko Oleg, Tyrsa Vera, Burtseva Larysa, Rivas López Moisés. Signal frequency measurement by rational approximations. Elsevier, "Measurement", Volume 42, Issue 1, January 2009, Pages 136-144. ISSN: 0263-2241 - doi:10.1016/j.measurement.2008.04.009.

28. Hernández B. Daniel, Rivas L. Moisés, Burtseva Larisa, Sergiyenko Oleg, Tyrsa Vera. Method for Phase Shift Measurement using Farey Fractions. IEEE-LEOS Proceedings "Multiconference on Electronics and Photonics"(MEP-2006), Guanajuato, Mexico, Guanajuato, 7-10 de noviembre 2006, 2006, p. 181 -185, ISBN 1-4244-0627-7, ISSN/Library of Congress Number 2006932321.

29. Herring T.A., The Global Positioning System, Scientific American, 1996 pp. 32-38.

30. Herrera V., Contreras H., " Aplicación del Sistema de posicionamiento satelital G.P.S. en la medición de deformaciones de muros de embalses y estructuras mineras", Revista, Teledetección, No. 9, 1998. Madrid, España.

31. Jim ray, Ken Senior, Geodetic techniques for time and frecuency comparations using GPS phase and code measurements, Metrologia, Institute of Physics Publishing, Vol. 2, No. 4, august 2005, pp. 215-232.

32. Kee, C.; Park, B.; Kim, J.; Cleveland, A.; Parsons, M. & Wolfe, D. (2008). A Guideline to Establish DGPS Reference Station Requirements. The journal of navigation. Royal Institute of Navigation-Cambridge Journals (2008), 61, pp.99–114.

33. Kihara Mitsuru, Ohno Hiroshige, Distributed Optical Fiber Sensor Using Brillouin Scattering, in Conference on Lasers and Electro-Optics/Quantum Electronics and Laser Science Conference, Technical Digest (Optical Society of America, 2003), paper CFC3.

34. Lavelle, J. P. ; Schuet, S. R. & Schuet, D. J. (2004). High Speed 3D Scanner with Real-Time 3D Processing. Proceedings of ISA/IEEE Sensors for Industry Conference, pp.102- 108, ISBN: 0-7803-8143-2, 2004.

35. , D. D. ; Stewart, M. P.; Tsakiri, M. & Snow, A. J. (2000). Benchmark tests on a Three-Dimensional Laser Scanning system. Department of Spatial Sciences of Curtin University of Technology, Geomatics Research Australasia, 23 p., 2000

36. Lombardi, M. A. Legal and Technical Measurement Requirements for Time and Frequency. Measure: The journal of Measurement Science. Vol1. No. 3. 2006. pp.60-69.

37. Leithold Louis, The Calculus 7, Interests International Inc., ISBN 0673-46913-1, 1994

38. Lee C. W., . Zhang X. M, Tjin1 S. C. and A. Q. Liu, Nano-Scale Displacement Measurement Ofmems Devices Using Fiber Optic Interferometry, Journal of The Institution of Engineers, Singapore, Vol. 44 Issue 5, 2004, pp 1-8.

39. Leng J.S.,Du S.Y.,Winter D.,Barner R.A. Mys G.C. and Fernando G.F.,Structural Strain Monitoring Of Smart Civil Structure Using Fibre Optic Sensor, publicado en Structural Health Monitoring, Advancements and Challenges for Implementation, Fu Kuo Chang(ed.), DEStech publications inc., Lancaster, Pennsylvania, U.S.A., 2005, pp. 331-339.

40. Mehta Vipin, El Zarki Magda, A Bluetooth Sensor Network for Civil Infraestructure Healt Monitoring, Wireless Network, No 10., pp 401- 412, Kluwer Academic Publishers, Netherlands 2004.

41. Norgia M., Donati S., D. d'Alessandro : ‘Interferometric Measurements of Displacement on a Diffusing Target by a Speckle-Tracking Technique’, IEEE Journal of Quantum Electronics, vol. QE-37 (2001), pp.800-806.

42. Olivera C., Fleta J., Susagna T., Figueras X., Roca A., “Sismicidad y Deformaciones actuales en el Nordeste de la Península Ibérica”, Revista Física de

la Tierra, No. 15, 2003, ISSN 0214-4557, pp. 111- 144, Universidad Complutense, Madrid, España.

43. Peng-Hsiang Weng & Fu-Jen Kao. (2004). Modulation Based Time Resolved Laser Scanning Microscopy. The Second Asian and Pacific Rim Symposium on Biophotonics, APBP 2004, pp.97- 98, ISBN: 0-7803-8676-0, december 2004.

44. Petrov, M.; Talapov, A.; Robertson, T. Lebedev, A.; Zhilyaev, A. & Polonskiy, L. (1998). Optical 3D Digitizers: Bringing Life to the Virtual World. IEEE Computer Graphics and Applications, Vol., 18, (May/Jun 1998), page numbers (28-37). Issue: 3, ISSN: 0272-1716.

45. Pierce, D.S.; Ng, T.S. & Morrison, B.R. (1992). A Novel Laser Triangulation Technique for High Precision Distance Measurement, Proceeding of IEEE Industry Aplications Society Annual Meeting, vol.2, pp. 1762-1769, USA, october, 1992, Houston.

46. Player J. Slade J., KristoffS.B, Kokkins J., Lusignea R. and Livingston R, Fiber Optic Sensor for Situ In Measurement Of Relative Humity in Concrete, publicado en Structural Health Monitoring, Advancements and Challenges for Implementation, Fu Kuo Chang(ed.), DEStech publications inc., Lancaster, Pennsylvania, U.S.A., 2005, pp. 340-348.

47. Pozo Ruz A.,Ribeiro A., García Alegre M.C., García L., Guinea D., Sandoval F., Sistema de Posicionamiento Global(GPS): Descripción,Análisi de errores, Aplicaciones y future, Instituto de Automática industrial, Consejo superior de Investigaciones científicas, Madrid, España 2005.

48. R. Cordero Raul, Roth Pedro, Revisiting the problem of the evaluation of the uncertainty associated with a single measurement, Short Communication, Metrologia, international Journal of pure and applied metrology, vol. 42, Num. 2, april 2005, Institute of Physics publishing, pp. L15-L19.Philadelphia,PA, USA.

49. Rivas L. Moisés, Sergiyenko Oleg,And Tyrsa Vera, Machine Visión:Approaches and Limitations, Computer Vision Book, ISBN9789537619-21-3, Viena Austria, 2008, pp396-428.

50. Rivas López Moisés, Sergiyenko Oleg, Tyrsa Vera, Hernandez Perdomo Wilmar, Hernández Balbuena Daniel, Devia Cruz Luis, Burtseva Larisa, Nieto Hipólito Juan Iván. Optoelectronic Method for Structural Health Monitoring. SAGE Publications, "International Journal of Structural Health Monitoring", Issue Online, September,24, 2009, ISSN 1475-9217 / doi: 10.1177/1475921709340975

51. Rivas López Moisés, Sergiyenko Oleg, Aguirre Mario, Devia Luis, Tyrsa Vera, and Rendón Ismael, Spatial data acquisition by laser scanning for robot or SHM task. IEEE-IES Proceedings "International Symposium on Industrial

Electronics”(ISIE-2008), Cambridge, United Kingdom, 30 de junio -2 de julio de 2008, 2008, p.1458-1463, ISBN 978-1-4244-1666-0, ISSN/Library of Congress Number 2007936380.

52. Rutledge David, Gnipp Jack and Kramer John. Advances in Real-Time GPS Deformation Monitoring for Landslides, Volcanoes and Structures, Session III: Software for Deformation Data Collection Processing, and Analysis, The 10th FIG International Symposium on Deformation Measurements. March 2001 Orange, California, USA. pp110-121.

53. Sergiyenko O, Tyrsa V., Hernandez-Balbuena D., Rivas López M., I., Rendón López. Devia Cruz L. Precise Optical Scanning for practical multiapplications. Proceedings of IEEE-34th Annual Conference of IEEE Industrial Electronics (IECON’08), Florida, USA, 10-13 November, 2008. pp.1656-1661, ISBN 978-1-4244-1766-7.

54. Sergiyenko Oleg Y., Tyrsa Vera V, Devia Luis F., Hernandez Wilmar, Starostenko Oleg, Rivas Lopez Moisés**.** Dynamic Laser Scanning method for Mobile Robot Navigation. Proceedings of ICCAS-SICE 2009, ICROS-SICE International Joint Conference, Fukuoka, Japan, August 18-21, 2009, pp. 4884-4889, PR0002/09/0000-4884 2009SICE

55. Staffan Johansson. New frequency counting principle improves resolution. Proceedings of the 36 Annual Precise Time and time interval (PTTI) Systems and Application Meeting, 7-9 December2004, Washington, D.C., ISBN 0-7803-9053-5, 2005 – 628p.

56. Surmann, H.; Lingemann, K.; Nuchter, A. & Hertzberg, J. (2003). A 3D laser range finder for autonomous mobile robots. Robotics and Autonomous Systems, Issues 3-4, vol. 45, pp. 181-198, december 2003

57. Tyrsa Valentin,Burtseva Larisa, Rivas López Moisés, Tyrsa Vera, Monitoring of Civil Engineering Structures, Healt Monitoring and Smart Nondestructive Evaluation of Structural and Biological Systems III, Editor: TribikranKundu,March, 2004 , San Diego CA., USA, pp485-492.

58. Tyson John and Schmidt Timothy, Trilion Quality Systems, Dr. Konstantin Galanulis, GOM mbH , Optical Deformation & Strain Measurement in Biomechanics, Biophotonics, September 2003.

59. Werner Lienhart, Fritz K. Brunner. Monitoring of Bridge Deformations Using Embedded Fiber Optical Sensors. Proceedings, 11th FIG Symposium on Deformation Measurements, Santorini, Greece, 2003.

60. Worden K., Farrar C.R., Manson G. Park G., Fundamental Axioms of Structural Health Monitoring, Structural Health Monitoring 205 Advancements and Challenges for Implementation, Edited by Fu-Kuo Chang, Destech Publications, Inc., pp 26-41,Lancaster Pensylvania, 2005.

61. Zippelt Karl. Geodetic Monitoring of Slow Deformations in a Seismic Active Region. Proceedings, 11th FIG Symposium on Deformation Measurements, Santorini, Greece, 2003.

ANEXO 1

(Publicaciones en extenso)

M. Rivas Lopez, Oleg Sergiyenko, Vera Tyrsa, “Computer vision” book. Edited by Xiong Zhihui / Chapter 22 “Machine vision: approaches and limitations” pp. 395-428. Editorial: IN-TECH, Vienna, Austria, 2008. - 538 p. ISBN 978-953-7619-21-3

Moisés Rivas López, Oleg Sergiyenko, Vera Tyrsa, Wilmar Hernandez Perdomo, Daniel Hernández Balbuena, Luis Devia Cruz, Larisa Burtseva, Juan Iván Nieto Hipólito. Optoelectronic method for structural health monitoring. SAGE Publications, “International Journal of Structural Health Monitoring”, Vol. 9. No.2, pp.105-120,March , 2010, ISSN 1475-9217 / doi: 10.1177/1475921709340975

Moisés Rivas, Oleg Sergiyenko, Mario Aguirre, Luis Devia, Vera Tyrsa, and Ismael Rendón Spatial data acquisition by laser scanning for robot or SHM task. IEEE-IES Proceedings “International Symposium on Industrial Electronics”(ISIE-2008), Cambridge, United Kingdom, 30 de junio -2 de julio de 2008, 2008, p.1458-1463, ISBN 978-1-4244-1666-0, ISSN/Library of Congress Number 2007936380.

O. Sergiyenko, V. Tyrsa, D. Hernandez-Balbuena, **M. Rivas López**, I. Rendón López, L. Devia Cruz. Precise Optical Scanning for practical multiapplications. Proceedings of IEEE-34th Annual Conference of IEEE Industrial Electronics (IECON’08), Florida, USA, 10-13 November, 2008. pp.1656-1661, ISBN 978-1-4244-1766-7.

Tyrsa Valentin,Burtseva Larisa, Rivas López Moisés, Tyrsa Vera, Monitoring of Civil Engineering Structures, Healt Monitoring and Smart Nondestructive Evaluation of Structural and Biological Systems III, Editor: TribikranKundu,March, 2004 , San Diego CA., USA, pp485-492.

Daniel Hernández Balbuena, Oleg Sergiyenko, Vera Tyrsa, Larysa Burtseva, **Moisés Rivas López.** Signal frequency measurement by rational approximations. Elsevier, “Measurement”, Volume 42, Issue 1, January 2009, Pages 136-144. ISSN: 0263-2241 - doi:10.1016/j.measurement.2008.04.009

Oleg Y. Sergiyenko, Vera V. Tyrsa, Luis F. Devia, Wilmar Hernandez, Oleg Starostenko, **Moisés Rivas Lopez.** Dynamic Laser Scanning method for Mobile Robot Navigation. Proceedings of ICCAS-SICE 2009, ICROS-SICE International Joint Conference, Fukuoka, JAPAN, August 18-21, 2009, pp. 4884-4889, PR0002/09/0000-4884 2009SICE

Daniel Hernández B., **Moisés Rivas L**., Larisa Burtseva, Oleg Sergiyenko, Vera Tyrsa. Method for Phase Shift Measurement using Farey Fractions. IEEE-LEOS Proceedings “Multiconference on Electronics and Photonics”(MEP-2006), Guanajuato, Mexico, Guanajuato, 7-10 de noviembre 2006, 2006, p. 181 -185, ISBN 1-4244-0627-7, ISSN/Library of Congress Number 2006932321

22

Machine Vision: Approaches and Limitations

Moisés Rivas López, Oleg Sergiyenko and Vera Tyrsa
Engineering Institute of Autonomous University of Baja California, Polytechnic University of Baja California
Mexicali, BC, México

1. Introduction

Machine vision in its common definition is a possibility of a machine (by sensing means and computer mathematic processing consecutively) to obtain an information about surrounding environment for further analytical treatment.
According to this common definition we can unite in a general classification various, sometimes quite different by its principle, technical systems.
These classification tables can be represented on the base of two different approaches: 1) practical causes (Soini, 2001) for necessity to "see surrounding environment", and 2) technical principle and means using for this task solution.
According to the common definition any complete Machine vision system combines two components: technical means (or hardware) and information processing mathematics and algorithm (or software). However, the various software analyses is not expedient in view of variety of mathematical methods and their object focused applications in each case (Mordohai & Medioni, 2006); and finally can't give clearer problem understanding.
We are now observing a rapid growth of 3D software and hardware capabilities for mainstream PCs, and 3D graphics accelerator boards with processing capabilities of roughly millions polygons per second are becoming commonplace (Petrov et al., 1998). At the same time, dynamic level-of-detail algorithms—built into standard 3D software packages— offer considerable acceleration of model viewing and progressive loading and transmission of 3D models. Despite the fast growth of computer 3D visualization capabilities, until recently data input technology has remained unchanged.
So, in our research for better understanding what is Machine vision, what is its modern state, which practical and technical tasks it decide, and which objective limitations and open problems recently it have, we'll based on the two mentioned above approaches.
In a part of practical reasons, which caused for necessity to develop Machine (or computer) vision concept, can be mentioned:

- security problems in static/dynamic image analysis in perimeter/volume protection (motion/dangerous object detection); (Chellappa et al., 2005), (Itti & Baldi, 2005)
- analysis of short/long term deformation of important engineering structures (more commonly known as 'structural health monitoring' or SHM); (Athavale et al., 1990), (Allen et al., 2005), (Mallet et al., 2004), (Tyrsa et al., 2004), (Ohno et al., 2002), (Benedetti et al., 2004), (Slob & Hack, 2004), (Stewart & Tsakiri, 2002), (Liwen Dai et al., 2002)

Source: Computer Vision, Book edited by: Xiong Zhihui,
ISBN 978-953-7619-21-3, pp. 538, November 2008, I-Tech, Vienna, Austria

- surface digital mapping and micro-surface analysis; (Winkelbach et al., 2006), (Slob & Hack, 2004), (Tunstel, 1995), (Vang et al., 2000), (Peng-Hsiang Weng & Fu-Jen Kao, 2004)
- automatic navigation of robot in unknown scene (Tunstel, 1995), (Diosi & Kleeman, 2005), (França et al, 2005), (Ibeanusi et al, 1999), (Chaumette & Hutchinson, 2006), (Surmann et al, 2003), (Kee et al, 2008), (Hada & Takase, 2001)

In a part of technical principle and means Machine vision system can be classified to:

- camera (or "stereo camera") principle with further image analysis algorithms; (Chellappa et al., 2005), (Itti & Baldi, 2005), (Selectes papers on CCD and CMOS imadges, 2003), (Lavelle et al., 2004)
- 2D-3D image reconstruction techniques (most frequently - 3D laser scanning on triangulation principle); (Tyrsa et al., 2004), (Peng-Hsiang Weng & Fu-Jen Kao, 2004), (França et al, 2005), (Surmann et al, 2003), (Lavelle et al., 2004), (*Handbook of Optical and Laser Scanning,* (2004), (Forman & Parry, 2001), (Pierce et al., 1992), (Lichti et al., 2000), (Petrov et al., 1998)
- terrestrial laser total stations, or airborne laser scanners; (Slob & Hack, 2004), (Baltsavias, b, 1999), (Baltsavias, a, 1999), (Wehr & Lohr U, 1999)
- obstacle detection y description techniques, based on signal "time-of-flight"(radar, lidar, sonar, rangefinders or UWB technologies); (Vang et al, 2000), (Pierce et al., 1992), (Yu et al., 2008)
- GPS-based systems for objects surface reconstruction; (Kee et al., 2008), (Stewart, & Tsakiri, 2002), (Hada & Takase, 2001), (Liwen Dai et al., 2002)
- combined systems, which use a certain combination of mentioned above basic means for increase total system resolution and noise robustness (Ohno et al., 2002), (Benedetti et al., 2004), (Lavelle et al., 2004), (Retscher, 2007), (Liu et al., 2006).

The goal of our work is to compare several of mentioned approaches to Machine vision design, compare their advantages over each other, and the most principal limitations for practical application.

In general, variety of practical applications which strongly requires the technical vision device it is just a confirmation of an actuality and high importance of a new technical vision methods development.

However, sometimes very different practical tasks use very similar techniques for practical task solution. And it has a different level of success. Because of various practical limitation and specific requirements which appears in each unique case. So, the key parameter for to analyze different technical principle for machine vision system design is a basic technical device for task solution.

2. Approaches to machine vision design

More attentive analysis of the mentioned above technical principle and means list permit us to make a simplified conclusion. There are four completely distinct technical approaches to technical vision device design. More truly, if to be rigorous in definitions, three relatively independent methods, and the fourth group which cannot be an independent basis for creation of the device, but possesses such important advantages, that at use of other methods it is not to forget about them, and it is desirable to use actively them as auxiliary means.

These four groups are:

- camera methods;
- laser scanning systems;
- GPS-based methods;
- numerous rangefinder devices (radar-, sonar- , laser-principle, etc.)

As evident the last one cannot be an independent basis for creation of the complete Machine vision system. Because of its physical nature this system it is only capable to estimate the distance to "averaged object", but not reconstruct its surface point-by-point.
Let us carefully review all mentioned principles of Machine vision design for establish their strong and weak points.

2.1 Camera based machine vision

The machine vision system includes (Selectes papers on CCD and CMOS images, 2003) a stereo TV camera assembly and a processing unit. It detects obstacles in real time within its field of view in a range from 5 m to 50 m ahead of the vehicle with a viewing angle of 40 degrees. The cameras are arranged vertically at the front part of the vehicle. The system locates obstacles in the trapezoidal field of view. The scanning of each camera is synchronized and the processing unit uses hard-wired logic instead of a programmable device in order to realize high speed processing of video signals from the cameras. The principle of the obstacle detection is parallax. When two images from both of the cameras are compared, the two images of an obstacle are identical except the positions in the frames. On the other hand each image of figures on the ground differs due to the positions of the cameras. Fig. 1 illustrates the principle of the obstacle detection.

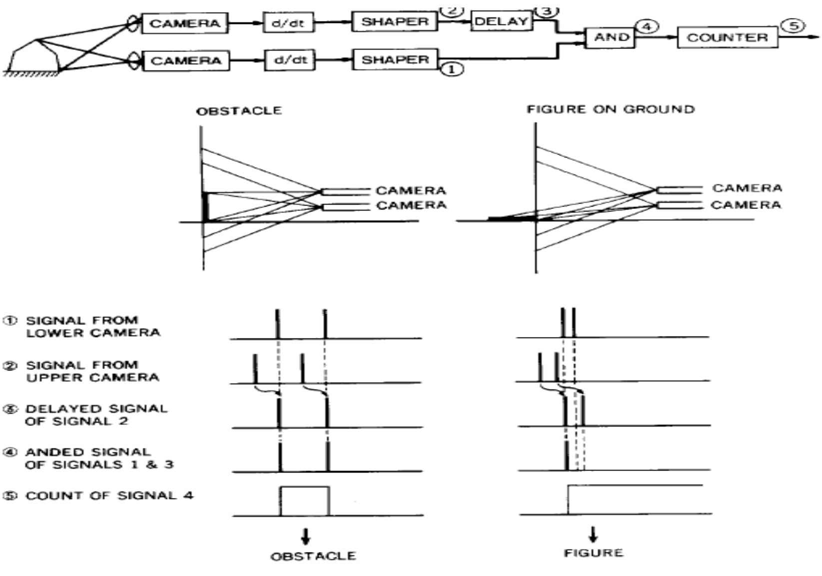

Fig. 1. The principle of the real time obstacle detection

The video signals are differentiated regarding time and the signals are shaped to obtain pulses that correspond to edges in the images. Each time interval of the pulses from each cameras, *(signal* 1 and *signal* 2 in Fig. l), discriminates an obstacle from a figure on a road.

An obstacle generates same time intervals, but a figure on a road generates different time intervals. The cameras have to be, thus, synchronized with each other, and have to employ vertical and progressive scanning techniques. The position of a scanning line corresponds to the direction to the obstacle, and the point where the optical axes of the cameras are crossing indicates the distance to the obstacle. Delaying of one of the signals from the TV cameras is equivalent IO rotation of the optical axis of the camera. Thus, varying the delay time enables us to detect obstacles at other locations. For enlargement of the field of view and detection of obstacle:; in the two-dimensional field of view during one scanning period, parallel processing with 16 kinds of delay time is employed, which yields the field of view of 16 zones arranged longitudinally at intervals of **1** m. Time required to detect obstacles is 35.6 ms, which consists of 33.3 ms of scanning OF one frame and 2.3 ms of processing to detect and locate obstacles. Fig. 2 shows an example of the obstacle detection. The guardrail is identified as a series of obstacles that are indicated by black elements in the figure at the bottom. Since the system had no measures against brightness, shadows, and shades, the operating condition was restricted.

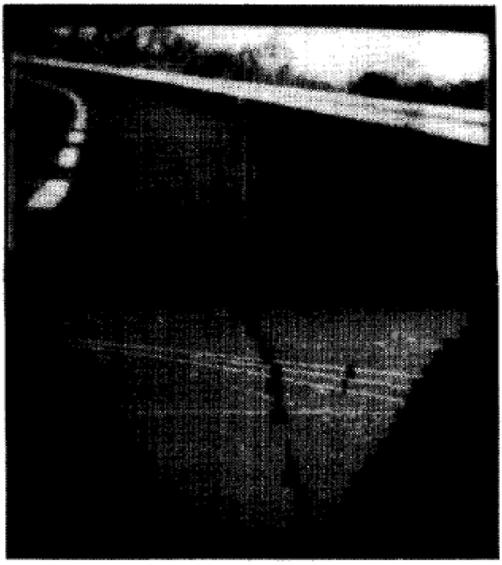

Fig. 2. The obstacle detection: a road scene (top) and obstacles in the scene (bottom) (Sadayuki Tsugawa, 1994)

In a basis of any camera method it is the principle of the human volumetric vision, capable to reconstruct a 3-dimensional picture and approximately estimate distances up to the objects within scene. That is in other words, stereovision.

Any stereovision technical system is approach to a multicamera system. In the elementary case under consideration it is two cameras system. If a stereovision system (Chaumette & Hutchinson, 2006) is used, and a 3-D point is visible in both left and right images (see Figure 3), it is possible to use as visual features s (vector *s* contains the desired values of the scene/features):

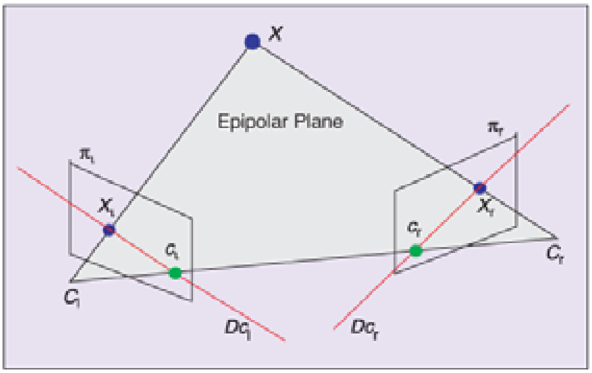

Fig. 3. A stereovision system

$$\mathbf{s} = \mathbf{x}s = (\mathbf{x}l, \mathbf{x}r) = (xl, y\,l, xr, yr),$$

i.e., to represent the point by just stacking in **s** the x and y coordinates of the observed point in the left and right images.

For a 3-D point with coordinates $X = (X,Y,Z)$ in the camera frame, which projects in two images as a 2-D point with coordinates $\mathbf{x} = (x, y)$, we have (Chaumette & Hutchinson, 2006):

$$\begin{cases} x = X/Z = (u - c_u)/f\alpha \\ y = Y/Z = (v - c_v)/f, \end{cases} \tag{1}$$

where image measurements matrix $\mathbf{m} = (u, v)$ gives the coordinates of the image point expressed in pixel units, and $\mathbf{a} = (c\,u, c\,v, f, \alpha)$ is the set of camera intrinsic parameters: $c\,u$ and $c\,v$ are the coordinates of the principal point, f is the focal length, and α is the ratio of the pixel dimensions. In this case, we take $\mathbf{s} = \mathbf{x} = (x, y)$, the image plane coordinates of the point.

Taking the time derivative of the projection equations (1), we obtain the result which can be written in general form

$$\mathbf{X} = \mathbf{L}_x \mathbf{V}_c, \tag{2}$$

where $\mathbf{V}_c$ is a spatial velocity of the camera be denoted by $\mathbf{v}_c = (v_c, \omega_c)$, (with v_c the instantaneous linear velocity of the origin of the camera frame and ω_c the instantaneous angular velocity of the camera frame) and the interaction matrix $\mathbf{L}_x$ (we consider here the case of controlling the motion of a camera with six degrees of freedom) related to **x** is

$$L_x = \begin{bmatrix} \frac{-1}{Z} & 0 & \frac{x}{Z} & xy & -(1+x^2) & y \\ 0 & \frac{-1}{Z} & \frac{y}{Z} & 1+y^2 & -xy & -x \end{bmatrix} \tag{3}$$

L_x is an interaction matrix related to s, *or* feature Jacobian. In the matrix $\mathbf{L}_x$, the value Z is the depth of the point relative to the camera frame. Therefore, any control scheme that uses this form of the interaction matrix must estimate or approximate the value of Z. Similarly

(Chaumette & Hutchinson, 2006), the camera intrinsic parameters are involved in the computation of x and y.

Let us analyze this basic “camera method” parameters regard to equations (1)-(3).

1. Focal distance f in (1), as well as the set of camera intrinsic parameters, shows us that camera uncertainty is strongly related to fabrication imperfections for each unique camera. And, hence the absolute value of this camera uncertainty is rising sufficiently with scene depth increase (proportionally to $1f$, $2f$ … nf).
2. $\mathbf{V}c$ in (2), which is camera velocity, shows us that any camera method error strongly related to any own camera motions. And, taking to account an arbitrary character of camera self-motions and consequently instant vector $\mathbf{V}c$ direction, it is very difficult to estimate real camera uncertainty.
3. Depth Z in (3) shows for components (1;1), (2;2) (2;3) for example, that method resolution and reasonable operating rate are strongly limited by own theory.

These reasons permits us to understand exactly clear a principal limitations for any practical application of camera based technical vision method. They are very critical for practical using in any application with self-moving camera positioning, are extremely sensible to any vibration and dynamic shocks. Moreover, in spite of significant achievements of camera technologies in last ten years, it still exist a possibility of “camera error”, i.e. when one typical object image is assigned with typical properties of another. And this possibility is proportionally increased with distance growth. Finally, camera methods application is naturally limited with distances up to 50 m.

2.2 Laser principle based machine vision systems

Modern laser sensor technologies have made fast and accurate 3-D data acquisition possible as evidence by several commercialized 3-D laser sensors (Tyrsa et al., 2004), (Peng-Hsiang Weng & Fu-Jen Kao, 2004), (Diosi & Kleeman, 2005), (França et al., 2005), (Surmann et al., 2003), (Lavelle et al., 2004), (Handbook of Optical and Laser Scanning, 2004), (Forman & Parry, 2001), (Pierce et al., 1992), (Lichti et al., 2000), (Petrov et al., 1998). Other than some existing 3-D technologies based on CCD 2-D image reconstruction, these 3-D sensors are based on laser scanning and geometric methodologies such as triangulation (Petrov et al., 1998), (Tyrsa et al., 2006, a), (Tyrsa et al., 2006, b), (Rivas et al., 2008) and have achieved more and more attentions in machine vision application due to its robustness and simplicity. However, to expand functional application of these laser sensors, powerful algorithm add-on is still needed to effectively process measured data from them, normally depending on individual application case.

Laser triangulation principle (Handbook of Optical and Laser Scanning, 2004) in general can be based on two schemes represented in Fig 4 (a and b). The first one uses a fixed angle of emission and variable distance; the second one, on the contrary, fixed triangulation base and variable scanning angle.

The first one works as follows.

A laser beam is projected onto the measurement surface (Fig. 4, a), where it is scattered from the surface and its image is detected by an optical detector, usually a CCD camera. By using a suitable angular arrangement between the laser and sensor positions, the detected location of the laser spot on the image plane produces an accurate measurement of the distance between the sensor and the surface. Therefore, the profile of a surface can be measured by using laser triangulation. The laser beam is made to scan across the surface of the object. The range data at each location is calculated according to its position within the image plane so that the whole 3-dimensional profile of the surface can be obtained. The positioning of the laser beam is normally controlled by an adjustable mirror system, which is able to change the angular direction of the laser beam over a 2-dimensional plane.

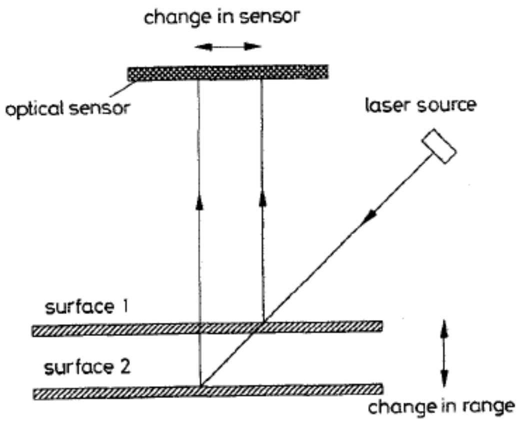

a)

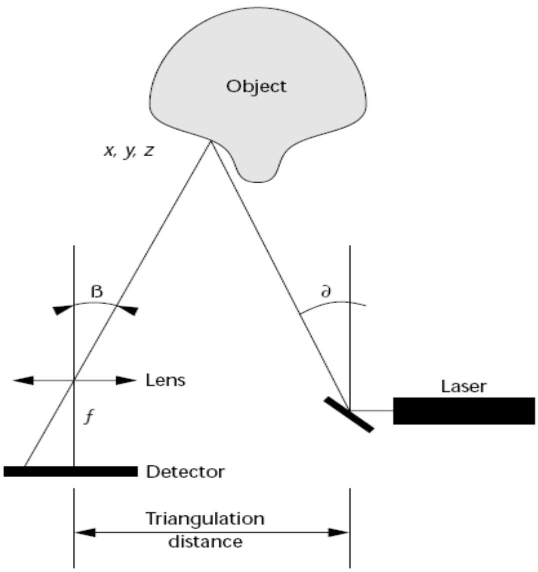

b)

Fig. 4. Two principles of laser triangulation (a – "with fixed angle of emission"; b - "with fixed triangulation distance", consists of a laser dot or line generator and a 1D or 2D sensor located at a triangulation distance from the light source (Petrov et al., 1998). Optionally, the laser light can be steered by a motor)

A second one basic triangulation scheme (Fig. 4, b) is an active optical triangulation 3D digitizing systems, which visualize real-life objects. These active optical systems provide photorealistic representations of shapes and textures with reasonable speed. Figure 4,b shows a simple diagram of a triangulation scanner. The laser beam—reflected from a mirror—is projected on the object. The diffusely reflected light is collected by the sensor, which is a linear array if a laser dot is projected or a 2D matrix (typically a charge coupled device camera) if laser stripes are projected.

The laser positioning circuitry controls the angle α and is known. The angle β is determined in the sensor measurements if the focal length *f* and the detector pixel size are given. The triangulation distance—the distance between the sensor and the mirror—is also known.

As Figure 4, b shows, since all geometric parameters are known, the *x*, *y*, *z* coordinates of the point on the object can be computed in a trigonometric fashion. If a single laser dot is projected, the system measures the coordinates of just one point of the object. When a laser stripe is projected, all points along the stripe are digitized. The basic triangulation scheme can be enhanced to improve the optical quality and depth of field (see www.vit.iit.nrc.ca for several good examples). The modifications, however, require custom-manufactured components and are relevant mostly for scanners used in high-accuracy reverse engineering tasks. In general, any other kind of structured light can replace the laser dot or stripe. For example, several dots or laser stripes can be projected. However, if the system projects multiple patterns, it's difficult to identify individual elements. If, say, two stripes are projected, then the image processing software must separate the first and second lines. Solutions to the identification problem include using a sequence of different colored stripes. Such schemes typically become sensitive to ambient light, as we'll discuss later.

The most well-known optical triangulation 3D scanner is the one developed by Cyberware of Monterey, California. This legendary scanner was used by a generation of computer scientists. The company has maintained essentially the same product line for more than 10 years. Cyberware products can capture photorealistic images of a range of objects—from apple-size models to fullsize human bodies. The scanner head contains a laserline generator, a system of mirrors, and black-and-white and color video cameras. Scanning occurs by moving the object on a rotation and translation platform, or by moving the sensor around the object in a circular motion. In the basic Cyberware scanner model, a system of mirrors collects laser light from left and right triangulation paths relative to the laser. This scheme helps avoid shadows in the scans caused by the triangulation angle. However, it imposes strict requirements on the optical assembly's quality and the system's calibration, and increases the scanner's size. The scanners are complex, not portable, and prohibitively expensive for many applications. One version, the full-body scanner, digitizes a complete human body as a combination of four scans in about 17 seconds. Each scan has 250 × 1000 points of resolution. The four scans can be glued using commercial software packages (Petrov et al., 1998).

Another typical method for laser scanners is a Circular laser scanning vision sensor for detecting position of singular points (Tao Dai et al., 2005). Usually it called data acquisition device-circular scanning sensor (CSS). By singular point in this case we mean small convex or concave points deviated from smooth surface manifold, caused by either faulty or normal production/machining. The platform for this devise features a three degree of freedom (hence, accommodate 3-D) motion control through a processor, three servo motors and a circular scanning sensor (CSS), as well as a computing system. An emulated head is attached rigidly with CSS to indicate the tracking and focusing actions. The circular scanning sensor (CSS) (Figure 5), with embedded data acquisition device, is a laser scanning multi-axis machine vision device which produces 3-D data sequences of a target work piece for reconstruction of geometry characteristics.

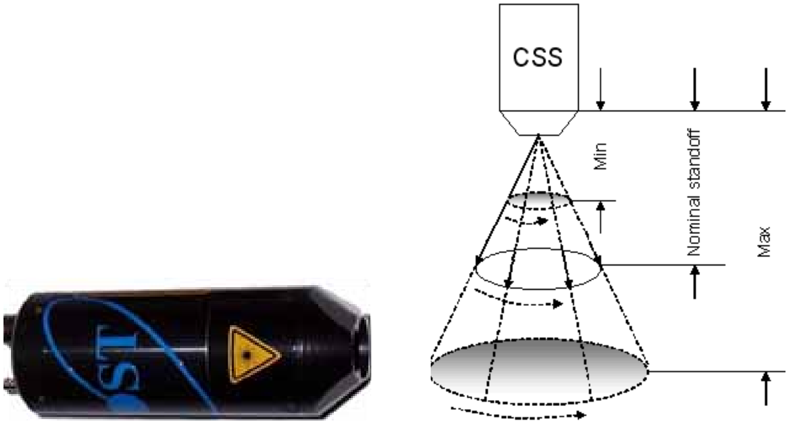

Fig.5. A Laser Circular Scanning Sensor and illustration of Circular Scanning Principle

The CSS and the emulated head are driven by three servo motors to generate 3-D (*x*, *y*, *z*-axis) motion: arbitrary planar scanning route, up and down motion. The main emulated head could track any 3-d singular point on the surface of the work piece while conducting scanning and concentrate on it at specified focusing distance.

The motors are controlled by a central processor which receives location information of singular points from a PC system. The loop is then closed by feedbacking 3-D geometric data of target points acquired by the CSS to the PC system which processes the data sequence continuously using DMA based algorithm (Fig. 6.) to return the location information of singular points, if any, on the surface of work pieces.

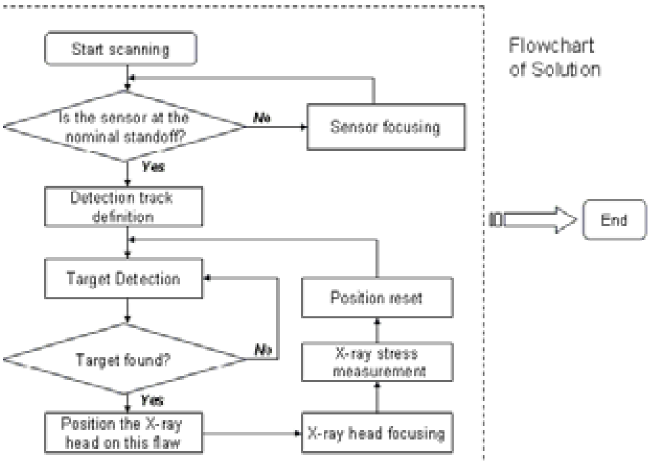

Fig. 6. Flow-Chart of DMA Based Operating Algorithm

For central laser scanning sensor, scanned data is obtained in sequence:

$$Xi = [x_0, x_2, \cdot\cdot\cdot, x_{N-1}], i = 1, 2, \cdot\cdot\cdot, \quad (4)$$

where Xi indicates the $i - th$ data sequence captured and N is the number of scanning times called the depth of the data sequence. This data sequence could represent data piece acquired by one sensor in different pre-set time period or by multiple sensors at same time. For example, a line or circular scanning laser sensor generates a geometric data sequence of objects in one scanning cycle. For circular scanned data is considered, hence the depth N is also the scanning cycle period. An example of a 1-D real circular scanning data cycle is illustrated in Figure 7, which is conducted, for example, on a horizontally flat iron plate placed on a table.

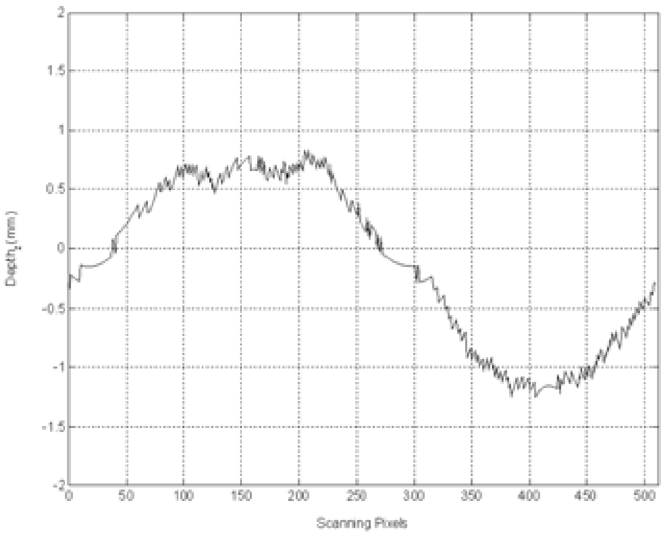

Fig. 7. A 1-D Circular Scanning Data Cycle

In ideal case, one would expect scanned data yields a horizontal line. However, this hardly happens in reality. Instead, as Figure 7 shows, a pseudo-sinusoid shape is presented reflecting either unevenness of plate surface or table leaning, or both. In the case that there is a hole-like singular point, caused by either normal or faulty machining, on the surface, the scanned data would normally reflect that point with a peak significantly deviated from the profile, unlike small peaks around the profile induced by noise. Such an example with a hole of depth 0.4 mm at the 100th pixel is shown in Figure 8 (1-D circular scanning data).
From these two examples, it is clear that two major tasks have to be performed in order for us to obtain accurate information of targets from laser scanned data: reduction of effect of noise on the measurement and detection of singular peak.
This method even it is a laser scanner practically is similar to 3-D technologies based on 2-D image reconstruction and posses all weak points, which are mentioned for these group of methods.
For static object shape monitoring also possible to use a multi-beam laser triangulation (Noll & Krauhausen, 2003) up to more than 120 laser beams are used to simultaneously measure geometric features of moving products such as e.g. the thickness, profile or surface topology. The laser beams form a series of measuring points or lines on the object surface.

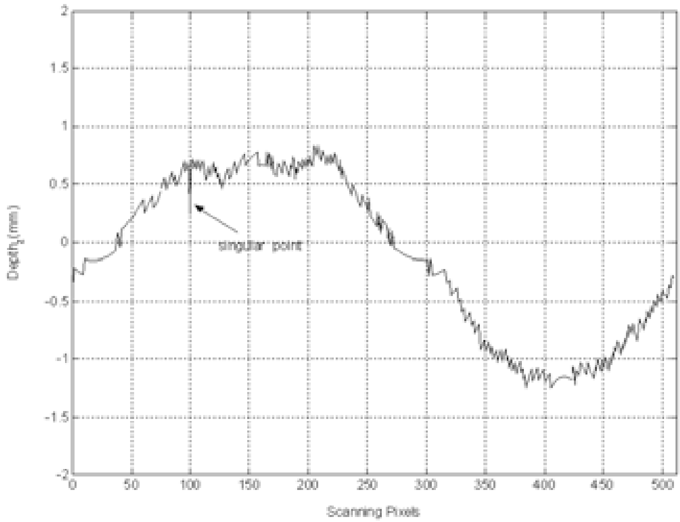

Fig. 8. A 1-D Circular Scanning Data Cycle with a Singular Point

By temporal modulation of the pulse width of the laser diodes and control of the exposure time of the CCD or CMOS detectors **a** dynamic range of more than $1 \div 10^4$ (without considering the dynamic range of the detector elements itself is realized enabling the measurement of object surfaces ranging from black to metallic bright. The use of different laser wavelengths allows suppressing cross-talking originating from overlapping laser projections on the surface of the specimen. However, this method is a good tool for dynamic surface control, but it is unsuitable for high-grade image reconstruction. It cannot be related to pure "camera methods" because CCD or CMOS devices are used only like "light 1/0 detectors", also for incident ray preliminary positioning. This example highlights those sometimes optical sensors matrixes are the better detectors because of their good sensitivity/resolution.

Another laser tools for static perimeter control is Laser radar (LADAR) (Sahba et al., 2006), (Stutz, 2005). LADAR scanning is far advanced over conventional active infrared (AIR) sensing. The transmitter and receiver units are usually coaxially located, making the installation less prone to misalignment or tremors than traditional opposed or retro-reflective sensor posts. Laser scanning also has much finer resolution that RADAR and microwave-RADAR, allowing the definition of the intruding target size. Time of flight pulse detection or continuous wave phase shift methods are used to derive range measurements. According to tests conducted to determine the feasibility of using laser scanning for perimeter protection (Sahba et al., 2006), it has been confirmed the capability of detecting humans and vehicles, with a maximum range of 25m and 80m respectively. The testing demonstrated large area coverage, the ability to determine intruder size, the definition of multiple detection zones, a good detection rate and low false alarm rate (Hosmer, 2004). It has also been claimed that camouflage and other methods for masking an object can deceive near infrared devices, but it is impossible to mask a physical volume moving through space, thereby implying that by scanning a plane at high speed and resolution, any object moving through this plane will be detected (Hancock et al., 1998). Riza, et. al. propose generic criteria for an ideal optical scanner including a wide scanning range, no moving parts, high resolution, high speed and low power consumption. Additionally, they place significance on reconfiguration (Riza & Muzammil, 2003). By projecting many spots, a laser curtain is produced and multiple range measurements from a dense array of laser spots provide a 3D contour of the perimeter. In current LADAR scanners, a laser beam is deflected by rotating mirrors as show in Fig. 9 where D is the incident beam diameter, α is the beam-feed angle, θ is the active scan angle and L is the scan length.

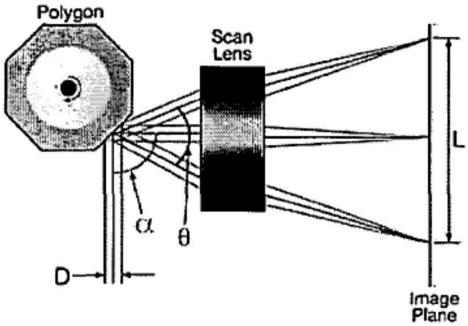

Fig. 9. Principal of laser beam deflection using a rotating mirror (Stutz, 2005)

As we can observe, commonly static object monitoring methods strongly related to basic optical property of focal distance and its practical consequence of a sharp image in a focal plane. From the other hand, it makes these technical solutions initially (apriori) unsuitable for such dynamic task like a mobile robot vision.

In applications where information from more than one physical point of an object needs to be derived, a scanning mechanism must be employed to deflect the light beam from the laser source, towards the desired point of interest on the object surface. This deflection is usually driven in two or three dimensions electro-mechanically. Laser scanning mechanisms have been used in a large variety of applications ranging from photo and document scanners to airborne topographic mapping, surveying of buildings and plants, counting and collision prevention. Approximately over the past ten years laser scanning has found new applications in photoelectric security sensing. Some common uses include providing light curtains in front of assets on a wall display or over the facade of a building. More commonly, laser scanners are employed to provide high resolution range measurements to the outer perimeter (e.g. fencing, walls) of a building and detect a change in range values when beams are intersected by an intruder.

To date, driving the deflection mirror in the desired direction has been accomplished using different devices such as electro-mechanics, rotating polygon shaped mirrors and galvanometers. Figs. 10. (c) and (d) show the layout of a typical commercially available laser scanner and its mirror driving mechanics. Typically, the whole optical head is rotated by a servo motor head around the azimuth in the order of a 1000 rpm, and the mirror rotates in elevation at the same time. This dual movement deflects the beam in the desired directions. However, the intrinsic motion of the mirror causes scanning problems which are the hardest to quantify and correct. Acceleration time taken to reach the constant scanning speed from a stationary position can result in range measurements being stored at the wrong corresponding points in the scanned image. Additionally, all mirrors and measurement components must be synchronized exactly. In general, laser scanning is much more sensitive to vibration than a multi-beam stationary optic approach. In particular, mirror device scanners are slow, bulky and expensive and being inherently mechanical they wear out as a result of acceleration, cause deflection errors and require regular calibration. Stutz in (Stutz, 2005) explains that the performance of polygonal scanners, especially with respect to maintaining an accurate deflection beam path, is prone to manufacturing tolerances.

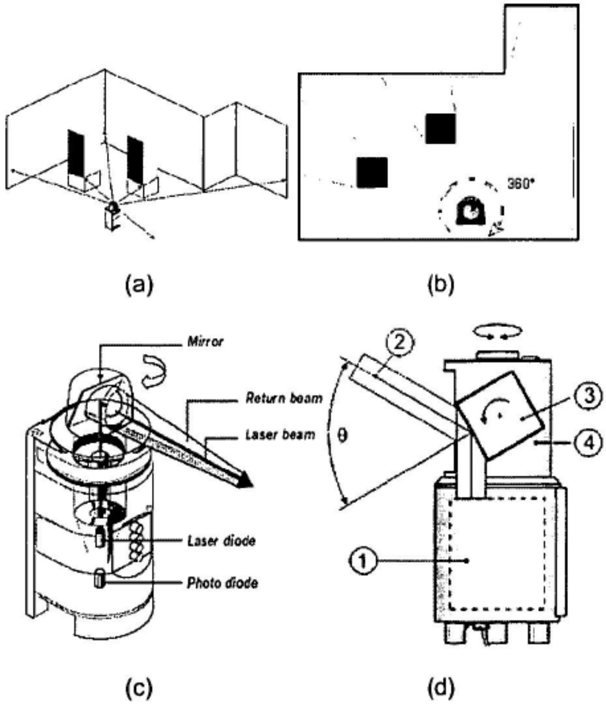

Fig. 10. (a) and (b) indoor room surveillance scanning, (c) scanner with mirror mounted on motor, (d) scanner with rotating mirror where 1 contains the range finding electronics, 2 is the deflected beam, 3 is the rotating mirror and 4 is the complete optical head which also rotates (Sahba et al., 2006)

Dynamic track and jitter errors are caused by tolerances for:

- Polygon machining errors
- Mounting errors
- Mounting-hub errors
- Random wobble caused by ball bearings
- Motor cogging
- Torque variations
- Noisy start of scan circuit

Machining and mounting errors directly cause the deviation of the deflection beam from the desired path of propagation towards the correct point at the image plane. Errors can range from 1 to 60 arc-seconds in angular deviation. Cogging, torque and facet flatness variations cause errors in the actual scan line.

Other problems listed with rotational scanners are as follows (Stutz, 2005):

- Synchronization with other time-dependent elements in the system is rather difficult.
- Motor stability and durability at higher rotation speeds also present problems.
- There is an upper limit to the rotation speed due to the tensile strength of the mirror material. The mirror must not disintegrate at the maximum rotation speed.

Another strong tool for 3D spatial data acquisition is terrestrial laser scanning (Slob & Hack, 2004), (Baltsavias, 1999, a), (Baltsavias, 1999, b). These are active scanners based on laser signals for measurement of slant distances to acquire information about the surface of the Earth and objects on it. As mentioned above, there are several laser scanning systems being operational. Concerning the measurement principle two different methods had been realized: *runtime* measurement using pulsed laser signals and *phase difference* measurement using continuous-wave lasers. Because most systems are based on the first mode, it will be described in more detail in the next section. A good overview on both topics can be found in (Wehr & Lohr, 1999). The pulsed mode laser scanner emits pulsed laser light in exactly determined time intervals. The system measures the runtime of these laser pulses, i.e. the elapsed time between emitting a signal and receiving it after reflection on the surface of the Earth or objects on it. Therefore, slant distances can be derived from these time differences by the wellknown formula v = Ds / Dt or Ds = v / Dt. By means of the exterior orientation of the sensor (recorded by differential GPS (dGPS) and INS systems) 3D co-ordinates of the illuminated surface points can be determined.

Laser systems need to be designed mainly regarding two components: the *emitting and receiving unit* and the *positioning unit*. Both will be described as the example by means of the operational system TopoSys (Wehr & Lohr, 1999) which was used to acquire the data sets about terrestrial landscape.

In this system, the emitting and receiving unit is realized by means of a glass fiber optic. The laser light is emitted on a nutating mirror, i.e. a rotating mirror which deflects it on a glass fiber bunch. The ends of the glass fibers are connected to a row-shaped optic, so the resulting measuring pattern on the surface of the Earth is a single scanning line. In addition to the movement of the airplane this results in a strip-wise data acquisition as shown in Figure 11.

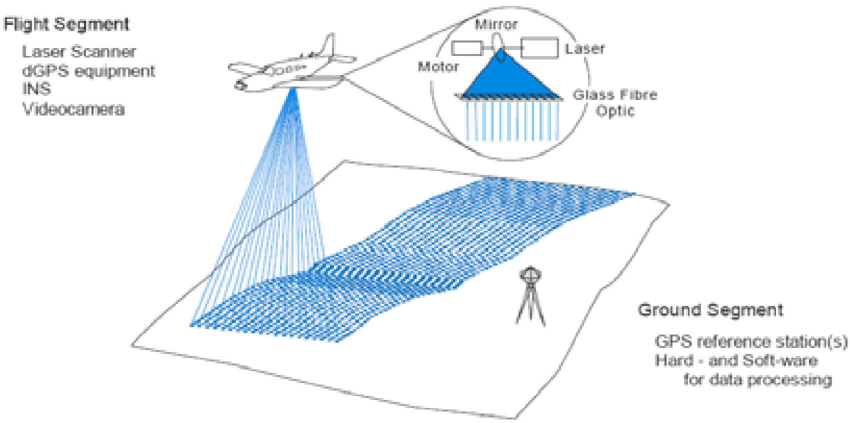

Fig. 11. Laser scanner system TopoSys (Wehr & Lohr, 1999)

The positioning component of the system consists of several elements. As navigation principle differential Global Positioning System (dGPS) is chosen. Therefore, GPS antennas

are mounted on the airplane, as well as on reference stations on the ground. Although this positioning strategy yields to good results concerning the accuracy of the obtained co-ordinates (in the range of some few centimeters), the measurement rate is lower than the one of the laser scanner. Therefore, additionally Inertial Navigation Systems (INS) are used, i.e. navigation units register the rotations of the airplane based on gyros. These are capable to determine a position with a higher temporal resolution.
In Table 1 the performance parameters of this system are listed. It should be mentioned that the system is capable of acquiring up to 5 points per m^2. This results in data sets of high point density and suitable accuracy in position as well as in elevation.

sensor type	pulse modulated laser Radar	range	< 1000 m
scanning principle	fibre optic line scanner	transmitter	solid state at 1.5 μm
measurement principle	run-time measurement	scan frequency	300 Hz (adjustable)
field of view	+/- 7°	number of pixels per scan	127
swath width (1000m flight height)	250 m	accuracy of a single distance measurement	< 0.3 m
accuracies of point coordinates x,y,z	˜ 0.3, 0.3, 0.1 m	resolution of a distance measurement	< 0.1 m

Table 1. Performance parameters of TopoSys laser system (Steinle & Vogtle, 2000)

It is relatively more expensive method over another laser application. Hence the principle limitation of it is the practical importance of the task. However, terrestrial laser scanning have a significant flexibility of provided practical use acts. For example, terrestrial scanning lidar (light detection and ranging) is applied to outcrop stratigraphic mapping enables researchers to capture laser range data at a rate of thousands of individual X, Y, Z and laser-intensity points per second (Bellian et al., 2005).

Fig. 12. A typical field setup in Patagonia in early 2002. All equipment was transported in a backpack by a single person (picture courtesy of Jeremy Willson, Shell Oil). Lithium Ion batteries have helped reduce battery weight to 1,540 grams (3.4 pounds) per approximately 2 hours of continuous scan time (Bellian et al., 2005)

Research group of (Bellian et al., 2005) store the 3D coordinates data set with an Optech Laser Imaging ILRIS 3D terrestrial (ground-based) scanning lidar (Fig.12). This instrument was chosen for its 1 km range, palm-type interface, and light weight. All data from the ground-based lidar surveys were processed on a standard laptop computer with at least a gigahertz processor speed, 1 gigabyte of RAM and Innovmetric Incorporated's Polyworks CAD (Computer Aided Design) software. The principal result of (Bellian et al., 2005) was: high-resolution lidar (approx. 1cm point spacing) is far more accurate in three dimensions than nearly all GPS currently available to the public.

2.3 GPS-based and combined machine vision principles

GPS-based solutions sometimes also are acceptable for machine vision, especially for navigation tasks. The good example of such system is presented in (Vang et al., 2000).
GPS based navigation for autonomous land vehicles has the capabilities of GPS to determine the locations of vehicles, as far as static objects, basing on satellites (Kee et al., 2008), (Stewart & Tsakiri, 2002).
GPS measurements consist of biased and noisy estimates of ranges to the orbiting satellites. The principal source of bias is the unknown receiver clock offset, whereas the remaining errors arise from:

- ′ modelling of the satellite clock and ephemeris.
- ′ modelling of the ionospheric and tropospheric delay.
- ′ measurement of the code and carrier phase influenced by both receiver noise and multipath.

DGPS is a technique that improves the user's position accuracy by measuring the infinitesimal changes in variables in order to provide satellite positioning corrections. It should contain a reference station, a data-link, and user applications. The reference station generates corrections by means of a measured pseudo-range or carrier-range, a calculated distance from the reference station to each satellite, and a satellite clock bias as well as an estimated receiver clock bias, and broadcasts them to the user application. The correction messages contain a Pseudo Range Correction (PRC) for DGPS, a Carrier Phase Correction (CPC) for CDGPS, and their time rates, Range Rate Correction (RRC) (Kee et al., 2008):

$$PRC = -(-b + I + T + \delta R) = d - \rho + \widehat{B} \tag{5}$$

$$CPC = -(-b - I + T + \delta R + N\lambda) = d - \varphi + \widehat{B} \tag{6}$$

Where:

ρ:	pseudo range measurement
φ:	carrier phase measurement
λ:	wavelength of the carrier phase
N:	integer ambiguity
d:	distance from the reference station to the satellite
b:	satellite clock bias error
$\widehat{B}$:	estimated clock bias of the receiver
I :	ionospheric delay
T:	tropospheric delay
δR:	orbit error

Unfortunately, the available accuracy for civilian applications is very poor because of all basic components in (5, 6). First of all, because of objective atmospheric delays (ionospheric and tropospheric). Although commercial DGPS (Differential GPS) service increases the accuracy up to several meters, it is still not sufficient for autonomous driving. Hence it is possible use an image processing to compensate this error. In spite of the fact that it is difficult to use image processing for recognition of a complex environment, it is possible to use it to determine some specified objects that haw obviously simple features. For example, lane tracking in highway, forward car tracking have been reported in (Vang et al., 2000). In this study, information about some specified objects is provided by a 3D map which is synthesized based on a real environment. The autonomous land vehicle uses these features to identify the indicated objects from the complex environments so as to position the vehicle's location. Because image processing consumes long time and positioning accuracy cannot satisfy the autonomous driving in many cases, environmental sensors, such as a 3D scanning laser rangefinder: ultrasonic environmental sensors, are also used.
Fig. 13 depicts the autonomous land vehicle used in the experiments (Vang et al., 2000). This vehicle was equipped with a color CCD camera, a GPS unit, a 3D scanning laser rangefinder, ultrasonic sensors, etc.

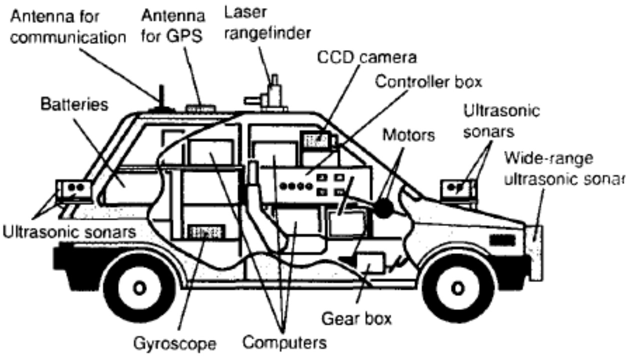

Fig. 13. The autonomous land vehicle used in the experiments (Vang et al., 2000)

Pedals and steering wheel are controlled with servomotors. The environmental sensing and control system is multitools. The position information from DGPS is used to retrieve environmental data from the 3D map. The 3D map provides the information about landmarks and features of some targets. Based the target features, the image processing system identify the landmarks by which the position of the vehicle is determined. An encoder attached to the wheel of a tire and a gyroscope are used for determination of the vehicle position and attitude. Because draft error may become unallowably large, these sensors are only for short distance measurement. A 3D scanning laser rangefinder is employed for compensation of the image processing system. The computers control the steering based on the information from the environmental recognition.
Positioning of GPS uses satellites. The resolution of the GPS used in the experiments is about 0.18m. However, the accuracy available for civilian applications is very poor. Even though DGPS makes the accuracy improved greatly, the positioning error is still insufficient for automatic driving. The positioning accuracy is not so good to navigate a vehicle, but enough to indicate the vehicle t o search some landmarks around the location. The synthesized 3D map provides geographic information that is referred by DGPS for positioning the vehicle's location. Because of the error of DGPS, some other information has

to be given for the vehicle to compensate the positioning error of GPS**.** In study (Vang et al., 2000) the information about landmarks and their geometry and features is contained in the 3D map. The vehicle locates itself position by referring to the landmarks. The 3D map was synthesized by using OpenGL[1]. In the scene some objects are specified as landmarks for the image processing system to recognize as well to correct the positioning error caused by GPS. For the sake of simplicity of the image processing, some obvious features of the indicated objects are provided. The image processing identifies some objects indicated by the 3D map. By detecting the relative position to the indicated objects, the vehicle can determine itself position. Image processing is not always effective in any situation. In such case, **a** 3D scanning laser rangefinder is used. A laser rangefinder measures distance using time-of-flight method. It has advantages in positioning accuracy, detection speed in comparison with image processing. By horizontal and vertical scanning 2D or 3D maps can be obtained. The above discussed environmental sensors are effective for long range detection. To guarantee a safe driving the near surroundings of the vehicle have to be monitored. For this purpose, ultrasonic sensors were used. 8 ultrasonic sensors that have detection range of several meters are arranged around the vehicle. A no-scanning wide-range ultrasonic sensor was also developed and mounted in the front, of the vehicle. The experimental results of (Vang et al., 2000) demonstrated a higher performance in comparison with a video camera only.

But, if we'll analyze presented system, it can be classified more like combined system, than GPS-based as declared by authors. It shows one more again that robust and secure systems nowadays more and more became combined system, which shares strong skills of mentioned above classical approaches.

It is important to note, that, in our opinion, the GPS have a strong potential in a field of future machine vision design. Because in last ten years there is a lot of financial and intellectual investments to GPS and GPS-based technologies application. But this branch still can not be adopted as an independent base for machine vision, because of impossibility to scan nearby environment, to detect an arbitrary object in the scene. We are consider, that with years comes detailed GPS-maps with marked details in landscape. It will give a possibility to navigate a mobile object using dead reckoning principle (Ibeanusi et al., 1999), (Sadayuki Tsugawa, 1994). In this case a quantity of arbitrary objects in the scene will be minimized, and their location it is possible to fix by simple locator or UWB (Yu et al., 2008). But recently it is problematic use GPS as an independent vision tool. Another principle limitation of GPS is a nonlinear uncertainty growth for such dynamic application like mobile robot navigation for example.

Also it is essential to note that in present time any GPS application still have a fundamental problem of the method. The GPS technology cannot be used outside the radio signals receiving zone such as tunnels, mines, complex indoor spaces, up to that sometimes can not functioning correctly at dense cloudiness or overcast, etc.

A good example of "combined system" design is presented in (Petrov et al., p. 32, 1998). It is given the detailed consideration to the optical 3D scanner developed by company MetaCreations Real-Time Geometry Lab (www.metacreations.com/products/rtgeom). The principal design goals are portability, low cost, fast scanning speed, and photorealistic quality of models. To fulfill these requirements, a scanner is built mostly from off-the-shelf components. Also a set of rather complex software algorithms to help facilitate the scanning process is developed. The basic image processing algorithms were implemented in hardware. The scanning resolution is better than 1 mm, while the acquisition time is sufficient. In the hardware design we avoided using complex optical schemes, instead transferring the complexity of the problem to algorithm development. This softwareoriented approach allowed us to use simple components in an easy-to-manufacture design. Figure 14 shows a block diagram of Galatea scanner.

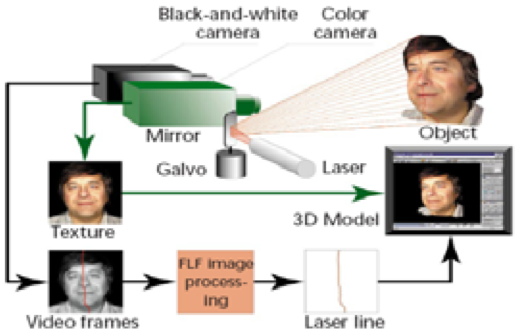

Fig. 14. Galatea scanner block-diagram. A galvanometric motor steers the laser stripe. The Fast Laser Finder (FLF) image processor processes the black-and-white camera's video stream. Merging the texture image of the color camera with the geometric model generates the final 3D model

The optical part consists of a laser-line generator, a galvanometric scanner, and black-and-white and color cameras. It's quite natural to use a laser as the light source in a triangulation system. Diode lasers are compact and inexpensive, and can be easily focused down to their diffraction limit. The depth of field is considerably larger than the sensor camera's depth of field. For this reason, the laser does not require focusing during normal operation. In general, a properly designed scanner is eye safe, so that the system can be certified as a Class 1 laser according to the CDRH (Center for Devices and Radiological Health, Food and Drug Administration) classification. One of the major advantages of a laser source is that it can be easily filtered out from the ambient illumination using a narrow-bandpass filter. This allows laser-based digitizers to be operated in daylight conditions. Also, the laser signal can be easily filtered out from the color camera data, allowing the color texture and geometry to be captured simultaneously. The laser projection system consists of a laser-line generator and an ultrafast galvanometric scanner. The repeatability of average galvanometric scanners is about 20 microradians, while the nonlinearities are small enough to be calibrated for, if necessary. The positioning speed of such a motor exceeds 1,000 angles per second. An NTSC formatted high resolution black-and-white camera senses the geometry. A color CCD camera—installed between the laser projection system and the black-and-white camera—captures the texture map. The scanning speed of 3D laser digitizers is limited by the rate of video cameras, typically 60 frames per second. Acquiring a 200-stripe resolution image would take about 3.3 seconds in a traditionally built digitizer. For many applications, including scanning the human body, this speed is not satisfactory. Using faster cameras provides a straightforward solution to increase speed. However, fast cameras tend to be rather expensive. To avoid using fast cameras, several solutions have been proposed.
Meanwhile, this system – as far as mentioned by authors collective - is designed as low cost solution for practical application where not necessary a high resolution. This example highlights the next fact. Any combined design always have larger coordinates error because a generalized system uncertainty is caused by complex cross-action of all components error sources and their interaction in this case is almost impossible to estimate by classic metrological methods.

3. Synthetic approach to machine vision system design

The first principle conclusion from the methods overview is the next. The machine vision can be divided in a two general groups of methods:

- relatively fast, but rough form estimation methods of scene analysis (with significant uncertainty of form reconstruction);
- metrological methods based on the precise coordinates measurement. These methods requires for insignificant form reconstruction uncertainty a lot operating time and gives a enormous data set for memory storage. Practically it is almost impossible to use this group in real time for any dynamic system.

The second principle conclusion from the methods overview is the next. Competitive machine vision can not be based on any of these two bases. It must to share the main advantages of them: fast operability of the first one and precise 3D coordinates accuracy of the second one.

The third conclusion. Many modern scanners use ‘’time of flight’’ to measure distance on the basis of the average speed of light in air. This measurement varies with air density, but because the speed of light is so great, these perturbations are very small for distances less than several kilometers. Other instruments use phase recognition to augment this technique for increased precision; however, this method is associated with an increase in data volume, which is undesirable.

The fourth conclusion from the methods overview: laser shows the high competitive ability over other scanning tools. It gives higher resolution, reasonable range and operation velocity. The weak point of laser technology is a limited power source of continuous scan time.

The key solution of this problem we are considering in a carefully thought over algorithm of information processing, very closely tied to each practical application. It must be flexibly used similar to human brain estimation: combine a very rough scene analysis in general, with furthering "zoom"-possibility for most problematic points surrounding (i.e. singular points). For this final fine stage it is only acceptable to provide a metrological accuracy method.

System optimized design according to open problem requirements will be explained on example of 3D laser Machine vision system, based on (Tyrsa et al., 2006, a), (Tyrsa et al., 2006, b), (Rivas et al., 2008).

4. Multipurpose scanning vision system design

It is considered in this paper a system with several characteristics previously referred; such as a high resolution, speed and versatility, can be used by our system in low cost.

In the most of fully autonomous navigation systems is used a vision system like this, our prototype can stand out among the other systems because has a very low cost; other advantage is the versatility, has a wide range of vision that can change to increase precision; and large sight depending of laser power.

This vision of environment is very similar to the human sight, has wide range of view, but can focus a specific area to get a high resolution and detailed image, so to make this task is not necessary modify hardware in prototype, just adjust some parameters in software

4.1 Original principle of 3D spatial coordinates measurement

On fig.15, basic elements of machine vision system (MVS), placed as example on mobile robot (MR), are shown.

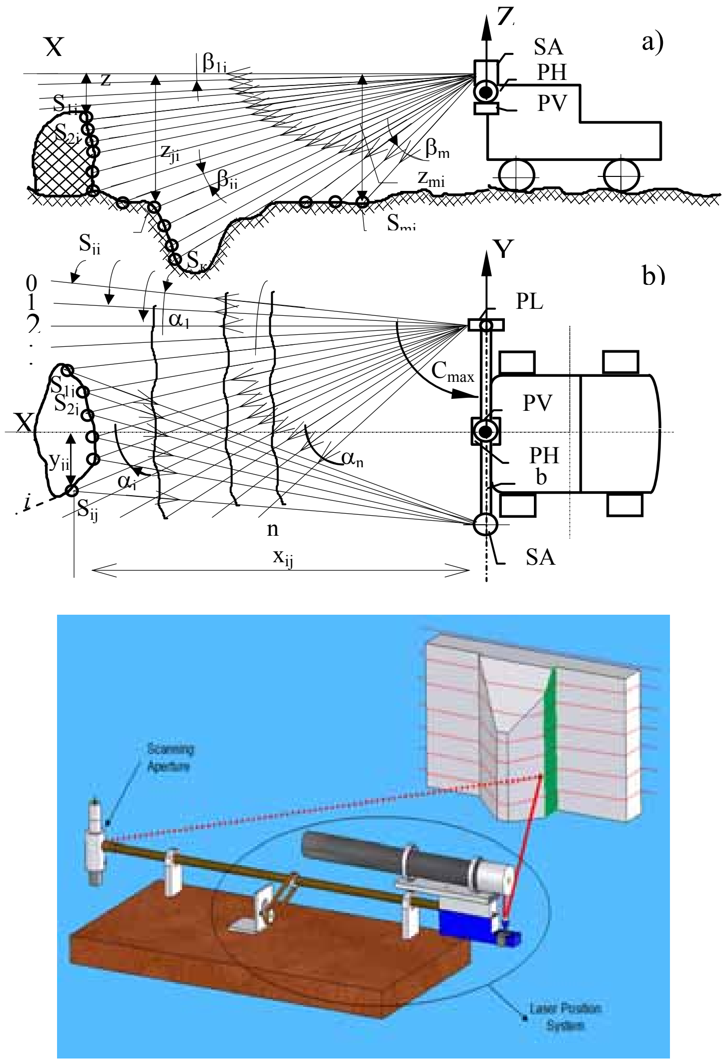

c)

Fig. 15. General principle of MVS functioning (a – lateral view; b - top view; c - laser scanner prototype view)

MVS represents laser angle-distance-measuring system located in the upper forward part of MR. MVS contains a rather high-power laser with a collimator. The laser and the collimator are installed in own laser positioning system (PL) (fig.15, b). PL has its step drive, which on a command from the onboard computer can turn PL in a horizontal plane at each for one angle pitch. PL is on one end of a horizontal bar b. On the other end of the bar is located a scanning aperture (SA), shown separately on fig.16. The SA axle is perpendicular to a bar and plane XOY. The bar b is installed by its middle part in its own positioning system, containing horizontal (PH) and vertical (PV) step drives (fig.1).

MVS works in the next way (Tyrsa et al., 2006, a). By the command from the computer the bar is installed so that the SA rotation axis becomes perpendicular to plane XOY of MVS reference system (fig. 15). PL puts the laser with the collimator, for example, in an extreme right position. The axis of the collimator (with the help of PV-step drive) then takes extreme top position (above the horizon). The laser and the SA are switched on. SA is rotated by the electromotor EM. At each SA turn a laser ray should hit an obstacle, is reflected difusely by it (point Sij) and returns to mirror M (fig.16). At the moment when three objects: the point of reflection Sij, the perpendicular to mirror M and the vertical axis of SA - takes their common plane, perpendicular to plane XOY while SA is rotating, an optical signal, having trevelled a path "Sij - mirror M - objective O - optical channel OC - photoreceiver PR ". It makes an electrical stop signal. A start signal is previously formed by SA by means of a zero-sensor (installed on a bar b axis).

Filling in a time interval $t_{B1} = B_1/\omega$, (where: B_1 - angle between the bar axis (zero-sensor direction) and direction SA – Sij (fig.3); ω - SA rotation rate) with pulses of reference frequency f_0, we shall receive a code $N_{B1} = t_{B1} \cdot f_0$. Rotation of SA cycle time $T_{2\pi 1} = 2\pi/\omega$ is simultaneously filled with same impulses of reference frequency f_0. The code $N_{2\pi 1} = T_{2\pi 1} f_0$ is formed. The angle $B_1 = 2\pi \cdot N_{B1}/N_{2\pi 1}$ is stored.

It is essentially to note, that this SA, or properly PSA (passive SA) as independent node have a very precise angle coordinates measurement accuracy. It can be used for navigation task as well as the static coordinates measurement (Tyrsa et al., 2004), for example for structural health monitoring of important civil engineering structures. Exactly, for inferior limit of stabilized reference oscillator of 1 MHz and scanning velocity of 1 rev per sec, consequently we have an exact measurement scale of 1,000,000 units for complete angle of 360˚. Even such resolution (0.00036˚ of angle) is an excellent for mentioned task. But it can be increased easy by reference frequency increase or scanner's velocity decrease.

When mirror SA has passed a direction towards point Sij, the laser is switched off to save power. The electric pulse goes to PL, the step-drive turns the laser with the collimator on an angle α_1 along horizon (fig.15, b). By approach of SA mirror M to the MR 'view sector' the laser is switched on. If the laser ray in its new position hits an obstacle, a new point of reflection is formed and the measurement is re-cycled. If the laser ray does not hit an obstacle, no reflection will be, and a new point will not be formed. In this case, as well as in case when a point of reflection exists, the formation of a code $N_{в2}$ begins with the signal of zero-sensor start pulse.

As soon as this code reaches some pre-determined value overlapping a range of possible code values corresponding to an operative sector, the counter, where codes N_{Bi} are formed, is installed on zero, and the laser is switched off. PL step-drive turns the laser on an angle α_2. Cycles with measurements of angles on reflection points, if these are formed by obstacles, or single cycles of scanning, when the obstacle is not present, are repeated in the same order. Values of angles Bi, in a cycle where reflection points took place, are stored. When the system PL stands in an extreme position *n*, stipulated by a minimum distance and a maximum angle of view, the bar positioning system step drive turns it round a horizontal axes by an angle β_1 (fig.15,a). The cycles with measurements of angles B_i are recurred. Angles α_i are fulfilled in the back order from a position *n* up to a position 0.

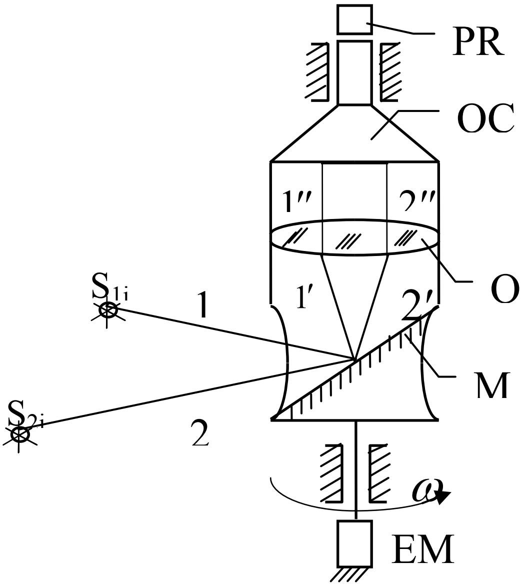

a)

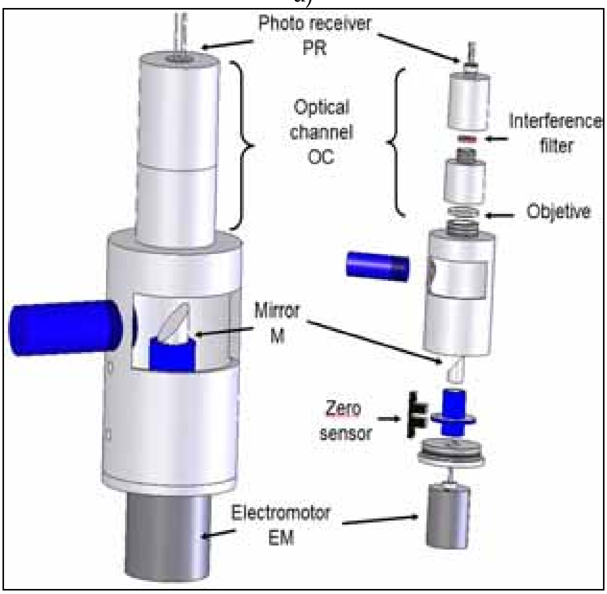

b)

Figure 16. Scanning aperture functioning principle (a), general design (b)

After some position of a plane, where the laser ray moves in the plan from the right to the left or reverse, all fixed laser rays hit a surface under research, making points of reflection S_{ij}. If in this case laser emission power and distance to points of reflection as well as sensitivity of the photoreceiver are sufficient for formation of stop pulses, empty cycles of SA scanning will not exist. The measurement cycles are repeated until the plane, formed by a horizontal axes of a bar b and the last point S_{ij}, deviates from a plane XOY by angle $\sum_{j=1}^{m}\beta_j$.

As mentioned above, data on angles B_{ij} measured will be accumulated in computer memory. One of these angles is shown on Fig.3. A related angle $C_{ij} = C_{\max} - \sum_{i=1}^{i}\alpha_i$, where C_{max} – is an initial angle of PL position. Angles C_{ij}, as well as angles $\sum_{j=1}^{j}\beta_j$, are fixed in memory simultaneously with the measured angles B_{ij} during each cycle.

Using the theorem of sines as well as correlation between the sides and the height in a triangle represented on Fig.17.

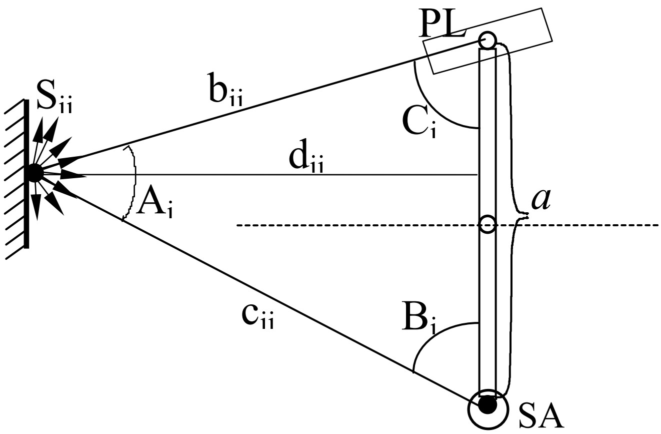

Fig. 17. Triangulation scheme for precise coordinates measurement

It is possible to find the formula for calculating sloping distances d_{ij} from basis *b* up to points highlighted by the laser

$$d_{ij} = a\frac{SinB_{ij}\cdot SinC_{ij}}{Sin\left[180^{\circ} - \left(B_{ij}+C_{ij}\right)\right]}, \quad (7)$$

where *a* - is basic distance between rotation axes of PL and SA. It is accurately enough pre-measured.

Using value of angles B_{ij} , C_{ij}, $\sum_{j=1}^{j}\beta_j$, and basis *a*, it is possible to calculate the Cartesian coordinates by each of the laser-highlighted points, in reference system OXYZ of MVS by the following formulas

$$x_{ij} = a \cdot \frac{SinB_{ij} \cdot SinC_{ij} Cos\sum_{j=1}^{j} \beta_j}{Sin\left[180^{\circ} - \left(B_{ij} + C_{ij}\right)\right]}, \tag{8}$$

$$y_{ij} = a \cdot \left(\frac{1}{2} - \frac{SinB_{ij} \cdot CosC_{ij}}{Sin\left[180^{\circ} - \left(B_{ij} + C_{ij}\right)\right]} \right) \text{at } B_{ij} \le 90^{\circ}, \tag{9}$$

$$y_{ij} = -a \cdot \left(\frac{1}{2} + \frac{SinB_{ij} \cdot CosC_{ij}}{Sin\left[180^{\circ} - \left(B_{ij} + C_{ij}\right)\right]} \right) \text{ at } B_{ij} > 90^{\circ}, \tag{10}$$

$$z_{ij} = a \cdot \frac{SinB_{ij} \cdot SinC_{ij} Sin\sum_{j=1}^{j} \beta_j}{Sin\left[180^{\circ} - \left(B_{ij} + C_{ij}\right)\right]}. \tag{11}$$

Thus, the onboard computer with the help of TVS provides digital map-description of the terrain in a MR sector of view in an actual time scale. If in a direction of observation any obstacles shaped as a dredging or as a big item above a surface (in these places points Sij are heaped), MR, with the help of vertical step drive PV, turns TVS by an angle $\sum_{i=1}^{n} \alpha_i$ To the left or to the right depending on a position of obstacles in relation with axis OX, and "searches" a new sector.

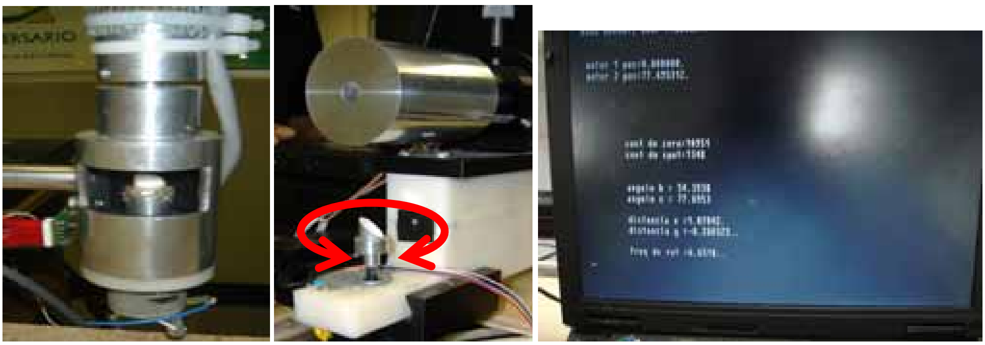

Fig. 18. Prototype parts (Scanning aperture; Emisor part (laser positioning system); and Software screen in function, taking epperimental data on obstacles

4.2 Prototype construction and experimentations

This prototype (Figs. 18 and 19) can be fabricated in very simple way using low-cost elements. A prototype was made with the follows elements: an aluminum base bar with 1m of length, step motors to make vertical and horizontal scanning, source of light in this case a laser, a pair of mirrors with 45 degrees cut to redirection the light beam, in laser emisor part and scanning aperture (Fig.18), a photo receiver to convert light signal to electrical signal, a lens in the aperture part to get a fine convergence of light in photo receiver, a sensor (start) in the aperture part to detect and count revolutions of mirror2, and a interference filter to get only the selected source of light; this hardware is controlled by a laptop IBM Pentium II using "turbo c" program in MS-DOS where the measurement distances is stored (Fig.18), the connection to transfer data between hardware and software is by parallel port. The complete prototype (Rivas et al., 2008) is no longer than 1m, data can be stored in another system, and the prototype fabricated with all elements is shown in Fig.19 in action.

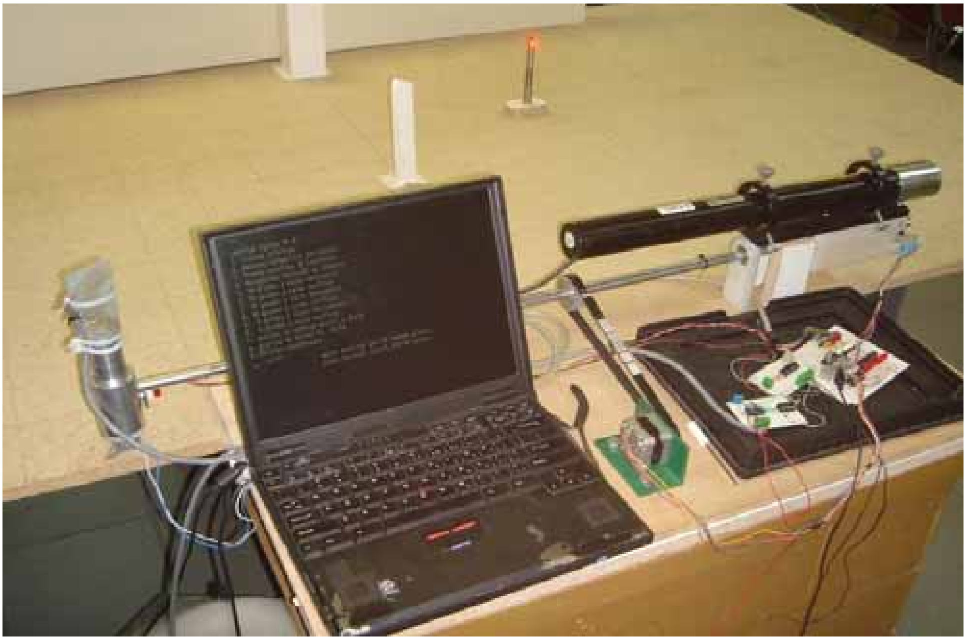

Fig. 19. Complete prototype system testing view.

This prototype was tested 100 times in different locations in grid nodes (see Figure 20) to verify accuracy on vision by different angles in 2D, making tests on reflective and absorptive objects; in Table 2 are partially shown the measurement values by the prototype on a plane surface with grid-scale.
The values in the table 2 are shown graphically in (Figure 20). The violet points are distance values taken by the prototype working usual way; the yellow points are distances measured by the prototype but using an independent source of light in each point to measure (without prototype laser), finally the real distances can be shown by squares in the table base.
As it is evident, the range of error is very small in the center of the table, this center is the center of the prototype sight, and near both sides of the prototype sight angle the error is minimal. This prototype is very similar to human sight, at front the image view is very detailed and precise, both borders of angle of view have no much accuracy, this can be resolved rotating the vision of focus of the prototype exactly humans sight do.
Analyzing the measurement results (Fig.20) and its numerical values (Table 2), it is possible to say that all the experiments were carried out not less at 95% confidence level. And measurement uncertainty, especially its offset error, not overcomes a 5% threshold in any point, even in extended angle of sight where such accuracy is not obligatory.

Test Point	Theoric Value				Measured Value			
	X (m)	Y (m)	B (°)	C (°)	*x(m)*	*y(m)*	*B (°)*	*C (°)*
B	120	120	120,26	35,22	124,21	128,68	123,43	34,8
D	100	100	116,57	33,69	99,83	104,48	118,46	32,87
F	100	80	106,70	37,57	95,3	76,86	106,4	36,91
H	120	60	94,76	47,49	122,92	63,49	96,38	47,28
J	80	60	97,13	36,03	77	58,62	96,57	35,33
L	80	40	82,87	41,63	79,99	42,15	84	40,95
N	120	40	85,24	53,13	119,86	40,04	84,48	53,08
O	120	20	75,96	59,74	119,22	19,48	76,01	59,76
P	100	20	73,30	55,01	97,6	19,15	72,94	54,67
Q	80	20	69,44	48,81	79,11	18,7	68,39	49,04
R	60	20	63,43	40,60	60,33	21,7	64,3	40,07
S	40	20	53,13	29,74	39,14	19,59	52,07	29,35
T	40	0	38,66	38,66	36,52	1,06	36,52	36,73
U	60	0	50,19	50,19	59,8	0,9	49,39	50,625
V	80	0	57,99	57,99	80,93	3,49	56,7	60,11
W	100	0	63,43	63,43	103,58	1,51	63,45	64,68
X	120	0	67,38	67,38	120,72	-4,7	66,23	69,43
Y	120	-20	59,74	75,96	118,54	-18,36	59,95	75,05
Z	100	-20	55,01	73,30	96,72	-18,37	54,7	71,9
A1	80	-20	48,81	69,44	75,79	-18,33	48,03	67,32
B1	60	-20	40,60	63,43	58	-18,53	39,5	61,52
C1	40	-20	29,74	53,13	36,17	-20,31	27,3	50,62
D1	60	-40	33,69	80,54	58,05	-38,63	33,6	78,92
E1	80	-40	41,63	82,87	77,46	-38,26	40,46	81,38
F1	100	-40	48,01	84,29	97,1	-38,02	46,94	82,96
H1	120	-60	47,49	94,76	123,68	-61,03	48,21	95,09
J1	80	-60	36,03	97,13	78,9	-59,73	35,37	97,03
L1	80	-80	31,61	110,56	80,52	-80,21	31,81	110,56
N1	120	-80	42,71	104,04	121,01	-78,73	43,34	103,35
P1	100	-100	33,69	116,57	101,65	-96,18	35,06	114,43
R1	100	-120	30,47	124,99	111,73	-126,15	32,09	124,27

Table 2. Experimental results of point-coordinates measurement (Rivas et al., 2008)

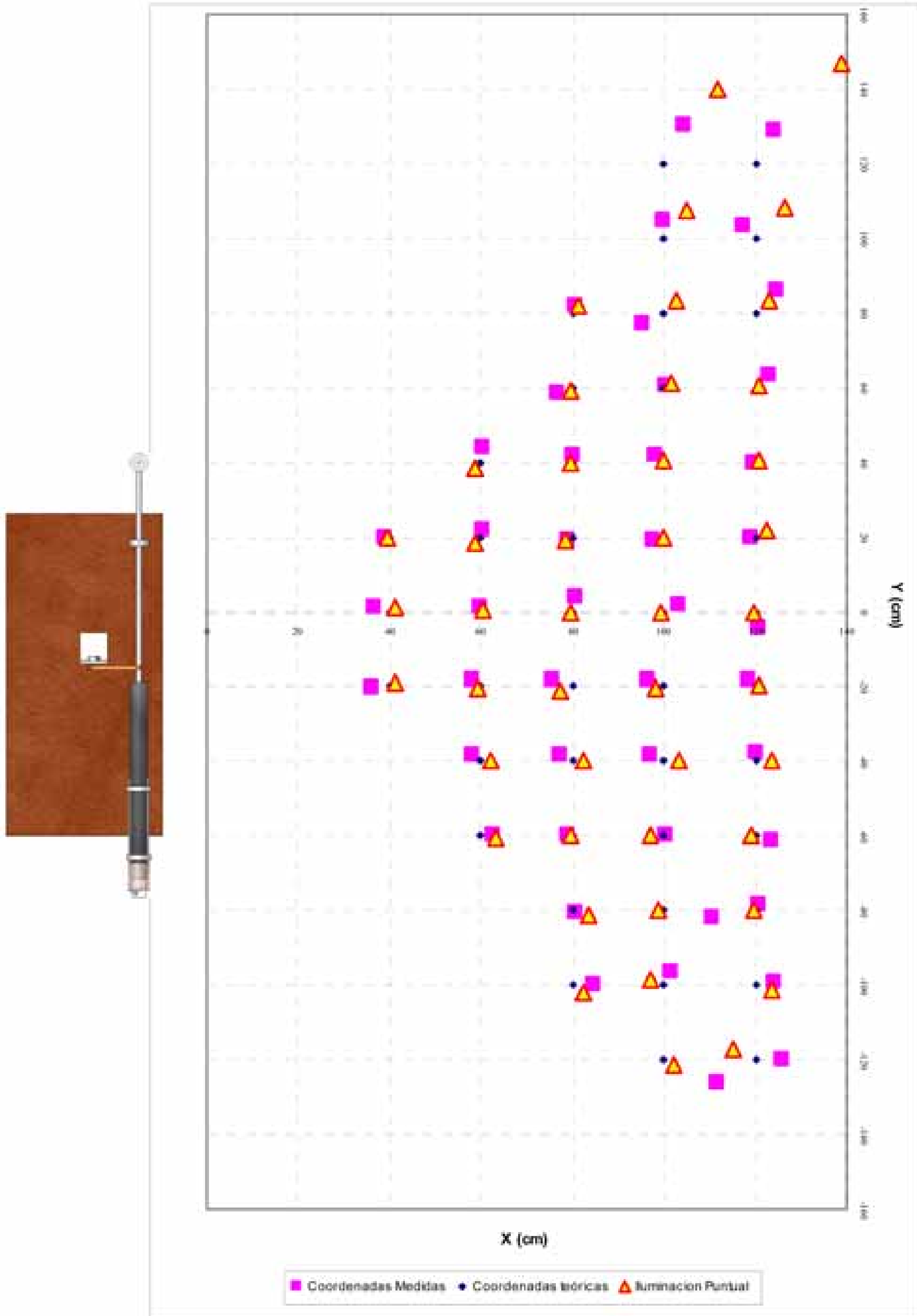

Fig. 20. Experimental graphic of 2D points measurement and obstacle positioning

Also detailed analyzis of scanning aperture original construction (Fig. 16, 18) and principle deduce us to conclusion that it is possible to obtain measurement results with the same uncertainty from highlighted points of the different attitudes inside precertain angle of view. It is significant advantage of the presented device over other known laser triangulation scanners (Forman & Parry, 2001), (Pierce et al., 1992), (Surmann et al., 2003). In general behavior of uncertainty repeats graphic presented on Figure 6 in (Pierce et al., p. 1765, 1992), however accuracy nearby edge in our system is more advanced. Also accuracy (coordinate measurement offset) in a central part of scanner's angle of view is 2-7 times better in a different checked points respect to (Pierce et al., 1992) for example.

4.3 Prototype application for static monitoring

The above-described passive scanning aperture (Figs. 16 and 18) (PSA) independently can be able for static object deformation monitoring (Tyrsa et al., 2004). PSA, or POS (passive optical scanner), using the vertical axis of rotation is destined for the measurement of the horizontal angles. Let's call it a vertical POS. The vertical angles between the "emissive beacons"(EBs) are measured by the POS with the horizontal axis of the rotation. This POS is the horizontal POS. The system, which consists of the vertical and horizontal POSs, permits to measure the displacement of the EB in horizontal and vertical planes.
Fig.2 shows the adoption of the horizontal POS for the realization of the bridge points monitoring in a vertical plane.

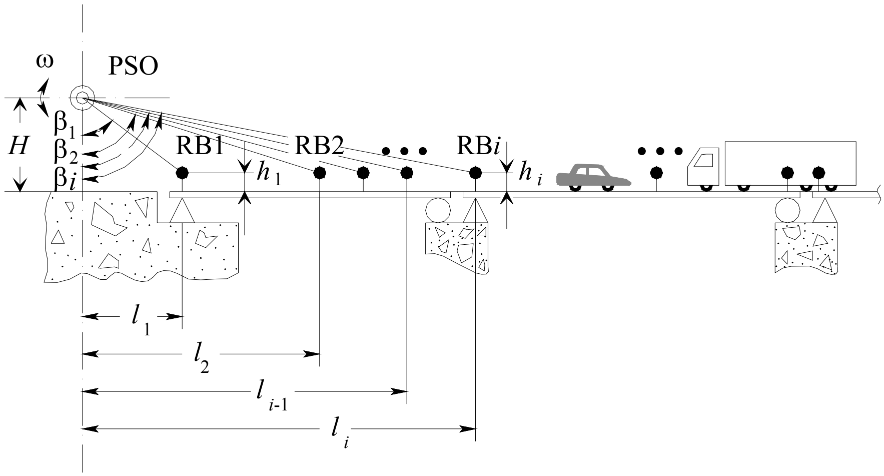

Fig. 21. Horizontal POS placement for bridge monitoring

The POS is placed outside the bridge and measures the vertical angles β_i . The EBs are installed with the same height h_i above the bridge surface. As EB it is possible to use any sufficiently cheap light source, for example mentioned above lamp HRQ3010-5071. The distances l_i are measured during the installation of the EB.
In the absence of a deformation, for each EB_i, the following expression is valid:

$$\frac{H-h}{l_i} = \tan(\frac{\pi}{2} - \beta_i) \tag{12}$$

For the bridge deformation with the magnitude Δh_i in the placement point of the beacon EB_i, the angle β_i, measured by the POS, will change on the magnitude $\Delta\beta_i$. As a result the expression (13) will receive the form:

$$\frac{H - h \pm \Delta h}{l_i} = \tan(\frac{\pi}{2} - \beta_i \pm \Delta\beta_i) \tag{13}$$

Therefore:

$$\Delta h_i = (H - h) - l_i \tan(\frac{\pi}{2} - \beta_i \pm \Delta\beta_i) . \tag{14}$$

In a similar manner the POS for tunnel monitoring is installed. In extended tunnels several functionally connected POS can be placed along its axis.

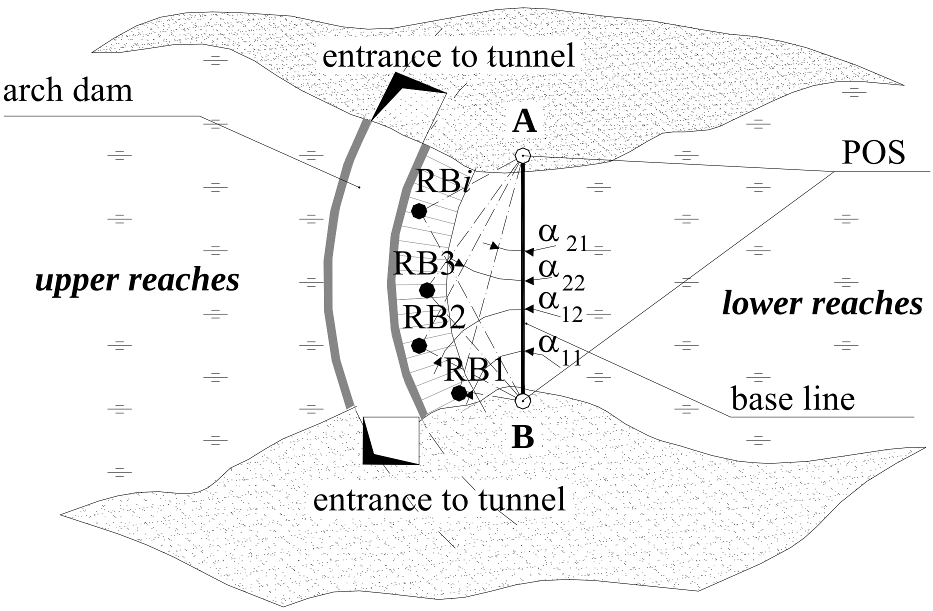

Fig. 22. Placement of two vertical POSs for arch dam monitoring.

Fig. 22 shows the placement of two vertical POSs for the arch dam monitoring of a hydroelectric power station. The POSs measure in pairs the horizontal angles α_{1i} and α_{2i} between the base line AB and the EB_i. The length of the base line D and the Cartesian coordinates of the POS are determined beforehand by known geodetic methods. The angles $\angle EB_i$ are found by the formula:

$$\angle RB_i = 180^\circ - (\alpha_{1i} + \alpha_{2i}) . \tag{15}$$

According the sine theorem we find the triangles sides, which have the vertex A, B, EB_i ; and the coordinates x_i, y_i of the points EB_i, in the national system or conditional Cartesian coordinate system. The change of coordinates of the points RB_i in the repeated measurements of the angles α_{1i} and α_{2i} reveal the dam deformation.

5. Conclusions

Presented research was provided with a general goal to design simple and secure method for 3D laser scanning of any unknown surface placed on a variable distance from scanner location. Other advantage of a present system over other laser triangulation system is a higher in principle order of exactitude in a part of 3D coordinates calculation. Preliminary prototype testing is shown

- This theoretical principle can be realized with modern electronic and electromechanic devices in low cost;
- With completely acceptable operation velocity this device can detect an obstacle and to cover it with digital 3D map of *n* points on it's surface;
- This factor *n* is easy possible to change as only one variable in software; such way provide basic principle "more points – less uncertainty, but more operating time". This task must be solved carefully for each practical application;
- Coordinates calculation uncertainty is less than any known laser triangulation with electronic scanning because of exact surveying techniques principle using;
- This system in a closest way simulates the human binocular vision; as shown, the best exactitude can be achieved in a center of angle of view, and nearby both edges the picture is not has so sharpness. It possible to overcome by base bar rotation;
- These techniques can be implemented with insignificant changes for various practical applications, such as large engineering structures Structural Health Monitoring, mobile robot navigation, microsurface inspections, etc.

6. References

Allen, D.; Park, G.; & Farrar, C. (2005). Overview of Wireless Active Sensing Systems for Structural Health Monitoring, In *Structural health monitoring*, Fu-Kuo Chang, page numbers (1578-1585), DEStech Publications, ISBN: 1-932078-51-7

Athavale, N.; Ragade, R.; Cassaro M.; & Fenske, T. (1990). *A prototype for KYBAS: the Kentucky Bridge Analysis System.* Proceedings of the 3rd international conference on Industrial and engineering applications of artificial intelligence and expert systems, pp. 781-789, Vol. 2, 1990

Baltsavias, E. P. (1999), a. A comparison between photogrammetry and laser scanning. *ISPRS Journal of Photogrammetry & Remote Sensing*, Elsevier, Vol. 54, (July 1999) page numbers (83–94)

Baltsavias, E. P. (1999), b. Airborne laser scanning: basic relations and formulas. *ISPRS Journal of Photogrammetry & Remote Sensing,* Elsevier, Vol. 54, (July 1999) page numbers (199–214)

Bellian, J. A.; Kerans, C. & Jennettem, D. C. (2005). Digital outcrop models: applications of terrestrial scanning lidar technology in stratigraphic modeling. *Journal of* *sedimentary research*, SEPM , Vol. 75, No. 2, pp. 166–176, ISBN 1527-1404/05/075-166, march, 2005

Benedetti, M.; Donelli, M.; Massa, A. & Rosani. A. (2004). *An innovative microwave imaging technique for non destructive evaluation: applications to civil structures monitoring and biological bodies inspection. IEEE Proceedings of International "Imaging Systems and Techniques, (IST-2004)"*,(may 2004) page numbers (91 – 94)

Chaumette, F. & Hutchinson, S. (2006). Visual servo control PART I: basic approaches. *IEEE Robotics & Automation Magazine*, December 2006, pp.82-90.

Chellappa, R.; Roy-Chowdhury, A. K. & Zhou, Sh. K. (2005). *Recognition of humans and their activities using video.* Morgan & Claypool Publishers, ISBN 1598290061

Diosi, A. & Kleeman, L. (2005). Laser scan matching in polar coordinates with application to SLAM. *Proceedings of IEEE/RSJ International Conference on Intelligent Robots and Systems (IROS 2005)*, pp. 3317- 3322, ISBN: 0-7803-8912-3, august 2005

França, J.; Gazziro, M.; Ide, A. & Saito, J. (2005). A 3D scanning system based on laser triangulation an variable field of view, *Proceedings of the 2005 International Conference on Image Processing (ICIP 2005),* pp. 425-428, IEEE Volume 1, Italy, 2005, Genoa

Forman, P. & Parry, I. (2001). Rapid Data Collection at Major Incident Scenes using Three Dimensional Laser Scanning Techniques. *2001 IEEE 35th International Carnahan Conference on Security Technology*, pp. 60-67, october 2001

Hada, Y. & Takase, K. (2001). Multiple Mobile Robot Navigation Using The Indoor Global Positioning System (iGPS). *Proceedings of IEEE/RSJ International Conference on Intelligent Robots and Systems,* Vol. 2, pp. 1005-1010, ISBN: 0-7803-6612-3, USA, Maui, HI, 10/29/2001 - 11/03/2001

Hancock, J. ; Langer, D.; Hebert, M.; Sullivan, R.; Ingimarson, D.; Hoffman, E.; Mettenleiter, M. & Fredlich, C. (1998). Active Laser Radar For High-Performance Measurements, *IEEE International Conference on Robotics & Automation*, pp 1465-1470, Belgium, Leuven, 1998

Handbook of Optical and Laser Scanning. (2004).Edited by Gerald F. Marshall, 769 p., ISBN: 0-8247-5569-3, Marcel Dekker, Inc., New York – Basel, 2004

Hosmer, P. (2004). Use of Laser Scanning Technology for Perimeter Protection. *IEEE Aerospace and Electronic Systems Magazine*, vol. 19, page numbers (13-17), 2004

Ibeanusi, U.; Lafond-Favieres, V. ; McLawhorn, L. & Anderson, S. (1999). Understanding robot navigation and control, Proceedings of the 37th annual *ACM Southeast Regional Conference*, 7p, CD version, 1999

Itti, L. & Baldi, P. (2005). A principled approach to detecting surprising events in video. *Proceedings of IEEE CVPR2005,* pp. 631- 637, vol. 1, International Conference on Computer Vision and Pattern Recognition, 20-25 June 2005

Kee, C.; Park, B.; Kim, J.; Cleveland, A.; Parsons, M. & Wolfe, D. (2008). A Guideline to Establish DGPS Reference Station Requirements. *The journal of navigation. Royal Institute of Navigation-Cambridge Journals* (2008), 61, page numbers (99–114)

Lavelle, J. P. ; Schuet, S. R. & Schuet, D. J. (2004). High Speed 3D Scanner with Real-Time 3D Processing. *Proceedings of ISA/IEEE Sensors for Industry Conference*, pp.102- 108, ISBN: 0-7803-8143-2, 2004

Lichti, D. D. ; Stewart, M. P.; Tsakiri, M. & Snow, A. J. (2000). Benchmark tests on a Three-Dimensional Laser Scanning system. Department of Spatial Sciences of Curtin University of Technology, Geomatics Research Australasia, 23 p., 2000

Liu, F.; Bhakar, S.; Fevens, T. & Mudur, S. (2006). Environment Lighting for Point Sampled Geometry. *Proceedings of International Conference on Computer Graphics, Imaging and Visualisation (CGIV'06)*, pp. 522-527, 2006

Liwen Dai, Jinling Wang, Rizos, C. & Shaowei Han. (2002). Pseudo-satellite applications in deformation monitoring. *GPS Solutions Journal, Springer Berlin / Heidelberg,* Vol. 5, No 3, (January, 2002), page numbers (80-87), ISSN: 1080-5370 (Print) 1521-1886 (Online)

Mallet, L.; Lee, B.; Staszewski, W. & Scarpa, F. (2004). Structural health monitoring using scanning laser vibrometry: II. Lamb waves for damage detection. *IOP electronic journals*; *Smart Mater. & Struct.*, 13, (2004), page numbers (261-269)

Mordohai, P. & Medioni, G. (2006). *Tensor Voting: A Perceptual Organization Approach to Computer Vision and Machine Learning*, Morgan & Claypool Publishers, ISBN: 1598291009

Noll, R. & Krauhausen, M. (2003). Multibeam laser triangulation for the measurement of geometric features of moving objects in production lines. *Conference on Lasers and Electro-Optics Europe CLEO/Europe,* p. 468, ISBN: 0-7803-7734-6, 22-27 June 2003

Ohno, H.; Naruse, H.; Kurashima, T.; Nobiki, A.; Uchiyama, Y. & Kusakabe, Y. (2002). Application of Brillouin Scattering-Based Distributed Optical Fiber Strain Sensor to Actual Concrete Piles. *IEICE TRANSACTIONS on Electronics*, Vol. E85-C, No.4, (2002), page numbers (945-951)

Peng-Hsiang Weng & Fu-Jen Kao. (2004). Modulation Based Time Resolved Laser Scanning Microscopy. *The Second Asian and Pacific Rim Symposium on Biophotonics, APBP 2004,* pp.97- 98, ISBN: 0-7803-8676-0, december 2004

Petrov, M.; Talapov, A.; Robertson, T. Lebedev, A.; Zhilyaev, A. & Polonskiy, L. (1998). Optical 3D Digitizers: Bringing Life to the Virtual World. *IEEE Computer Graphics and Applications,* Vol., 18, (May/Jun 1998), page numbers (28-37). Issue: 3, ISSN: 0272-1716

Pierce, D.S.; Ng, T.S. & Morrison, B.R. (1992). A Novel Laser Triangulation Technique for High Precision Distance Measurement, *Proceeding of IEEE Industry Aplications Society Annual Meeting,* vol.2, pp. 1762-1769, USA, october, 1992, Houston

Retscher, G. (2007). Test and Integration of Location Sensors for a Multi-sensor Personal Navigator. *The Journal of Navigation*, 60 (1), page numbers (107–117)

Rivas, M.; Sergiyenko, O.; Aguirre, M.; Devia, L.; Tyrsa, V. & Rendón, I. (2008). Spatial data acquisition by laser scanning for robot or SHM task. *Proceeding of IEEE/IES International Conference ISIE-2008 pp.*1458-1463, ISBN 978-1-4244-1666-0, UK, Cambridge, 30June – 2 July, 2008

Riza N. A. & Muzammil, A. A. (2003). Code-multiplexed optical scanner, In: *Applied Optics*, vol. 42, pp. 1493-1501, 2003

Sadayuki Tsugawa. (1994). Vision-Based Vehicles in Japan: Machine Vision Systems and Driving Control Systems. *IEEE Transactions on industrial electronics*, Vol. 41, No. 4, pp.398-405, august, 1994

Sahba, K.; Alameh, K. E. & Smith, C. (2006). A Proposed Motionless Laser Scanning Architecture for Perimeter Security. *Proceedings of 40th ICCST2006*, pp. 9-16, ISBN: 1-4244-0174-7, Lexington, KY, October 17, 2006

Slob, S. & Hack., R. (2004). 3D Terrestrial Laser Scanning as a New Field Measurement and Monitoring Technique, In: *Engineering Geology for Infrastructure Planning in Europe*, *Springer Berlin*, page numbers (179-189), Heidelberg

Selectes papers on CCD and CMOS imadges. (2003). SPIE Press Bellingham, editor Moon Gi Kang, General editor Brian J.Thompson,Vol. MS177, 636p., ISBN 0-8194-5114-2 USA, Washington, 2003

Soini, A. (2001). Machine vision technology take-up in industrial application. *Proceedings of the 2nd International Symposium on Image and Signal Processing and Analysis ISPA,* pp. 332-338, ISBN: 953-96769-4-0, Pula, Croatia

Steinle, E. & Vogtle, T. (2000). Effects of different laser scanning modes on the results of building recognition and reconstruction. *International Archives of Photogrammetry and Remote Sensing*, 2000 - www-ipf.bau-verm.uni-karlsruhe.de. 8p.

Stewart, M. P. & Tsakiri, M. (2002). The Application of GPS to Dam Surface Monitoring. *Journal of Geospatial Engineering*, Vol.3, No.1, page numbers (45-57)

Stutz, G. (2005). Guiding Light, *SPIE's magazine*, vol. 5, page nnumbers (25-27), 2005

Surmann, H.; Lingemann, K.; Nuchter, A. & Hertzberg, J. (2003). A 3D laser range finder for autonomous mobile robots. *Robotics and Autonomous Systems, Issues 3-4,* vol. 45, pp. 181-198, december 2003

Tao Dai; Xiang Chen; Drake, R. & Jun Yang. (2005). Vision Sensor Based Tracking and Focusing of 3-D Singular Points. *Proceedings of 2005 IEEE International Conference on Mechatronics and Automation,* Vol. 3, pp. 1312-1317, ISBN: 0-7803-9044-X, Canada, 2005, Niagara Falls, Ont.

Tunstel, E. (1995). *Fuzzy spatial map representation for mobile robot navigation.* Proceedings of the 1995 ACM symposium on Applied computing, pp. 586 – 589, ISBN:0-89791-658-1, USA, (1995), Nashville, Tennessee

Tyrsa, V.E.; Burtseva, L.; Rivas Lopez, M.; & Tyrsa, V.V. (2004) Monitoring of civil engineering structures. *Proc. of SPIE Int. Conf. Health monitoring and smart nondestructive evaluation of structural and biological systems III, 5394*, pp. 485-492, USA, 2004, San-Diego

Tyrsa, V. Ye.; Sergiyenko, O.; Burtseva, L.; Bravo-Zanoguera, M.; Devia, L.; Rendon, I. & Tyrsa, V. V. (2006), a. Mobile Transport object control by technical vision means. *Proceeding of IEEE International Conference CERMA2006*, Vol. II, p.74-79, ISBN: 0-7695-2569-5/ ISBN13 978-0-7695-2569-3, Mexico, Cuernavaca, September 2006

Tyrsa, V.Ye.; Sergiyenko, O.Yu.; Tyrsa, V.V.; Bravo, M.; Devia, L. & Rendon, I. (2006), b. Mobile Robot navigation by Laser Scanning Means. *Proceeding of 3rd International "Conference on Cybernetics and Information Technologies, Systems and Applications CITSA – 2006"*, Vol. I, p. 340-345, ISBN: 980-6560-82-5 (collection)/ 980-6560-83-3 (volume I), USA, July 20-23, 2006, Orlando, Florida

Vang, L.; Emura, T. & Ushiwata, T. (2000). Automatic Guidance of a Vehicle Based on DGPS and a 3D Map, *Proceedings of IEEE Intelligent Transportation Systems*, pp.131-136, ISBN: 0-7803-5971-2, USA, october 2000, Dearborn, MI

Wehr, A. & Lohr, U. (1999). Airborne laser scanning—an introduction and overview. *ISPRS Journal of Photogrammetry and Remote Sensing,* Elsevier, Vol. 54, Issues 2-3, (July 1999) page numbers (68-82) et al.,

Winkelbach, S.; Molkenstruck, S. & Wahl, F. (2006). Low-cost Laser Range Scanner and Fast Surface Registration Approach. *Proceedings of DAGM 2006, Springer Berlin Heidelberg*, (2006) page numbers (718-728)

Yu, H.; Aguado, E.; Brodin, G.; Cooper, J. ; Walsh D. & Strangeways H. (2008). UWB Positioning System Design: Selection of Modulation and Multiple Access Schemes. *The Journal of Navigation*, 61, page numbers (45–62)

SHM Structural Health Monitoring

Optoelectronic Method for Structural Health Monitoring

M. Rivas Lopez,[1,2] O. Yu. Sergiyenko,[1,*] V. V. Tyrsa,[1] W. Hernandez Perdomo,[1] L. F. Devia Cruz,[1] D. Hernandez Balbuena,[1] L. P. Burtseva[1] and J. I. Nieto Hipolito[1]

[1]*Engineering Institute of Autonomous University of Baja California Blvd. Benito Juarez, Calle de la Normal S/N Col.Insurgentes Este 21280 Mexicali, BC, México*
[2]*Polytechnic University of Baja California, Mexico*

Important engineering constructions require geometrical monitoring to predict their structural health during their lifetime. Monitoring by geodetic devices, vibration-based techniques, wireless networks or with GPS technology is not always optimal; sometimes it is impossible as shown in this article. A method based on geodetic measurements automation applying local optical scanners for monitoring is proposed. Its originality and contribution is based on the novel method of precise measurement of plane spatial angles. It considers robust invariant AD-conversion angle-to-code for dynamic angle, signal energetic center search method, initial reference scale adjustment, and uncertainty decrease using mediant fractions formalism for result approximation. An algorithm of electromechanic parts interaction for spatial angle encoding with beforehand set accuracy is described. It is shown that by its nature it is appropriate for practically unlimited uncertainty reduction: it is only limited by reasonable ratio "uncertainty/operation velocity". The operation range, accuracy, scanner operation velocity, and its adaptation to objects are determined and described. The experimental results confirm that optical device of presented passive scanning aperture overcomes all recently known compared optical devices for 3D coordinates recognition in a part of offset uncertainty. It is shown that the presented optoelectronic scanning aperture is a universal tool for various practical solutions.

Keywords optical instruments · scanning aperture · solid angle · surface figure measurement · measurement result rational approximations · mediants

1 Introduction

Several of important engineering structures like bridges, electric plants, tunnels, historical buildings, dams, etc. require observation of their integrity and deformation throughout their operation time. Usually, this observation is called structural health monitoring (SHM). The structure deformation is observed by the periodic determination of their reference point coordinates, fixed on an object. In this

*Author to whom correspondence should be addressed.
E-mail: srgnk@iing.mxl.uabc.mx
Figures 1 and 4–7 appear in color online: http://shm.sagepub.com

Vol 9(2): 105–16
[1475-9217 (201003) 9:2;105–16 10.1177/1475921709340975]

framework, nowadays, we are using various techniques for SHM. From the classics of geometrical and trigonometrical leveling up to the GPS NAVSTAR technologies are used. In the present work, on the basis of cross-comparing of advantages and limitations of the several approaches to the SHM task, we introduce a new method of optical scanning with posterior analytic information processing for precise measurement of 3D coordinates convenient for continuous monitoring of large volume constructions. This method proposes an optimal trade-off between exactitude, own low price, and operating range in real time.

This article is arranged as follows, the next section presents the analysis of existing approaches to structural health monitoring and surface recognition, and on the basis of their common shortcomings are defined desirable properties of the system under construction. Section 3 presents the problem formulation and stated requirements to the desired system; in Section 4, we describe the system design, and also explain the advantages of spatial angle measurement for precise resolution of 3D coordinates and introduce the mathematical formalism of Farey fractions as a tool for it. In Section 5, we present calculations of the most important operational parameters of the designed system. In Section 6 are shown both adoptions of the proposed system for bridge and dam/tunnel monitoring. Section 7 introduces the concept of energetical center search (ECS), which permits sufficient increase in spatial resolution of the optical scanner in the case of significant striking distance. The results of system control experiments for the measurements of target location are presented in Section 8. Conclusions are finally given in Section 9.

2 State-of-art

Let us try to classify these SHM methods for better problem understanding and verification of their advantages and shortcomings. This analysis has to be useful for the final design of the structural monitoring system. It should present clear understanding of the limitations that are critical, and, alternatively, discuss which system properties are strongly recommended for optimal final design. Such an analysis has been partially presented in [42] and [43]. In general, in our opinion, all these methods of Civil Engineering Objects Structural Health Monitoring can be grouped into four groups:

- Vibration-based and time-frequency wave propagation damage detection methods [1–6];
- Wireless remote sensor networks [7–10];
- Embedded fiber-optics sensors and networks [10–13];
- Optical inspection methods and optoelectronic scanning [14–17,37].

The first one is the most advanced and well-investigated branch recently. There are various localized experimental methods such as acoustic or ultrasonic methods, magnet field methods, radiographs, eddy-current methods and thermal field methods. Most of the papers on this group of SHM represent reports about adaptive and self-calibrating networks of strain sensors for monitoring the deformation of concrete poured highway structures, usually well-known bridges (Z24-bridge [2], Ashidagawa or Kishwaukee bridges [3], I-40 Bridge [4], etc.). As the rule, there are wire networks. These methods are strong tools for any internal and external damage detection during the early stages. However, all these methods provide too much information in an indirect form. Complex algorithms are used for object structural health verification. These algorithms: (1) have been processed over extended time, and (2) cannot completely exclude invalid interpretation of damage type and localization. But in a case of integrity monitoring of large engineering structures, first of all, we are interested in a fast and accurate detection of pre-disaster situation at the early stages. It can give only fixed information about directed and continued movement of all reference points set and not about small local displacement of material. In this case the above- mentioned techniques are not very efficient tools.

In the wireless active SHM hardware, most off-the-shelf solutions currently available have a deficit in processing power that limits the complexity of the software and the SHM process that can be implemented. Also, many integrated systems are inflexible because of tight integration between the embedded software, the hardware, and sensing [18, p. 1583]. Current damage-detection methods for the ‘‘wireless group’’ is the most recent and promising branch of SHM. Therefore, there is not enough statistical information about security and reliability of such nets. But it is logical to note that for thousands wireless sensors in the case of a large object, we need the same thousands of independent radio channels. This structure is very complex to operate and, very sensitive to any kind of electromagnetic noise. For example, in a case of bridge monitoring by system [8] the main problem can occur because of using cellular phones on this bridge.

Fiber optics embedded nets can be very efficient for initial point damage recognition. Any internal microdisplacements of material can be detected with extremely high accuracy by destroyed wavelet or sensor location. But this solution also isn't a perfect solution for our task. Firstly, it can be applied only for new constructions, by "embedding" at creation stage. For historic buildings, or for already existing bridges, tunnels, etc. this method is inapplicable. Another important question in articles in this field is a question about the influence of fiber-optical embedded nets on properties of constructional material durability. And finally, we can note that this group of materials is not very economical in power consumption, especially with enhancement of monitored object volume.

The optical inspection methods and optoelectronic scanning were developed in 1970–1980s, parallely with surveying techniques. Further achievement was stopped because of natural limitations of hardware capacity and accuracy. Also during this time intensive development of various remote sensors started. But in the last 20 years technical parameters (especially technical reliability and accuracy) of electromechanic systems, as well as laser sources and optical sensing developed essentially. So, we are considering that it is reasonable to use the properties of optical systems. Some studies in this branch of SHM [14,15] offer many interesting ideas. But unfortunately, these systems do not have technically completed solutions [15], or are not convenient for automation in the proposed form [14].

Thus, we can conclude that SHM is a prospective technical branch, which is being actively developed now, using various methods. We are considering that the best results can be obtained by synthetic SHM-techniques, which combine most competitive skills of various technical solutions.

Also, it is reasonable to take to account some achievements of other technical systems that are not directly dedicated to SHM, but have some very useful properties that could develop our understanding of the problem decision.

For such properties or existing completed solution overview, it is necessary to observe other techniques.

For the last 20 years, laser scanning systems are being used successfully in the field of 3D-object visualization and recognition, which uses unique properties of laser rays for surface highlighting. These properties are: fixed frequency of light emission, and correspondingly response; high ability of scanning element to be focused, spatially compressed; well-known methods of the noise protection of optical channel.

On the other hand, there exist "laser scanning systems", which usually use one laser source and one camera [19,20]. The difference between various systems is only in the laser emission power, camera resolution, and the price. However, according to their geometry, such systems need a "reference background base" (geometric standard for dimensions measurement) [19]. These systems are not acceptable for SHM because of the natural difficulties with such "reference background". Also, the triangulation principle is a rule based on only one angle measurement, and therefore this is a cause of additional systematic error. On the other hand, these systems prove that the laser rays have many properties useful for recognition of spatial coordinates, which do not possess any other scanning element.

The next advanced step in the field of spatial coordinate's determination is terrestrial laser scanners. 3D terrestrial laser scanning is a relatively new, but already revolutionary, surveying technique [21,22]. The survey yields a digital data set, which is essentially a dense "point cloud" where each point is represented by a coordinate in 3D space. The most important advantage of the method is that a very high point density can be achieved, in the order of 5 to 10 mm resolution. But this technique is designed for large area observation from a relatively long distance [22].

And resolution of 5–10 mm is practically 3D-coordinates measurement error. For surveying tasks it has been corrected at the surface reconstruction stage (Delaunay triangulation, Voronoy diagrams, NURBS, Fast RBF, etc.), but for SHM this error is not acceptable. Because of the reconstruction, algorithms have a probabilistic character. Moreover, for this kind of a task, 3D terrestrial laser scanners use very expensive units, like super-power laser source, supersensitive receivers, etc. So, as the conclusion we can say that terrestrial laser scanners is a good tool for surveying tasks, not for SHM.

We can find another interesting solution [23] in a group of spatial surface scanning by the structured light (not only lasers!). But the maximum unambiguous range of such systems is essentially limited by usual light sources. It cannot be sufficiently localized and focused on a long distance.

Sometimes, SHM tasks use GPS- and, especially, DGPS-technologies (with special pseudosatellite as additional "terrestrial reference point" for accuracy enhancement). However, these techniques are still too expensive. Also the GPS technology cannot be used outside the radio signal receiving zone such as tunnels, mines, etc.; in this case, it is possible to provide only traditional geodetic means. Geodetic tools using the structure in a process has a low productivity and frequently it is associated with difficulties. The controllable object vibrations, transport movement, etc. inevitably cause some systematic errors or even damage during the functioning of geodetic devices. Sometimes the operator of geodetic devices cannot be located in a working zone (radioactivity, strong electromagnetic fields, chemical pollution, etc.).

This is one of the reasons for automated geodetic measurement tools development.

3 Problem Formulation

The main idea of this work is to monitor the progress of recent stage of the electronic, optic, electromechanic techniques progress, and modern computing capacity to design the novel system for objects monitoring. Taking into account that such a system must to possess some advantages of the above-mentioned techniques, but not their lacks.

We suppose that the other advantages can be useful for exact, robust, secure and low-price system:

- remote systems like various wireless sensor nets presented in references overview. The sensing part and the analyzing part must be distanced and electrically independent of each other;
- present total information about object statement in a form convenient for storage and mathematical treatment. It must to be easy to compare recent object data with any previous stage for professional analysis;
- register small deformation of the structure at the earliest stage and to show clearly the general character of this deformation.
- provide control with minimal reference points and have very short and clear algorithm of estimation. In other words, the deformation estimation must be sufficient, but not redundant. Like optical control methods, it must give fast and clear response.
- adaptable to its fast and non-destructive installation on the controlled object. It must not influence any own object properties.

On this basis, the automatic monitoring system would be created.

4 Plane Angles Automatic Measurement

Any spatial location of the point in 3D can be represented by polar coordinates (radial distance and two plane angle projections) in Cartesian coordinates introduced by Rene Descartes. This postulate is the basis of spatial coordinates determination by now. It is evident that the same unique spatial location of the point can be described using the third plane angle projections instead of the radial distance. This circumstance explains why the central question of geodetic surveying is the angle measurement method. To measure the direction to any certain point always is faster and more precise than to measure the distance up to the same point [43]. This is a point why we are focused in precise spatial angle measurement and its uncertainty reduction for our task solution. This is the key for adequate estimation of slow/fast 3D coordinates changes in a real time system.

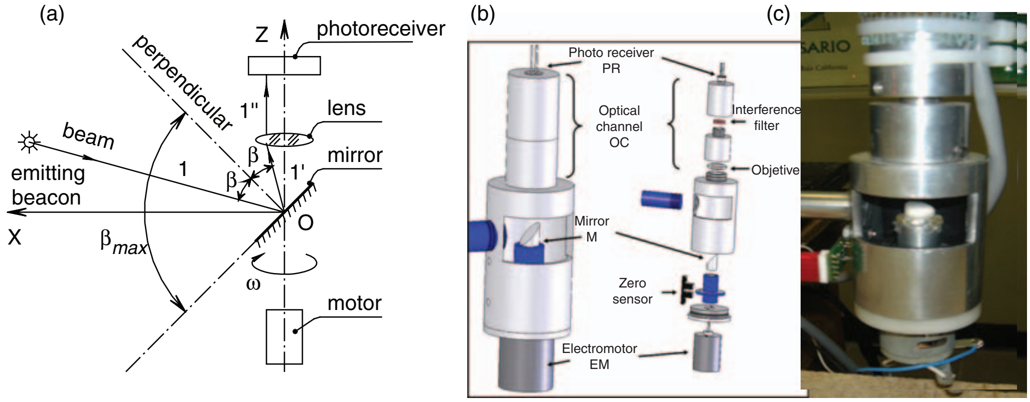

Figure 1 POS operating principle (a) and a prototype design (b,c).

Usually in geodetic practice, angles and distance measurement tools are used. Up to Bergstrand's invention of a range finder in the middle of the 20th century [24], the geodesy basic tools were: a theodolite, a surveying tape and a level. In many cases, for the vertical surveying, a level can be replaced with a theodolite with additional distance reference; such an operation is called a trigonometric leveling. A theodolite was invented by Leonard Digges in 1571; and its principle was kept up to the present time in all modern plane angle measurement systems.

In practice, the plane angles can be formed (1) by mutual turning of the shafts or (2) by the intersection of lines (spatial plane angle). In the first case, the plane angle can be measured automatically, using the shaft angle encoder. In the second case, the special means constructed according to the principle of the theodolite design are necessary for the measurement of the spatial plane angles.

The search for a guidance point of the sighting telescope inside the solid angle 4π sr is carried out for the measurement of a spatial plane angle with a theodolite. The sighting telescope has an expression for the visual solid angle [25]

$$\Omega_t = 4\pi \cdot \sin^2 \frac{\beta_t}{4} \quad (1)$$

where β_t is the theodolite's sighting telescope plane angle of vision [25, (3.6) on p. 35]. For $\beta_t \approx 2^\circ$, $\Omega_t = 9.57 \times 10^{-4}$ sr. According to (1), the points quantity m_e examined with a theodolite in the solid angle 4π sr is:

$$m_e = 1/\sin^2(\beta_t/4) \geq 1.31 \cdot 10^4. \quad (2)$$

So, it becomes the evidence of complexity of the task automation of the given point in the space search, and all the difficulties of the device guidance during this task solution.

The problem of a spatial plane angle automatic measurement can be solved by active [15] or passive [16] optical scanners (AOS and POS correspondingly). Against an AOS, a POS solves the double-uniform task: the guidance point search and the plane angle measurement in space.

The principal elements of a POS are represented in Figure 1. Some variations of this unit are presented in [16,35,37,43]. The emitting beacon (EB) light by a mirror rotation gets through a lens on a photoreceiver, which forms a stop-pulse. A start-pulse is formed by a special independent zero-sensor. The time interval $T_\alpha = \alpha/\omega$ corresponds to the spatial plane angle α between the zero-sensor and the direction on an EB. The intervals T_a and $T_{2\pi} = 2\pi/\omega$ are filled by standard frequency pulses f_0, generating the codes $N_\alpha = T_\alpha f_0$ and $N_{2\pi} = T_{2\pi} f_0$. From the proportion $\alpha/(2\pi) = N_\alpha/N_{2\pi}$ is received:

$$\alpha = 2\pi \frac{N_\alpha}{N_{2\pi}}. \quad (3)$$

It is invariant with respect to ω and f_0. In other words, one of the most important advantages of our system is the independence of the measurement result on "time walking effect" or reference source instability. Because a real time system's electronic circuit in two independent counters saves two independent counts. They are codes proportional to values of 360° (or 2π) angle and desired (unknown) angle α. It means, practically, that the parallel two-channel AD-conversion of the geometrical basis in real time. It permits elimination of the absolute error component of both codes after their division according to (3) because of their natural equality in real time. It is experimentally verified by the research group of Dr.Valentyn Tyrsa [15] uncertainty of the single measurement of the angle a, for one rotation period of the mirror, is about 10 s of arc. The multiple averaging in the automatically repeated measurements permits to obtain the uncertainty measurement of the angle a no more than 1 s of the arc. Because it is widely known that with n consecutive repetitions of a single act of measurement, it is possible to decrease a measurement uncertainty up to $\sqrt{n}$ times.

In its general optical design the proposed system have some similarities with [38] and [39]. However, as compared to [38] we can note that the device in US Patent No.5455708 have very similar optical channel, but its principle is completely different. The patented system has a rotating drum with at least one reflective binary diffractive optical element facet and a normal, which is perpendicular to the said binary diffractive optical element facet. The system design is further arranged to substantially maintain beam collimation whenever the beam is reflected from any binary facet, through the post scan lens means that this beam is received by photoreceptor medium with a scan plane radius of curvature (see Figure 3, 5 or 6 of [38]). Figure 3 of [38] is repeated on Figure 8. This optical design obviously permits sufficient increase in the optical resolution of the scanned object at significant striking distance, but at the same time makes the system sensitive to any kind of mechanical noise. Because of small geometrical sizes of binary facets and strong dependence of uncertainty on the position of the reflected points in a certain location on the curve photoreceptor medium, it is practically impossible to use the above-mentioned system at conditions of mechanical vibrations or dynamical indistinctness of the optical beam projection on the sensitive surface.

Three-dimensional optical scanner of [39] is dedicated to the microoptical bench. In this case authors are not limited in accuracy by striking distance. They do not need to solve this additional complex problem.

Observing these opposite approaches [38] and [39], we can note that the main difficulty is in a reasonable trade-off between acceptable exactitude of spatial coordinate measurement and a reasonable operating range (striking distance).

In our case, we are reaching an acceptable exactitude in conventional distances by application of two factors: (1) diminution of the scanning velocity gives us practically unlimited possibility of angle coordinate resolution (for example, for reference source frequency of 1 MHz and scanner rotation velocity 1 revolution per second we have 1,000,000 distinguishable units per 360°); (2) energetic center search method, which permits use as a reference not all light ray cone, but only its geometrical sizeless axis. And, conversely, our electromechanical design is extremely simplified as compared to [38] and robust to any mechanical noise.

The average angle is determined as:

$$\overline{\alpha} = 2\pi \frac{\sum_{i=1}^{n} N_{\alpha i}}{\sum_{i=1}^{n} N_{2\pi i}}. \tag{4}$$

The ratios $N_{\alpha i}/N_{2\pi i}$ and $N_{\alpha(i+1)}/N_{2\pi(i+1)}$ represent the rational fractions which possess the properties of Farey fractions [26–28]. The ratio of the numerators sum to the denominators sum for such fractions in the formula (4) represents the mediants of the Farey fractions [29]. Mediant is a standard term in theory of numbers: for given a Farey sequence with consecutive terms h/k and h'/k' the mediant is defined as the reduced form of the fraction $(h + h')/(k + k')$ [27, pp. 152–154; 26, Lemma on p. 14 of US edition]. In mathematics, a rational number is a number which can be expressed as a ratio of two integers. Non-integer rational numbers (commonly called rational fractions) are usually written as the vulgar fraction a/b, where b is not zero. Numbers $N_{\alpha i}$ and $N_{2\pi i}$ in any i-th position are count results of two independent counters, so they are integers naturally.

Each rational number can be written in infinitely many forms, such as 3/6 = 2/4 = 1/2, but it is said to be in simplest form when a and b have no common divisors except 1 (i.e., they are coprime). The Farey sequence F_n for any positive integer n is the set of irreducible rational numbers a/b with

$0 \le a \le b \le n$ and $(a,b) = 1$ arranged in increasing order. The first six for example are

$$F_1 = \left\{\frac{0}{1}, \frac{1}{1}\right\},$$
$$F_2 = \left\{\frac{0}{1}, \frac{1}{2}, \frac{1}{1}\right\},$$
$$F_3 = \left\{\frac{0}{1}, \frac{1}{3}, \frac{1}{2}, \frac{2}{3}, \frac{1}{1}\right\},$$
$$F_4 = \left\{\frac{0}{1}, \frac{1}{4}, \frac{1}{3}, \frac{1}{2}, \frac{2}{3}, \frac{3}{4}, \frac{1}{1}\right\}$$
$$F_5 = \left\{\frac{0}{1}, \frac{1}{5}, \frac{1}{4}, \frac{1}{3}, \frac{2}{5}, \frac{1}{2}, \frac{3}{5}, \frac{2}{3}, \frac{3}{4}, \frac{4}{5}, \frac{1}{1}\right\}$$
$$F_6 = \left\{\frac{0}{1}, \frac{1}{6}, \frac{1}{5}, \frac{1}{4}, \frac{1}{3}, \frac{2}{5}, \frac{1}{2}, \frac{3}{5}, \frac{2}{3}, \frac{3}{4}, \frac{4}{5}, \frac{5}{6}, \frac{1}{1}\right\}$$

These two statements are actually equivalent [30, p. 24]. For a method of computing a successive sequence from an existing one of n terms, insert the mediant fraction $(a+b)/(c+d)$ between terms a/c and b/d when $c + d \le n$ [27; 30, pp. 25–26; 31]. Given $0 \le a/b < c/d \le 1$ with $bc - ad = 1$, let h/k be the mediant of a/b and c/d. Then $a/b < h/k < c/d$, and these fractions satisfy the unimodular relations [31, p. 99]:

$$bh - ak = 1$$
$$ck - dh = 1.$$

For a n-th mediant generation in the form of the fraction $\sum_{i=1}^{n} N_{\alpha i} / \sum_{i=1}^{n} N_{2\pi i}$, the sum $\sum_{i=1}^{n} N_{\alpha i}$ discretely on each turn of the POS's mirror is formed. The sum $\sum_{i=1}^{n} N_{2\pi i}$ is formed continuously from the first start-pulse up to the $n+1$ pulse. A computer performs the division operation only once, after the generation of the both the sums $\sum_{i=1}^{n} N_{\alpha i}$ and $\sum_{i=1}^{n} N_{2\pi i}$ in the POS.

The average $\overline{\alpha}$ founded with the mediants use, has the higher exactness, in comparison with the classical arithmetic middle averaging exactness for the given value n. We can approve it on the base of [26, p. 30, in the US edition p. 21]: it is immediately clear that the apparatus of systematic fractions is completely unsuitable for approximation problem solving, since denominators of the approximating fraction that it provides are determinated exclusively by the chosen system of calculation (in the case of decimal fraction, they are powers of ten); hence, the denominators are completely independent of the arithmetic nature of the number represented. On the other hand, in the case of continued fraction, the denominators of the convergents are completely determined by the number represented. We, therefore, have every reason to expect that these convergents (since they are connected in a close and natural way with the number represented, and are completely determinated by it) will play a significant role in the solution of the problem of the best approximation of a number by a rational fraction. Rigorous proof of this fact is given by Theorems 15, 16, 17 proofs in [26, pp. 22–28 of US edition].

This benefit also seems comparably small to other similar problems in various practical applications.

Thus, the proposed system for precise spatial coordinates measurement have some obvious advantages over other similar methods [19–21,36,38,39]: using the robust and precise mechanical scanning and registering principle instead of the electronic scanning which is extremely sensible to any kind of vibration and mechanical noise and using special mathematical processing for measurement uncertainty decreasing.

Precise measurement of spatial coordinates were taken, first of all, considering the scanning tool is not the real light beam, but the geometrical axis of this beam of a conic form. Thanks to the concept of the energetic center search of the noisy electrical pulse, it is possible to increase spatial resolution of the EB location. This method will be described below.

Also, it can be additionally increased accuracy of the angle measurement using original method [40,41] for precise adjustment of initial and final scale coincidence between angle pulse-marks and reference pulse train. This method can minimize the influence of reference frequency source own jitter.

5 POS Operation Range

The analysis of the possible positions of a beam, traveling from the EB to the mirror, shows that the maximum value of the angle β between the beam and the perpendicular to the mirror (look Figure 1), can reach 90°. Thus, the POS aperture angle is $\beta \leq 90^\circ$. During the mirror rotation, the solid angle of an all-round vision of a POS is:

$$\Omega = 4\pi\left(1 - 2\sin^2\frac{180^\circ - \beta_s}{4}\right) \quad (5)$$

where β_s is the POS's desirable angle of sight. If $\beta_s = 90^\circ$ for example, then $\Omega = 2.83\pi$ sr; so it is more than half of the space around a POS.

We shall determine the POS coverage. Let assume that EB have the diffuse emission power P. The uniform emission density in the solid angle 4π sr is

$$I = \frac{P}{4\pi}. \quad (6)$$

Let the aperture diameter of the POS be $2r = 3 \times 10^{-2}$ m, and then the emission power, getting in the POS be:

$$P_a = I\Omega_a \quad (7)$$

where

$$\Omega_a = \frac{S_a}{D^2} = \frac{\pi r^2}{D^2} \quad (8)$$

where S_a is the scanning aperture area, and D is the distance between EB and the center of SA mirror (detailed distance toward current light source under consideration).

According to the expressions (6) and (7), from the proportion (8) we find the expected operating range

$$D = \frac{r}{2}\sqrt{\frac{P}{P_a}}. \quad (9)$$

Let P_a be equal to the minimum threshold optical power value $P_{\min}$. It can be determined, for example, by the technique given in reference [32, p. 70] (this reference is taken intentionally to show that it is possible for very basic hardware, not so advanced):

$$P_{\min} = NEP\frac{R_{\max}}{R(\lambda)}\sqrt{B}[\mathrm{W}]. \quad (10)$$

Here NEP is the noise equivalent of the power, $R_{\max}$ and $R(\lambda)$ are the maximum sensitivity and the sensitivity on the detecting wave, respectively; B is the frequencies band in Hz. For example, the length of the wave for the photoreceiver Model # 2007 [32, pp. 56, 66] is 400–1070 nm; $NEP = 3 \times 10^{-12}$. For $B = \omega/2\pi \approx 100$ Hz, $R_{\max} = 0.55A/W$ and $R(\lambda) = 0.5A/W$, then:

$$P_{\min} = 3 \times 10^{-12} \times 0.55 \times \frac{\sqrt{100}}{0.5} = 3.3 \times 10^{-11}\mathrm{W}. \quad (11)$$

Using as a power source, for example, the lamp HRQ3010-5071 of catalog [33] with power 1.75 W, from the expression (9) we find:

$$D_{\max} = 0.5 \times 1.5 \times 10^{-2} \times \sqrt{\frac{1.75}{3.3 \cdot 10^{-11}}} = 1727\,\mathrm{m}. \quad (12)$$

This analysis shows that with a POS it is possible to design networks of polygonometry and triangulation of a high accuracy, which allows observation of large spaces on monitoring objects. This distance covers our requirements even taking to account different types of losses inside the optical channel because the optimal distance between the scanner and the controlled object is 150–500 m. Also it is possible to use more expensive light sources, like special automobile lamps (Philips H11 CrystalVision, type 12362 CV, 12 V, 55 W) or even CW-lasers, which have proved unambiguous range up to ≥150 m according to [34, p. 200-201]. Of course, it has a reason only for civil engineering structures of enhanced importance.

6 POS Adoption on the Monitored Objects

The above-described POS with the vertical axis of rotation is used for the measurement of the horizontal angles. Let us call it a vertical POS. The vertical angles between the EBs are measured by the POS with the horizontal axis of rotation. This POS is the horizontal POS. The system, which consists of the vertical and horizontal POSs permits one to measure the displacement of the EB in horizontal and vertical planes.

Figure 2 shows the adoption of the horizontal POS for the realization of the bridge points monitoring in a vertical plane. The POS is placed outside the bridge and measures the vertical angles β_i. The EBs are installed with the same height h_i above the bridge surface. It is possible to use any

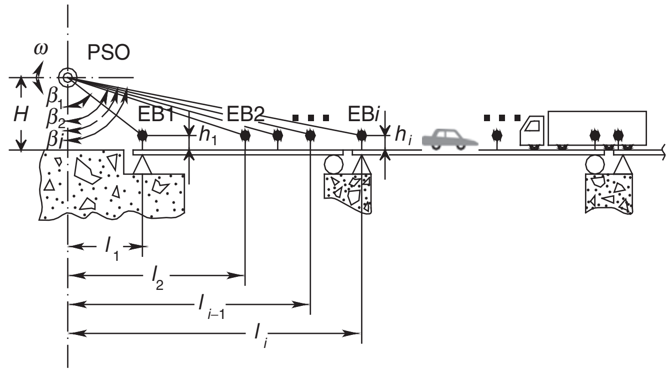

Figure 2 Horizontal POS placement for bridge monitoring.

sufficiently cheap light source, for example lamp HRQ3010-5071. The distances l_i are measured during the installation of the EB.

In the absence of a deformation, for each EB_i, the following expression is valid:

$$\frac{H-h}{l_i} = \tan\left(\frac{\pi}{2} - \beta_i\right). \quad (13)$$

For the bridge deformation with the magnitude Δh_i in the placement point of the beacon EB_i, the angle β_i, measured by the POS, will change on the magnitude $\Delta\beta_i$. As a result the expression (13) will receive the form:

$$\frac{H-h\pm\Delta h}{l_i} = \tan\left(\frac{\pi}{2} - \beta_i \pm \Delta\beta_i\right). \quad (14)$$

Therefore:

$$\Delta h_i = (H-h) - l_i \tan\left(\frac{\pi}{2} - \beta_i \pm \Delta\beta_i\right). \quad (15)$$

Similarly the POS for tunnel monitoring is installed. In extended tunnels several functionally connected POS can be placed along its axis.

Figure 3 shows the placement of two vertical POSs for the arch dam monitoring of a hydroelectric power station. The POSs measure in pairs the horizontal angles α_{1i} and α_{2i} between the base line AB and the EB_i. The length of the base line D and the Cartesian coordinates of the POS are determined beforehand by known geodetic methods. The angles $\angle EB_i$ are found conform to the formula:

$$\angle EB_i = 180^\circ - (\alpha_{1i} + \alpha_{2i}). \quad (16)$$

According to sine theorem we find the triangles sides, which have the vertex A, B, EB_i; and the

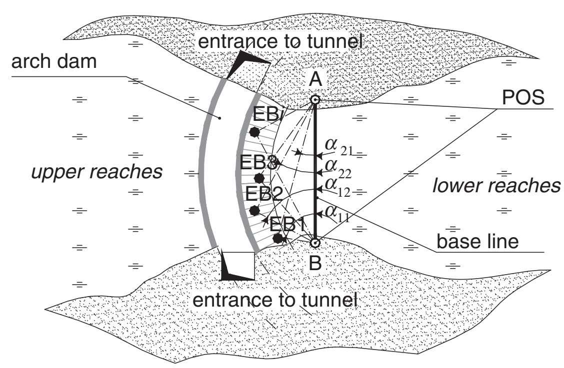

Figure 3 Placement of two vertical POSs for arch dam monitoring.

coordinates x_i, y_i of the points EB_i, in the national system or conditional Cartesian coordinate system. The change of coordinates of the points EB_i in the repeated measurements of the angles α_{1i} and α_{2i} reveal the dam deformation.

7 Accuracy Improvement by the Method of Pulse Energetic Center Search

The above-mentioned considerations are still strongly theoretical, because in the geometrical scheme we consider a pure geometrical object, i.e. the straight line is precisely straight, without any curvature, have only length, all another sizes are zero; points have no sizes and its location is characterized only by three Cartesian coordinates in the space.

Practically it is different. The optical ray is a cone in general, or of an even more complex shape depending on medium properties. The vertex of this cone also is not a point, but distributed in some small spatial scope. The divergence inside this cone is caused by many natural factors.

It causes that practically the stop-pulse in photo receiver is not a short pulse of the standard form, but it is formed as shown on Figure 6(a–e).

It grows (Figure 6a) and falls down (Figure 6e), and fluctuating around its maximum area in Figures 6(b–d). Taking to account the presence of some natural noise (as a rule, white Gaussian noise) in this process, we can conclude that finally we need to operate the single electric signal of non-regular shape presented on Figure 7a. Moreover, the shape and width of this pulse are closely related to scanning velocity. But the scanning velocity in practical case is not a constant also. In this case the best problem solution is adequate signal processing. And our contribution is based on simple idea. What is the red point on the Figure 7a? In the point of view of electric signals, area on the graphic limited by signal curve is the energy transferred by this electric signal. So, this red point with certain small uncertainty is the signal energetic center. It is essential to note that position of the energetic center coincides for both pulses on the Figure 7a: ideal theoretical square pulse and its real noisy performance. It is much more essential is to note in this case that at the energetic center position uncertainty the less depends on noise, than the pulse area. Our task is the same as less scanning velocity.

On the other hand, as we consider this pulse as the optic blur equivalent registered by photosensor, it is the center of optical ray spatial cone. Thus we can detect in noisy electric signal the truth position of the unique straight line which belongs to the center of light source (active target or EB) and the center of the photoreceiver.

To find the correct point in noisy electric pulse, it is necessary to find the maximum of energy. For normalized electrical signal the maximum point it is exactly that point where the first derivative of its function is equal to zero. So, using the standard differentiator circuit, we are finding this point instantly by hardware (see Figure 7b). In another words, after finding the zero-cross position of the first derivative function of the registered signal, we can find a real position of the EB in our coordinate system.

The practical realization of described operation is possible in several ways. The most efficient among them in this case is a complex question. We still consider it as a whole problem for furthering research and a topic of another publication. However, in our primary experimentation we realize that this operation uses standard differentiator circuit (Figure 7b). On the operation screenshot on Figure 7b it is clearly evident that it is completely possible in a real time scale to obtain an electrical mark of the real light source position. It causes a certain delay between real maximum position and its mark by pin-pulse (Figure 7b) because of the differentiator circuit operating time. But it is strongly evident that it has a constant character and can be eliminated on the processing stage by a simple correction factor.

Combining our above-mentioned method of spatial angle measurement it permits us to

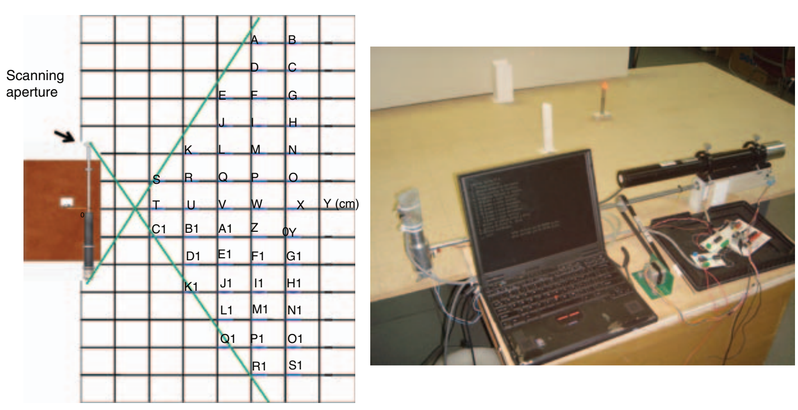

Figure 4 EBs' and POS positioning on the experimental table with a grid-scale.

Table 1 Experimental results of the coordinates measurement and its relative error (offset) estimation.

	Theoretical value				*Measured value*				
Test point	X *(m)*	Y *(m)*	B *(°)*	C *(°)*	X (m)	Y (m)	B *(°)*	C *(°)*	*Relative error [%] (offset)*
A	100	120	124.99	30.47	111.94	140.3	128.89	30.47	3.12
B	120	120	120.26	35.22	139.01	146.93	124.89	35.22	3.85
C	120	100	112.62	38.66	126.53	108.16	114.69	38.66	1.83
D	100	100	116.57	33.69	104.91	107.37	118.67	33.69	1.81
E	80	80	110.56	31.61	81.2	81.949	111.48	31.61	0.83
F	100	80	106.70	37.57	102.73	83.555	108.09	37.57	1.30
G	120	80	104.04	42.71	123.21	83.475	105.2	42.71	1.12
H	120	60	94.76	47.49	120.52	60.481	94.97	47.49	0.22
I	100	60	95.71	42.27	101.36	61.499	96.472	42.27	0.80
J	80	60	97.13	36.03	79.405	59.182	96.596	36.03	0.54
K	60	40	80.54	33.69	58.935	38.403	78.868	33.69	2.07
L	80	40	82.87	41.63	79.567	39.513	82.492	41.63	0.46
M	100	40	84.29	48.01	100.17	40.157	84.388	48.01	0.12
N	120	40	85.24	53.13	120.67	40.499	85.498	53.13	0.31
O	120	20	75.96	59.74	122.59	21.509	76.916	59.74	1.25
P	100	20	73.30	55.01	99.755	19.829	73.172	55.01	0.18
Q	80	20	69.44	48.81	78.538	18.721	68.284	48.81	1.67
R	60	20	63.43	40.60	58.791	18.59	61.886	40.60	2.44
S	40	20	53.13	29.74	39.652	19.391	52.334	29.74	1.50
T	40	0	38.66	38.66	41.083	1.3538	40.182	38.66	3.94
U	60	0	50.19	50.19	60.67	0.5579	50.822	50.19	1.25
V	80	0	57.99	57.99	79.392	−0.3799	57.602	57.99	0.68
W	100	0	63.43	63.43	99.259	−0.3703	63.094	63.43	0.54
X	120	0	67.38	67.38	119.63	−0.1522	67.256	67.38	0.18
Y	120	−20	59.74	75.96	121.09	−19.729	60.064	75.96	0.54
Z	100	−20	55.01	73.30	98.417	−20.475	54.394	73.30	1.12
A1	80	−20	48.81	69.44	77.312	−21.008	47.434	69.44	2.83
B1	60	−20	40.60	63.43	59.276	−20.362	40.112	63.43	1.21
C1	40	−20	29.74	53.13	41.172	−19.121	30.78	53.13	3.48
D1	60	−40	33.69	80.54	62.278	−39.62	34.796	80.54	3.28
E1	80	−40	41.63	82.87	82.325	−39.709	42.542	82.87	2.18
F1	100	−40	48.01	84.29	103.12	−39.688	48.986	84.29	2.03
G1	120	−40	53.13	85.24	123.5	−39.708	54.006	85.24	1.65
H1	120	−60	47.49	94.76	119.04	−59.92	47.282	94.76	0.44
I1	100	−60	42.27	95.71	96.858	−59.686	41.446	95.71	1.96
J1	80	−60	36.03	97.13	79.77	−59.971	35.956	97.13	0.20
K1	60	−60	28.61	99.46	63.354	−60.559	29.814	99.46	4.21
L1	80	−80	31.61	110.56	83.619	−81.357	32.48	110.56	2.76
M1	100	−80	37.57	106.70	98.923	−79.677	37.338	106.70	0.61
N1	120	−80	42.71	104.04	119.63	−79.908	42.642	104.04	0.16
O1	120	−100	38.66	112.62	123.77	−101.57	39.234	112.62	1.49
P1	100	−100	33.69	116.57	96.833	−98.416	33.122	116.57	1.69
Q1	80	−100	28.07	122.01	82.59	−101.62	28.578	122.01	1.80
R1	100	−120	30.47	124.99	102.2	−121.54	30.786	124.99	1.05
S1	120	−120	35.22	120.26	115.43	−117.33	34.598	120.26	1.76

conclude that our method gives more accurate angular resolution than any of those known in [15,21,38].

8 Experimental Results

Practical working capacity of the given method has been checked out on a scanning aperture prototype, with preliminary experimentations, however still without ECS-circuit implementation. This experimentation was made using a movable light source, varying its position on a table with a grid-scale, in which was situated a network with 45 designated points (see Figure 4). The points were chosen according to the detection pattern of the system within a maximum range of 1 m. The separation distance between each point is of 20 cm in coordinate X and Y, with an error of ±0.1 cm. The light source used in the experiment, is a regular incandescent automobile lamp of 12 V DC. Also the prototype gives the possibility to highlight the same points with laser rays by 20 mW laser (JDS Uniphase, model 1136P). The lamp was located in each point of the network, where 10 optical scannings were made. An average of the reception angle for each point was obtained (see Table 1). Additionally, the value of the emission angle (angle C) for each point in the test was obtained using trigonometrical formalism in [35, p. 342]. Using the value of angle C, the final coordinates X and Y that describe the experimental position of each point, were obtained. The coordinate value of each point has measurement error. This error must be due to many causes, but mainly due to the errors in reflection angle measurement at the optical aperture. The Principal known causes of error are detected:

– instability of motor speed in optical aperture.
– electrical signal center shifting caused by low operating velocity.
– improper calibration of reference instrument.

All these causes have been taken into account in the present process of a second prototype design.

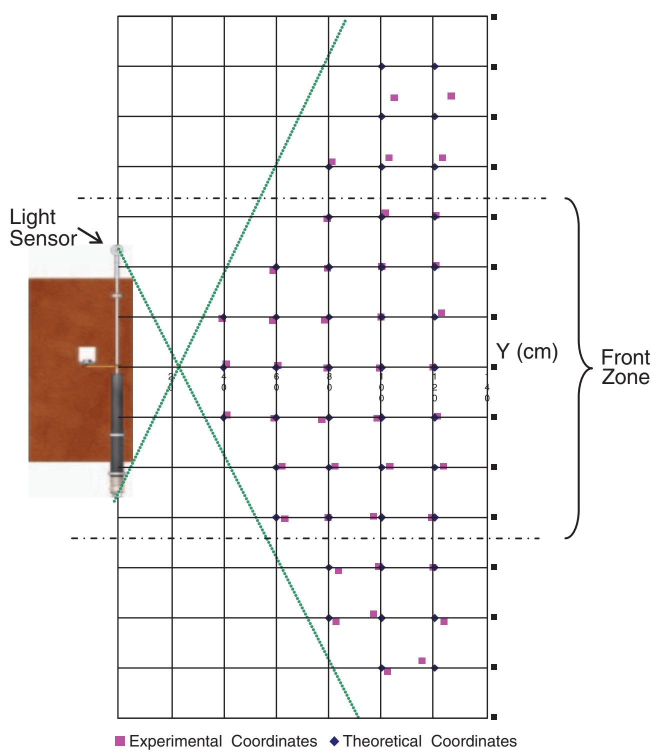

Figure 5 Measured coordinates points positioning on the grid-scale.

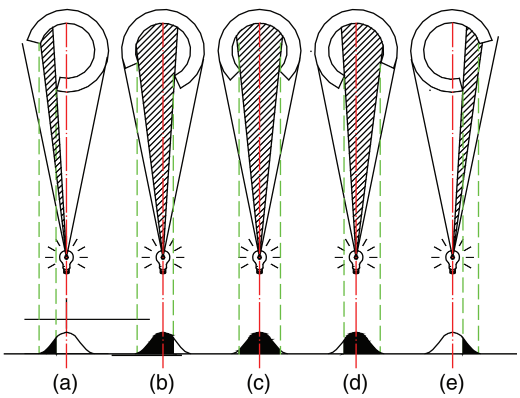

Figure 6 The principle of noisy electrical stop-pulse formation during rotational scanning.

From data analysis it is possible to determine a zone in the Table 1 where the obtained data is more accurate. It is shown on a Figure 5. All the experiments were carried out at not less than 95% confidence level. But in the Figure 5 are presented real points and measured points, and it is evident that there appears two zones of different accuracy in this measurement. Further exact data was obtained in the frontal zone, where the experimental data have an error less than in the zones near the edge. Thus, the zone of more accurate measurement from the system can be known.

In general, the behavior of uncertainty repeats the graphic on Figure 6 in [36, p. 1765], however, accuracy near the edge is advanced. Also, accuracy in the central part of the angle of view is 2–7 times better in different checked points respect to [36] for example.

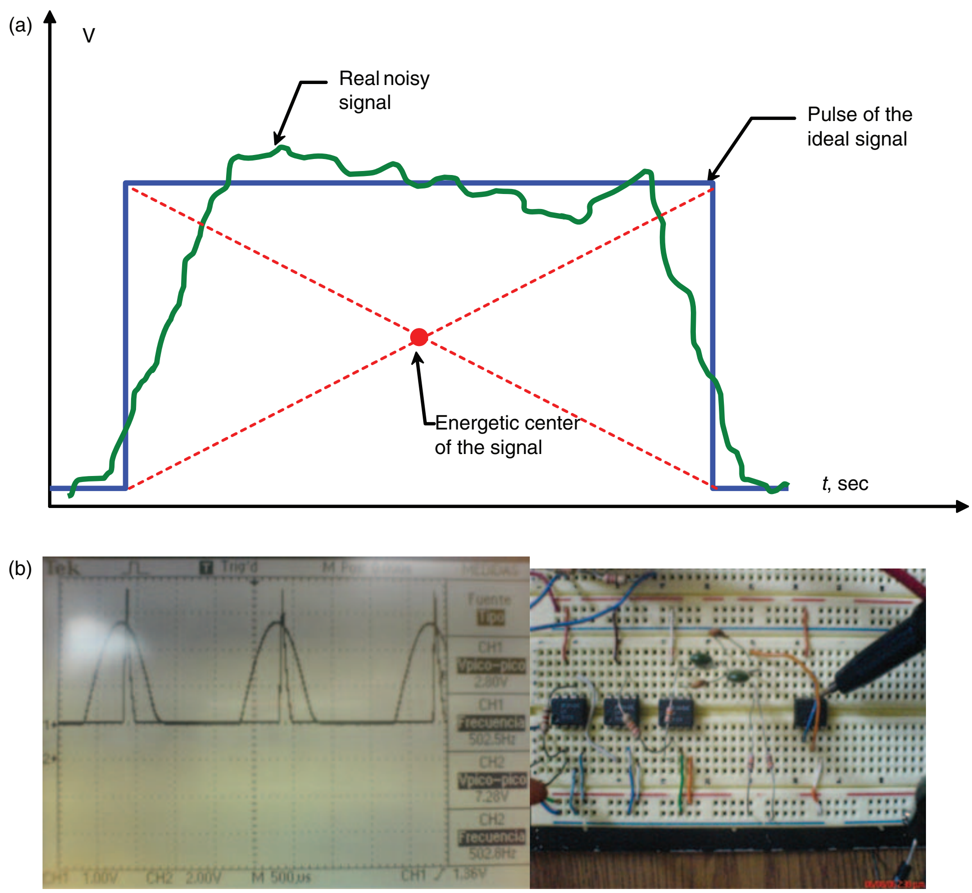

Figure 7 Method of the signal energetic center search: (a) general purpose; (b) differentiator circuit functioning screenshot.

U.S.Patent Oct. 3,1995 Sheet 2 of 8 5,455,708

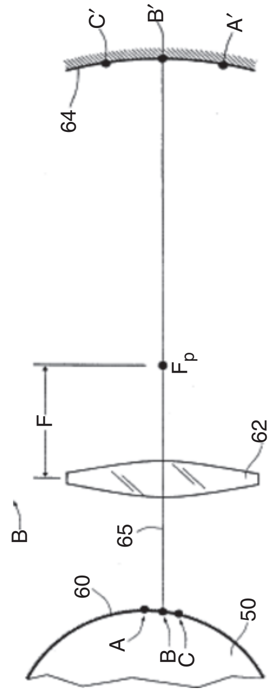

Provided by Patent Storm, http//www.patentstorm.us

Figure 8 Optical channel of the Harris–Wilson scanner (Figure 3 of [38]).

9 Conclusions

(1) The stationary system of the structure deformation monitoring, based on the POS, possesses the following inherent properties:

– A possibility of receiving the data about structure deformation every minute, in all check points, with a millimeter's uncertainty, for the structure of any size and configuration;
– The complete measurement automation, the data registration for the significant distance between the processing center and the observable structure;
– The operation of the monitoring system without interruption of the structure functioning;
– A possibility of the operation underground: in tunnels, subways, mountain excavation;
– High durability and a simple service;
– The possibility of many years round-the-clock control of the earthquakes development centers with it prediction purpose.

(2) On the POS-base the mobile robots navigation systems, the automatic adjustment system for the compound space crafts, the mutual orientation system for the six freedom degrees structures, the ships and aircrafts deformation monitoring system in dynamics, automatic region mapping systems and others can be constructed.

Acknowledgements

The Present work is partially supported by the Autonomous University of Baja California, the projects No. 2352, in 2003–2004 and N2386, in 2005–2006. Particular results of this investigation herein described were reported in several congresses [16,17,35,37]. The authors dedicate this article to the grateful memory of our teacher, Dr. Valentyn Tyrsa; and would like to thank anonymous reviewers for valuable comments and remarks.

References

1. Doebling, S.W., Farrar, C.R. and Prime, M.B. (1998). Summary review of vibration-based damage. *The Shock and Vibration Digest*, *30*(*2*), 91–105.
2. Fritzen, C.-P. (2005). Recent developments in vibration-based structural health monitoring. In: Chang, F.-K. (ed.), *Structural Health Monitoring*, pp. 42–60, USA: DEStech Publications.
3. Wang, M.L. (2005). Damage assessment and monitoring of long-span bridges. In: Chang, F.-K. (ed.), *Structural Health Monitoring*, pp. 61–79, USA: DEStech Publications.
4. Farrar, C.R., Cornwell, P.J., Doebling, S.W. and Prime, M.B. (2000). Structural health monitoring studies of the Alamosa Canyon and I-40 Bridges, Los Alamos National Laboratory Report, LA-13635-MS, pp. 182.
5. Salvino, L.W., Purekar, A.S. and Pines, D.J. (2005). Damage identification using time-frequency wave propagation data. In: Chang, F.-K. (ed.), *Structural Health Monitoring*, pp. 582–589, USA: DEStech Publications.
6. Benedetti, M., Donelli, M., Massa, A. and Rosani, A. (2006). An innovative microwave imaging technique for non destructive evaluation: applications to civil structures monitoring and biological bodies inspection. In: *IEEE Proceedings of International Imaging Systems and Techniques, (IST-2004)*, Braunschweig, Germany, 14 May, Vol. 35, pp. 91–94, ISSN: 0018-9456.

7. Chintalapudi, K., Fu, T., Paek, J., Kothari, N., Rangwala, S., Caffrey, J., Govindan, R., Johnson, E. and Masri, S. (2006). Monitoring civil structures with a wireless sensor network. *IEEE Internet Computing*, *10*(*2*), 26–34.
8. Mehta, V. and El Zarki, M. (2004). *A Bluetooth based Sensor Network for Civil Infrastructure Health Monitoring*, pp. 401–412, The Netherlands: Kluwer Academic Publishers.
9. Lee, R.G., Chen, K.C., Lai, C.C., Chiang, S.S., Liu, H.S. and Wei, M.S. (2007). A backup routing with wireless sensor network for bridge monitoring system. *Measurement*, *40*(*1*), 55–63.
10. Inada, H., Kumagai, H. and Okuhara, Y. (2005). Experimental study on structural health monitoring of concrete structures using self-diagnosis materials and wireless measurement systems. In: Chang, F.-K. (ed.), *Structural Health Monitoring*, pp. 253–260, USA: DEStech Publications.
11. Ohno, H., Naruse, H., Kurashima, T., Nobiki, A., Uchiyama, Y. and Kusakabe, Y. (2002). Application of Brillouin scattering-based distributed optical fiber strain sensor to actual concrete piles. *IEICE Transactions on Electronics*, *E85-C*(*4*), 945–951.
12. Horiguchi, T., Shimizu, K., Kurashima, T., Tateda, M. and Koyamada, Y. (1995). Development of a distributed sensing technique using Brillouin scattering. *Journal of Lightway Technology*, *13*(*7*), 1296–1302.
13. Salgado, R. and Cruz, P. (2005). Detecting damage in structures using Wavelet analysis. In: Chang, F.-K. (ed.), *Structural Health Monitoring*, pp. 1809–1816, USA: DEStech Publicationsin.
14. Athavale, N.N., Ragade, R.K., Cassaro, M.A. and Fenske, T.E. (1990). A prototype for KYBAS: the Kentucky Bridge Analysis System. In: In: *Proceedings of the 3rd International Conference on Industrial and Engineering Applications of Artificial Intelligence and Expert Systems*, Charleston, South Carolina, United States, Vol. 2, pp. 781–789, ISBN: 0-89791-372-8.
15. V.E. Tyrsa (1973). Technique of a determination of an object coordinates, Author's Certificate on the Invention No. 402736, G 01.C1/00 (in Russian).
16. Tyrsa, V.E., Sauseda-Carvajal, A., Burtseva, L.P., Rivera Castillo, J. and Tyrsa, V.V. (2001). Navigation of spacecraft and mobile robot. In: *Proceedings of the IASTED International Conference on Robotics and Manufacturing*, Cancun, Mexico, May 21–24, pp. 83–87. XP001131961 2001, Calgary, Alta, Canada, IASTED/Acta Press, Canada, ISBN: 0-88986-281-8.
17. V.E.Tyrsa, L.P.Burtseva, M.Rivas Lopez, V.V.Tyrsa (2004). Monitoring of civil engineering structures. In: *Proceedings of SPIE International Conference Health Monitoring and Smart Nondestructive Evaluation of Structural and Biological Systems III*, 5394, San Diego, USA, pp. 485–492.
18. Allen, D.W., Park, G. and Farrar, C.R. (2005). Overview of wireless active sensing systems for structural health monitoring. In: Chang, F.-K. (ed.), *Structural Health Monitoring*, pp. 1578–1585, USA: DEStech Publications.
19. Winkelbach, S., Molkenstruck, S. and Wahl, F. (2006). Low-cost laser range scanner and fast surface registration approach. In: *Proceedings of DAGM 2006*, pp. 718–728, Berlin: Heidelberg.
20. França, J.G.D.M., Gazziro, M.A., Ide, A.N. and Saito, J.H. (2005). A 3D scanning system based on laser triangulation an variable field of view. In: *Proceedings of the 2005 International Conference on Image Processing (ICIP 2005), IEEE*, Vol. 1, pp. 425–428, Genoa, Italy.
21. Slob, S. and Hack, R. (2004). 3D terrestrial laser scanning as a new field measurement and monitoring technique. In: Hack, R., Azzam, R. and Charlier, R. (eds), *Engineering Geology for Infrastructure Planning in Europe*, pp. 179–189, Berlin, Heidelberg: Springer.
22. Baltsavias, E.P. (1999). A comparison between photogrammetry and laser scanning. *ISPRS Journal of Photogrammetry & Remote Sensing*, *54*, 83–94.
23. Tsai, M.J. and Hung, C.C. (2005). Development of a high-precision surface metrology system using structured light projection. *Measurement*, *38*(*3*), 236–247.
24. Bergstrand, E. (1949). Velocity of light and measurement of distance by high frequency light signalling. *Nature*, *4139*, 338–339.
25. Wyatt, C.L. (1991). *Electro-Optical System Design: For Information Processing*, p. 343, NY: McGraw-Hill.
26. Khinchin, A. Ya. (1992). *Continued Fractions*, 3rd edn, Moscow: The State Publishing House of the Physical And Mathematical Literature, pp. 111, 1961 (translated to English in 1964, by Dover Publications Inc., Mineola, New York, Licensed by Chicago University Press, 1992, p. 94).
27. Conway, J.H. and Guy, R.K. (1996). *Farey Fractions and Ford Circles. The Book of Numbers*, p. 332, New York: Springer-Verlag.
28. Carmichael, R.D. (2004). *The Theory of Numbers and Diophantine Analysis*, p. 118, New York: Courier Dover Publications, Dover Phoenix Editions.
29. Farey, J. (1816). On a curious property of vulgar fractions. *London, Edinburgh and Dublin Philosophical Magazine and Journal*, *47*, 385.
30. Hardy, G.H. and Wright, E.M. (1979). Farey series and a theorem of Minkowski. In: *An Introduction to the Theory of Numbers*, 5th edn, Ch. 3, pp. 23–37, Oxford, UK: Clarendon Press.

31. Apostol, T.M. (1990). Farey fractions. In: Axler, S., Gehring, F.W. and Ribet, K.A. (eds), *Modular Functions and Dirichlet Series in Number Theory*, §5.4, 2nd edn, pp. 97–99, New York-Berlin-Heidelberg: Springer-Verlag, Available at: http://books.google.com.mx/books?id=lyqDSjLY6zEC&printsec=frontcover&source=gbs_navlinks_s#v=onepage&q=&f=false
32. 1999/00 Catalog (New Focus, Inc., 10, 1999).
33. Harison Toshiba Lighting Inc. Catalog, 2007.
34. Baltsavias, E.P. (1999). Airborne laser scanning: basic relations and formulas. *ISPRS Journal of Photogrammetry & Remote Sensing*, *54*, 199–214.
35. Tyrsa, V.Ye., Sergiyenko, O.Yu., Tyrsa, V.V., Bravo, M., Devia, L. and Rendon, I. (2006) Mobile robot navigation by laser scanning means. In: *Proceedings of 3rd International Conference on Cybernetics and Information Technologies, Systems and Applications CITSA – 2006*, Vol. I, Orlando, Florida, USA, 20–23 July, 2006, pp. 340-345.
36. Pierce, D.S., Ng, T.S. and Morrison, B.R. (1992). A novel laser triangulation technique for high precision distance measurement. In: *Proceedings of IEEE Industry Applications Society Annual Meeting*, Vol. 2, October, Houston, USA, pp. 1762-1769.
37. Rivas, M., Sergiyenko, O., Aguirre, M., Devia, L., Tyrsa, V. and Rendón I. (2008) Spatial data acquisition by laser scanning for robot or SHM task. In: *IEEE-IES Proceedings International Symposium on Industrial Electronics (ISIE-2008)*, Cambridge, UK, June 30 to July 2, pp.1458-1463.
38. Harris, E.D. and Wilson, J.M. (1995). US Patent N 5455708, pp. 15, October 3.
39. Sasaki, M., Yamaguchi, T., Song, J.H., Hane, K., Hara, M. and Hori, K. (2003). Optical scanner on a three-dimensional microoptical bench. *Journal of Lightwave Technology*, *21*(*3*), 602–608.
40. Balbuena, D.H., Sergiyenko, O., Tyrsa, V., Burtseva, L. and López, M.R. (2009). Signal frequency measurement by rational approximations. *Measurement*, *42*(*1*), 136–144, Available at: http://www.sciencedirect.com/science?_ob=ArticleURL&_udi=B6V42-4SD29MF-1&_user=10&_rdoc=1&_fmt=&_orig=search&_sort=d&_docanchor=&view=c&_searchStrId=991768478&_rerunOrigin=scholar.google&_acct=C000050221&_version=1&_urlVersion=0&_userid=10&md5=b45f993b1fd1d6d5c5f27c6257dab79d
41. Balbuena, D.H., López, M.R., Burtseva, L. Sergiyenko, O. and Tyrsa, V. (2006). Method for phase shift measurement using Farey fractions. In: *IEEE Proceedings of Multiconference on Electronics and Photonics (MEP-2006)*, Guanajuato, 7–10 November, pp. 181–185.
42. Strand, T.C. (1985). Optical three-dimensional sensing for machine vision. *Optical Engineering*, *24*(*1*), 033–040.
43. Lopez, M.R., Sergiyenko, O. and Tyrsa, V. (2008). Machine vision: approaches and limitations. In: Zhihui, X. (ed.), *Computer Vision,* Ch. 22, pp. 395–428, Vienna, Austria: I-TECH.

Spatial data acquisition by laser scanning for robot or SHM task

Moisés Rivas [1,2], Oleg Sergiyenko[1], Mario Aguirre[1], Luis Devia[1], Vera Tyrsa[2], and Ismael Rendón[3]
[1] *Engineering Institute of Autonomous University of Baja California,*
[2] *Politechnical University of Baja California*
[3] *Technological University of Hermosillo*
mrivas@upbc.edu.mx, srgnk@iing.mxl.uabc.mx, moaeaz@hotmail.com, lfdevia7@gmail.com, vera-tyrsa@yandex.ru

Abstract- **This paper presents through of the principle of laser triangulation a technique to acquisition data from an environment. The prototype can discover obstacles or objects in a unknown environment. Using a light source (laser) and very simple but efficient scanning unit is possible determinate distances and angles of any point on object in environment based in data acquisition by these elements. The most important parameters are: accuracy, functioning speed, range of action, and power requirements; the main characteristics is based in simplicity, versatility and economical accessibility. Fully automatic navigation and monitoring system is able to implement this prototype.**

I. INTRODUCTION

About the control in the motion of autonomous robots [1] or similar systems indisputably is necessary to collect some data to take a decision for specific task. For example in some case a system has to know the environment, for cause of navigation or explore a terrain. The same task also seems comparably mall to other similar problem: structural health monitoring (SHM) of big engineering structures. Visual Data Acquisition is basic for these systems; in searching for match human binocular sight for this task; the most popular techniques are based on laser scanning and geometric methodologies such as triangulation [2] and have achieved more and more attentions in machine vision application due to its robustness and simplicity.

Triangulation has the significant advantage over interference techniques in that the absolute distance to the target is measured [3, p.1762].

In industrial environments guided vehicles by a magnetic or optical track are standard [4] for present day. Autonomous mobile service systems not restricted by a track, are used extremely rarely although many research groups are working on this since several years – particularly with mobile systems for transportation tasks. One of several reasons for the gap between prognoses and reality is the lack of good, cheap and fast sensors that allow the robots to sense the environment in real-time and to act on the basis of the acquired data.

Several terrestrial laser-imaging systems have been recently released [5, 6]. These types of imaging system provide a user with a dense set of three-dimensional vectors to unknown points relative to the scanner location. Given the volume of points and high sampling frequency, laser-imaging systems offer surveyors and photogrammetrists an unprecedented density of geospatial information coverage. For this reason, there is enormous potential for use of this instrumentation in monitoring applications where such dense data sets could provide great insight into the nature envioronment.

Most commercial laser scan systems use a camera and a laser beam or laser plane [7]. The surface recovery is based on triangulation, i.e. the intersection of the illuminating laser beam and the rays projected back to the camera. Expensive high-precision actuators are often used for rotating/translating the laser plane or for rotating/translating the object.

Implementing this principle we can obtain data more fast and precise than other means like vision with cameras, in some case can be good option, but about volume and versatility our prototype get more advantages, so can has sufficient range of visibility and depth including high precision.

Almost mechanisms of autonomous control without human intervention in decision choice need information, for example in navigation vehicles [8] either explore a terrain field or make task in unknown field, basically "a first watch" of the environment is very important, but to get high precision in task of system is necessary a detailed image of the environment.

In the future this kind of systems can be used to explore new fields or environments like dangerous areas or inaccessible areas for the humans, so this mechanism is able to collect data either recognition of environment or give information to a fully autonomous robot to make specific task.

II. STATE OF ART

This system is based in triangulation principle; the principle of triangulation cares on the projection of a light pattern, i.e., a line is projected by the laser over an object and captured by the optical receiver (digital camera). The distance from object to system can be calculated by trigonometry, as long as you know a priori distance between the scanning system and the camera [9].

Is possible classify triangulation techniques into active and passive methods [10]. Active techniques, such as laser scanning and structured light, intentionally project illumination into the scene in order to construct easily identifiable features in order to minimize the difficulty involved in determining correspondence. In contrast, passive stereo algorithms attempt to find matching image features between a pair of general images about which nothing is known a priori. This classification has become so pervasive that we believe it is

978-1-4244-1666-0/08/$25.00 ©2008 IEEE

artificially constraining the range of techniques proposed by the research community.

There are a lot of systems to get an image from collect data to view an environment using a triangulation principle. Majority of such systems required an expensive camera set whit high resolution, so this aspect make a very careful and delicate system; other way is using two or more laser to found a convergence beam.

It is considered in this paper a system with several characteristics previously referred; a high resolution, speed and versatility can be used by our system in low cost.

In the most of fully autonomous navigation systems is used a vision system like this, our prototype can stand out among the other systems because has a very low cost; other advantage is the versatility, has a wide range of vision that can change to increase precision; and large sight depending of laser power.

This vision of environment is very similar to the human sight, has wide range of view, but can focus a specific area to get a high resolution and detailed image, so to make this task is not necessary modify hardware in prototype, just adjust some parameters in software

III. SYSTEM FUNCTIONING DESCRIPTIONS

Basically this prototype takes the triangulation principle to calculate distances from a known point to other unknown point. We have a "base bar" (Fig.1) of 1m of length, in a first extreme is positioned a cylindrical mirror with 45 degrees cut (mirror A) to redirection the source of light placed on, this is mounted in a step motor (motor1); in this case laser beam is a source, but can be another kind of light, laser was taked because has a good coherency, good directivity and fine convergence in long distance; in the other extreme of the "base bar" has the "scanning unit" with an aperture to collect a diffusely reflected laser beam in another mirror (mirror B) with 45 degrees cut mounted in another DC motor (motor2).

So the laser beam is reflected in the "mirror A" toward scene in a front of prototype making a horizontal scanning by rotation of motor1 placing a set of spots of laser light in every object in front of prototype.

The vertical scanning is made by a third step motor placed in the center of the base bar for drive the vertical scanning axis (base bar).

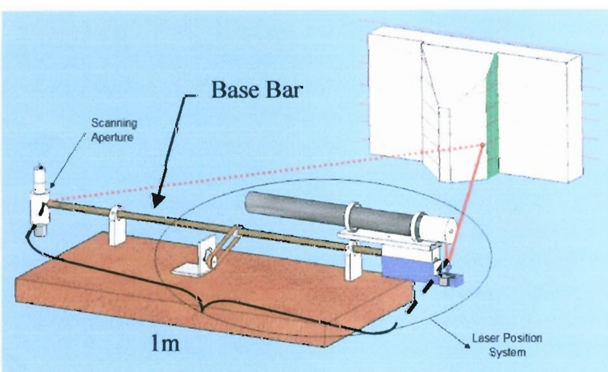

Fig 1. Prototype Laser scanning view

The scanning aperture (Fig.2) is compound by the "mirror B" to collect the spots reflection of the laser beam in the objects or obstacles, that signal is redirected by the "mirror B" into a lens for get a fine convergence of light, this signal is collected by another lens to ensure get a laser beam reflection.

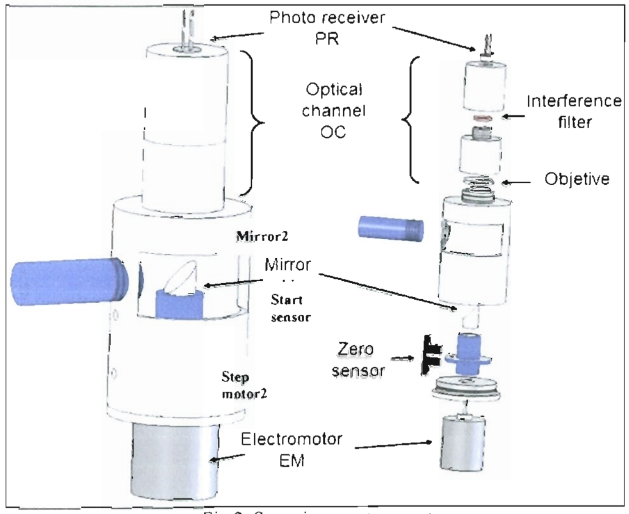

Fig 2. Scanning aperture parts

This prototype works as follows. The laser beam is positioned toward front perpendicular to "base bar" axis, then by software from a computer send a signal to start, the spot of laser L begins travel path to cover the horizon by motor1, a variable operator in the software (named "spot" in a text of program) is counting and store steps of this motor1; at same time in the scanning aperture, motor2 is revolving the second mirror scanning for optical signal reflected from objects, each revolution of this motor2 is counted by a sensor (start) inside of the aperture and stored in a software variable ("start"). When a spot S is reflected to the aperture SA this light signal is converted to an electrical signal by a photo receiver PR to be stored in software variable ("stop") (Fig. 3). When this happens, the system calculates the angle of rotation of the motor 2, calculating the relationship between the amount of reference pulses generated by the software (between START-STOP signals) and the amount of reference pulses existing in one rotation of motor 2 (between two START signals) and find the angle of coincidence with the reflected spot [11].

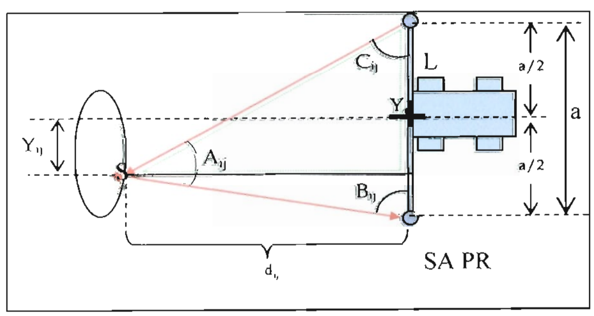

Fig 3 Distance Measurement through triangulation. (Top view)

Using triangulation is possible to calculate distances from the base bar toward front (Fig.3). In this process, if the variable "stop" its not detected there is no obstacles, when variable "stop" gets a value in the travel path of the scanning, the calculation begins, in that moment the position of motor1 and motor2 are stores in respective variables, so making a relation between the position of motor1 and motor2, and we know two angles: Cij and Bij (where i- number of step in horizontal scanning, and j - number of step in vertical scanning), distance "a" is known also (Fig.3), now about this data thought using the sine theorem as well as the relation between the sides and the height in a triangle we can calculate [11,12] distance "d" for each point reflected in a object, all this data is stored to make a graphic shape of an obstacle.

After a horizontal scanning is complete by the motor1 step by step and all data is stored in software, finished this 2D scanning the third motor makes a move to the next plane and the motor1 get back step by step sweeping reversely the horizon in other plane. This was providing 3D scanning.

The angle Dij given by the third motor is well known because each step is controlled (Fig.4), and is possible store data of each vertical level to after make a 3D image with horizontal and vertical scanning with formulas in [11,12].

We can modify resolution for scan increasing number of steps of dc motors, so in small area we have a lot of points (spot) and can be collect more data for more detailed environment.

This prototype was design for identify obstacles in totally unknown environment; this can help to another system giving essential information, for example described in [1].

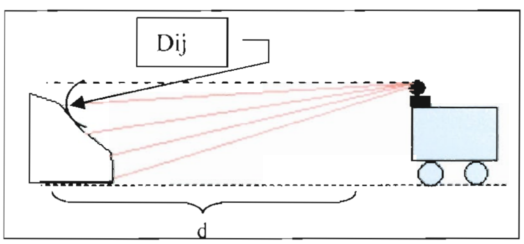

Fig.4 Scanning Lateral View

IV. PROTOTYPE CONSTRUCTION AND EXPERIMENTATIONS

This prototype can be fabricated in very simple way using low-cost elements. A prototype was made with the follows elements: an aluminum base bar with 1m of length, step motors to make vertical and horizontal scanning, source of light in this case a laser, a pair of mirrors with 45 degrees cut to redirection the light beam, in laser emisor part and scanning aperture (Fig.5, Fig.6), a photo receiver to convert light signal to electrical signal, a lens in the aperture part to get a fine convergence of light in photo receiver, a sensor (start) in the aperture part to detect and count revolutions of mirror2, and a interference filter to get only the selected source of light; this hardware is controlled by a laptop IBM Pentium II using "turbo c" program in MS-DOS where the measurement distances is stored (Fig.7), the connection to transfer data between hardware and software is by parallel port.

Fig. 5 Scanning aperture

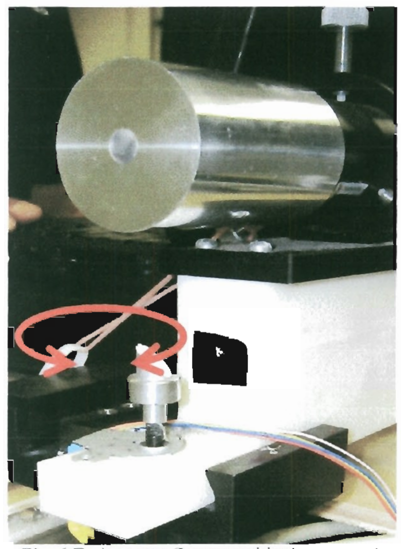

Fig. 6 Emisor part (Laser positioning system)

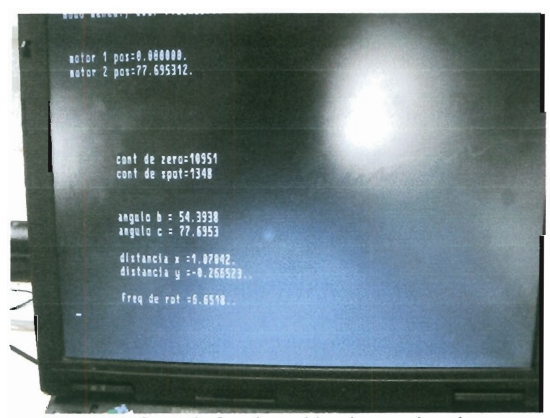

Fig.7 Software in function, taking data on obstacles.

The complete prototype is no longer than 1m, data can be stored in another system, and the prototype fabricated with all elements is shown in Fig.8 in action.

Fig.8 Complete prototype system testing view

This prototype was tested 50 times in different locations in grid nodes to verify accuracy on vision by different angles in 2D, making tests on reflective and absorptive objects: in Table.1 is partially shown the measurement values by the prototype on a plane surface with grid-scale.

TABLE I
EXPERIMENTAL RESULTS OF 2D POINTS MEASUREMENT

Test Point	Theoric Value				Measured Value			
	X (m)	Y (m)	B (°)	C (°)	x(m)	y(m)	B (°)	C (°)
B	120	120	120,26	35,22	124,21	128,68	123,43	34 8
D	100	100	116,57	33,69	99,83	104,48	118,46	32,87
F	100	80	106,70	37,57	95,3	76,86	106,4	36 91
H	120	60	94,76	47,49	122,92	63,49	96,38	47,28
J	80	60	97,13	36,03	77	58,62	96,57	35,33
L	80	40	82,87	41,63	79,99	42,15	84	40,95
N	120	40	85,24	53,13	119,88	40,04	84,48	53,08
O	120	20	75,96	59,74	119,22	19,48	76,01	59,76
P	100	20	73,30	55,01	97,6	19,15	72,94	54,67
Q	80	20	69,44	48,81	79,11	18,7	68,39	49,04
R	60	20	63,43	40,60	60,33	21,7	64,3	40,07
S	40	20	53,13	29,74	39,14	19,59	52,07	29,35
T	40	0	38,66	38,66	36,52	1,06	36,52	36,73
U	60	0	50,19	50,19	59.8	0,9	49,39	50,625
V	80	0	57,99	57,99	80,93	3,49	56,7	60,11
W	100	0	63,43	63,43	103,58	1,51	63,45	64,68
X	120	0	67,38	67,38	120,72	-4,7	66,23	69,43
Y	120	-20	59,74	75,96	118,54	-18,36	59,95	75,05
Z	100	-20	55,01	73,30	96,72	-18,37	54,7	71,9
A1	80	-20	48,81	69,44	75,79	-18,33	48,03	67,32
B1	60	-20	40,60	63,43	58	-18,53	39,5	61,52
C1	40	-20	29,74	53,13	36,17	-20,31	27,3	50,62
D1	60	-40	33,69	80,54	58,05	-38,63	33,6	78,92
E1	80	-40	41,63	82,87	77,46	-38,26	40,46	81,38
F1	100	-40	48,01	84,29	97,1	-38,02	48,94	82,96
H1	120	-60	47,49	94,76	123,68	-61,03	48,21	95,09
J1	80	-60	36,03	97,13	78,9	-59,73	35,37	97,03
L1	80	-80	31,61	110,56	80,52	-80,21	31,81	110,56
N1	120	-80	42,71	104,04	121,01	-78,73	43,34	103,35
P1	100	-100	33,69	116,57	101,65	-96,18	35,06	114,43
R1	100	-120	30,47	124,99	111,73	-126,15	32,09	124,27

The values in the table.1 are shown graphically in (Fig.9). The violet points are distance values taken by the prototype working usual way; the yellow points are distances measured by the prototype but using an independent source of light in each point to measure (without prototype laser), finally the real distances can be shown by squares in the table base.

As it is evident, the range of error is very small in the center of the table, this center is the center of the prototype sight, and near both sides of the prototype sight angle the error is minimal. This prototype is very similar to human sight, at front the image view is very detailed and precise, both borders of angle of view have no much accuracy, this can be resolved rotating the vision of focus of the prototype exactly humans sight do.

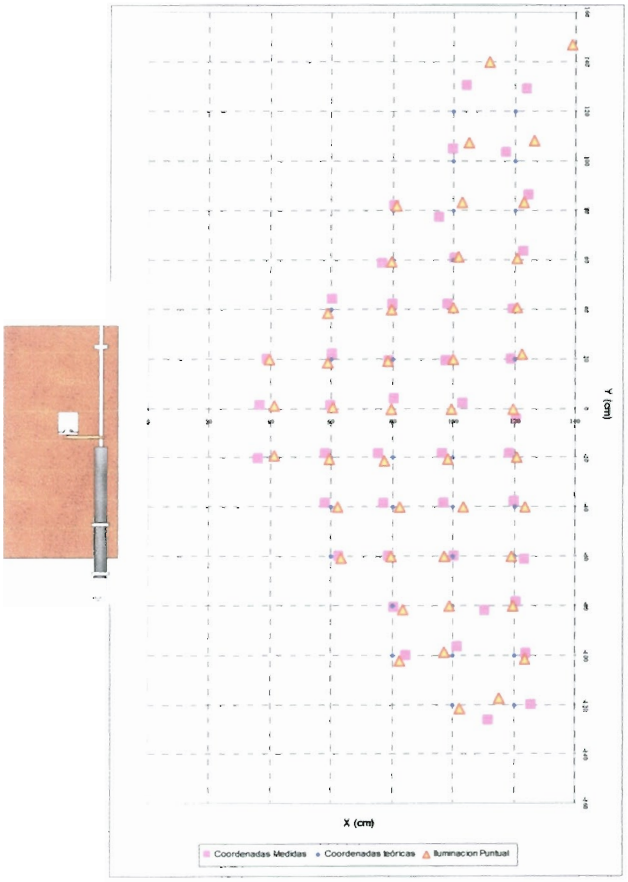

Fig.9 Experimental graphic of 2D points measurement and obstacle positioning.

Analyzing the measurement numerical results and its numerical values, it is possible to say that all the experiments were carried out not less at 95% confidence level. And measurement uncertainty, especially its offset error, not overcomes a 5% threshold in any point, even in extended angle of sight where such accuracy is not obligatory.

Also detailed analyzis of scanning aperture original construction (Fig. 2, 5) and principle deduce us to conclusion that it is possible to obtain measurement results with the same uncertainty from highlighted points of the different attitudes inside precertain angle of view. It is significant advantage of the presented device over other known laser triangulation scanners [2,3,4].

In general behavior of uncertainty repeats graphic presented on figure 6 in [3, p.1765], however accuracy nearby edge in our system is more advanced. Also accuracy (coordinate measurement offset) in a central part of scanner's angle of view is 2-7 times better in a different checked points respect to [3] for example.

V. Conclusions

Presented research was provided with a general goal to design simple and secure method for 3D laser scanning of any unknown surface placed on a variable distance from scanner location. Other advantage of a present system over other laser triangulation system is a higher in principle order of exactitude in a part of 3D coordinates calculation. Preliminary prototype testing is shown

- This theoretical principle can be realized with modern electronic and electromechanic devices in low cost;
- With completely acceptable operation velocity this device can detect an obstacle and to cover it with digital 3D map of *n* points on it's surface;
- This factor *n* is easy possible to change as only one variable in software; such way provide basic principle "more points – less uncertainty, but more operating time". This task must be solved carefully for each practical application;
- Coordinates calculation uncertainty is less than any known laser triangulation with electronic scanning because of exact surveying techniques principle using;
- This system in a closest way simulates the human binocular vision; as shown, the best exactitude can be achieved in a center of angle of view, and nearby both edges the picture is not has so sharpness. It possible to overcome by base bar rotation or robot turn;
- These techniques can be implemented for various practical applications, such as large engineering structures SHM, mobile robot navigation, etc.

VI. Future work

Preliminary design and construction of a prototype of passive scanning aperture based on the precise triangulation principle was made using commercial available digital circuits and hand made electromechanical devices and units. Direct comparison of theoretical reliability and operation velocity of the proposed system with first experimental results shows that it has redundant causes of uncertainty on the assembly stage.

Present days it is under construction the second device prototype, which should be assembled under industrial conditions.

On the second stage it will under investigation the possibility and advantages/losses of the pulse mode implementation for described optical channel.

Also it is important to determine experimentally period of interrogation (scanning) for different practical applications and the rate of factors, which are affects this process in real circuits functioning.

Acknowledgment

The authors dedicate this article to the grateful memory of our teacher, Dr. Valentin E. Tyrsa. The authors would like to thank to various congresses organizers [11, 12], where was discussed different aspects of the present work. We appreciate Daniel Hernandez-Balbuena's invaluable assistance.

References

[1] François Chaumette, Seth Hutchinson. Visual servo control PART I: basic approaches. IEEE Robotics & Automation Magazine, pp.82-90 , December 2006

[2] Paul Forman, Iwan Parry Rapid Data Collectiom at Major Incident Scenes using Three Dimensional Laser Scanning Techniques. 2001 IEEE 35th International Carnahan Conference on Security Technology, pp. 60-67, Oct 2001.

[3] D.S Pierce, T.S. Ng, B.R. Morrison. A Novel Laser Triangulation Technique for High Precision Distance Measurement, Proceeding of IEEE Industry Aplications Society Annual Meeting, vol.2, Houston USA, pp. 1762-1769, October 1992.

[4] Hartmut Surmann, Kai Lingemann, Andreas Nuchter and Joachim Hertzberg. A 3D laser range finder for autonomous mobile robots. Robotics and Autonomous Systems, Volume 45, Issues 3-4, pp. 181-198, 31 of December 2003.

[5] Siefko Slob and Robert Hack. 3D Terrestrial Laser Scanning as a New Field Measurement and Monitoring Technique. – in book "Engineering Geology for Infrastructure Planning in Europe", Springer Berlin / Heidelberg, pp. 179-189, 2004.

[6] D. D. Lichti, M. P. Stewart, M. Tsakiri, A. J. Snow. Benchmark tests on a Three-Dimensional Laser Scanning system. Department of Spatial Sciences of Curtin University of Technology, Geomatics Research Australasia, 23 p , 2000.

[7] S.Winkelbach, S.Molkenstruck, and F.Wahl, Low-cost Laser Range Scanner and Fast Surface Registration Approach. Proceedings of DAGM 2006, Springer Berlin Heidelberg, pp. 718-728, 2006.

[8] Ugonna Ibeanusi, Valerie Lafond-Favieres, Latresa McLawhorn, Scott D. Anderson. Understanding robot navigation and control, Proceedings of the 37th annual ACM Southeast Regional Conference, CD version, 7p., 1999.

[9] João Guilherme D. M. França, Mário A. Gazziro, Alessandro N. Ide, José H. Saito. A 3D scanning system based on laser triangulation an variable field of view. Proceedings of the International Conference on Image Processing (ICIP 2005), IEEE Volume 1, pp. 425-428, Genoa, Italy, 2005.

[10] James Davis, Ravi Ramamoorthi, Szymon Rusinkiewicz. Spacetime Stereo: A unifying framework for depth from triangulation, Proceedings of 2003 IEEE Computer Society Conference on Computer Vision and Pattern Recognition, Volume: 2, pp: II- 359-366, 18-20 June 2003.

[11] Tyrsa V.Ye., Sergiyenko O.Yu., Tyrsa V.V., Bravo M., Devia L., Rendon I. Mobile Robot navigation by Laser Scanning Means – Proceeding of 3rd International "Conference on Cybernetics and Information Technologies, Systems and Applications CITSA – 2006", Volume I, Orlando, Florida, USA, P. 340-345, July 20-23, 2006.

[12] Valentyn Tyrsa, Oleg Sergiyenko, Larisa Burtseva, Miguel Bravo-Zanoguera, Luis Devia, Ismael Rendon, Vera Tyrsa. Mobile Transport object control by technical vision means. Proceeding of IEEE International Conference CERMA2006, Cuernavaca, Mexico, Volume II, p.74-79, September 2006

Precise Optical Scanning for practical multi-applications

O. Sergiyenko[1], V. Tyrsa[3], D. Hernandez-Balbuena[1], M. Rivas López[3], I. Rendón López[2], L. Devia Cruz[1]
[1] Engineering Institute, Autonomous University of Baja California, [2] Technologic University of Hermosillo,
[3] Polytechnic University of Baja California, México. *srgnk@iing.mxl.uabc.mx*

Abstract- **At last decade many approaches for non-contact measurement techniques for object surfaces and approaches for 3D object recognition have been proposed; but often they still require complex and expensive equipment. Not least due to the rapidly increasing number of efficient 3D hardware and software system components, alternative low cost solutions are in great demand. We propose such a low-cost system for 3D data acquisition and fast surface registration by digitized points Cartesian coordinates matrix keeping. There is presented two examples of practical application of the passive optical scanning aperture under proposition.**

I. Introduction

A very common method for fast, safe and cheap information obtaining, is optical scanning. This kind of information collection has many practical applications because of a lot of experience and strong theoretical backgrounds. But on the other hands, some of the optical fundamentals put rigorous limits for universal optical scanners. In this paper we will present a new passive optical scanning method and equipment which permits a multifunctional use with simple according to certain practical task by basic working parameters changing.

A. Civil structures health Monitoring

Large civil infrastructures include various units and systems such as buildings, bridges, dams of hydroelectric plants, offshore platforms, transportation systems and communication systems. Significant amount of expenditures and long time periods are necessary for a society to build up its infrastructure systems; indeed, any advanced society has already put enormous effort toward this goal. The continued performance of these infrastructure units and systems is vital to our human and economic activities. Even a short-term malfunction affects the society tremendously [1, 2].

The built environment supported by infrastructures is an advantage if they are well maintained and properly operated. However, if they are degraded by improper maintenance, they can be a big debt to the society. To prevent this, it is absolutely necessary to develop maintenance technology for inspection, monitoring, repair, rebuilding and even financial planning. Structural health monitoring is one of the important components in the maintenance technology for civil infrastructures, and until now, some methods of structural monitoring have been used successfully and newly proposed methods offer the possibility of extending applications and improving efficiency.

Damage in a structure generally causes a local increase in flexibility, which depends on the extent of the damage. Currents methods of damage detection include visual inspections, classical non destructive techniques (NDT) and vibration/modal-based methods [1-3]. The majority of NDT techniques are based on regular ground inspections which are time consuming and thus expensive. Typical NDT methods for damage evaluation include: sonic, ultrasonic, acoustic-ultrasonic, acoustic emissions, pulse-echo, x-ray imaging, ground penetrating radar (GPR), and dye penetrant for crack determination [4].

Global Positioning System (GPS) technology and the use of Pseudo-Satellites has been widely used for monitoring the deformation of civil structures, but cannot be used when the signals are completely blocked by obstacles, natural and man-made, in addition to the high cost of receivers and pseudo satellites [5].

Recent advances in the development of new techniques it involves the use of embedded smart sensor and actuator technology for reduce the need for visual inspection to assess structural integrity and mitigate potential risk in large civil structures such as highways, bridges and buildings. These sensors and actuators are typically made up of a variety of materials including piezoelectric, shape memory alloy, magneto-strictive, electro-rheological and magneto-rheological fluids and fiber optic sensors. These materials can typically be embedded into the host matrix material of the structure to either excite or measure its state [6, 7].

Today's bridges and roads do not have ''intelligence'' built in, so they cannot take advantage of the benefits of the advancing technologies available for structural health monitoring. They are also in a poor state of repair due to inadequate maintenance, excess loading (relative to their original design and expected usage), and adverse environmental conditions (salt, acid rain, etc.).

In this paper, the design and the potential of the passive optical scanning aperture in deformation monitoring of civil structures are discussed. It is based on an optical exploration of luminous reference points previously fixed to the civil structure, measuring its coordinates periodically to determine, based on a historical information data base, the damage level of the structure. The most important technical part of this innovation and its operation principle and general design are shown in section 2.

978-1-4244-1766-7/08/$25.00 ©2008 IEEE

B. *Machine vision system for robot navigation*

Position determination for a mobile robot and the ability to measure surfaces and objects in 3D is an important part of autonomous navigation and obstacle detection, quarry mapping, landfill surveying, and hazardous environment surveying. In many cases, dead reckoning is insufficient because it leads to large inaccuracies over time. Beacon- and landmark-based estimators require the emplacement of beacons and the presence of natural or man-made structure respectively in the environment [8]. A significant number use landmark recognition, either extracting relevant natural features (corners, objects, etc.) using a camera or identifying prelocated beacons using both a camera and an optical scanner. Because image processing consumes long time and positioning accuracy, cannot satisfy the autonomous navigation in many cases. Major drawbacks of beacon-based navigation are that the beacons must be placed within range and must be appropriately configured in the robot work space.

The GPS based navigation for autonomous land vehicles has the capabilities to determine the locations of vehicles basing on satellites. Although commercial DGPS (Differential GPS) service increases the accuracy to several meters, it is still not sufficient for autonomous driving. It is well known that with the different type of GPS implementations we can obtain position fixes with errors of the order of 2cm to 100m. Nevertheless this accuracy cannot be guarantee all the time in most working environment where partial satellite occlusion and multipath effects can prevent normal GPS receiver operation [10]. Environmental sensors, such as 3D scanning laser rangefinder, ultrasonic environmental sensors, are also used.

Given the current state-of-the art [13-15] we believe that a 3-D laser scanner would be the best choice for building 3-D maps. However, 3-D scanners are expensive for most mobile robot applications and many are not fast enough for map building in real time on a fast-moving vehicle, due to the relatively slow vertical scan. A cost-effective alternative for 3-D mapping is to mount a 2-D laser scanner on the front-top of a mobile robot. During motion the fanning beam of the scanner sweeps over the terrain in front of the robot, effectively creating a 3-D map.

Triangulation-based laser range finders and light-striping techniques are well-known since more than twenty years. Beside other active techniques – like structured light, coded light, time of flight, etc. – laser range scanners are commonly used for contact-less measuring of surfaces and 3d scenes in a wide range of applications. Most commercial laser scan systems use a camera and a laser beam or laser plane. The surface recovery is based on triangulation, i.e. the intersection of the illuminating laser beam and the rays projected back to the camera [12]. Expensive high-precision actuators are often used for rotating/translating the laser plane or for rotating/translating the object.

We have designed scanning vision system that overcomes these limitations and provides a system that will meet the existing demand for more advanced mobile vehicle navigation. It has been developed for visual inspection tasks in both indoor and outdoor environments. The offered Passive Optical Scanning system, that along with a Laser Positioning System, allows to obtain three dimensional information of possible obstacles in front of a robot mobile and it can takes decisions and makes tasks of automatic navigation. The POS system does not require new elements and devices and can be designed on the basis of items currently in full-scale production.

This paper focuses on some of the design and applications issues of the passive optical scanning aperture in detail. The paper considers potential applications.

II. Problem Statement

The base to solve the tasks of navigation and civil structures monitoring, is the creation of the passive optical scanning system (POS) (Fig. 1). The POS must be fixed, and is compound of a fixed assembly to support and to align the electro-optical elements of the system. A double convex lens, a interference filter, and a micro rod of 45 degrees cylindrical mirror are used like optical elements The mirror is mounted on the shaft of a DC motor that causes that it turns the mirror on his vertical axis. It has two sensors, an opto-switch to indicate the starting point of the turn of the mirror (START signal) and photodiode to detect light emission points (STOP signal).

The main task of the POS is to make a search in the horizontal plane of light emission points $\mathbf{S_{ij}}$ that they are within its field of view. These emission points can be fixed previously on a study surface or to be reflection points of light on a surface. The POS works in the following way: The mirror turns at constant speed and whenever it it passes over an initial reference point, a START signal is generated. beginning the count pulses of a reference signal with high frequency and constant f_o, until the moment when the scanning plane will coincide with emitting point Sij. In this case the scanning plane we mean the plane formed by two intersected straight lines: motor rotation axis and the gravitational force line projection to the plane of mirror. When the point Sij belong to this imaginable plane can be formed the STOP pulse. Only at this short moment when the check point Sij coincides with the scanning plane exist the physical possibility to transmit a certain part of a light energy emitted by point Sij. When that happens, the ray caught by the mirror is reflected with same angle with which it arrived, towards the double convex lens. And it passes through the interference filter until arriving to the photo detector, generating a STOP signal. In another case, if during a complete turn of the mirror an emitted ray of light was not detected, then the counter of f_o pulses it will be reset.

In this process we can find the horizontal coincidence angle B_i between START signal and STOP signal,

$$B_i = 2\pi \cdot N_{Bi} / N_{2\pi 1} \qquad (1)$$

N_{Bi} it corresponds to the number of f_o pulses between START-STOP signals, and $N_{2\pi I}$ it is the number of f_o pulses in a complete turn of the mirror. These codes depend on the motor speed rotation (ω) and f_o frequency [16].

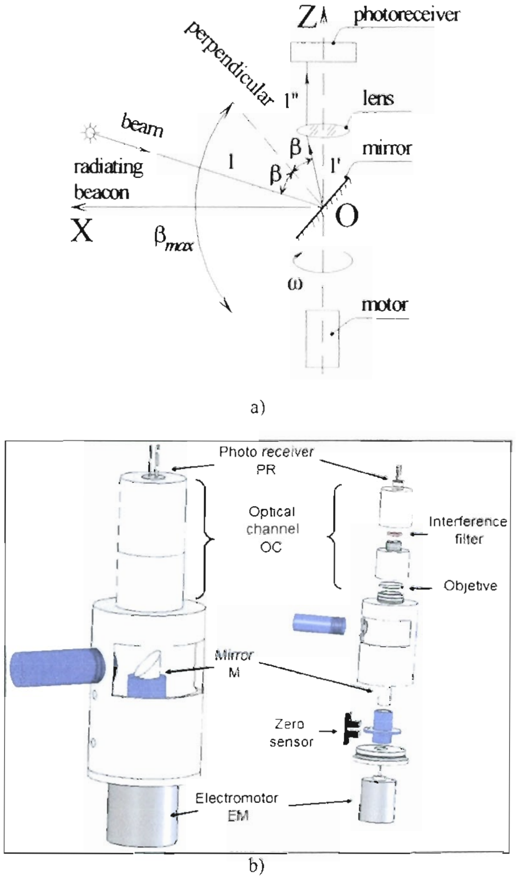

Fig. 1. Passive scanning aperture a) functioning principle, b) general design.

III. MONITORING OF CIVIL STRUCTURESFUL

One of the possible applications of the POS is the health of civil structures engineering monitoring. As example we can see the bridge of Figure 2. It is necessary to install Radiating Beacons (RB) on the surface of the structure with the same height h_i. The distance l_i between each RB is measured during the installation. In order to measure the horizontal and vertical displacements of each RB, two POS are installed, one POS to measure horizontal angles (HPOS) with vertical axis rotation and other POS to measure elevation angles (VPOS) with Horizontal axis rotation.

Then the following expression is valid for each RB$_i$ when deformation does not exist,

$$\frac{H-h}{l_i} = \tan(\frac{\pi}{2} - \beta_i) \qquad (2)$$

When there is deformation with magnitude Δh_i in the position of point RB$_i$, the measured angle by the pos $\Delta\beta_i$ will change in magnitude $\Delta\beta_i$ and the expression (2) would be in the following form,

$$\frac{H-h\pm\Delta h}{l_i} = \tan(\frac{\pi}{2} - \beta_i \pm \Delta\beta_i) \qquad (3)$$

Therefore:

$$\Delta h_i = (H-h) - l_i \tan(\frac{\pi}{2} - \beta_i \pm \Delta\beta_i) \qquad (4)$$

In this case, the system does not to be affected by the vibrations of the structure. The rotation velocity of the POS it´s fixed based on the natural vibration frequency of the monitoring structure and on the distance "POS – structure", to be able to observe abnormal distortions.

Fig.3 shows the placement of two vertical POSs for the arch dam monitoring of a hydroelectric power station. The POSs measure in pairs the horizontal angles α_{1i} and α_{2i} between the base line AB and the RB$_i$. The length of the base line D and the Cartesian coordinates of the POS are previously determined by known geodetic methods.

The angles ∠RB$_i$ are calculated with the following equation.

$$\angle RB_i = 180^\circ - (\alpha_{1i} + \alpha_{2i}) \qquad (5)$$

According the sine theorem we find the triangles sides with vertex A, B, RB$_i$ and the x_i, y_i Cartesian coordinates of the

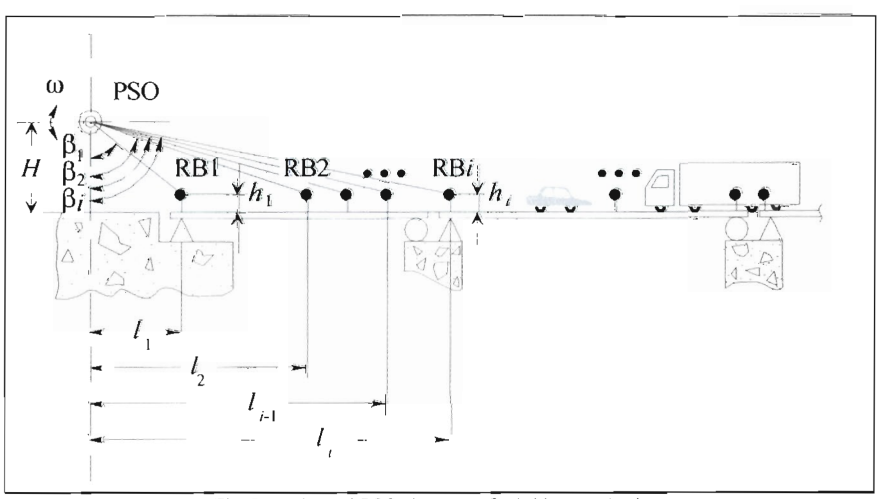

Fig. 2. Horizontal POS placement for bridge monitoring.

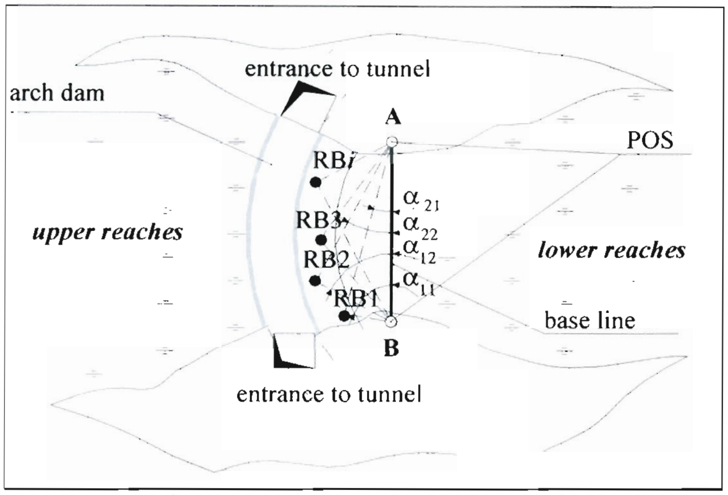

Fig.3. Placement of two vertical POSs for arch dam monitoring.

points RB_i. If there are changes in RB_i coordinates, then changes in angles α_{1i} and α_{2i} would be registered, which would indicate dam deformation.

In a similar manner is installed the POS system for tunnel monitoring. In extended tunnels several functionally connected POS can be placed along its axis.

IV. Scanning vision system

The Scanning Vision system is another application of a POS. In this manner, only is necessary installing one POS with a scanning laser position system (LPS).

Figure 4 shows a simple diagram of a triangulation scanner. The laser beam—reflected from a mirror in the LPS —is projected on the object. The diffusely reflected light is collected by the POS, if laser spots are projected.

The laser positioning circuitry controls the C_{ij} angle and $\Sigma\beta_i$ elevation angle are known. The angle B_{ij} is determined in the POS measurements. The triangulation distance, the a distance between the POS mirror and the LPS mirror, is also known.

As Figure 4 shows, since all geometric parameters are known, the x, y, z coordinates of the point on the object can be computed in a trigonometric form. If a single laser dot is projected, the system measures the coordinates of just one point of the object [16]. When a laser discrete stripe is projected, all points along the stripe are digitized. The basic triangulation scheme can be enhanced to improve the optical quality and depth of field by simple variation of "motor step size/steps quantity". It's easy to provide by software.

If we'll place the fast-operation POS on the autonomous mobile object, such as robot, vehicle, transportation carriage or any military techniques, we can use it like an artificial technical vision system for an automatic navigation task solution.

V. Experimental results

Practical working capacity of the given method has been checked out on a scanning aperture prototype, with preliminary experimentations. This experimentation was made using a movable light source, varying its position on a table with grid-scale, in which was situated a network with 45 designated points (See figure 5). The points were chosen according to the detection pattern of the system within a maximum range of 1 m. The separation distance between each point is of 20 cm in coordinate X and Y, with an error of

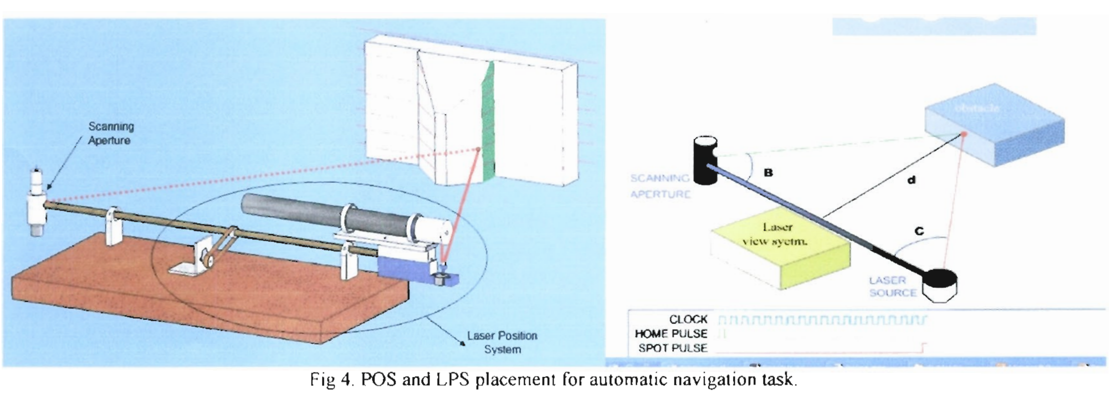

Fig 4. POS and LPS placement for automatic navigation task.

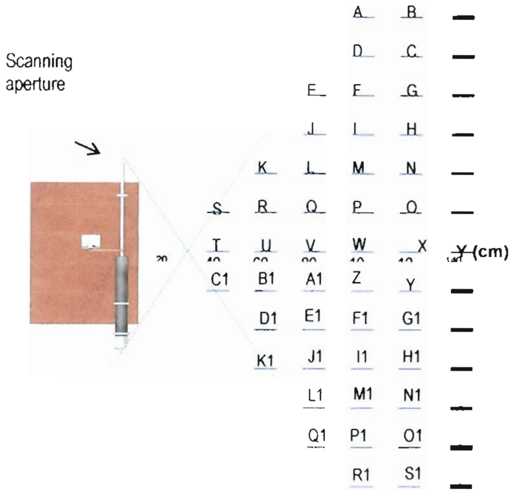

Fig.5. EBs' and POS positioning on the experimental table with grid-scale.

±0.1 cm. The light source used in the experiment, is a regular incandescent automobile lamp of 12 volts DC. Also the prototype gives the possibility to highlight same points with laser ray by 20mW laser (JDS Uniphase, model 1136P). The lamp was located in each point of the network, where 10 optical scannings were made. An average of the reception angle for each point was obtained (see table 1). Additionally, the value of the emission angle (angle C) for each point in test was obtained using trigonometrical formalism in [16, p.342].

Using the value of angle C, the final coordinates X and Y that describe the experimental position of each point, were obtained. Each point coordinate value has an measurement error. This error must due to many causes, but mainly due to the errors in reflection angle measurement at optical aperture.

Principle known causes of error are detected:

- Instability of motor speed in optical aperture.
- Electrical signal center shifting caused by low operating velocity.
- Improper calibration of reference instrument.

All these causes are been taking to account in the present process of a second prototype design.

Table 1. Experimental results.

Test Point	Theoretical Value				Measured Value				Relative Error [%]
	X (m)	Y (m)	B (°)	C (°)	*X(m)*	*Y(m)*	*B (°)*	*C (°)*	*(offset)*
A	100	120	124.99	30.47	111.94	140.3	128.89	30.47	3.12
B	120	120	120.26	35.22	139.01	146.93	124.89	35.22	3.85
C	120	100	112.62	38.66	126.53	108.16	114.69	38.66	1.83
D	100	100	116.57	33.69	104.91	107.37	118.67	33.69	1.81
E	80	80	110.56	31.61	81.2	81.949	111.48	31.61	0.83
F	100	80	106.70	37.57	102.73	83.555	108.09	37.57	1.30
G	120	80	104.04	42.71	123.21	83.475	105.2	42.71	1.12
H	120	60	94.76	47.49	120.52	60.481	94.97	47.49	0.22
I	100	60	95.71	42.27	101.36	61.499	96.472	42.27	0.80
J	80	60	97.13	36.03	79.405	59.182	96.596	36.03	0.54
K	60	40	80.54	33.69	58.935	38.403	78.868	33.69	2.07
L	80	40	82.87	41.63	79.567	39.513	82.492	41.63	0.46
M	100	40	84.29	48.01	100.17	40.157	84.388	48.01	0.12
N	120	40	85.24	53.13	120.67	40.499	85.498	53.13	0.31
O	120	20	75.96	59.74	122.59	21.509	76.916	59.74	1.25
P	100	20	73.30	55.01	99.755	19.829	73.172	55.01	0.18
Q	80	20	69.44	48.81	78.538	18.721	68.284	48.81	1.67
R	60	20	63.43	40.60	58.791	18.59	61.886	40.60	2.44
S	40	20	53.13	29.74	39.652	19.391	52.334	29.74	1.50
T	40	0	38.66	38.66	41.083	1.3538	40.182	38.66	3.94
U	60	0	50.19	50.19	60.67	0.5579	50.822	50.19	1.25
V	80	0	57.99	57.99	79.392	-0.3799	57.602	57.99	0.68
W	100	0	63.43	63.43	99.259	-0.3703	63.094	63.43	0.54
X	120	0	67.38	67.38	119.63	-0.1522	67.256	67.38	0.18
Y	120	-20	59.74	75.96	121.09	-19.729	60.064	75.96	0.54
Z	100	-20	55.01	73.30	98.417	-20.475	54.394	73.30	1.12
A1	80	-20	48.81	69.44	77.312	-21.008	47.434	69.44	2.83
B1	60	-20	40.60	63.43	59.276	-20.362	40.112	63.43	1.21
C1	40	-20	29.74	53.13	41.172	-19.121	30.78	53.13	3.48
D1	60	-40	33.69	80.54	62.278	-39.62	34.796	80.54	3.28
E1	80	-40	41.63	82.87	82.325	-39.709	42.542	82.87	2.18
F1	100	-40	48.01	84.29	103.12	-39.688	48.986	84.29	2.03
G1	120	-40	53.13	85.24	123.5	-39.708	54.006	85.24	1.65
H1	120	-60	47.49	94.76	119.04	-59.92	47.282	94.76	0.44
I1	100	-60	42.27	95.71	96.858	-59.686	41.446	95.71	1.96
J1	80	-60	36.03	97 13	79.77	-59.971	35.956	97.13	0.20
K1	60	-60	28.61	99.46	63.354	-60.559	29.814	99.46	4.21
L1	80	-80	31.61	110.56	83.619	-81.357	32.48	110.56	2.76
M1	100	-80	37.57	106.70	98.923	-79.677	37.338	106.70	0.61
N1	120	-80	42.71	104.04	119.63	-79.908	42.642	104.04	0.16
O1	120	-100	38.66	112 62	123.77	-101.57	39.234	112.62	1.49
P1	100	-100	33.69	116.57	96.833	-98.416	33.122	116.57	1.69
Q1	80	-100	28.07	122 01	82.59	-101.62	28.578	122.01	1.80
R1	100	-120	30.47	124.99	102.2	-121.54	30.786	124.99	1.05
S1	120	-120	35.22	120.26	115.43	-117.33	34.598	120.26	1.76

Basing in data analysis is possible to determine a zone in the Table 1 where the obtained data is more accurate. It is shown on a Fig.6. All the experiments were carried out not less at 95% confidence level. But in the Fig.5 are presented real points and measured points, ant it is evident that appears two zones of different accuracy in this measurement. Most exact data was obtained in frontal zone, where the experimental data's have an error less than in the zones nearby edge. Thus, the zone of more accurate measurement from the system can be known.

In general behavior of uncertainty repeats graphic on figure 6 in [17, p.1765], however accuracy nearby edge is advanced. Also accuracy in a central part of angle of view is 2-7 times better in a different checked points respect to [17] for example.

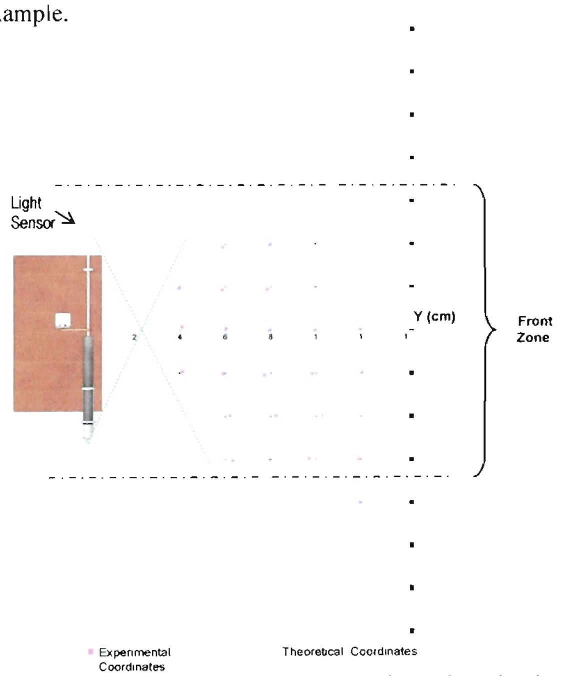

Fig.6. Measured coordinates points positioning on the grid-scale.

VI. CONCLUSIONS

The offered system has the next advantages over other 3D triangulation scanners:

- It not requires expensive no telescope tubes for scanning ray positioning neither megapixel sensors matrix;
- Uncertainty of angles measurement depend only on well known technical parameters, and can be preliminary fixed according to certain task requirements.

REFERENCES

[1] George James, Randy Mayes, Thomas Carne, and Garth Reese. 6-11 Nov 1994, *Damage detection and Health Monitoring of operational structures*. Experimental Structural Dynamics Department. Sandia National Laboratories. Conference: American Society of Mechanical Engineers' winter annual meeting, Chicago, IL (United States), Technical report, 10p.

[2] Scott W. Doebling, Charles R. Farrar, Michael B. Prime, Daniel W. Shevitz. 1996. *Damage Identification and Health Monitoring of Structural and Mechanical Systems from Changes in Their Vibration Characteristics: A Literature Review. Report LA-12767-MS*, Los Alamos National Laboratory, University of California. Los Alamos, NM, 136p.

[3] L. Mallet, B. C. Lee, W. J. Staszewskil and F. Scarpa. 2004. *Structural health monitoring using scanning laser vibrometry: II. Lamb waves for damage detection*. Smart Material and Structures. Vol.13, p. 261–269.

[4] Sohn H. et al., 2004. *Review of Structural Health Monitoring Literature from 1996 – 2001. Report LA-13976-MS*, Los Alamos National Laboratory, University of California. Los Alamos, New Mexico.

[5] Liwen Dai, Jinling Wang, Chris Rizos, Shaowei Han. January, 2002. *Pseudo-Satellite Applications in deformation Monitoring*. GPS Solutions journal. SpringerLink, Volume 5, Number 3, p. 80-87.

[6] Darryll J. Pines and Philip A. Lovell, 1998. *Conceptual framework of a remote wireless health monitoring system for large civil structures*. Department of Aerospace Engineering, University of Maryland, College Park, MD, USA. Smart Material and Structures journal. 7 p.627- 636. Printed in the UK.

[7] R. C. Tennyson, A. A. Mufti, S. Rizkalla, G. Tadros and B. Benmokrane. 2001. *Structural health monitoring of innovative bridges in Canada with fiber optic sensors*. ISIS Canada, A Network of Centres of Excellence, University of Manitoba, Winnipeg, Manitoba, Canada. Smart Material and Structures. 10 p.560–573.

[8] John Hancock, Dirk Langer, Martial Hebert, Ryan Sullivan, Darin Ingimarson, Eric Hoffman, Markus Mettenleiter, Christoph Froehlich. May 1998 *Active Laser Radar For High-Performance Measurements*. Proceedings of the 1998 IEEE International Conference on Robotics & Automation Leuven, Belgium. P. 1465-1470.

[9] J. Inigo Thomas, John Oliensis. 1993 *Automatic Position Estimation of a Mobile Robot*. Proceedings of Ninth Conference on Artificial Intelligence for Applications, Orlando, FL, USA, p.438-444.

[10] Lei Wang. Takashi Emura. and Takashi Ushiwata October 1-3, 2000. *Automatic Guidance of a Vehicle Based on DGPS and a 3D Map*. 2000 IEEE Intelligent Transportation Systems Conference Proceedings, Dearborn (MI), USA, p.131-136.

[11] Jose Guivant, Eduardo Nebot, Stefan Baiker. April 2000. *High Accuracy Navigation Using Laser Range Sensors in Outdoor Applications*. Proceedings of the 2000 IEEE International Conference on Robotics & Automation,V.4 San Francisco, CA, p. 3817-3822.

[12] Simon Winkelbach, Sven Molkenstruck, and Friedrich M. Wahl. 2006. *Low-Cost Laser Range Scanner and Fast Surface Registration Approach*. DAGM, LNCS 4174, p. 718–728, 2006, Springer Berlin Heidelberg.

[13] A. Wehr, U. Lohr. 1999. *Airborne laser scanning - an introduction and overview*. ISPRS Journal of Photogrammetry & Remote Sensing, Vol. 54, Elsevier, p.68–82

[14] Kenichi Nishide, Moritomo Hanawa and Toshio Kondo. 1986. *Automatic Position Findings of Vehicle By Means of Laser*. IEEE International Conference on Robotics and Automation Proceedings, p. 1343-1348.

[15] Cang Ye and Johann Borenstein. May, 2002. *Characterization of a 2-D Laser Scanner for Mobile Robot Obstacle Negotiation*. Proceedings of the 2002 IEEE International Conference on Robotics & Automation, Washington, DC, USA, p.2512-2518.

[16] Tyrsa V.Ye., Sergiyenko O.Yu., Tyrsa V.V., Bravo M., Devia L., Rendon I., July 20-23, 2006. *Mobile Robot navigation by Laser Scanning Means* - 3rd International "Conference on Cybernetics and Information Technologies, Systems and Applications CITSA – 2006", Volume I, Orlando, Florida, USA, p. 340-345

[17] D.S. Pierce, T.S. Ng, B.R. Morrison (1992). A Novel Laser Triangulation Technique for High Precision Distance Measurement, Proceeding of IEEE Industry Applications Society Annual Meeting, vol 2, October 1992, Houston USA, pp. 1762-1769

Monitoring of civil engineering structures

Valentin Tyrsa*[a], Larisa Burtseva[a], Moises Rivas Lopez[a], Vera Tyrsa[b]
[a]Engineering Institute of Autonomous University of Baja California, Calle de La Normal S/N, 21270, Mexicali, Mexico;
[b]Automobile and Highway Technical University, Petrovsky str., 28, Kharkiv, 61002, Ukraine

ABSTRACT

Civil engineering structures require geometrical monitoring to assure their integrity during their life time. The monitoring by geodetic devices or according to GPS technology is not always appropriate, sometimes it is unrealizable. Means for monitoring based on automatic geodetic measurements applying optical scanners are proposed. The sensor for integrity and deformation control of the structure elements and components was designed.

Keywords: monitoring, geometrical measurement, engineering structure, tunnel, deformation, optical scanning system, radiating beacon.

1. INTRODUCTION

Large engineering structures like bridges, tunnels, high-rise buildings, dams of hydroelectric plants, etc. require frequent observation of their integrity and deformation during all their operation time.

The deformation of a structure is observed by the periodic determination of their reference points coordinates, fixed on object. For this purpose a geometrical and a trigonometrical leveling, a tacheometrical survey or the GPS NAVSTAR technology are used. The GPS technology cannot be used outside the zone of radio signals reception such as tunnels, mines, etc. In this case, only traditional geodetic means remain.

Work with geodetic tools on functioning structures has a low productivity and frequently it is associated with difficulties. Sometimes the interruption of the main work is required, for example during vibrations; in that case the work of geodetic devices is suspended, since the operators can not work, and then appropriate tools for automatic geodetic measurements should be created. Therefore, built-in systems are invented and implemented.

The integrity of the observable object fragments is checked visually, by photo or TV cameras. The labors are executed manually by qualified workers. Such works not only are labour-consuming; they are dangerous for the executors life. On especially important objects, if the condition permits, the automatic control systems include a set of sensors and the transmitting and receiving stations.

For the creation of such systems, the problem consists in the selection or the development of sensors able to detect the formation of cracks in reinforced concrete constructions, or the deformation of steel structures.

2. AUTOMATIC MEASUREMENT OF PLANE ANGLES

Geodesy in its practical part measures corners and distances.

Up to Bergstrand invention of a range-finder in the middle of the XX century, the geodesy basic tools were: a theodolite, a surveying tape and a level. In many cases for the vertical surveying a level was replaced with a theodolite. It is called trigonometrical leveling. A theodolite was invented by Leonard Digges in 1571 and its diagram was kept up to our time in all measurement systems of plane angles.

In practice, the plane angles can be formed 1) by the shafts mutual turning or 2) by the lines intersection (spatial plane angle). In the first case, for the measurement of a spatial plane angle we need a special tools constructed in accordance with the theodolite diagram.

The measurement of a spatial plane angle by a theodolite is done by a search of an aiming point of a sighting telescope inside the solid angle 4π sr.

A sighting telescope has the visual solid angle [1]:

* v_tyrsa@iing.mxl.uabc.mx

Health Monitoring and Smart Nondestructive Evaluation of Structural and Biological Systems III, edited by Tribikram Kundu, Proc. of SPIE Vol. 5394 (SPIE, Bellingham, WA, 2004) · 0277-786X/04/$15 · doi: 10.1117/12.537411

$$\Omega_t = 4\pi \cdot \sin^2 \frac{\beta_t}{4} \qquad (1)$$

Here β_t is the visual plane angle of the theodolite. For $\beta_t \approx 2^\circ$ from (1) $\Omega_t = 9.57 \times 10^{-4}$ sr. The points number m_e examined by a theodolite in the solid angle 4π sr is:

$$m_e = 1/\sin^2(\beta_t/4) \geq 1.31 \cdot 10^4.$$

Hence it is clear a process automation difficulty of a space given point search and its device guidance.

The problem of a spatial plane angle automatic measurement can be solved by active [2, 3] or passive [4, 5] optical scanning systems (POS). As against an active system, a POS solves the two-uniform task: the search of the sighting point and the measurement of the plane angle in space.

The principal elements of a system are represented on Fig. 1 [4, 5], the light of a radiating beacon (RB) by a mirror rotation gets through a lens on a photoreceiver, which forms a stop - pulse. A start-pulse is formed by a special independent zero-sensor. The time interval $T_\alpha = \alpha/\omega$ corresponds to the spatial plane angle α between the zero-sensor and the direction on a RB. The intervals T_α and $T_{2\pi} = 2\pi/\omega$ are filled by pulses of the standard frequency f_0, generating the codes $N_\alpha = T_\alpha f_0$ and $N_{2\pi} = T_{2\pi} f_0$. From the proportion $\frac{\alpha}{2\pi} = \frac{N_\alpha}{N_{2\pi}}$ is received:

$$\alpha = 2\pi \frac{N_\alpha}{N_{2\pi}}$$

invariant respect ω and f_0. The experimentally verified uncertainty of the single measurement of the angle α, for one rotation period of the mirror is about 10 arc seconds.

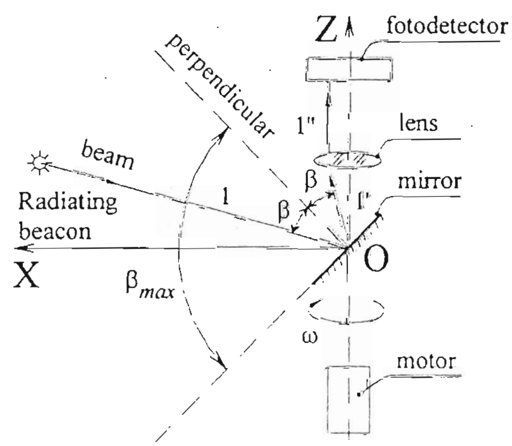

Fig. 1. Operating principle of a POS

The average of the multiple, automatically repeated measurements permit to obtain the uncertainty measurement of the angle α no more then 1 second of arc. The average angle is determined as:

$$\bar{\alpha} = 2\pi \frac{\sum_{i=1}^{n} N_{\alpha i}}{\sum_{i=1}^{n} N_{2\pi i}} \qquad (2)$$

The relations $N_{\alpha i}/N_{2\pi i}$ and $N_{\alpha(i+1)}/N_{2\pi(i+1)}$ represent the rational fractions that possess the property of Farey Fractions [6]. The ratio of the numerators sum to the denominators sum for such fractions in the formula (2) represents the mediants of the Farey fractions. For a formation of the mediant n in the form of the fraction $\sum_{i=1}^{n} N_{\alpha i} / \sum_{i=1}^{n} N_{2\pi i}$, the sum $\sum_{i=1}^{n} N_{\alpha i}$ forms discretely on each turn of the POS's mirror is formed. The sum $\sum_{i=1}^{n} N_{2\pi i}$ is formed continuously from the first start-pulse up to the $n+1$. A computer performs the operation of a division only once, after the formation of the sums $\sum_{i=1}^{n} N_{\alpha i}$ and $\sum_{i=1}^{n} N_{2\pi i}$ in the POS. The average $\overline{\alpha}$ found with the mediants use, has the higher exactness, than the classical arithmetic middle exactness for the given meaning n.

3. A COVERAGE OF A POS

From the analysis of a possible position of a beam going from the RB to the mirror, is clear, that the maximum value of the angle β between the beam and the perpendicular to the mirror, can reach 90°. Thus, the POS aperture angle is $\beta \le 90°$. At the mirror rotation, the all-round vision of a POS is:

$$\Omega = 4\pi\left(1 - 2\sin^2 \frac{180° - \beta_s}{4}\right). \tag{3}$$

If $\beta = 90°$ then $\Omega = 2.83\pi$ sr. It is more than half of the all space around of a POS.

We shall determine the coverage of a POS from the following assumptions:

Let the RB represent the diode laser with the radiation power P, the uniform radiation density in the solid angle 4π sr is

$$I = \frac{P}{4\pi} \tag{4}$$

Let the aperture diameter of the POS be $2r = 3\times10^{-2}$ m, then the radiation power, getting in the POS is:

$$P_a = I\Omega_a, \tag{5}$$

where

$$\Omega_a = \frac{S_a}{D^2} = \frac{\pi r^2}{D^2}. \tag{6}$$

According to the expressions (4) and (5), from the proportion (6) we find the coverage

$$D = \frac{r}{2}\sqrt{\frac{P}{P_a}} \tag{7}$$

Let the P_a be equal to the minimum value of the liminal optical power $P_{\min}$. It can be determined by the technique given in reference [7, p.70]:

$$P_{\min} = NEP\frac{R_{\max}}{R(\lambda)}\sqrt{B} = \text{W}.$$

Here NEP is the noise equivalent of the power, $R_{\max}$ and $R(\lambda)$ are the maximum sensitivity and the sensitivity on the detecting wave, B is the frequencies band (in Hz). For example, the length of the wave for the photoreceiver Model#2007 [7, p.56; 66] is 400-1070 nm; $NEP = 3\times10^{-12}$. For $B = \omega/2\pi \approx 100$ Hz, $R_{\max} = 0.55A/W$ and $R(\lambda) = 0.5A/W$:

$$P_{\min} = 3\times10^{-12} \times 0.55 \times \frac{\sqrt{100}}{0.5} = 3.3\times10^{-11}\ \text{W}.$$

From the expression (7) we find:

$$D_{\max} = 0.5\times1.5\times10^{-2}\times\sqrt{\frac{2}{3.3\cdot10^{-11}}} = 1846\ \text{m}.$$

4. PLACEMENT OF THE POS ON THE MONITORING OBJECTS

The above described POS with the vertical axis of the rotation is destined for the measurement of the horizontal angles. Let's call it as a vertical POS. The vertical angles between the RBs are measured by the POS with the horizontal axis of the rotation. This POS we denote as the horizontal POS. The system consisting from a vertical and horizontal POSs permit to measure the displacement of the RB in horizontal and vertical planes.
Figure 2 shows the placement of the horizontal POS for the realization of the bridge points monitoring in a vertical plane. The POS is placed outside the bridge and measures the vertical angles β_i, the RBs are established at the identical height h_i above the bridge surface. The distances l_i are measured during the installation.
At the absence of a deformation for each LB_i, the following relation is valid:

$$\frac{H-h}{l_i} = \tan(\frac{\pi}{2} - \beta_i). \tag{8}$$

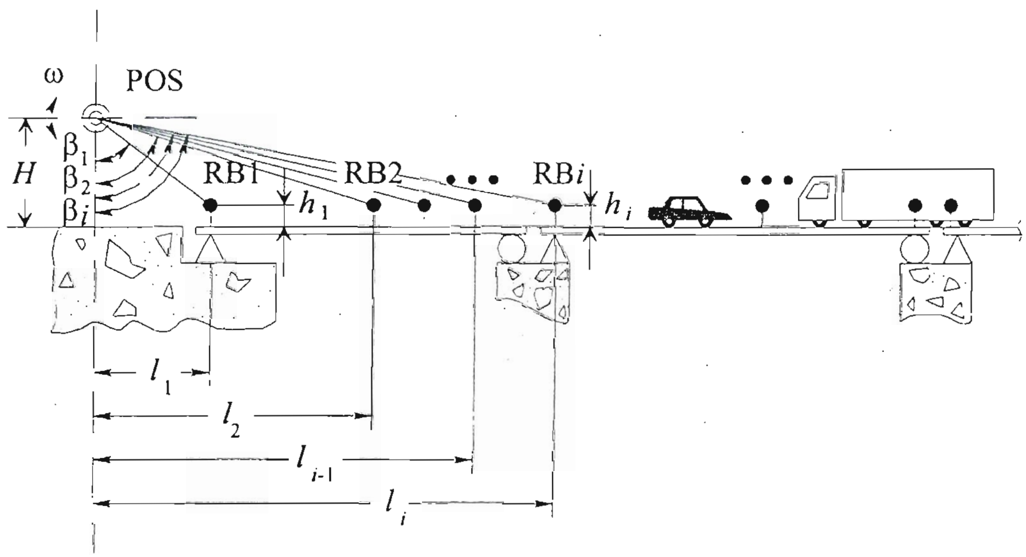

Fig. 2. Placement of the horizontal POS for bridge monitoring

As a result of the bridge deformation with the size Δh_i, at the point, where the beacon LB_i is established, the angle β_i measured by the POS will change on the size $\Delta\beta_i$, and the relation (8) will receive the form:

$$\frac{H-h \pm \Delta h}{l_i} = \tan(\frac{\pi}{2} - \beta_i \pm \Delta\beta_i),$$

and therefore:

$$\Delta h_i = (H-h) - l_i \tan(\frac{\pi}{2} - \beta_i \pm \Delta\beta_i).$$

In a similar manner a POS is placed also for tunnels monitoring. In extensive structures, along the monitoring object, we can place a few POSs, functionally connected with each other.
Fig. 3 shows the placement of two vertical POSs for the arch dam, monitoring a hydroelectric power station.
The POSs measure in pairs the horizontal angles α_{1i} and α_{2i} between the base line AB and the RB_i. The length of the base line D and the cartesian coordinates of the POS are determined by known geodetic methods beforehand. The angles $\angle RB_i$ are found conform to the formula:

$$\angle RB_i = 180^\circ - (\alpha_{1i} + \alpha_{2i}).$$

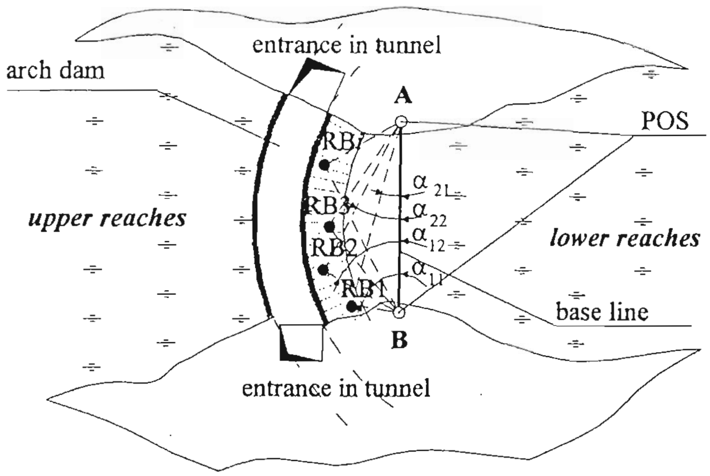

Fig. 3. Placement of two vertical POSs for arch dam monitoring

According the sine theorem we find the triangles sides, which have the vertex A, B, RB$_i$.; and the coordinates x_i, y_i of the points RB$_i$, in the state or conditional cartesian coordinate system. The changes of coordinates of the points LB$_i$ and the repeated measurements of the angles α_{1i} and α_{2i} reveal the dam deformation.

Fig. 4 shows the monitoring system of the pyramid UXMAL, Yucatan State, Mexico is presented as an example of the monitoring system of a three-dimensional object.

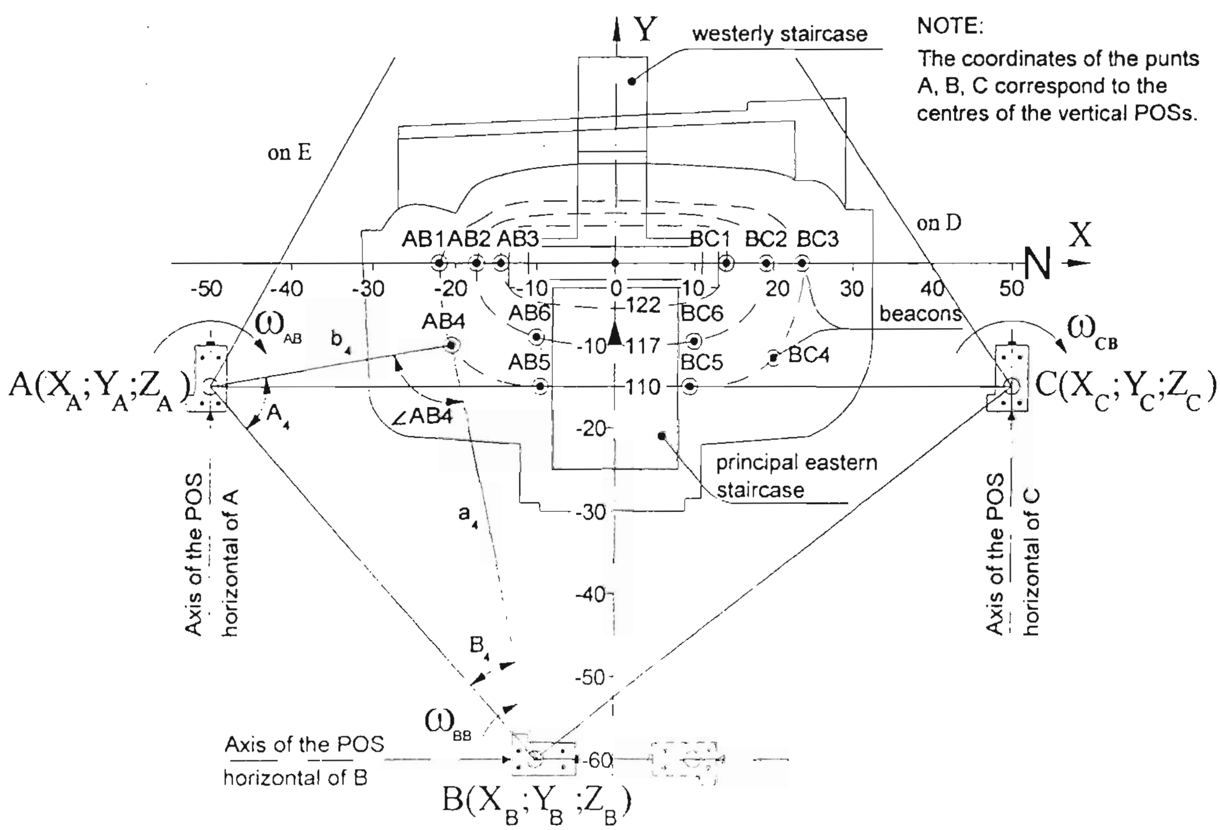

Fig. 4. Schematic diagram of the POSs placement for the monitoring the pyramid UXMAL. Yucatan State. Mexico.

5. SENSORS FOR A CONCRETE INTEGRITY MONITORING SISTEM

Concrete is one of the most popular building materials. For example, the large bridges connecting the island del Carmen, Campeche State, Mexico, with the continent, are constructed from reinforced concrete (Fig. 5).

The concrete peculiarity is its high compression strength, around 2×10^7 N/m^2, but it is fragile, and it does not withstands a tension load. The deterioration occurs in the form of cracks, which are visible in Fig. 6.

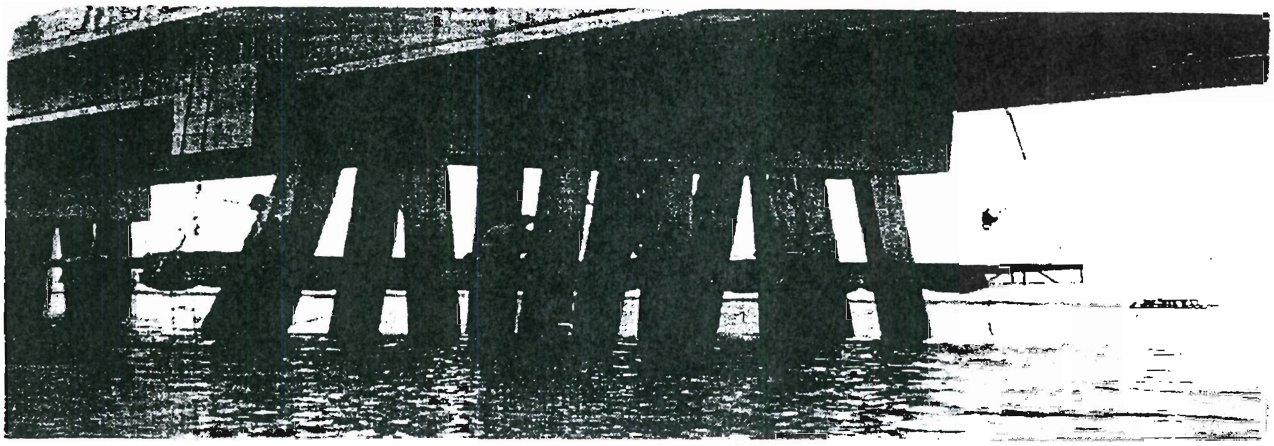

Fig. 5. The reinforced concrete bridge in Campeche State, Mexico

Fig. 6. A crack on the bridge column (dark line on bottom right)

It is evident the need of the urgent monitoring of concrete structures integrity. The resister sensors used for the measurement of steel deformation cannot be used for concrete integrity monitoring.
Fig. 7 shows the diagram of the simple sensor for concrete integrity control. It represents a ceramic or glass plate. more fragile than concrete. The external surface of the plate is covered with a conducting layer. It can be a graphite or metal powder protected by a waterproofed insulation.

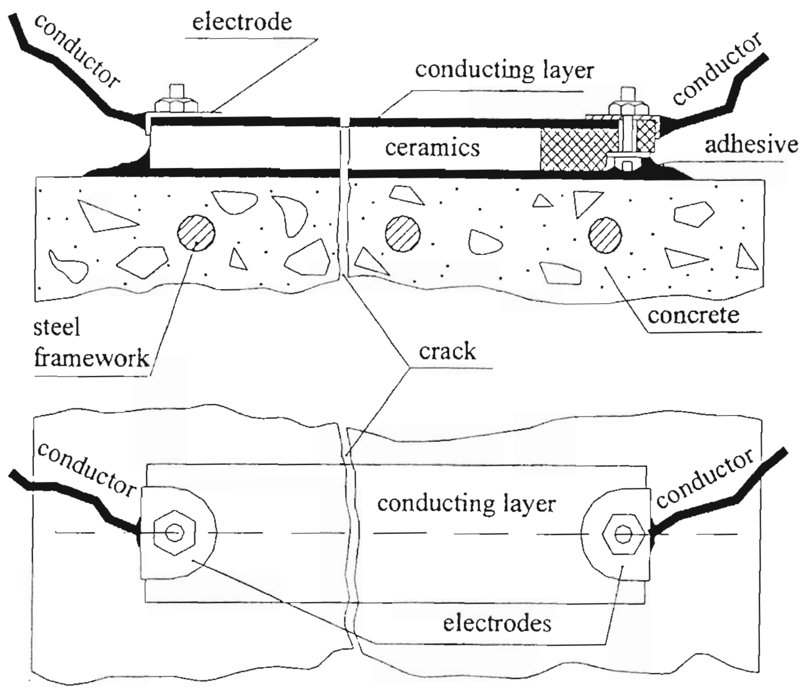

Fig. 7. Elementary sensor for concrete integrity control.

Along with the current source and the conductors, connected to the plate through the contact electrodes, the plate represents a continuous electric circuit, connected with the active perceiving element, which is not shown on the figure. The plate is adhered to the concrete surface in that manner, that its longitudinal axis is located perpendicularly to the probable direction of cracks.

With the formation of a crack in concrete, in the fragile plate, represented solid mass with the concrete, the crack also is formed, which creates the break in an electrical circuit. The perceiving element of the monitoring system with a POS detects the break. The sensor can be designed also in such a manner, that the formed crack will close an electrical circuit or an optical channel. This signal is registered by the POS.

6. CONCLUSIONS

1. The built-in stationary system monitoring of structure deformation, based on the POS, possess the following inherent qualities:

An opportunity to receive the data about deformation every minute, in all control points, with the smallest uncertainties on the object of any size and configuration;

The complete automatization of the measurement process, the data registration for the significant distance between the processing center and the observable object;

The operation of the monitoring system without interruption of the object functioning;

A possibility of the operation under ground: in tunnels, Metro, mountain excavation;

High durability and a simple service;

The possibility of the lasting round-the-clock control of the earthquakes development centers with the purpose of their prediction.

2. On the base of a POS the navigation systems of a mobile robots, the system automatic adjustment of the compound space crafts, the mutual orientation system of the objects with the six degrees of freedom, the deformation monitoring system for the navy and aircrafts in dynamics, the systems of automatic region mapping [4] and others can be constructed.

REFERENCES

1. Clair L. Wyatt, *Electro-Optical System Design. For Information Processing*, p. 344, McGraw-Hill, New York, 1991.
2. V.E.Tyrsa, "Technique of a Determination of a Object Coordinates", Author's Certificate on the Invention No 402736, G 01.C1/00, Moscow, 1973.
3. V.E.Tyrsa. "On Automation of Geodetic Measurements Intended for Earthquakes Prediction", Geodesy and Kartography, **2**, pp.18-21, 1996 (in Russian).
4. V.E.Tyrsa, "Geodetic Measurements Automation by Means of Optical Scanning Systems", Geodesy and Kartography, **9**, pp.16-20, 1996 (in Russian).
5. V.E. Tyrsa, A. Sauseda-Carvajal, L.P.Burtseva, J. Rivera Castillo, and V.V.Tyrsa, "Navigation of Spacecraft and Mobile Robot", *Robotics and Manufacturing*, IASTED/ACTA Press, pp. 83-87, Proc. of the IASTED Int. Conf., Cancun, Mexico, 2001.
6. J.H. Conway and R.K. Guy, *The Book of Numbers*, Springer-Verlag, New York, 1996.
7. 1999/00 Catalog, New Focus, Inc., **10**, p.193, 1999.

Author Index

Banerjee, Sauvik, 1, 42
Banerjee, Sourav, 89
Banerji, Pradipta, 139
Berkley, Robert B., 23
Burtseva, Larisa P., 485
Carroll, David, 23
Chang, Chih-Chen, 192, 399, 438
Chang, L., 317
Chen, Chi-An, 288
Chen, Chun-Kuang, 288
Chen, Yih-Fan, 288
Chien, Chia-Nan, 288
Chiu, Nan-Fu, 288
Chung, Jaycee H., 210
Cobb, Adam C., 363
Cowles, Bradford A., 23
Cuc, Adrian, 66
DeGiorgi, Virginia G., 298
Derriso, Mark M., 340
Dong, Qinxi, 118
Endo, Katsura, 118
Epureanu, Bogdan I., 340
Erickson, K., 317
Farrar, Charles R., 53, 157
Finlayson, Richard D., 428
Frederick, Amanda, 169
Ghoshal, Anindya, 180
Giurgiutiu, Victor, 11, 66
Godínez-Azcuaga, Valery F., 428
Gopalakrishnamurthy, Sharath H., 210
Grill, Wolfgang, 233, 263
Grisso, Benjamin L., 99, 222
Hachiya, Yoshitaka, 118
Himeno, Kenji, 118
Holmes, Richard A., 23
Huang, Jhen-Gang, 288
Huang, Lu, 210
Hymer, Wes C., 248
Inman, Daniel J., 99, 222
Iwasaki, Atsushi, 411
Jacobs, Laurence J., 33
Jaw, Fu-Shan, 288
Jayaraman, Subash, 248
Jin, Ming-Hui, 288
Kaneshige, Kenichi, 375
Kao, Cheng-Yan, 288
Kaukuri, Nagaswaroopa, 385
Kawamura, Akira, 118
Kim, Heung Soo, 180
Kirikera, Goutham, 180
Knauth, Stefan, 233
Komsky, Igor N., 201
Krafft, Christoph, 255
Kreinovich, Vladik, 385
Kundu, Tribikram, 89, 263
Laforsch, Christian, 233
Lanza di Scalea, Francesco, 78
Larsen, James M., 23
Law, Kincho H., 157
Lee, Chih-Kung, 288
Lee, K., 317
Lemistre, Michel B., 148
Leo, Donald J., 222
Li, Po-Ching, 446
Liao, Fang-Jen, 288
Lin, Chii-Wann, 288
Lin, Shi-Ming, 288
Lin, Yun-Han, 288
Littles, Jerrol W., Jr., 23
Lowe, Michael J. S., 33
Lu, Shey-Shi, 288
Luangvilai, Kritsakorn, 33
Lynch, Jerome P., 157
Ma, Tian-Wei, 192
Mal, Ajit K., 1, 42
Mamishev, Alexander V., 493
Mares, Jose Rodrigo, 385
Margasahayam, Ravi N., 99
Marzani, Alessandro, 78
Mastro, Andrea M., 273
Matsui, Kunihito, 118
Matsuzaki, Ryosuke, 239
Meo, Michele, 108
Mercer, Robyn R., 273
Michaels, Jennifer E., 363
Michaels, Thomas E., 363
Minnicino, Michael A., II, 419
Miyasaka, Chiaki, 248, 273
Nayak, Subrata, 139
Ngwa, Wilfred, 233, 263
Nicholas, Nicholas C., 248
Nichols, Jonathan M., 307, 317, 329
O'Donnell, Bruce W., 428
Ogiyama, Kazuki, 475
Osegueda, Roberto A., 385
Page, Kenneth R., 99
Pai, P. Frank, 210
Pan, Min-Chun, 446
Panergo, Reynold R., 280
Park, Gyuhae, 53
Peairs, Daniel M., 99
Pettit, Richard G., 23
Pines, Darryl J., 351
Placko, Dominique, 148
Poon, Chun-Wing, 399
Prosser, William H., 180

Qu, Jianmin, 33
Rasmussen, Erik A., 351
Ricci, Fabrizio, 1
Rivas Lopez, Moises, 485
Rizzo, Piervincenzo, 78
Rosenberger, Andrew H., 23
Rowe, Gabriel I., 493
Russ, Stephan M., 23
Saewong, Mark, 375
Sakai, Shinsuke, 411
Salvino, Liming W., 351
Salzer, Reiner, 255
Sato, Tadanobu, 454, 464, 475
Schirra, John J., 23
Schulz, Mark J., 180
Seaver, Mark, 307, 329
Shu, Fong, 428
Shukla, Amit, 169
Sohn, Hoon, 53, 157,
Sommer, Henry J., III, 419
Steiner, Gerald, 255
Sugiya, Tsuneya, 411
Sun, Zhi, 438
Sundararajan, Arvind, 157
Syrmos, Vassilis, 375
Sze, K. W., 438
Tai, Hsiang, 180
Tanaka, Yohei, 464
Tang, Hesheng, 454
Thomas, Dustin T., 11
Tittmann, Bernhard R., 248, 273
Todd, Michael D., 317
Todoroki, Akira, 239, 411
Trickey, Stephen T., 307, 329
Tunç, Sibel, 255
Tyrsa, Valentin E., 485
Tyrsa, Vera V., 485
Wait, Jeannette R., 53
Wang, Wei-Chih, 280
Wang, Xudong, 375
Warnemuende, Kraig L., 127
Wen, Chih-Min, 288
Welsch, Jill, 248
Welter, John T., 11
Wilcox, Paul, 33
Wimmer, Stephanie A., 298
Wu, Hwai-Chung, 127
Wu, Wen-Jong, 288
Yang, Henry T., 192
Yen, Jia-Yush, 288
Yin, Shih-Hsun, 340
Yu, Shih-An, 288
Zimmerer, Cordelia A., 255
Zumpano, Giuseppe, 108

Measurement 42 (2009) 136–144

Contents lists available at ScienceDirect

Measurement

journal homepage: www.elsevier.com/locate/measurement

Signal frequency measurement by rational approximations

Daniel Hernández Balbuena, Oleg Sergiyenko *, Vera Tyrsa, Larysa Burtseva, Moisés Rivas López

Engineering Institute of Autonomous University of Baja California, Blvd. Benito Juárez y Calle de la Normal S/N, Col. Insurgentes Este, Mexicali, BC, Mexico

ARTICLE INFO

Article history:
Received 18 April 2007
Received in revised form 4 February 2008
Accepted 21 April 2008
Available online 29 April 2008

Keywords:
Frequency measurement
Rational fraction approximation
Approximants
Mediant fraction
Measurement uncertainty
Measurement time

ABSTRACT

An alternative method of signal frequency measurement based on the direct frequency comparison principle is presented. Based on a model of its measuring process, it is shown that the resulting measurement is a rational approximation to the true value, and that this approximation has a higher accuracy than approximations by systematic fractions. The properties of mediant fractions are used in the measurement model for two given fractions. The results obtained from the simulation of the measurement model are presented. It is shown that the accuracy of frequency measurement that can be obtained with this method is equivalent to the repeatability of the atomic standard of frequency and time. This method can be implemented in a short time using low cost hardware.

1. Introduction

Measurement of many physical parameters is possible after their transformation to more convenient physical parameters, usually electric parameters. Usually, conversion to frequency or time intervals is used. Therefore, the need for measuring these electric parameters is ever increasing.

Various technologies and applications depend on precise measurements of time and frequency including financial markets, the wired and wireless telephone networks, radio broadband stations, the electrical power grid, radionavigation systems, and GPS-applications [1–6,27].

Many analog and digital frequency measurement techniques have been proposed [2–6]. In a basic digital measurement technique, the zero crossing of a signal is counted and the average frequency is determined by the number of whole cycles occurring during a fixed time interval which is determined by the counter's time base [6]. These are the classic methods for frequency measurement. The sources of error for these methods are analyzed satisfactorily in [7–9].

In other digital techniques, the gate time is determined by electronic detection of two kinds of the same phase difference situation between two signals [10], or by electronic detection of two coincidence pulses of regular independent pulse trains [5,7,11]. In these methods the quantization error (±1 cycle) can be overcome satisfactorily [7,10]. For these techniques in a best case in measurements results the ±1 period measurement error is almost eliminated, because the gate time is not fixed, this is defined by two consecutives electronics events, and quantization error is limited only by pulses overlapping area (coincidence pulse width). Also, in [10] a phase coincidence detection circuit with high distinguishability is required.

All the methods previously mentioned are not independent of instrumental errors. By instrumental error we refer to any kind of error caused by objective phenomena like: jitter, thermal noise, Gaussian white noise, etc., which always are present as a source of error inside measuring equipment, and cannot be eliminated.

When the frequency to be measured increases sufficiently, these factors more strongly affect the measurement results. According to Allan [12], the way to exactly verify the error is through long term observation. It is possible, for example, in the National Institute of Standards and Technologies of the USA (NIST USA), to carry out a

* Corresponding author. Tel./fax: +52 686 566 41 50.
E-mail address: srgnk@iing.mxl.uabc.mx (O. Sergiyenko).

0263-2241/$ - see front matter © 2008 Elsevier Ltd. All rights reserved.
doi:10.1016/j.measurement.2008.04.009

comparison of frequency and time standards with a margin of error $\beta_0 \leqslant 1 \times 10^{-15}$ within 24 h [13].

However, for some practical applications it is impossible to observe a real time process over such a long time interval [1, p. 68] Thus, an extremely important and innovative task is to release the measurement process from the necessity of long term observation. In principle, it is impossible for all methods based on the "Allan algorithm" (accuracy enhancement by the observation time prolongation). The Allan variance (Avar) remains a strong tool for the slow frequency calibration laboratory [14,15], because Avar is important for characterizing the stability of oscillators.

According to Allan variance definition the measurement uncertainty is decreasing slowly, as rule with exponential character, after measurement time growing up. But the Allan variance is obtained on the infinite quantity of constant time intervals (units) by statistical treatment of data set. The Allan variance curve always has a monotone character. So, minimal measurement uncertainty (or the best approximation of the measured value) we can obtain only after sufficiently long term of observation. Then, this method of accuracy estimation is unacceptable for fast physical processes or phenomena because of own definition. But as we will show below, the real discrete events comparison process not has a monotone character. And in a short time interval we can have various points when the error is equal or even less, than estimation by Allan variance after long time. And our principle goal is to detect criterion for such points verification.

For most practical tasks, short term exact frequency estimation can be achieved with specific mathematic information processing. Some types of such mathematic methods are described in articles of Tyrsa and Wei [3,4,7,10,11,16]. However, for common applications this theory is not sufficiently general and has still not defined the general criterion for exact frequency estimation. In this paper we will try to develop a generalized theory.

2. Pulse coincidence measurement method and its features. Extended analysis

In this method, a desired frequency is measured by comparing it with a standard frequency. The zero crossings of both frequencies are detected, forming two regular independent narrow pulse trains. The desired and standard trains of narrow pulses are compared for coincidence. This comparison is made using an AND gate. A coincidence pulse train is generated. The coincident pulses can be used as triggers to start and stop a pair of digital counters. The standard and desired pulse trains are applied to the counters and a measure of the desired frequency is obtained by multiplying the know standard frequency by the ratio of the desired count and the standard count obtained with the two digital counters [5,11].

Consider f_x as the desired or unknown frequency and f_0 as the standard frequency. In Fig. 1, S_x and S_0 are the unknown and standard trains of narrows pulses, respectively. The pulses' widths are τ.

Consider ΔT as the greatest common divisor (g.c.d) of both periods $T_x = 1/f_x$ and $T_0 = 1/f_0$. ΔT represents a minimally distinguishable time interval and indirectly a quantum, which as shown below, is defined by the stability of the standard frequency. τ and ΔT are independent parameters.

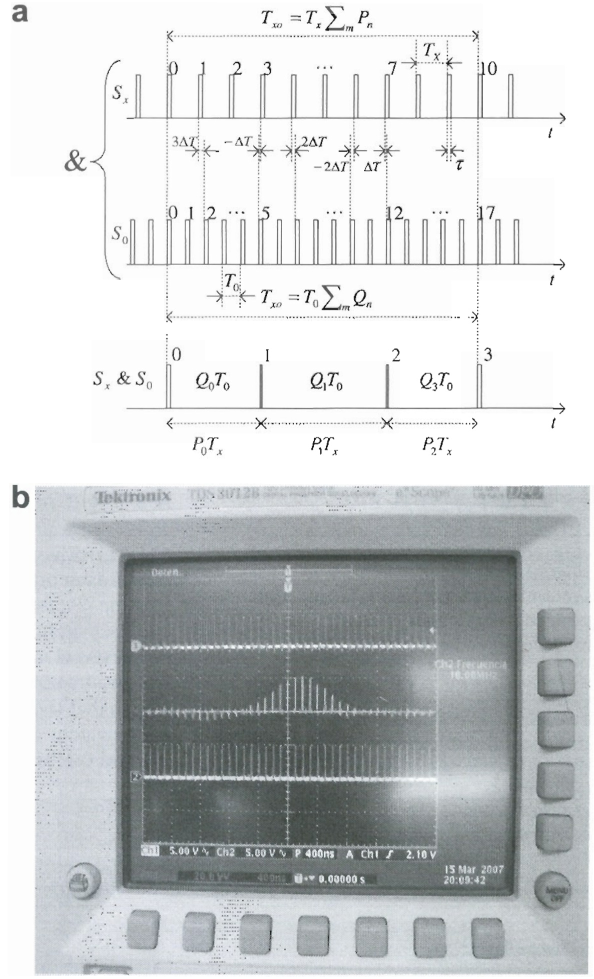

Fig. 1. Process of direct frequency comparison: (a) geometric theory of coincidence trains formation and (b) practical view of coincidences on the oscilloscope screenshots.

The next section describes the functioning of the ideal method.

Let us admit that there exists a pair of narrow pulses in the pulse trains which exactly coincide on the time axis.

This first, completely coincident pair of pulses (Fig. 1) is designated with zero indexes. This pair of pulses is a command to start the frequency measurement. P_n and Q_n are the numbers of counted pulses from the S_x and S_0 sequences that occur between adjacent coincidences. Between two completely coincident pairs (which correspond to pulses number 0 and 17 of the reference frequency sequence II) there also exist some partial coincidences. Adjacent coincidences may be either partial or total. The index n refers to both partial or total coincidences. In Fig. 1 for the second and the third, partially coincident pairs, respectively, $P_1 = 3$, $Q_1 = 5$; $P_2 = 7$, $Q_2 = 12$.

Fractions $P_1/Q_1 = 3/5$, $P_2/Q_2 = 7/12$ each independently can be used for an estimation of the unknown frequency, as shown in [5]. On the other hand, according to [17,18], if we have any two fractions P_1/Q_1, P_2/Q_2 they can form a mediant fraction, as follows:

$$\frac{P_2}{Q_2} < \frac{P_1 + P_2}{Q_1 + Q_2} < \frac{P_1}{Q_1}. \tag{1}$$

Mediant fractions are known to lie between their approximants (progenitors), viz., for

$$\frac{P_2}{Q_2} < \frac{P_1}{Q_1}. \tag{2}$$

So, in our case P_1/Q_1, P_2/Q_2 are approximants to each other and to the mediant formed by them [17,18]:

$$\sum_m P_n / \sum_m Q_n = (P_1 + P_2)/(Q_1 + Q_2) = (3 + 7)/(5 + 12) = 10/17. \tag{3}$$

3. Problem formulation

The mediant and its approximants have the common fundamental property [17,18] and [19, p. 19, III]:

$$P_n Q_{n+1} - P_{n+1} Q_n = \pm 1. \tag{4}$$

The mediant can be generally written in the form

$$\sum_m P_n / \sum_m Q_n \quad (n = 1, 2, \ldots;\ m = 2, 3, \ldots, n - 1), \tag{5}$$

where n is the number of the fraction, m is the number of the mediant. The comment in parenthesis in (5) means that we can form a mediant with a minimum of two fractions. In this case the number of the fraction $n = 2$, and the corresponding number of the mediant $m = 1$, i.e. the number of the mediant is always one unit less than number of the fraction under consideration. The mediant also can be formed by three fractions with numbers $n = 1, 2, 3$ [17,18]. In this case their mediant is formed using the last fraction $n = 3$ and the previous mediant of the fractions $n = 1$ and $n = 2$.

So, the indexes n and m in formula (5) mark only the step of approximation.

As mentioned in (5) we can consider the two sums

- $\sum_m P_n$ sum of numerators of all n fractions, which form the mediant m.
- $\sum_m Q_n$ sum of denominators of all n fractions, which form the mediant m.

At the same time, these sums automatically provide back-to-back continuous (without dead-time) averaging throughout the measurement time. This method is really more like "continuous time stamping" than [15], for example.

According to measurement fundamentals [20–22] the measurement result can never be represented as the ratio of two integers. This is because the probability than n standard units can coincide with true desired value is close to zero. We can suppose the ratio of frequencies is an irrational number, $\alpha = f_x/f_0$. Since the mediant $\sum_m P_n/\sum_m Q_n$ 10/17 is closer to α, than its forming fractions, it is possible to accept $f_x/f_0 = \sum_m P_n/\sum_m Q_n$, and

$$f_x = f_0 \sum_m P_n \Big/ \sum_m Q_n. \tag{6}$$

We shall express the systematic error of f_x in the form of: $\Delta f_x = f_x - f_0 \sum_m P_n/\sum_m Q_n$. We shall divide the right and left parts of this expression by f_0. This gives us $\Delta f_x/f_0 = f_x/f_0 - \sum_m P_n/\sum_m Q_n$. Since $f_x/f_0 = \alpha$, and according to [17] $|\alpha - \sum_m P_n/\sum_m Q_n| \leqslant 1/(\sum_m Q_n)^2$, so $\Delta f_x \leqslant f_0/(\sum_m Q_n)^2$.

The relative value of the systematic measurement error β_{xm} (frequency offset [23]), using (6) we can write

$$\beta_{xm} = \frac{\Delta f_{xm}}{f_x} = \frac{1}{\sum_m P_n \times \sum_m Q_n}, \tag{7}$$

where Δf_{xm} is the average frequency measurement error.

That was an ideal picture. It shows that approximants and their mediants can be used to directly compare an unknown frequency with a known one. Using approximants and their mediants we can define the value of unknown frequency and its systematic error.

But at the conjunction (Boolean algebra operation by &-gate) of real pulse sequences, the positions of impulses from the sequence S_x along the time axis is arbitrary in relation to impulses of the sequence S_0. It is known [24], that the conjunction of two periodic trains of impulses with frequencies f_x, f_0, generates an infinite sequence of arbitrary coincidences. For impulses with duration (pulse width) $\tau_x \approx \tau_0 = \tau$ the average frequency of coincidences is $\bar{f}_{x0} = 2\tau f_x f_0$, with a period of

$$\bar{T}_{x0} = \frac{1}{2\tau f_x f_0}. \tag{8}$$

The duration of impulses from the output of an &-gate is random and between $0 < \tau_c \leqslant \tau$.

To obtain quantitative information about the direct comparison of frequencies during their conjunction it is possible to begin the analysis of pulses starting from any coincidence. At the next coincidence we have numbers P_n, $Q_n (n = 1, 2, \ldots)$ with the corresponding periods $T_x = 1/f_x$ and $T_0 = 1/f_0$. P_n, Q_n form the fraction P_n/Q_n. The third and any subsequent coincidences have mediants $\sum_m P_n/\sum_m Q_n$ $(n = 1, 2, \ldots; m = 1, 2, \ldots, n - 1)$. Any of these consecutive mediants can determine the value of frequency f_x using formula (6) and can estimate a relative systematic error using formula (7).

If the value of frequency f_x is approximated by a particular mediant with index i, then the relative value of an instrumental error is limited by two factors: (1) the duration of the pulses participating in coincidences, and (2) the time of measurement t_m. Thus $\beta_{xi} = \Delta f_{xi}/f_x \leqslant 2\tau/t_m$.

It is experimentally known, that the specified instrumental error is two to three orders less than in a classical frequency meter [7]. At a pulse width $\tau \approx 7 \times 10^{-9}$ s the measured values of frequency $f_x = 1 \times 10^6$ Hz of the thermostatic quartz generator had root-mean-square (RMS) error $s_x = 1.79 \times 10^{-3}$ Hz at 50 observations during total measurement time $t_m \leqslant 1$ s.

But the estimation of relative systematic error using formula (7) for the method of coincidences used in

[7,16], is $\beta_{xm} \cong 1 \times 10^{-12}$. This level of error is close to the reproducibility of nuclear standards of frequency and time: $\beta_0 = 5 \times 10^{-13}$ [25, p. 185]. This circumstance encourages us to more fully investigate the opportunities given by the approach using mediants.

In [15] the author indirectly proves our method: he tries to process several periods of adjacent coincidences mathematically beginning from the second coincidence. The mathematical process he offered is well known and is a strong method for statistical posterior processing. It is a very good tool, but the quantity of calculations in this case is too large. Consequently, it is a relatively slow method. According to their data, $\Delta f/f \approx 10^{-14}$ Hz. This result is 10 times worse than in NIST [26]. So, we still consider best approximation search the best way for fast and precise measurement of true frequency value.

4. The best approximation. Problem solution

The numerator and denominator of every mediant m corresponds to intervals of time $T_x\sum_m P_n$ and $T_0\sum_m Q_n$. Random overlapping of pulses at coincidences lead to specific segments of time $T_x\sum_m P_n$ and $T_0\sum_m Q_n$ that have different duration. The boundaries of their difference is

$$0 \leqslant \left| T_x \sum_m P_n - T_0 \sum_m Q_n \right| < 2\tau. \tag{9}$$

This expression shows, that in sequence of mediants $\sum_m P_n / \sum_m Q_n$ ($n = 1, 2, \ldots; m = 1, 2, \ldots, n-1$). It is possible to choose one, which satisfies the expression

$$0 \leqslant \left| T_x \sum_m P_n - T_0 \sum_m Q_n \right| < \Delta T. \tag{10}$$

From Archimedes axiom [19, p. 7, property V] it follows that product of two numbers $ab = c$ can be considered as the sum $a + a + \cdots + a$, in which the number of summands is equal to b or as the sum $b + b + \cdots + b$, in which the number of summands is equal to a. The number $c = ab$ represents the common multiple (CM) of numbers a, b.

By means of the g.c.d. ΔT it is possible to represent the periods T_x, T_0 by numbers $a = T_x/\Delta T$, $b = T_0/\Delta T$. Then $c = T_x/\Delta T \times T_0/\Delta T = T_{x0}/\Delta T$ is a common multiple as described mentioned above. Thus we have

$$T_{x0} = T_x T_0 / \Delta T. \tag{11}$$

Thus in formula (10) each of the segments $T_x\sum_m P_n$ and $T_0\sum_m Q_n$ within ΔT are equal to each other, and to the segment $T_{x0} = T_x T_0/\Delta T$. Considering this, we can write $T_x\sum_m P_n = T_{x0}$. Thus we find $\sum_m P_n = T_{x0}/T_x = T_0/\Delta T$.

From the statements above it follows for the accepted decimal notation that the mediant which provides the best approximation for $\alpha = f_x/f_0$ and the greatest possible accuracy for f_x has a numerator of the form $\sum_m P_n = 1 \times 10^r$. That is, the numerator is in the form of "one with r zeros".

It is easy to achieve a desired accuracy in hardware when the form of "r zeros" of least significant bits is registered using the unknown frequency's period counter. This is a stop signal for the end of the measurement process. It allows constructing time keeping systems or a frequency meter with a set accuracy and duration of measurement. A simplified functional diagram of a frequency meter is presented in Fig. 2. Pulse signals with frequencies f_x and f_0 inputs into three &-gates. Prior to the first coincidence in the gate &1 the trigger Tr prevents elements &2, &3 from being active.

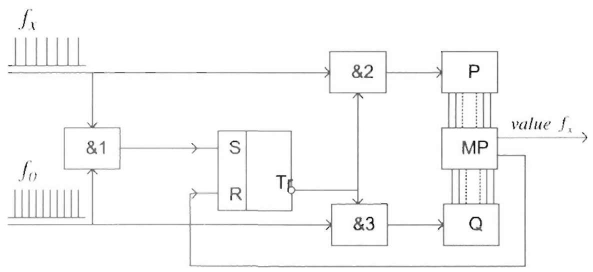

Fig. 2. The frequency meter block diagram for frequency measurement through direct comparison with a reference. Gates &1, &2, &3 are schemes of coincidences (&-gates); Tr is the trigger; P, Q are T_x, T_0-periods counters of unknown frequency f_x and reference frequency f_0, and the MP is microprocessor.

After the occurrence of a coincidence, the counters P and Q keep a count of the pulses of both frequencies until counter P receives a result in the form of $\sum_m P_n = 1 \times 10^r$. This signal results in feedback that resets the trigger to its initial state. The measurement is completed.

We assert that at the end of the measurement, the readout result in the counter $\sum_m Q_n$ is the best proportional approximation of the measured frequency's true value on the given interval of time. We can prove it through analysis of the numerical results of a computer simulation of a coincidence process of two pulse trains using set parameters.

5. Task simulation

In order to provide a clear explanation, we will divide the simulation into two steps. The first step is a demonstration of the real physical process. The second step is the analysis of the numerical results.

First, step one.

In the simulation two pulse trains of unitary amplitude are generated. One of them is a reference signal with the following parameters: $T_0 = 1 \times 10^{-7}$ s and $\tau_0 = 1.5 \times 10^{-9}$ s. The other is assumed to be the unknown frequency signal with hypothetical parameters $T_x = 1.701023 \times 10^{-7}$ s and $\tau_x = 1.5 \times 10^{-9}$ s.

For a given simulation time t_{sim}, two time partitions are generated according to the equations

$$t_{sx}(n_x) = (n_x - 1)T_x + \tau_x, \tag{12}$$

$$t_{s0}(n_0) = (n_0 - 1)T_0 + \tau_0. \tag{13}$$

where n_x, n_0, are integer numbers, representing the pulse number in each train, and t_{sx}, t_{s0} are the time position of each end of a pulse.

The coincidence condition is used as

$$\tau_0 < t_{sx}(n_x) - t_{s0}(n_0) < \tau_x. \tag{14}$$

Arrays of pulse numbers for each pulse train are calculated.

The number of pulses between all adjacent coincidences is calculated for each train, thus obtaining P_n (unknown frequency signal) and Q_n (standard).

The numerator and denominator of the mediants are calculated with $\sum_m P_n$ and $\sum_m Q_n$.

Desired frequency is calculated using

$$f_{xm} = \frac{\sum_m P_n}{\sum_m Q_n} \cdot f_0. \tag{15}$$

The relative frequency error is calculated using

$$\beta_x = \frac{\Delta f}{f_x} = \frac{f_x - f_{xm}}{f_x}. \tag{16}$$

A simplified flow chart of the algorithm is presented in Fig. 3.

5.1. First simulation results analysis

In Fig. 4 the calculated frequency relative error or relative resolution is presented. The simulation time is 0.2 s. In this graphic, we can see a global convergence to zero of this parameter.

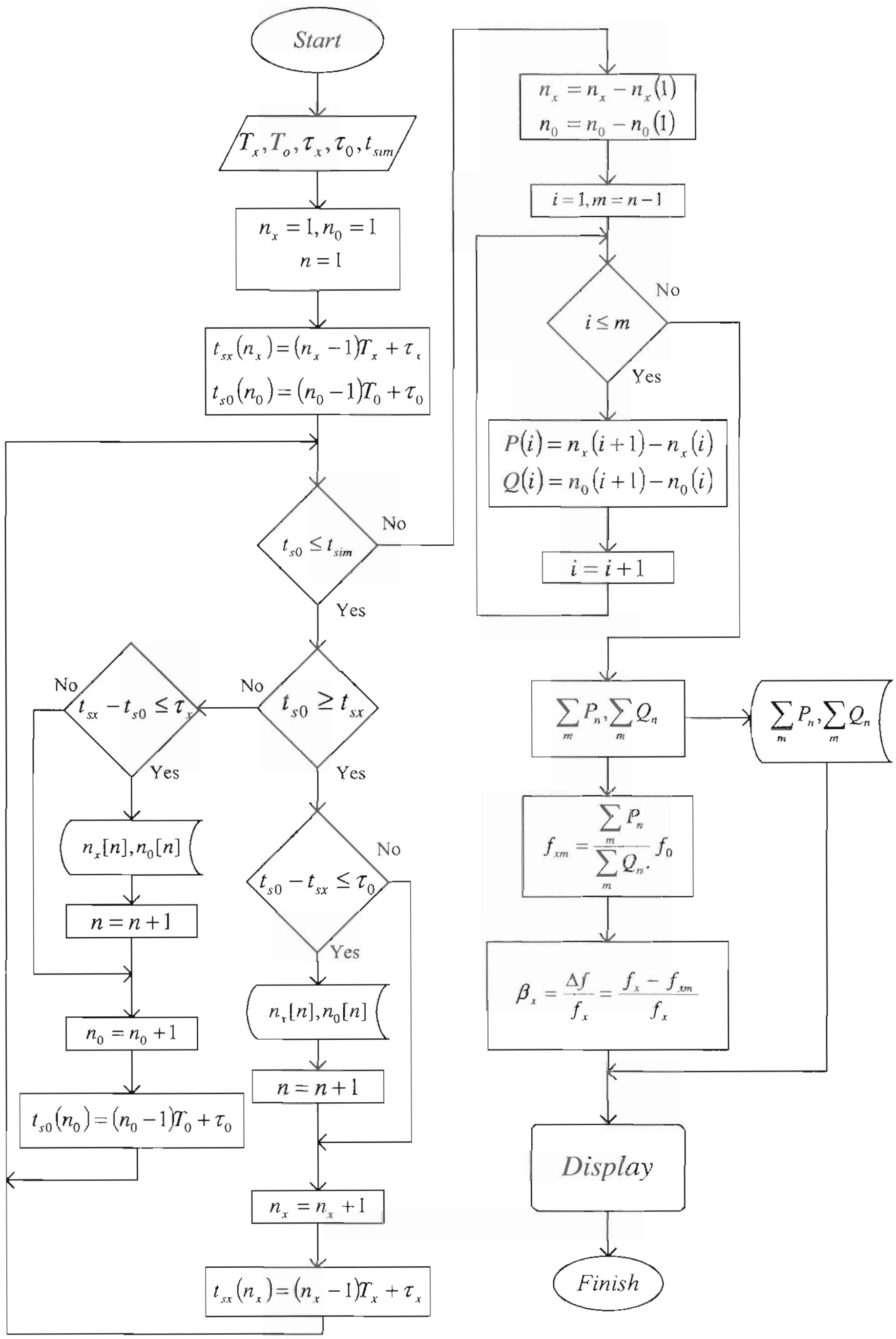

Fig. 3. Simplified flow chart algorithm of task simulation.

Relative resolution for the best coincidences, obtained under condition (6) with $\Delta T = 1 \times 10^{-12}$ is presented in Figs. 5 and 6.

In this graphic, we can observe a convergence by the left and a divergence by the right around 0.17 s. This condition is repeated with time, and in Fig. 7 we can

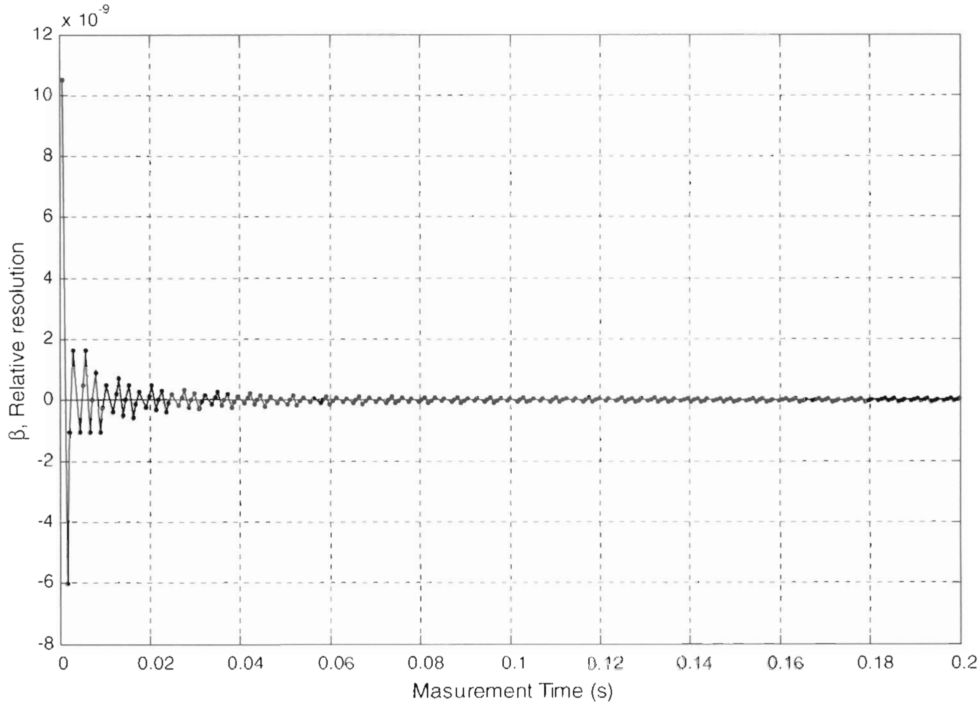

Fig. 4. Frequency relative error (relative resolution) convergence (according to Allan variance).

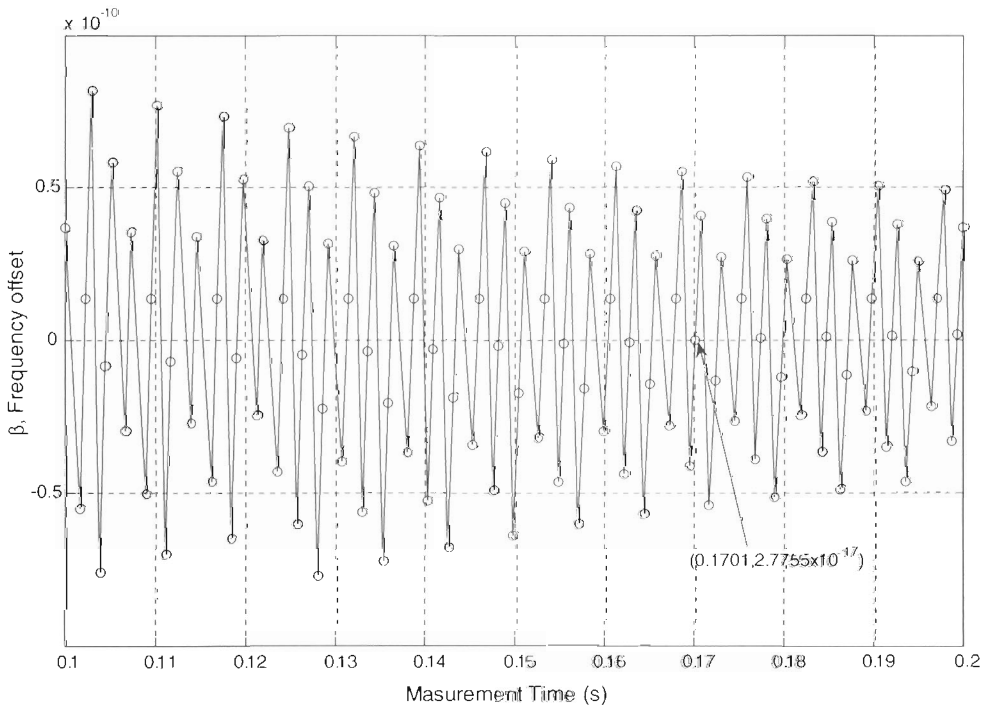

Fig. 5. Frequency offset alternated non monotone convergence (our principle backgrounds).

see five points where $|\beta_x|$ is minimum, for a simulation time of 1 s.

Our simulation is considering the flow of discrete events like coincidence along time axis the discrete pulses of unknown and standard trains. So, the real events of simulation in these graphics are points, not lines. And when we tell "the minimum is really for 0.17 s" it means that in simulation point closest to 0.17 s, for example in Fig. 5

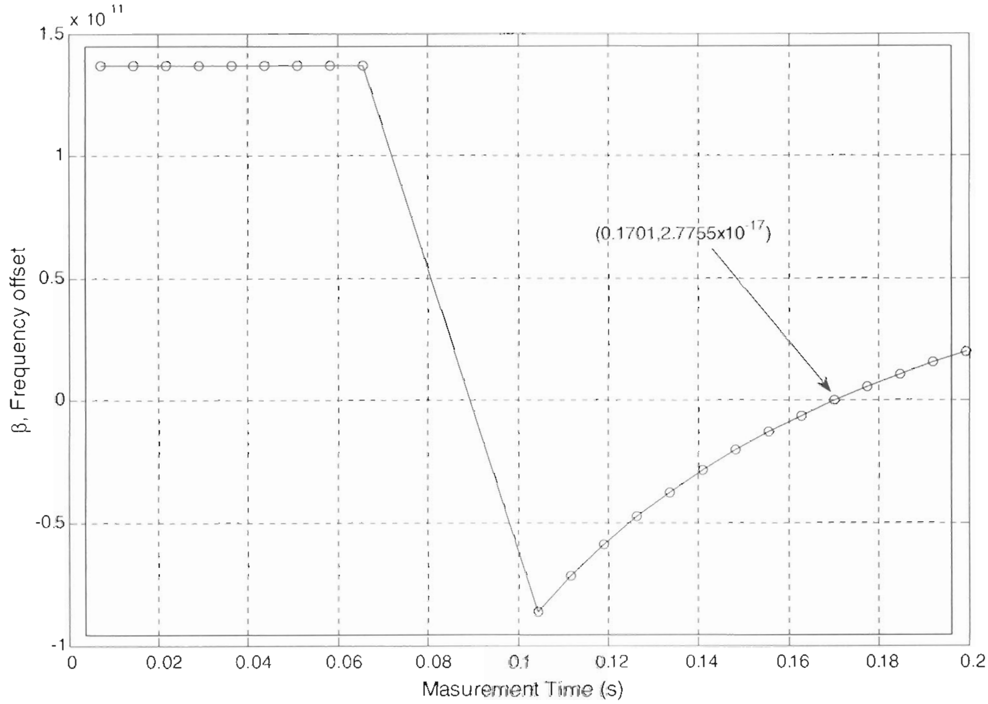

Fig. 6. Frequency offset for the best coincidences selection (the mediant's numeric value).

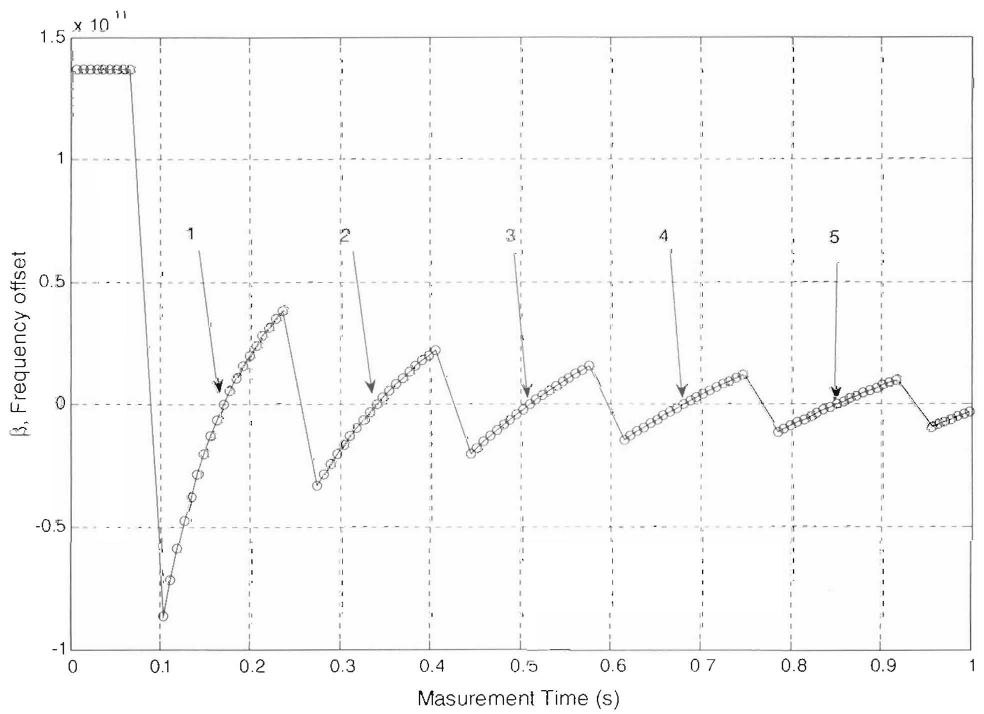

Fig. 7. Frequency relative resolution for a series of best coincidences.

(or Fig. 6 as a zoom of this point in Fig. 5) theoretical error of measurement is strictly equal to zero. Than we can conclude that between various good approximations to true value are some of them, which are the best ones on the interval under consideration. The lines in Figs. 4–7 we need to underline the alternate (but not chaotic) character of comparison process.

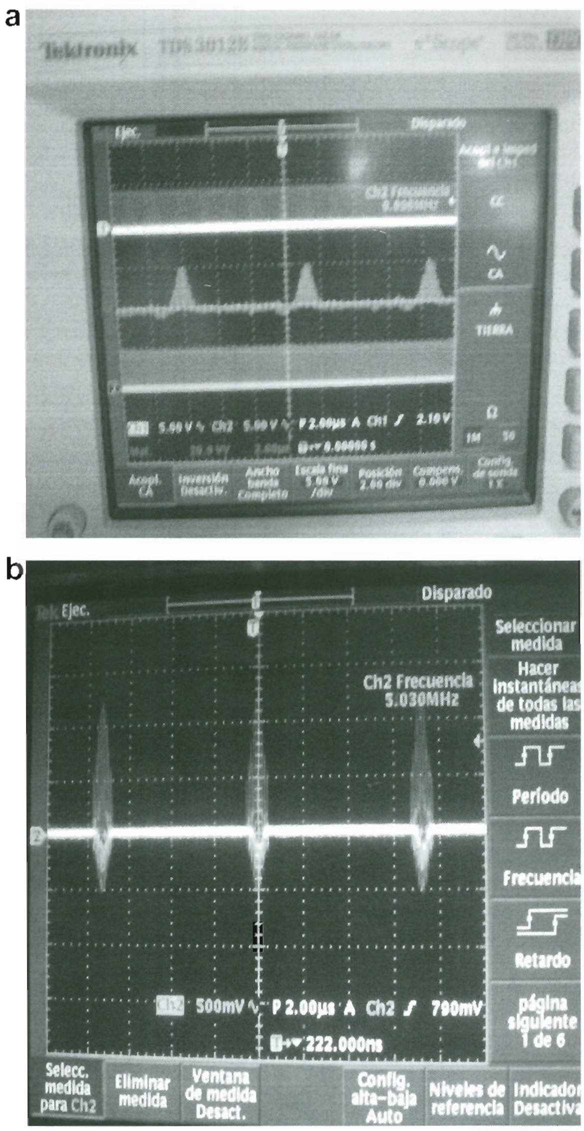

Fig. 8. Experimental screenshots for a series of best coincidences.

However, in the zoom of this graphic presented in Fig. 5, an alternated convergence and a non monotone decreasing characteristic are evident. However, we can identify a point where $|\beta_x|$ (subtitle x means relation to unknown frequency) is minimum for an approximated time of 0.17 s.

We can also see this repetitive character of the appearance of best coincidences in experimental research. For the very similar frequencies of the real crystal oscillators we have obtained the screenshots of signals coincidences (Fig. 8).

These two screenshots are obtained in a different ways. One of them (Fig. 8 a) is using a "Tektronix" TDS 3012B oscilloscope option "multiplication" for two independent pulse trains, formed by two different signal generators ("Agilent" 33250A and "Tektronix" AFG 3101). The second screenshot (Fig. 8 b) represents the pure physical modeling of the coincidence process on the &-gate MC74HC08AN.

5.2. Second step of task simulation

For the second measurement process simulation the value of reference frequency was accepted as $f_0 = 1 \times 10^7$ Hz, $T_0 = 1 \times 10^{-7}$ s. The hypothetical value of unknown frequency $f_x = 5{,}878{,}815.277629991$ Hz is a result of the accepted value of the period $T_x = 1.701023 \times 10^{-7}$ s. $T_x/\Delta T$ and $T_0/\Delta T$ have the common denominator and are mutually prime numbers, $\Delta T = 1 \times 10^{-13}$ s.

The simulation algorithm provided continuous formation of segments $T_x\sum_m P_n$, $T_0\sum_m Q_n$ and compares the magnitude of their difference with parameter 2τ. When the value of the specified difference was less than 2τ on corresponding steps, it was identified with coincidence of pulses from sequences I and II. "Measurement" began at $P_n = 0$, $Q_n = 0$ and considered completed at $\sum_m P_n$ 1×10^6. Values of $\sum_m P_n$, $\sum_m Q_n$ were registered and frequency f_x was calculated (see Table 1).

In the 1st and 2nd columns of the table three pairs of numbers $\sum_k P_n$, $\sum_k Q_n$ from the set of received values are shown. The first and third pairs represent numerators and denominators of approximants. The second pair of numbers is their mediant, which gives the best approximation. These approximants with the mediant satisfy the condition (1). Digits in 4th column are the calculated values of unknown frequency f_x at the time of measurement $t_{m0} \geq 0.17$ s.

Using formula (4) we can estimate the systematic and instrumental errors $\beta_{xm} = \Delta f_{xm}/f_x = 1/(1{,}701{,}023 \times 1{,}000{,}000) = 5.88 \times 10^{-13}$ (average unknown frequency offset). It is easy to see that for the standard $\beta_0 \cong 1 \times 10^{-17}$ (frequency offset, subtitle 0 means relation to reference frequency) and its frequency of $f_0 = 100$ MHz, with an

Table 1
Results of frequency measurement process simulation

Unknown frequency summatory count $\sum_m P_n$	Standard frequency summatory count $\sum_m Q_n$	Absolute error $\lvert T_x\sum_m P_n - T_0\sum_m Q_n\rvert$, s	Measurement result f_x, Hz
957,087	1,628,027	1.00×10^{-13}	5,878,815.277633602
1,000,000	1,701,023	2.78×10^{-17}	5,878,815.277629991
1,042,913	1,774,019	1.00×10^{-13}	5,878,815.277626677

averaging time of 2 s, the error of the measurement of frequency f_x will be on the rate of reproducibility of standard NIST PARCS, USA [13,26].

6. Conclusions

In the offered model for frequency measurement, the result is fixed on the equality of intervals $T_x\sum_m P_n$ and $T_0\sum_m Q_n$. Therefore the model is invariant (independent) to parameters of coincidence circuits, duration and the shape of coincidence pulses, and the parameters of "zero-crossing" pulses in both sequences.

For measuring systems which can be constructed on the basis of the specified model, systematic and instrumental errors have the same infinitesimal order. Instrumental errors are caused only by the reproducibility of the reference frequency. For measurements of high values of frequency f_x it is expedient to use higher values of reference frequency in order to have an equivalent reduction of measurement time.

Acknowledgement

The authors dedicate this article to the grateful memory of our teacher, Dr. Valentin Tyrsa; and would like to thank two anonymous reviewers for valuable comments and remarks. We appreciate Prof. Christopher Druzgalsky and Jason McDowell's invaluable assistance.

References

[1] M.A. Lombardi, Legal and technical measurement requirements for time and frequency, Measure: The Journal of Measurement Science 1 (3) (2006) 60–69.
[2] D. Vakman, New high precision frequency measurement, Measurement Science and Technology 112000) 1493–1497.
[3] Z. Wei et al., A novel Frequency measurement method suitable for a large frequency ratio condition, Chinese Physics Letters 21 (5) (2004) 786–788.
[4] Z. Wei, Z. Xuan, J. Yu, Some developments of precision frequency measurement technique, in: Proceedings of the 1995 International Frequency Symposium, 1995, pp. 354–359.
[5] J.C. Fletcher, Frequency measurement by coincidence detection with standard frequency, US Patent 3, 924,183, 1975.
[6] S.R. Stein, Frequency and Time – Their Measurement and Characterizations, Precision Frequency Control, vol. 2, Academy Press, New York, 1985. pp. 191–416.
[7] V.E. Tyrsa, V.V. Dunashev, Accuracy of frequency measurement based on the pulses coincidence principle, Measurement Techniques 24 (43) (1981) 308–312.
[8] J.J. Gonzales de la Rosa et al, Characterization of frequency instability and frequency offset using instruments with incomplete data sheets, Measurement 39 (2006) 664–673.
[9] C.A. Greenhall, Frequency stability review, TDA progress report 42-88, Communications Systems Research Section, Jet Propulsion Laboratory, vol. 1 (1), 1988, pp. 200 – 212.
[10] Z. Wei, The greatest common factor frequency and its application in the accurate measurement of periodic signals, in: Proceedings of the 1992 IEEE Frequency Control Symposium, 1992, pp. 270–273.
[11] V.E. Tyrsa, Error reduction in conversion of analog quantities to digitized time intervals, Measurement Techniques 18 (3) (1975) 357–360.
[12] David W. Allan, Time and frequency (time-domain) characterization estimation and prediction of precision clocks and oscillators, IEEE Transactions on Ultrasonics, Ferroelectrics, and Frequency Control 34 (752) (1987) 647–654.
[13] NIST-F1, PDF file NISTIR 6610, NIST Frequecy Measurement and Análisis Service. <http://www.boulder.nist.gov/timefreq/>.
[14] D.A. Howe, Interpreting oscillatory frequency stability plots, in: IEEE Proceeding of International Frequency Control Symposium and PDA Exhibition, 2002, pp. 725–732.
[15] Staffan Johansson, New frequency counting principle improves resolution, in: Proceedings of the 36 Annual Precise Time and time interval (PTTI) Systems and Application Meeting, 7–9 December 2004, Washington, DC, ISBN 0-7803-9053-5, 2005, 628 p.
[16] V.E. Tyrsa, V.V. Dunashev, About an error of frequency measurement base on the pulses coincidence principle, Measuring Technique (4) (1981) p.42–44 (in Russian).
[17] A.Ya. Hinchin, Continued Fractions, third ed., The State publishing house of the physical and mathematical literature, Moscow, 1961. 111p. (translated to English in 1964, by Dover Publications Inc., Mineola, New York).
[18] J.H. Conway, R.K. Guy, Farey Fractions and Ford Circles, The Book of Numbers, Springer-Verlag, New York, 1996. pp. 152–154, 332p.
[19] Robert Daniel Carmichael, The Theory of Numbers and Diophantine Analysis, Courier Dover Publications, 2004, ISBN 0486438031. Dover Phoenix Editions, 118p.
[20] N.M. Downie, Fundamentals of Measurement: Techniques and Practices, Oxford University Press, New York, 1967. 482p.
[21] Michael Grabe, Measurement Uncertainties in Science and Technologies, first ed., Springer-Verlag GmbH, 2006. 270p.
[22] Bob Frost, Measuring Performance, second rev. ed., Measurement International, 2000. 96p.
[23] Michael A. Lombardi, Fundamentals of time and frequency, in: Robert H. Bishop (Editor-n-Chief), The Mechatronics Handbook, Chapter 17-1, CRC Press, Boca Raton, London, New York, Washington, 2002.
[24] N.M. Sedyakin, Elements of the theory of random pulses streams 1965, The Soviet Radio, Moscow. 261p.
[25] Test & Measurement Catalog, Hewlett-Packard Press, USA, 1996, 668p.
[26] Nikolas K. Pavlis, Marc A. Weiss, The relativistic redshift with 3×10^{-17} uncertainty at NIST Boulder Colorado USA, Metrologia, Bureau International des Poids et Mesures 40 (2003) 66–73.
[27] Yuriy S. Shmaliy, An unbiased FIR filter for TIE model of a local clock in applications to GPS-based timekeeping, IEEE Transactions on Ultrasonics, Ferroelectrics, and Frequency Control 53 (5) (2006) 862–870.

ICROS-SICE International Joint Conference 2009
August 18-21, 2009, Fukuoka International Congress Center, Japan

Dynamic Laser Scanning method for Mobile Robot Navigation

Oleg Y. Sergiyenko[1], Vera V. Tyrsa[2], Luis F. Devia[1], Wilmar Hernandez [3], Oleg Starostenko[4], Moisés Rivas L. [2,]
[1]Engineering Institute of Autonomous University of Baja California, [2]Polytechnic University of Baja California, Mexicali, BC, Mexico; [3]Polytechnic University of Madrid, Spain; UDLA,[4] Puebla, Mexico.

Abstract

A low cost and non-contact system to obtain tridimentional data about a surface of an obstacle, using a new way of laser triangulation (where both emitter and sensor are rotating) principle is offered. The system uses a revolving laser emitter and a revolving optical scanner working together, which by means of a mathematical processing on a computer, is able to obtain spatial data from laser projected spots. Detailed analysis of priciple, functioning, interaction of mechanical elements and electronic signals is presented in this paper. The mathematical processes for distance and angular measurement are exposed. Results of experiments are shown.

Keywords : mobile robot, obstacle, distance measurement, triangulation, laser scanning.

1. Introduction

In practice, mobile robot routing planning can be classified in two types: first when the robot has stored a pre designed digital route. The second type corresponds to a mobile robot driving in a unknow enviroment, when each changing of direction due to obstacles in the way, cause new route trajectory, to achieve this task is basic to know the dimensions of the osbtacle and the distance to it. The reliability is inversely proportional to the complexity of a system, therefore, systems wich make a lot of calculus and where their output depends on enviroment light conditions, like CCD or CMOS cameras vision systems, are not reliable for special navigation tasks [1]. A typical LIDAR based on time of flight sensor is not suitable for tracking at the close-in distance [2].

The presented system uses the triangulation technique, to obtain tridimensional data from a scene. The three dimensional data from scene is based on intersection of the illuminating laser beam and the rays projected back to the revolving sensor [3]. Using the known emitter incidence angle, the known distance between emitter and sensor, and the reception angle, is possible to determine the heigh of triangle. The reception angle is calculated evaluating the period of each revolution and the time from home position to spot detection position [4]. Other two coordinates can be obtained by means of trigonometricals operations on the computer.

2. Basic operation principle.

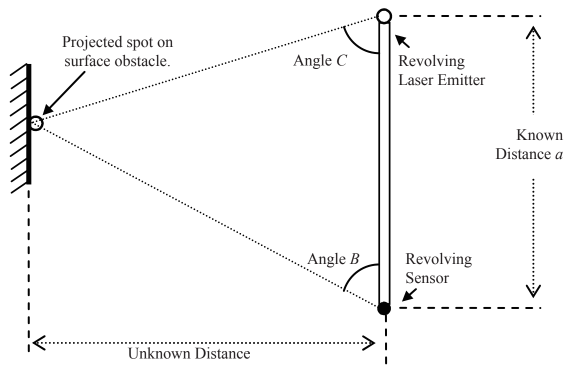

Fig 1. Triangulation principle based on two dynamic angles, *B* and *C*.

Triangulation method was reviewed for several authors [5],[6],[7],[8]. To obtain 3D-data of scene by trangulation method, a virtual triangle must to be created in the scene, and one of its vertexes is the desired point on obstacle surface. Straight line nature of laser light makes it apropppiative to perform lines into a space [9]. Triangulation consist of characteristics determitacion of a triangle usign at least three known elements of it [10]. One side of this triangle is the emitted laser ray, second side correspond to the diffusely reflected ray to the revolving receiver. Third side is the known distance between centers of laser revolving emitter, and the revolving sensor.

Figure 1. Laser triangulation with revolving emitter and sensor

The distance *d* from system up to highlighted points on by the laser, in terms of knowables values :

$$\mathrm{d(a,B,C)} = \frac{a.sen(B).sen(C)}{sen(180-(B+C))}, \quad (1)$$

Threedimensional point $P_{m,n}$ (x, y, z) of each study point depends directly of :*Horizontal emission angle (C), Vertical emission angle (θ) and Horizontal light detection angle (B)*.

Based on initial coordinate *d* measurement system is able to obtain the rest of three dimentional data about the study point by follow equations:

$$y = a\left[\frac{\sin(B).\cos(C)}{\sin(180-(B+C))} - \frac{1}{2} \right], \quad (2)$$

$$x = \frac{a.\sin(B).\sin(C)}{\sin(180-(B+C))} \cdot \cos\left(\sum_0^i \theta_i\right) \quad (3)$$

$$z = \frac{a.\sin(B).\sin(C)}{\sin(180-(B+C))} \cdot \sin\left(\sum_0^i \theta_i\right) \quad (4)$$

On Fig.2, basic elements of proposed system on mobile robot and also the related coordinate system are shown.

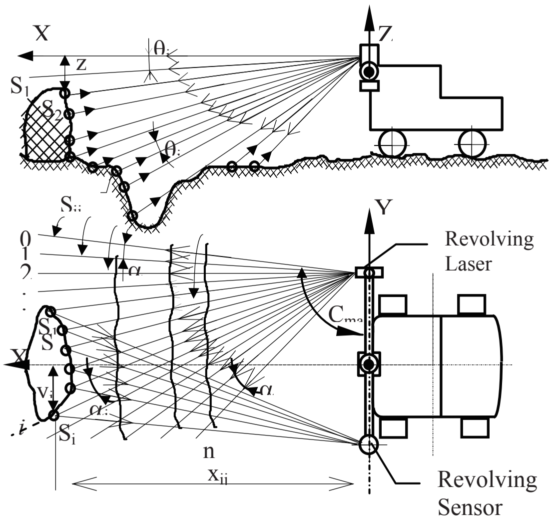

Fig.2. Triangulation system installed on a mobile robot.

3. System construction

This prototype was made using low-cost elements, as follows: an aluminum base bar with one meter of precise length, step motors for vertical and horizontal scanning, a laser source of light, a pair of mirrors with 45 degrees to redirectioning of the light beam, in laser emisor subsection. The emitter use a 632.8 um wave length HeNe Laser as radiation source, placed over horizontal aluminium bar, a group of two mirrors, one of them fixed, the other one, rotating over the shaft of a vertical stepper motor (Fig. 3). On scanning aperture subsystem (Fig. 4 and Fig. 5), a photo receiver, a len in the aperture to get a fine convergence of light in photo receiver. The scanning procedure must cover the entire desired scene surface.

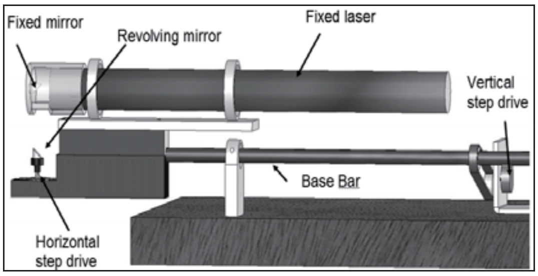

Fig. 3. Emission subsystem.

Steppers motors on system are cotrolled by computer and a power interface, and rotates with small step angle: 0.09118 degrees, due to 1: 82.25 built in reduction gear. Scanning subsystem consist of rotating axle motor with a mirror mounted on, wich change the reflected ray direction up to fixed photo receiver PR on top (Fig. 6).

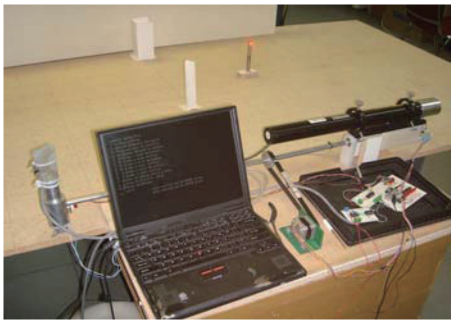

Figure 4. Complete prototype system testing view

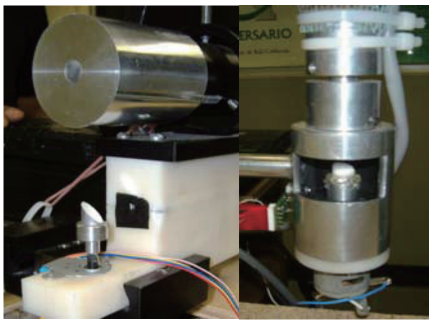

Figure 5. Emitter and scanning aperture.

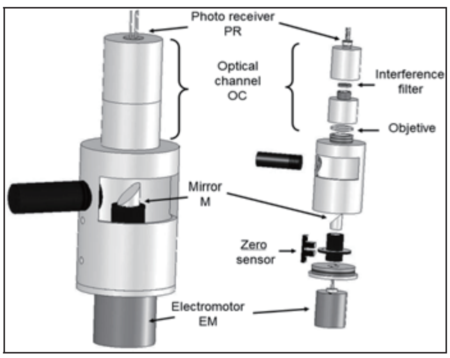

Fig. 6. Explode view of scanning subsystem.

The passive aperture technique PSA, as independent node has a high accuracy of angle measurement. It can be used for navigation task as well as the static coordinate measurement [11], [12].

Zero sensor generates an electric signal to determine each motor turn period, it signal is used for start counting (Fig.7).

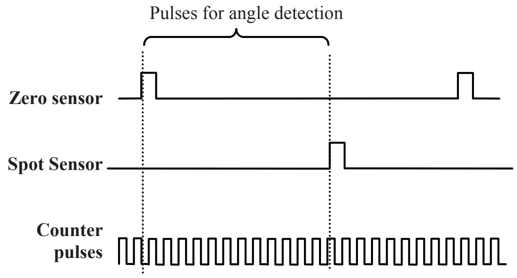

Figure 7. Photoelectric signals and angle detection.

When a reflected laser signal is detected, an electric signal is generated and it stops the angle counter, to calculate it. Pulse overlapping special algoritm in [13] could also increase the system accuracy.

Furthermore, simulation of power axial distribution on laser beam using real parameters was made on Matlab from Poon and Kim Algoritm [16]. Figure 8. shows the power distribution pattern for 0 meter and 15 meter from laser source. This data was useful to determine parameters on conditioner signal system on photodiode output.

4. Prototype experimental testing

Functional ability of the mentioned novel triangulation principle was tested experimentally (see Fig. 9). Oscilloscope yellow line represents real signal fron Zero Sensor, used to synchronize each turn with internal counter. Blue line represents real signal from phtoelectric sensor. It presence means that an obstacle in scene has refleted the laser bean. The time measured between last yellow pulse and blue pulse is proportional to reception angle. The precision of this measurement depends directly on internal counter frequency.

Motors movements control and digital signal processing was made in a host computer. Two digital signals from optical sensors come into device trough the parallel port. Stand alone program developed in C++ language scans continuosly the status port.

The port scanning frequency was 114,670 Hz. According with Zero Sensor and port scanning frequency: 11467 pulses correspond to a complete turn (2π rad).

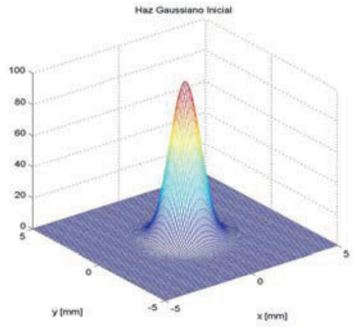

a)

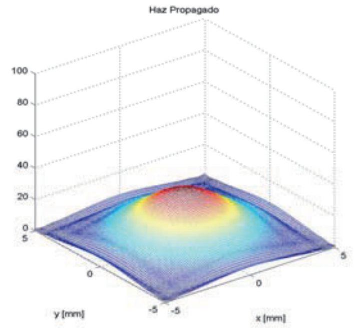

b)

Figure 8. a) Power distribution pattern for 0 meter from laser source. b) Power distribution pattern for 15 meters from laser source

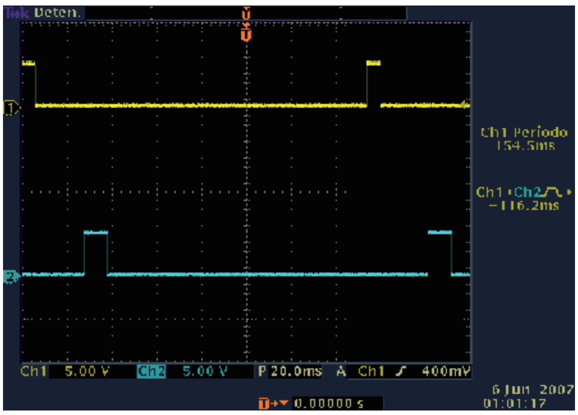

Figure 9. Angle B measurement: pulses from sensors.

Each time that spot signal appears, means that trigonometrical functions determines 3D coordinates of current point (see flow chart on Fig. 10).

All generated data are stored in a data matrix, that can be used to take decisions about mobile robot route i.e. the reconstructed surface can subsequently be visualized using a variety of 3D visualization techniques [14].

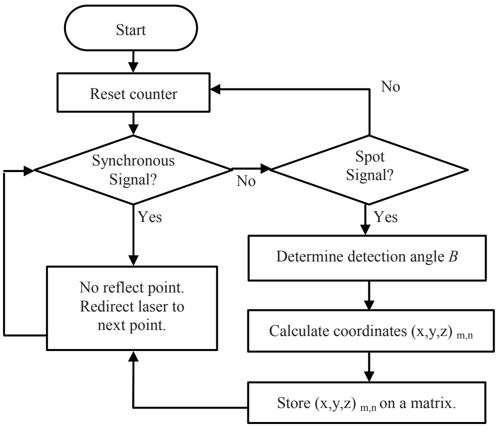

Figure 10 . Software flow chart.

The output signal from photodiode was analyzed in order to determine the dynamic limits of this system. Images on Figure 11 shows output amplitude changes respect to changes in the speed of the DC motor.

As the speed of the DC motor increases, the signal amplitude decreases due to the capacitance of the photodiode model**. I**ncreasing speed affects both the STOP-pulse amplitude and the STOP-pulse width, as shown in the Fig.11.

According to Fig.11, for a scanning velocity variation from 2-3 rps up to 25 rps, there are variations in both the pulse amplitude (from 400 mV up to 1.10 V) and the pulse width (from 2.02 ms up to 3.66 ms). Such variations can be easily corrected by using signal conditioning techniques. However, as can be seen from the above mentioned reasons that for SHM task these speed parameters are already acceptable for normal operation.

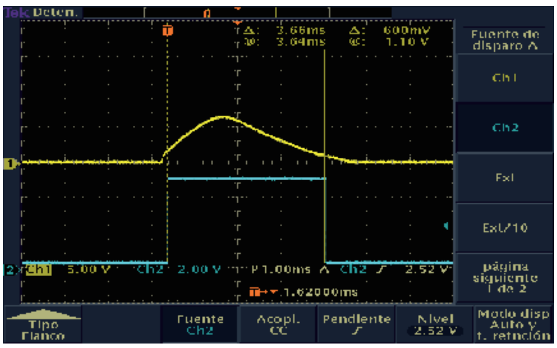

a)

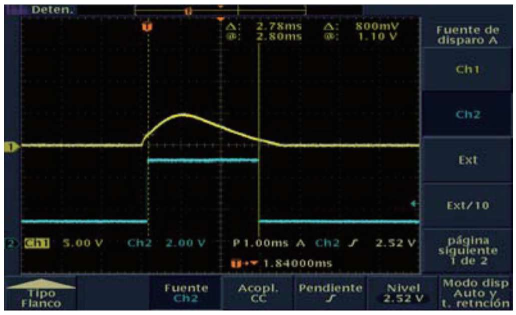

b)

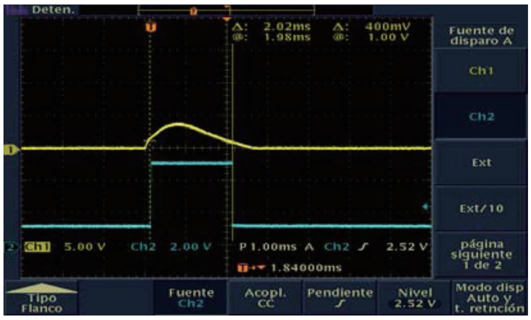

c)

Figure 11. a) Mirror on scanning aperture rotating at 3 RPM approx. b). Mirror on scanning aperture rotating at 12 RPM approx. c) Mirror on scanning aperture rotating at 25 RPM approx.

4.1. Angular Reflection Angle

Diffuse reflection is produced when a light beam fall on a surface, which scatters the light from all directions. Many areas makes it unevenly. In experiments with SVA, was used an obstacle surface as close as possible to a surface lambertian, ie a uniform circular pattern of reflection.

The intensity of light reflected in a perfectly diffusing surface varies as the angle formed by the incident light beam with the normal (vector perpendicular) to the surface. Thus, for a reflection angle of 0 degrees, the reflection is maximum, because the cosine of 0 degrees is 1, and decreases as the angle increases.

In Figure 12. rhombs shows pattern of reflection angle of a lambertian surface and squares shows pattern of the surface in test is case was white paper. This graphic shows that for the selected TVS configuration the registered signal of the reflected light varies within 3-6 volts, and it is completely suitable for implemented regular amplifier.

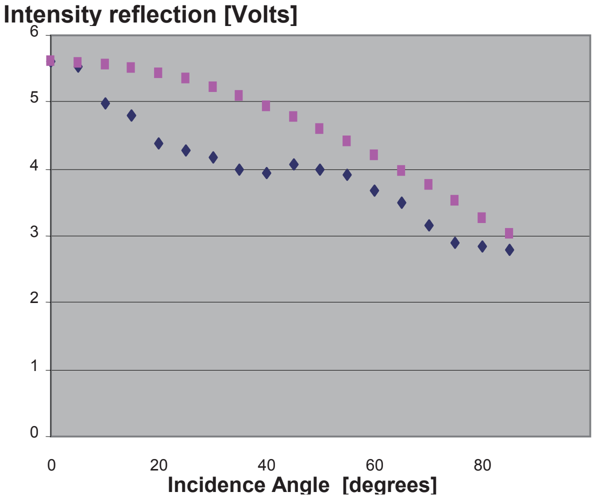

Figure 12. Pattern of reflection angle of a lambertian surface

The experiment starts for the value of the maximum reflected intensity, which occurs at an angle of zero degrees, according to Lambert law:

$$I_{reflected} = K_{\lambda}.I_{initial}.\cos\phi$$

4.2. Distance Reflection attenuation

The second experiment was based on measuring the intensity of the reflected light, when the distance between the laser light emitter and the obstacle was variying, keeping a constant distance between the photo receiver and the obstacle. See Figure 13.

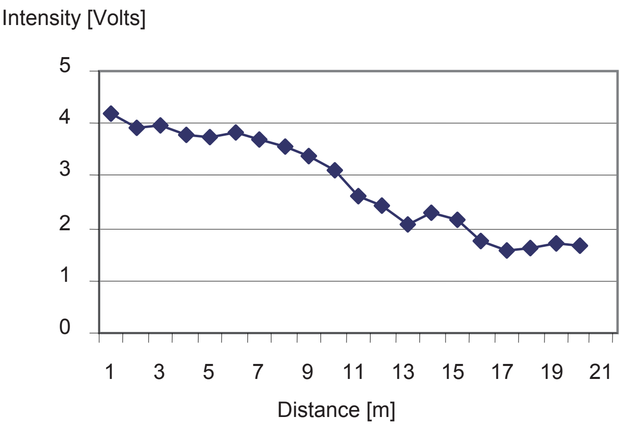

Figure 13. Intensity Vs. emitter distance

4.3. Bidimensional coordinates measurement.

A white paper obstacle was placed at each point in the network. Each point was scanning to 10 times the by optic aperture, and which was an average angle of reception of each item. Additionally, we calculated the value of the emission angle (angle C) for each test point, using trigonometric formulas. Using the value of C, gives the final coordinates X and Y, describing the position of each experimental point.

The figure 14, show the network. Rhombs indicates where real obstacle was placed on explorable area. Squares shows the points based on the calculated coordinates. Each of these points are on a 10 cm square network

From image results we conclude that exists an area on explorable scene where the calculated points (x,y), presents high accuracy. Far points have a bigger error due to reflection phenomenon on illuminated surface and low reflectance according with Lambert´s law.

5. Conclusions

The offered 3D vision system (TVS) completely solve a problem of MR navigation: it allows to search space in front of the robot and to locate obstacles in front of robot's position. Also, the TVS do not require new elements and devices, and can be designed on the basis of items currently in full-scale production. In addition, it represents the realization of an idea of a computer vision in the form of a analogue-digital model of space in front of the robot.

Acknowledgements

Presented system was partially supported by the Autonomous University of Baja California, Mexico (projects No. 2352, in 2003-2004 and N2386, in 2005-2006).

We have also appreciates the Ministry of Science and Innovation (MICINN) of Spain for their support under the research project TEC2007-63121, and the Universidad Politecnica de Madrid (EUIT).

Special thanks to the administration of the Baja California Polytechnical University for the experimental base maintenance.

References

[1] CCD or CMOS cameras vision systems Selectes papers on CCD and CMOS imadges / editor Moon Gi Kang, General editor Brian J.Thompson, SPIE Press: Bellingham, Washington, USA, Volume MS177, 2003.

[2] Javier Gonzales et al. A Mobile Robot Iconic Position Estimator Using a Radial Laser Scanner. Journal of Intelligent and Robotic Systems. © 1995, Springer, Netherlands, p 161-179.

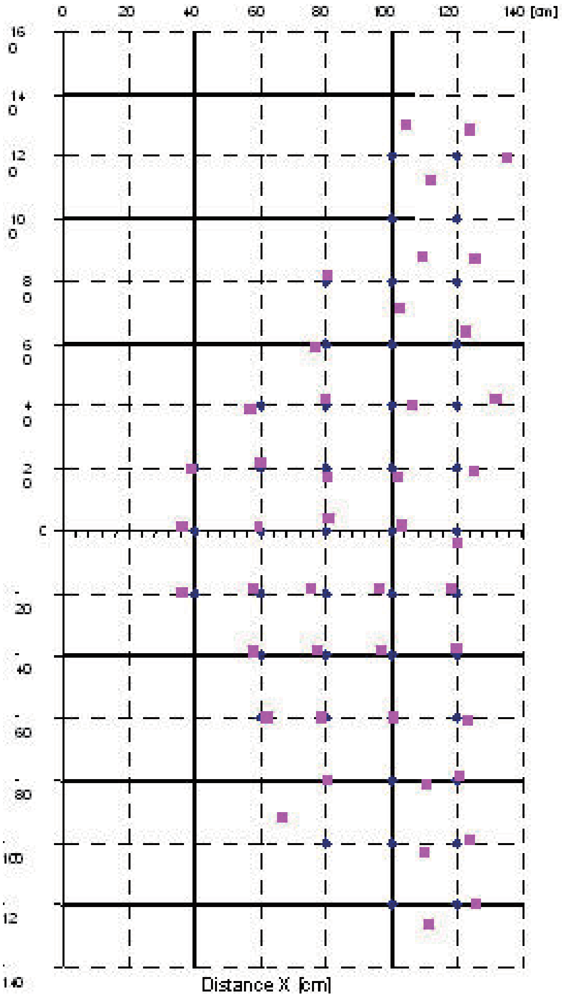

Figure 14. Bidimensional measurements XY.

[3] Oleg Sergiyenko, et al. Precise Optical Scanning for practical multiapplications. Proceedings of IEEE 34th Annual IEEE Conference IECON'08, Florida, USA, 2008, p. 1656-1661.

[4] "Computer vision" book. Edited by Xiong Zhihui, Chapter 22 "Machine vision: approaches and limitations". Authors: M. Rivas Lopez, Oleg Sergiyenko, Vera Tyrsa, pp. 395-428. Editorial: ITECH, Vienna, Austria, 2008. p. 538.

[5] Handbook of Optical and Laser Scanning (2004), *edited by Gerald F. Marshall*, Marcel Dekker, Inc., New York,p. 769.

[6] Paul Forman, Iwan Parry. Rapid Data Collectiom at Major Incident Scenes using Three Dimensional Laser Scanning Techniques.IEEE 35th International Carnahan Conference on Security Technology, Oct 2001, p. 60-67.

[7] D.S. Pierce, T.S. Ng, B.R. Morrison. A Novel Laser Triangulation Technique for High Precision Distance Measurement, Proceeding of IEEE Industry Aplications Society Annual Meeting, vol.2, Houston USA, 1992, p.1762-1769.

[8] D. D. Lichti, M. P. Stewart, M. Tsakiri, A. J. Snow. Benchmark tests on a Three-Dimensional Laser Scanning system. Department of Spatial Sciences of Curtin University of Technology, Geomatics Research Australia, 23 p., 2000.

[9] GLASSNER, Andrew S. An Introduction to Ray Tracing. Morgan Kaufman. San Francisco. 1989. p. 327.

[10] COLLADO, J. Forest. New Methods for Triangulation Based shape acquisition using laser scanners. University of Girona. 2005.

[11] Moisés Rivas, Oleg Sergiyenko, et al. Spatial data acquisition by laser scanning for robot or SHM task. IEEE-IES Proceedings of ISIE-2008, Cambridge, United Kingdom, June 2008, p.1458-1463.

[12] Tyrsa V.Ye., Sergiyenko O.Yu., et al. Mobile Robot navigation by Laser Scanning Means. Proceeding of Conference on Cybernetics, Systems and Applications CITSA, 2006, Volume I, Orlando, Florida, USA, 2006, p. 340-345.

[13] Daniel Hernández Balbuena, Oleg Sergiyenko, et al. Signal frequency measurement by rational approximations. Elsevier, "Measurement", Volume 42, Issue 1, January 2009, Pages 136-144.

[14] SLOB, Siefko. HACK, Robert. 3D Terrestrial Laser Scanning as a New Field Measurement and Monitoring Technique**.** LNES 104, pp. 179–189, 2004. Springer Verlag Berlin Heidelberg 2004

[15] WEHR, Aloysius. LOHR, Uwe. Airborne laser scanning an introduction and overview ISPRS Journal of Photogrammetry & Remote Sensing, 54 1999.pp. 68–82. ELSEVIER, *Germany,* 1999.

[16] POON, Ting-Chung. Engineering optics with Matlab. Ting-Chung Poon, Taegeun Kim: New Jersey : World Scientific, cop.2006.

METHOD FOR PHASE SHIFT MEASUREMENT USING FAREY FRACTIONS

Daniel Hernández B.[1], Moisés Rivas L.[1], Larysa Burtseva[1], Oleg Sergiyenko[1], Vira Tyrsa[2].

[1] *Autonomous University of Baja California, 21280, Mexicali, BC, México, Phone/Fax: 52-686-5664270, e-mail: dhernan@uabc.mx, {lpb,srgnk}@iing.mxl.uabc.mx.*
[2] *Kharkiv Automobile and Highway National University, 61002, Petrovsky Street 25, Ukraine, Phone: 380 57 700 38 65, Fax: 380 57 700 38 66, e-mail: tyrsa@khadi.kharkov.ua*

Abstract-The phase shift of coherent signals and the time intervals can be measured with the method of coincidences of electrical pulses. The results are automatically obtained and represented like simple fractions. These fractions are rational approximations of the unknown parameter, which generally is an irrational number. Such approximations can be represented with continued fractions or Farey fractions.
Definitions and properties of Farey fractions are presented. An original method for phase shift measurement based on the pulses coincidence principle, whose result is a Farey fraction, is described. In order to increase the measurement accuracy, the continuous formation of rational means is performed, to represent the measurement result. These simplify the data processing and provide more accurate results than traditional methods.
Keywords: Phase shift measurement, Farey fraction, mediant.

INTRODUCTION

On this paper, an application of the method of approach by rational approximations in metrology is presented. This method can be used to find the solution of several measurement problems, particularly, to increase the accuracy and speed of automatic digital measurements of physics magnitudes, such as frequency, phase shift and time intervals. The application of this method can be successful where the possibilities of the classic methods already were exhausted. On this article, an original algorithm based on the Farey succession is presented. The algorithm allows a quick and high accuracy way of measuring the phase shift between two coherent sine signals.

FREQUENCY MEASUREMENT USING THE COINCIDENCE PULSE METHOD

Consider an electrical sine signal with unknown frequency f_x, in order to measure it, its frequency is converted to an electrical pulse train signal. In the classical frequency measurement method the result is a digital code N_x, which is the output of a digital counter, and represent the amount of periods $T_x=1/f_x$, in 1 s. The measure frequency result is N_x and has an uncertainty $\Delta f_x \leq 1$ Hz. The fractional measurement uncertainty is $\beta=\Delta f_x/f_x$, which is inversely proportional to the measure frequency. For high frequencies such as f_x=1 GHz, the fractional measurement uncertainty is $\beta \leq 10^{-9}$. For accurate measurements fractional measurement uncertainties in the order of $\beta \leq 10^{-12}$ are necessaries, comparables with the reproducibility of time and frequency standards [1].

In order to increase the measurement accuracy, the frequency measurement method by rational approximations is proposed [2]. In this method the measurement system is a digital system, which counts the amount pulses of a couple of pulse trains. The first one is associated

1-4244-0627-7/06/$20.00 ©2006 IEEE

with the standard and has a repetition rate f_0. The other one is associated with the sine signal of unknown frequency and has an unknown repetition rate f_x. Periodic coincidences of these pulse trains are observed in time. Its mean frequency is [2]:

$$f_{0x} = 1/T_{0x} = (\tau_0 + \tau_x) f_0 f_x, \tag{1}$$

where T_{0x} is the mean coincidence period; τ_0, τ_x are the pulse duration of the pulse trains being compared in time, whose frequencies are f_0 and f_x respectively. The measurement time is the time interval between a couple of those coincidence pulses. The measurement result is represented like a simple fraction and is a rational approximation of the unknown frequency, which generally is an irrational number. A computation of the number of pulses $N_0 = T_{0x} f_0$ and $N_0 = T_{0x} f_x$ between a pair of coincidences allows the determination of the unknown frequency f_x for a know frequency f_0: $f_x = N_x f_0 / N_0$.

MEASUREMENT RESULT REPRESENTATION IN FAREY FRACTIONS FORM

Let φ be the phase shift between two electrical sine signals of frequency f_1. And consider two pulse trains of periods T_1 associated with the electrical sine signals. The phase shift is representing by the time interval t_φ as shown in Figure 1. Also consider a third pulse train signal of period T_0 associated with an electrical sine signal of frequency f_0, with $T_1 > T_0$. In order to explain the method, let us call to the first signal the *start pulse train* (Figure 1a), and to the second one *stop pulse train* (Figure 1b) and to the third signal *quantizing pulse train* (Figure 1c). The start and stop pulses delimit the time interval t_φ, see Figure 1.

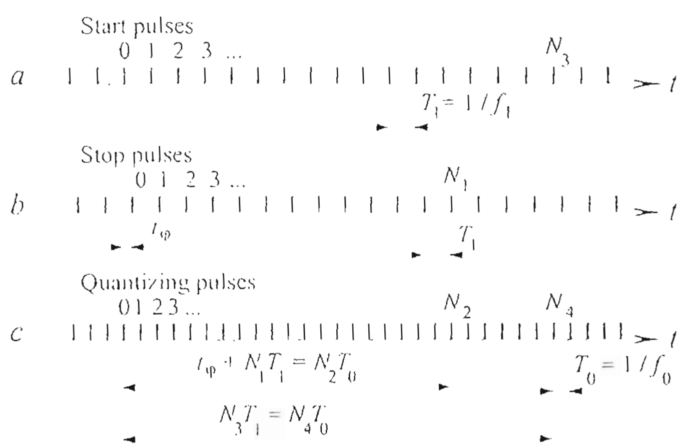

Figure 1. Phase shift measurement by pulse coincidences.

The start measurement criterion is the first coincidence between the start pulses and the quantizing pulses. This is the starting signal to count of the pulse in the three signals. However two stop measurement criterions exist. The first stop criterion is the second coincidence between the start pulses and the quantizing pulses, and they define the digital codes N_1 and N_2. The second stop criterion is the second coincidence between the stop pulses and the quantizing pulses, and they define the digital codes N_3 and N_4 as shown in Figure 1.

From Figure 1, is easy to see that $N_3 T_1 = N_4 T_0$ and $t_\varphi + N_1 T_1 = N_2 T_0$, consequently

$$T_1 = T_0\, N_4 / N_3,$$

and

$$t_\varphi = T_0 \left(N_2 N_3 - N_1 N_4\right)/N_3. \qquad (2)$$

Since $\varphi = t_\varphi / T_1$ then

$$\varphi = \left(N_2 N_3 - N_1 N_4\right)/N_4 \qquad (3)$$

whit $0 \leq \varphi < 1$. The phase shift magnitude is expressed in relative units.

From (3) the time interval t_φ can be written as

$$t_\varphi = T_1 \left(N_2 N_3 - N_1 N_4\right)/N_4 \qquad (4)$$

Is known that in order to increase the measurement accuracy, is necessary to measure the parameter n times and calculate the mean of the n measurements. The calculated mean is $\sqrt{n}$ times more accurate than only one measurement. In order to use this procedure is necessary to calculate (3), with n digital codes obtained n times with the digital measurement system. Therefore the method is inefficient. The Farey fractions are an option to increase the process efficiency and measurement accuracy.

Since $0 \leq \varphi < 1$, the fraction $(N_2 N_3 - N_1 N_4)/N_4$ in (3) y (4) represent the Farey fraction of order N_4.

On the other hand, it is possible to continually form the terms $\sum_k N_{3k}$ and $\sum_k N_{4k}$, and discreetly the terms $\sum_k N_{1k}$, $\sum_k N_{2k}$. Then

$$T_1 = T_0 \sum_k N_{4k} / \sum_k N_{3k}$$

and by similarity with (3) y (4)

$$\varphi_m = (\textstyle\sum_k N_{2k} \sum_k N_{3k} - \sum_k N_{1k} \sum_k N_{4k}) / \sum_k N_{4k} \qquad (5)$$

$$t_{\varphi m} = T_1 (\textstyle\sum_k N_{2k} \sum_k N_{3k} - \sum_k N_{1k} \sum_k N_{4k}) / \sum_k N_{4k} \qquad (6)$$

In (5) and (6) the right part of equations is a Farey fraction of order $\sum_k N_{4k}$. This is the *n-1* rational mean of the Farey fractions of order N_4.

The time intervals defined by the coincidences between the star and stop pulses and the quantizing pulses, are a variable magnitude [2]. Therefore, the Farey frequencies that are possible to be formed throughout the time are not constants number.

The summatory functions in equations (5) and (6) are obtained by the digital measurement system. The measurement result is calculated a single time and is invariant whit f_1 and f_0, and their instabilities. The methodical uncertainty is

$$\Delta t_{\varphi m} = \tau / (\textstyle\sum_k N_{4k})^2$$

The instrumental uncertainty is

$$\Delta t_{\varphi i} = \tau \sqrt{2/k}$$

where τ is the pulse width in all pulse trains.

Taking to $f_1 = 10^7$ Hz, $f_0 = 10^8$ Hz, $\tau = 10^{-9}$s, and the measurement time equal to 1 s. The methodical uncertainty is $\Delta t_{\varphi m} = 10^{-25}$s and the instrumental uncertainty is $\Delta t_{\varphi i} = 10^{-12}$ s. Such uncertainty level is only presented by a high resolution phase comparator for primary standards [4], based on heterodyne system.

Conclusions

The Farey fractions are a good mathematical base to the phase shift measurement. The measurement result is a rational approximation of the unknown parameter, automatically obtained by the digital measurement system. The results have high measurement accuracy without to use a heterodyne system.

References

56. http://www.boulder.nist.gov/timfreq/ Standards, 2003.
57. Burtseva L., Tyrsa V. "Medición de la frecuencia según el método de las aproximaciones racionales". ELECTRO 2002, ITCH, Chihuahua, México, p.441-446.
58. Conway J.H. and Guy R.K. *The Book of Numbers*. NY: Springer-Verlag, USA, 1996.
59. Construcción de un comparador de fase de alta resolución para patrones primarios de frecuencia. CNM-MTF-PT-0001,CENAM, Los Cues, Querétaro, México, 1996.

IEEE CN 06EX1524
ISBN 1-4244-0627-7
LC 2006932321